# HEAT VARIATIONS CAUSED BY GROUNDWATER FLOW IN GROWTH FAULTS OF THE SOUTH TEXAS GULF COAST BASIN

APPROVED:

John M. Sharp, Jr.

W. E. Galloway

Printed in the United States of America

# HEAT VARIATIONS CAUSED BY GROUNDWATER FLOW IN GROWTH FAULTS OF THE SOUTH TEXAS GULF COAST BASIN

by

DANIEL PAUL BODNER, A.B.

**THESIS**

Presented to the Faculty of the Graduate School of
The University of Texas At Austin
in Partial Fulfillment
of the Requirements
for the Degree of

MASTER OF ARTS

THE UNIVERSITY OF TEXAS AT AUSTIN

December, 1985

# ACKNOWLEDGEMENTS

The pages of this volume represent the largest single project I have ever undertaken. Throughout its duration, I have had the unfailing support and counsel of my advisor, who is also my friend, Jack Sharp. I am grateful to him.

I also thank my committee members, Dr. Lynton S. Land and Dr. William E. Galloway, for sharing their advice and knowledge, and for their valuable contributions to the editing process. Lynton is also gratefully acknowledged for providing the original idea which grew into this thesis, and which proved to be rewarding and stimulating.

The research stimulated not only myself, but also the Texas Mining and Mineral Resource Research Institute of the Department of the Interior, whom I thank for providing one of the most tangible rewards, the support of my research.

Technical support was provided by the Bureau of Economic Geology, who supplied the well logs and computer facilites used in obtaining and processing my temperature data. I especially acknowledge Graham Fogg for his advice and time, which was always given freely.

My colleague Paul Blanchard has been very helpful in sharing ideas, references, and computer frustrations. Immessurable moral support has been generoulsy provided by my friends, who have made my tenure at the University of Texas a very enjoyable one.

Finally, I owe a gratitude of a much grander scale to my parents, and also to my brother and the rest of my family, who have provided me with the tools to make of my self what I choose, and who have always loved and supported me, and whom I love and support in return.

## Abstract

Zones of above average subsurface temperatures have been noted in certain areas of the Gulf Coast basin. Their cause has often been credited to geopressure, which presumably traps heat because of higher porosity and consequently lower thermal conductivity. I determined the temperature distribution in a portion of South Texas by collecting and analyzing over 1600 bottom-hole temperature measurements. The analysis included correcting the temperatures with the Kehle correction scheme; constructing isothermal surfaces by both interpolating and extrapolating the data, and Kriging the result. Temperature profiles were plotted for twelve subregions of the study area. The greatest temperature anomalies are associated with the Tertiary Wilcox growth fault zone, and the simple presence of geopressure is insufficient to account for the temperature anomaly.

Numerical modeling indicates that growth faults act as zones for concentrated vertical flow. The upwelling of deep basinal fluids advects heat and causes the high temperatures observed in the growth fault zone. The model, by Smith (1983), is two-dimensional, finite element, steady state, and couples heat and fluid transport. It indicates that the source of these fluids is deep, perhaps over 20,000 feet (6096 m) below the surface. The modeling results also suggest that an unidentified region of high thermal and hydraulic conductivity could exist coastward of the Wilcox faults at a depth of about 15,000-20,000 feet (4572-6096m).

# TABLE OF CONTENTS

# LIST OF FIGURES

# INTRODUCTION

In the Gulf Coast Basin, as well as in most sedimentary basins, temperatures are unevenly distributed. The source of heat is the earth itself, which radiates heat from within in a relatively uniform fashion as a result of dispersed radioactive decay. There are many factors which cause uneven thermal patterns to emerge from this uniform heat source. These can be grouped into the following broad categories: heat transport by basinal fluids, heat transport through the solids, the presence of plutons or other heat sources or sinks, chemical reactions, and mass and energy exchanges across basinal boundaries. Of these, conduction and transport of heat via the movement of ground water, which saturates the sediments of the basin, are perhaps the most important processes in the Gulf Coast. Water has a high specific heat (ie., it can absorb heat without greatly raising its temperature). Thus flowing ground water has the potential to transport a significant amount of heat. Conversely, the heat content itself influences groundwater movement by altering the fluid's hydraulic properties. Thus one process influences and is in turn

influenced by the other. These are said to be coupled. This thesis explores the importance of coupled ground water and heat transport in controlling the deep basinal thermal regime of the Gulf Coast Basin.

Knowledge of groundwater movement in the deep basin has practical consequences in both the energy and mineral industries, as well as in academic inquiries into basinal diagenesis. It is, however, often difficult to observe groundwater movement, especially where rates are slow and/or in the remote deep-basin. It is less difficult to measure temperatures at such points. The coupled flow phenomena provides a method by which groundwater movement in the deep basin can be inferred from available temperature data. This is the approach of this research.

The research required two distinct stages. The initial step was data collection and analysis. These are presented in Part I. Part I includes discussion of the data, their collection and preparation, descriptions of the thermal patterns that emerged from analysis of these data, and implications of these patterns for groundwater flow. After the completion of the first stage, it was evident that too many factors were involved in the thermal regime of the basin to make any definitive conclusions possible from this largely empirical approach. However, the data were consistent and anomalous thermal trends were evident. Therefore, the second stage required computer modeling of the basin using the acquired thermal data. The details of the model, its results, and its implications are covered in Part II. Finally, the analysis allows us to make some definite conclusions about heat flux and groundwater flow in the deep portions of the Gulf of Mexico Basin and to offer

suggestions for further investigation.

# PART I

## 1.1 BACKGROUND

### 1.1.1 THE STUDY AREA

The study was conducted on a regional scale, covering a large portion of South Texas (Fig 1.1). The total area is over 17,000 square miles (44,030 $km^2$) and includes all or part of the counties of Webb, Zapata, Jim Hogg, Kleberg, Duval, Jim Wells, Nueces, Lasalle, McMullen, Live Oak, Refugio, San Patricio, Aransas, Bee,Atascosa, Karnes, Goliad, and Victoria. The area features low topographic relief, with greatest elevations of about 600 feet (183 m) to the west, dropping gradually to sea level at the coast. The maximum depth investigated is 20,000 feet (6096 m), which is wholly within Tertiary sediments.

### 1.1.2 REGIONAL GEOLOGY

The onshore lower Tertiary Gulf Coast section is composed of several terrigenous clastic wedges, which thicken down dip toward the Gulf of Mexico. The sediments prograded over and basinward of the rapidly subsiding Cretaceous Stuart City shelf margin, where

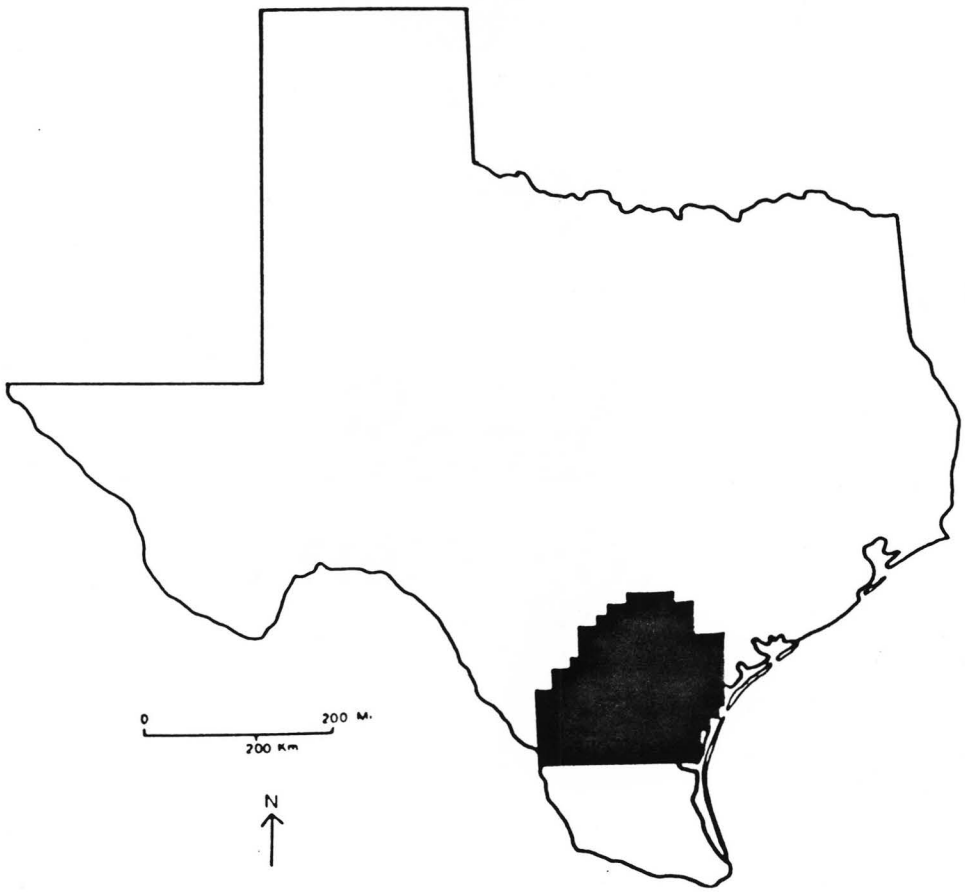


**Figure 1.1:** State of Texas with study area indicated in black.

contemporaneous growth faulting ensued in bands along the shelf edge. As sedimentation and subsidence continued, the shelf edge prograded seaward, establishing other growth fault zones (Fig 1.2). The major growth fault zones have been named after large sediment packages associated with them. The three major ones are the Wilcox, Vicksburg and Frio growth fault trends as shown on the cross section in Fig 1.2 which also identifies other major clastic groups.

### 1.1.3 THERMAL HISTORY

Potentially dominant heat sources are recent tectonic events, which can cause high basement heat fluxes, and volcanic activity, which causes localized heat-source variations.

The most recent tectonic event involving the Gulf Coast was the late Triassic/early Jurassic rifting episode. This event probably featured typical rift-level heat fluxes. Figure 1.3 (Royden and others, 1980) indicates a return to background heat-flux levels by Cretaceous time. Therefore, "normal" levels of heat flux have presumably prevailed since the Cretaceous. While local Cretaceous and Tertiary volcanic activity may have perturbed this pattern, their effects were minimal.

### 1.1.4 GENERALIZED FLOW SYSTEMS

Generalized groundwater flow through Gulf Coast sediments can be conceptualized as occurring in three distinct zones closely correlated with depth. Flow in each of these zones is controlled by different mechanisms. The three, from shallowest to deepest, are the

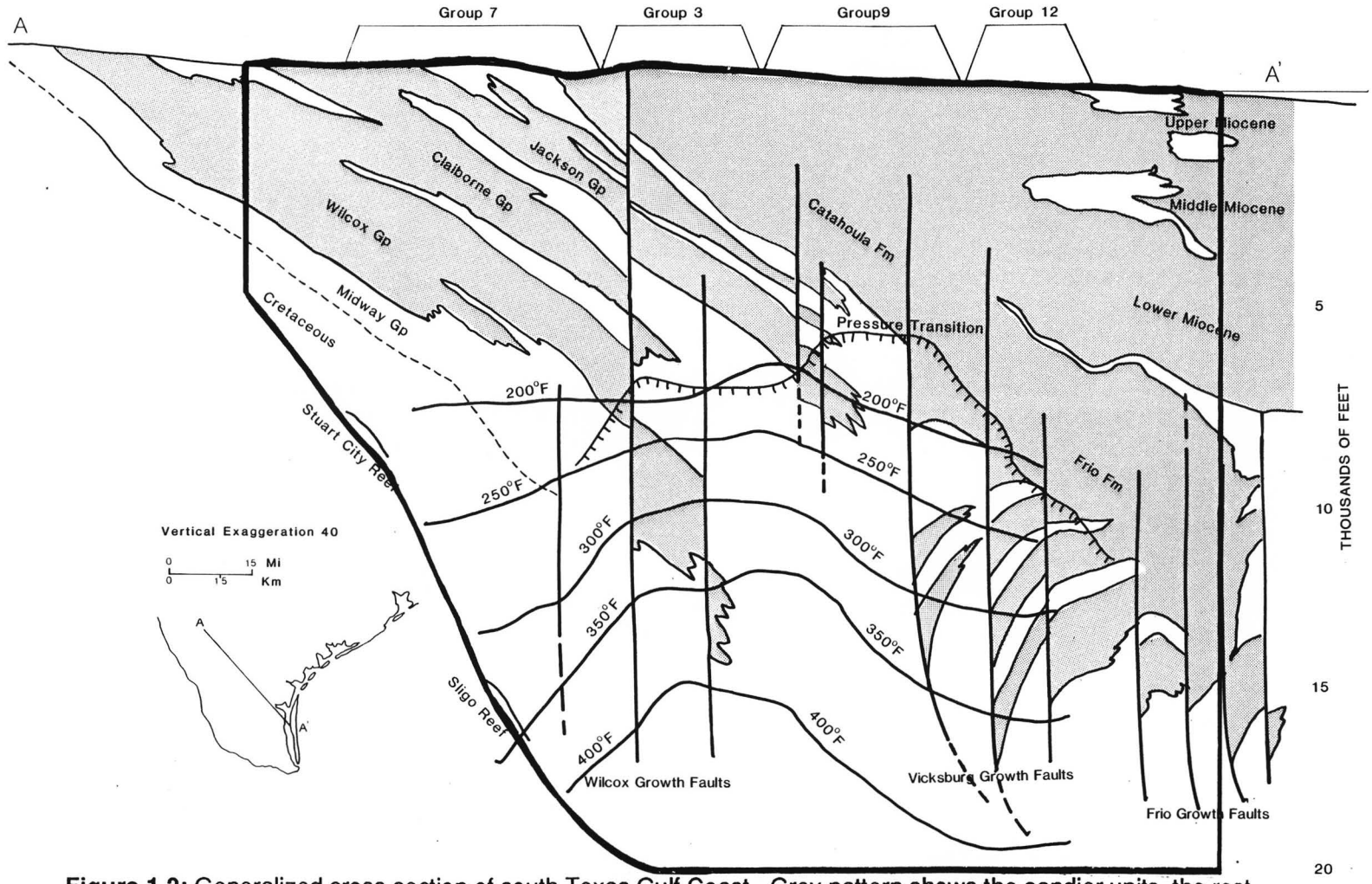


**Figure 1.2:** Generalized cross section of south Texas Gulf Coast. Grey pattern shows the sandier units, the rest of the section being predominantly argillaceous (modified from W.,E. Galloway, written communication). Also indicated are isotherms and the top of the geopressure Transition zone as determined by drilling mud weights. Heavy outline indicates position of finite element grid used in modeling (Part 2).

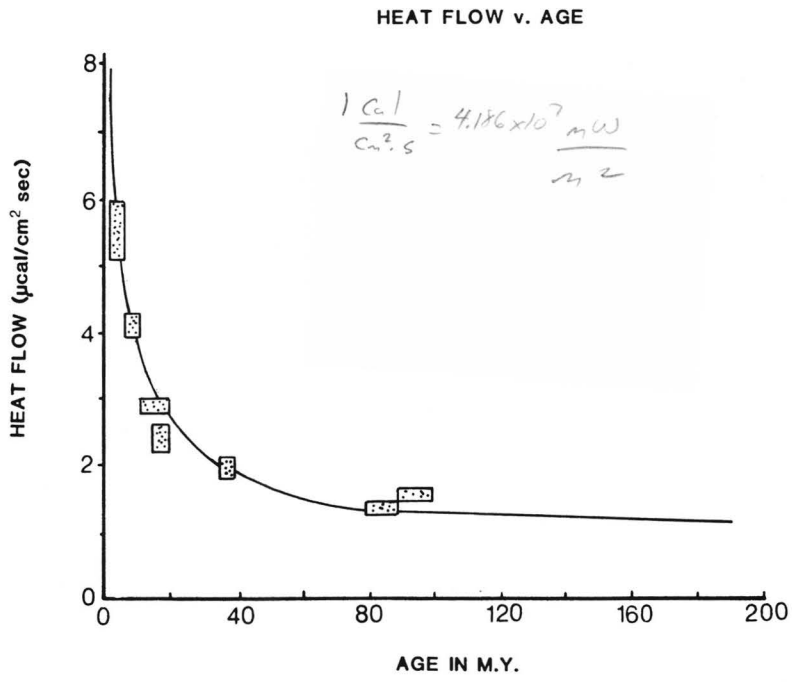


**Figure 1.3:** Generalized plot of mean heat flow versus time after a rifting event. Stippled boxes indicate various heat flow data (redrawn from Royden and others., 1980)

meteoric, compactional/overpressured and thermobaric zones. These are shown for a generalized sedimentary basin in Figure 1.4 from Galloway and Hobday (1983).

Meteoric Zone. Groundwater flow in the meteoric zone is controlled by the elevation of the water table (i.e., ground water moves from areas of high hydraulic potential, usually under topographic highs, to areas where the potential is low, usually at rivers and streams). It has been demonstrated by Back (1966) for the Atlantic Coastal Plain and also by Smith and others (1982) for the Oakville aquifer of Texas that most ground water discharges to rivers. This is contrary to the common misconception that meteoric water flows only down dip towards the coast, a condition that occurs primarily near the coast where there is little topographic relief and in deeper, more inactive portions of the meteoric zone. For these cases, discharge is by diffuse, upward, cross-formational flow in the vicinity of the shoreline and is not concentrated near rivers and streams. The term *meteoric* implies water of an atmospheric origin, but connate water may also enter the meteoric system.

Compactional/overpressured zone. The compactional/overpressured system lies below the meteoric one. Here groundwater movements are not significantly influenced by surficial conditions, but rather are controlled by excess pore-fluid pressure gradients. Excess pressures are partially caused by the weight of the accumulated overlying sediments which causes this zone to compress or compact. As the sediment grains come closer together, the intergranular

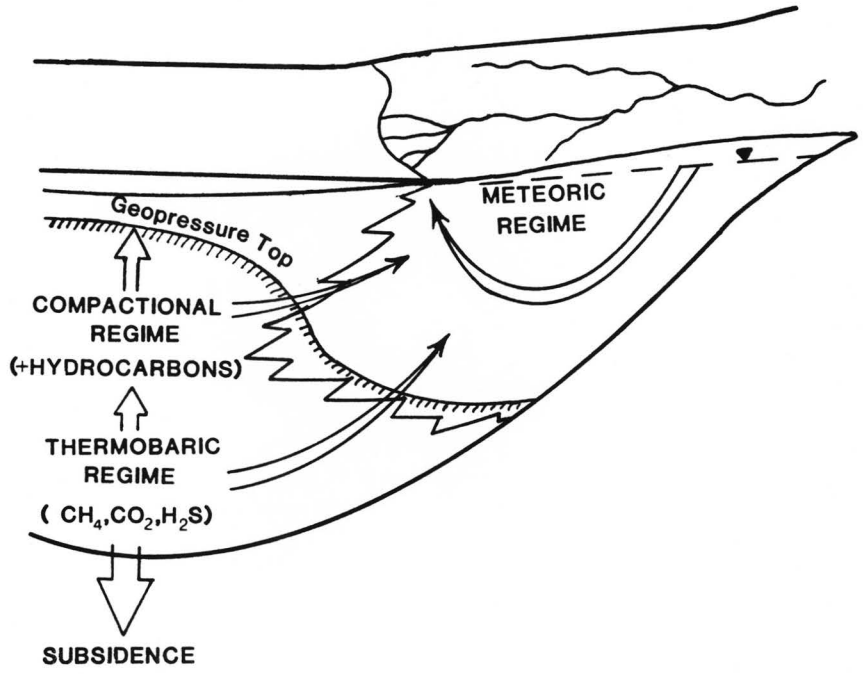


**Figure 1.4:** Generalized hydrogeologic model of a sedimentary basin (redrawn from Galloway and Hobday, 1983).

spaces become smaller and the pore fluid is expelled concommitantly. If permeability is not sufficiently high, as is the case in Gulf Coast clays and shales, the fluid becomes trapped for a time. Higher porosities may thus be maintained in the sediment, kept open by trapped pore fluids which are also subjected to greater than normal pressures. This circumstance is variously known as *overpressuring* , *excess pressuring*, or *geopressuring* and represents a compactional disequilibrium. Eventually, the trapped fluids will bleed off, the sediments will compact, and equilibrium will be reestablished, unless the pressuring processes are continued (Gibson, 1956; Magara, 1976; Sharp, 1976; Sharp and Domenico, 1976; and Keith and Rimstidt, 1985). Other mechanisms have been proposed as contributing to excess pressuring, including aquathermal pressuring (Barker, 1972), mineral phase transformations such as clay dehydration(Burst, 1969; Weaver & Beck, 1971; Bruce, 1984), and hydrocarbon maturation (Hedberg, 1980).

Much of the Gulf Coast Basin is overpressured. The hachured line in Figure 1.2 indicates the top of overpressure derived from mud weights. Figure 1.5 shows generalized plots of fluid pressure versus depth for the Gulf Coast, depicting inflection points where pressure deviates from the normal hydrostatic condition. The sediments beneath these points are considered to be overpressured, although discontinuous zones of lesser overpressures may exist above this depth.

Thermobaric Zone. The thermobaric regime is transitional with the compactional regime and encompasses the deepest parts of the basin. This regime is defined as the zone where the temperatures and pressures

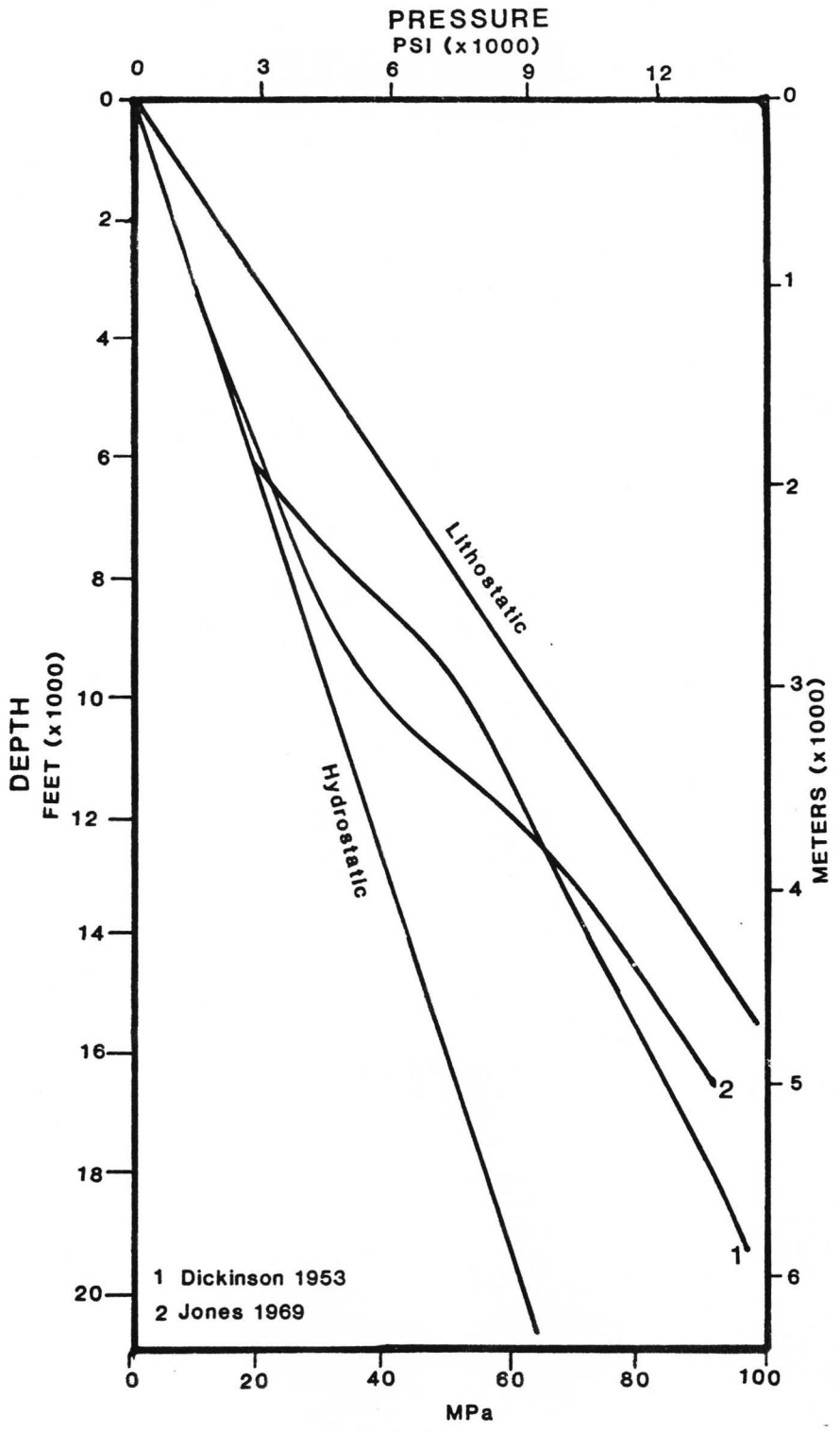


**Figure 1.5:** Generalized variation of fluid pressure versus depth in the Gulf Coast.

are great enough to cause low-grade metamorphism. The subsequent release of metamorphic fluids is presumed to be the major hydrologic process. Rocks above and/or below the Louann Salt may currently be producing water in addition to large quantities of carbon dioxide as the result of metamorphic reactions. The importance of these fluids on the hydrology of the rest of the basin is unknown because direct sampling of this portion of the basin has not yet been accomplished.

## 1.2 DATA COLLECTION AND PREPARATION

The data collected for this research consists of over 1600 bottom-hole temperatures (BHTs) from over 725 separate wells (see pocket map for locations). The BHT readings where taken off of well headers, ie., the first page of an electric log. The headers also list other information about the well including the Company that drilled it,the depths of each run, the land owner, sometimes the elevation of the well head, and its location. The logs listed in Appendix A are all from the files of the Bureau of Economic Geology (BEG), but are in the public domain and may be purchased from the appropriate well libraries. To collect them, all logs held by BEG for wells within the study area were examined. Of those, all that were readable, that included the well head elevation, and that had BHTs above 170°F were recorded. It should be noted that data for shallow measurements below 170°F were not recorded, though such measurements did exist on many logs. It was later apparent that this information would have been quite useful, but time

constraints ruled out their aquisition. Any additional research should include adding shallow measurements to the data base.

### 1.2.1 TEMPERATURE CORRECTIONS

A bottom-hole temperature is a temperature reading taken at the bottom of a well. In the case of deep oil wells, such as those used in this study, a logging tool equipped with a thermometer is lowered periodically as the hole is deepened. Thus several runs, each with a separate BHT reading, are commonly available from a deep well.

When a well is logged, the bottom-hole temperature is just one of many different types of measurements taken. Many different measuring instruments are usually lowered into the hole strung together in a pipe-like bundle known as a *sonde*. When logging, drilling operations must be halted, and the sondes are lowered into the hole without removing the drilling mud. There are many sources of error that are introduced when taking the bottom-hole temperature, mostly linked to temperature equilibration problems. When drilling, the drilling mud which fills the hole and surrounds the drill stem is circulated to remove the drilling debris and to keep the drill bit cool. As a consequence, the rocks surrounding the hole are also cooled. When logging, mud circulation is halted, but the time elapsed between halted circulation and temperature measurement is usually not enough for the bottom-hole temperature to reequilibrate with the actual temperature of the rock at that depth. Of course, it would be useful to record this elapsed time so that some estimate of the degree of equilibration could be made, but

unfortunately this is seldom included on the well log. It is clear, however, that some sort of correction is needed for the BHT reading.

The correction scheme adopted for these data is that of Kehle (1971), an empirical correction determined by comparing equilibrium and well-log bottom-hole temperatures from 602 selected West Texas and Louisiana wells. The apparent temperature from well-log BHTs was subtracted from the temperature obtained using equilibrium BHTs and the difference was plotted as a function of depth. A polynomial was fitted to these data using a least square error criterion, resulting in the correction curve shown in Appendix B.

### 1.2.2 CREATING THE COMPUTER FILE

In order to use the data in computer applications, a computer data file was created. The file was first loaded with well identification numbers and corresponding location coordinates. This was done using a digitizing tablet and BEG software. The well maps were placed on the digitizing tablet, and the well positions were recorded by manually positioning a cursor over the selected wells. An arbitrary numbering system was used to keep track of each well, and a notebook was used to record all the corresponding log information. When all the wells were digitized, the elevation, temperature, and depth readings recorded in the notebook were free-formatted into the file from a terminal, one computer line per well. The completed file contained over 725 lines, each line containing one well's identification number, location coordinates, multiple BHT and depth readings, and its elevation.

### 1.2.3 MANIPULATING THE FILE

Once the raw data was entered into the file, a program was written to calculate the Kehle temperature corrections for each paired BHT and depth reading. The program created a new file which contained the corrected temperatures in a formatted form. Appendix B shows the correction scheme.

In order to produce isothermal surfaces, the depth data had to be converted to a depth relative to sea-level, and interpolated or extrapolated to arbitrarily chosen temperatures. I choose 50°F increments from 200°F to 400°F. A program was written to produce files for each isothermal surface from the main data file. Since the thermal trends which were being investigated were assumed to vary with depth, it was essential to limit the amount of interpolation or extrapolation to a fairly narrow temperature range. The program thus requires the user to specify a temperature range limit. If a well has no BHT values within the specified temperature range of that isotherm, then that well is disregarded. If there is a value within the range, than the depth to the isotherm is either interpolated between it and the next closest temperature/depth pair that the isotherm value straddles, or , if there are no other values, the data is extrapolated to the isotherm. The range was set at 30°F for the 200,250, and 300°F isotherms, and was 50°F for the 350 and 400°F isotherms, for which data are more scarce. Appendix C shows the FORTRAN program used to create the isothermal data files.

Data scatter had to be eliminated to contour isotherms. This was accomplished by the geostatistical technique of kriging. The kriging process smooths the data by analyzing the variation in the data and weighting each data point accordingly. The technique also provides a determination of the accuracy of the contoured surface by supplying standard deviations at gridded intervals. Appendix D provides extensive information on the procedures for kriging.

Finally, to produce contour maps and three-dimensional drawings, Radian Corporation's CPS1 graphics subroutines were employed. Appendix E briefly covers the use of CPS1, which is sophisticated and cumbersome. Large amounts of computer and personal time were consumed before the figures presented in this chapter were successfully produced. The temperature profiles and linear regressions were executed in the statistics package SPSS.

## 1.3 OBSERVED THERMAL PATTERNS

The following series of twenty illustrations (Figs. 1.6-1.10, a through d) depicts the temperature patterns that were resolved from the data. These patterns are viewed from the perspective of five isotherms (200, 250, 300, 350, 400 °F). Four illustrations are shown for each isotherm: **a**, a three-dimensional representation of the surface; **b**, the corresponding contour map; **c**, the selected data; and **d**, a contour map of the standard deviations for the isothermal surface. With each succeeding temperature increment the depths increase, as one would expect. Also increasing with temperature is the prominence of a thermal

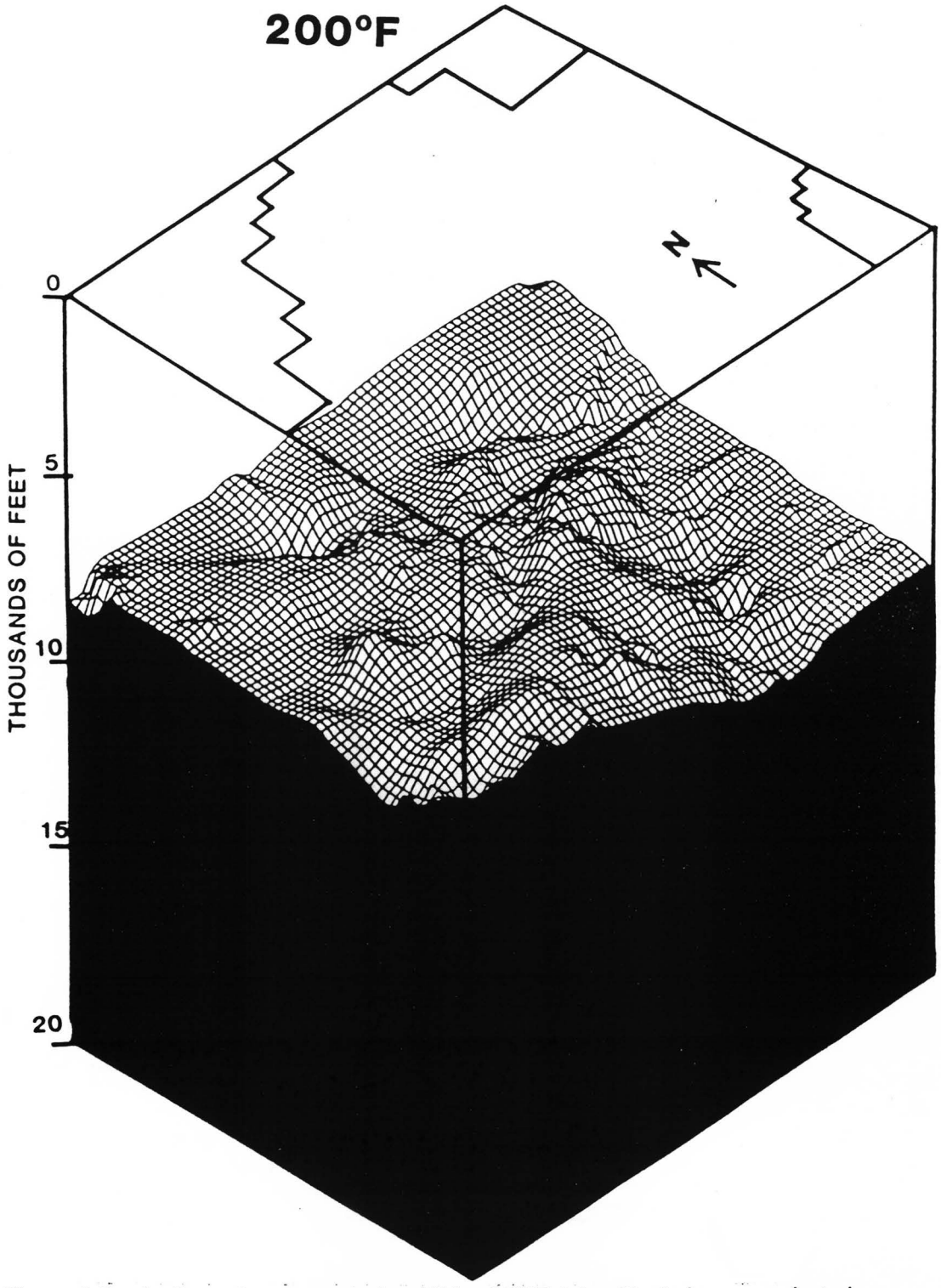


**Figure 1.6a**: Isotherm from corrected and Kriged BHT data with study area projected above.

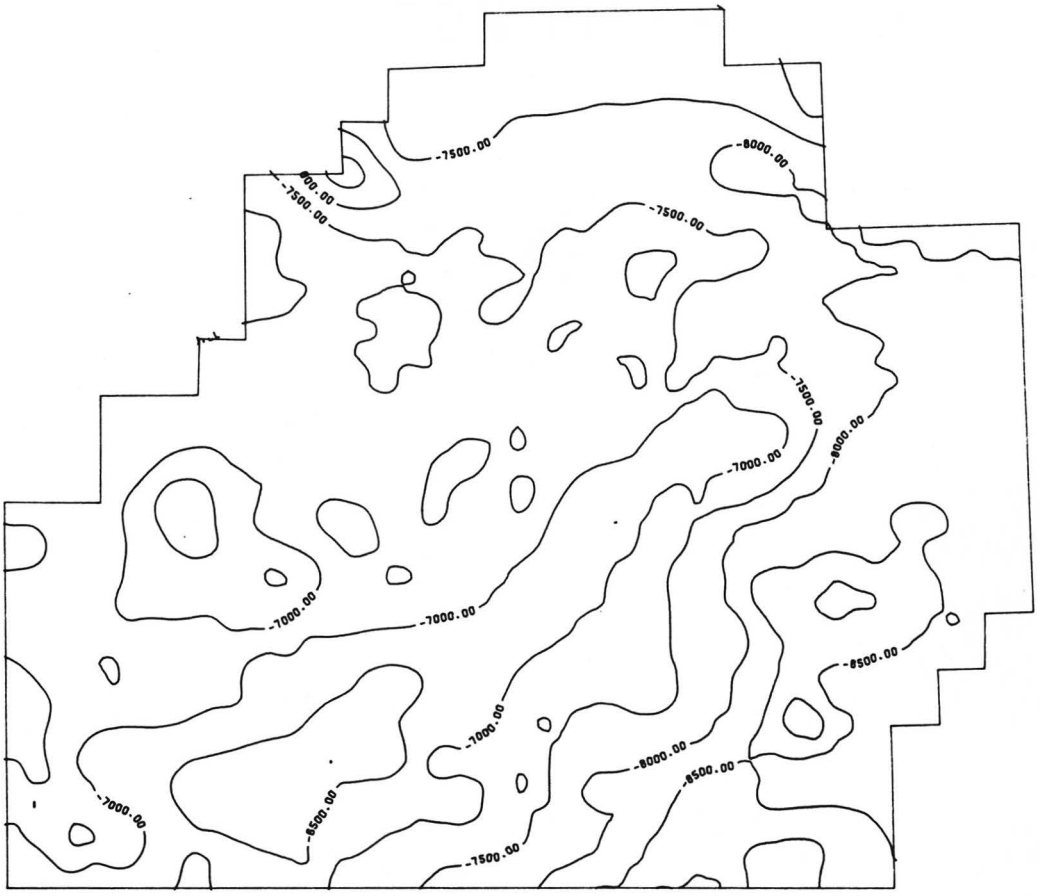


**Figure 1.6b**: Contoured 200°F isotherm within the study area.

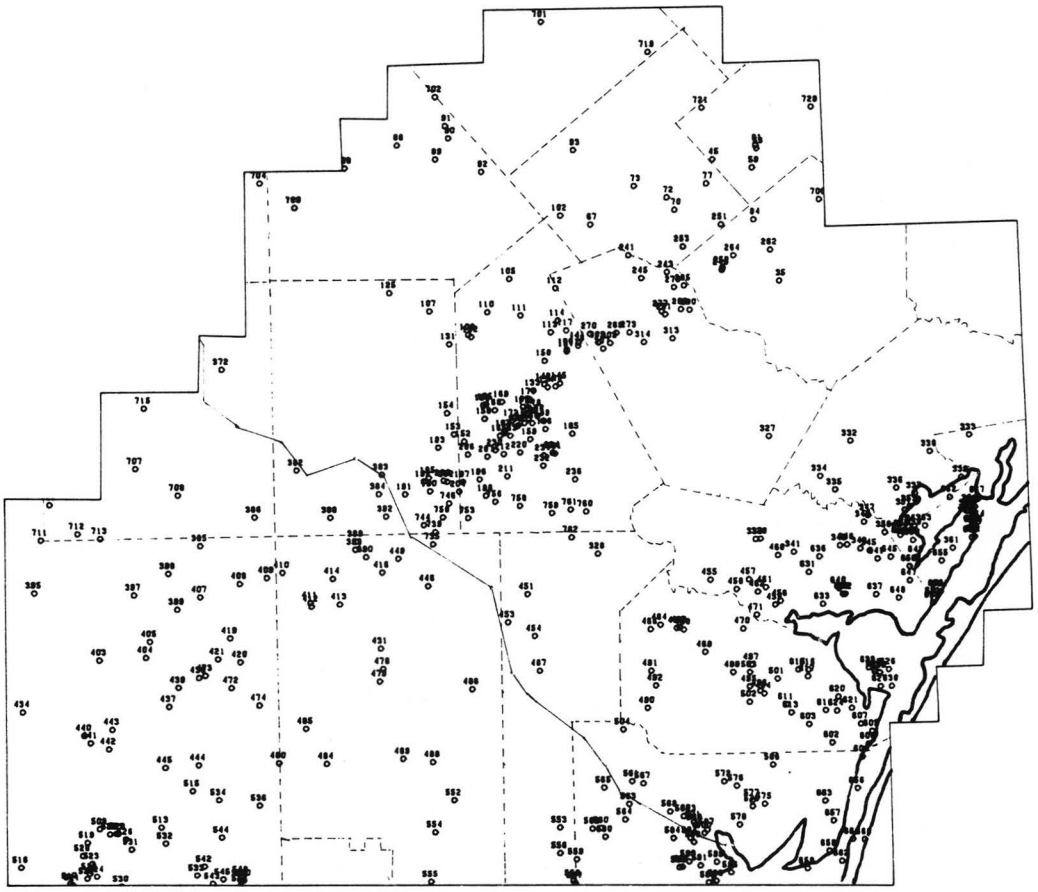

**Figure 1.6c**: Well locations for the 200°F isotherm.

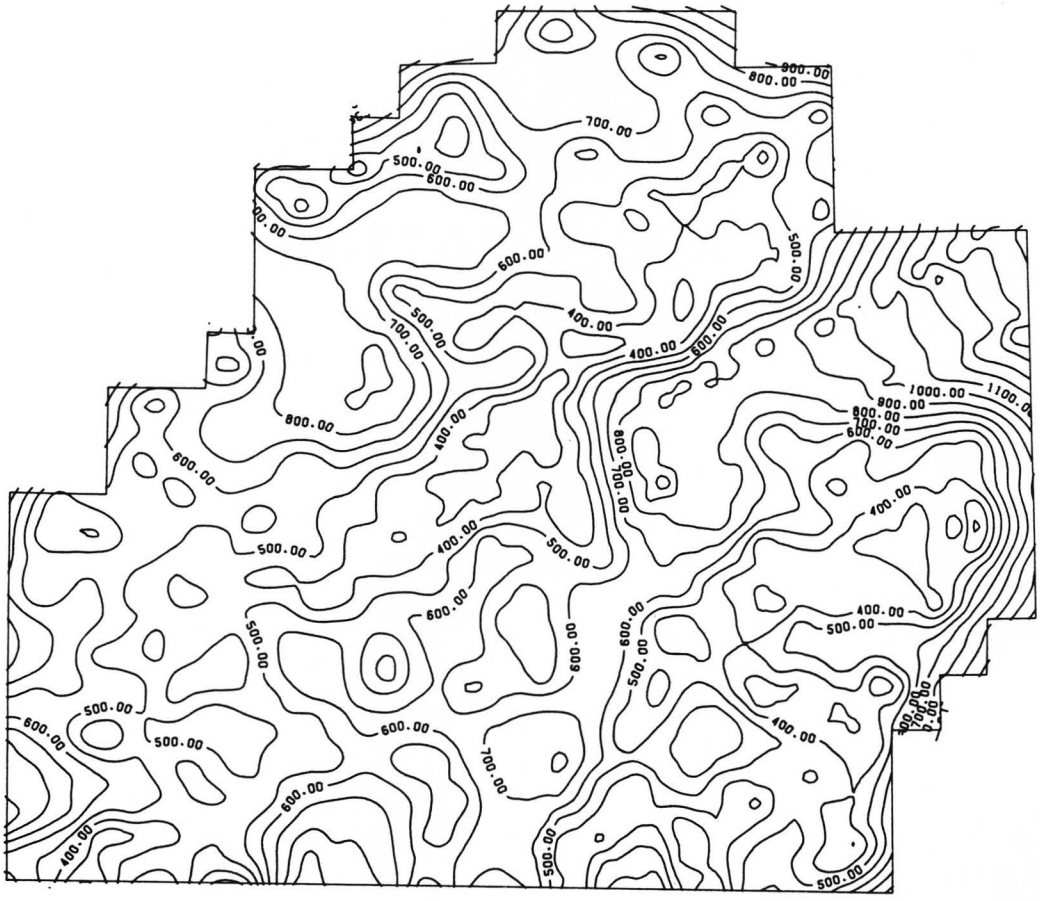


**Figure 1.6d**: Standard Deviation of contoured 200°F isotherm (computed by Kriging).

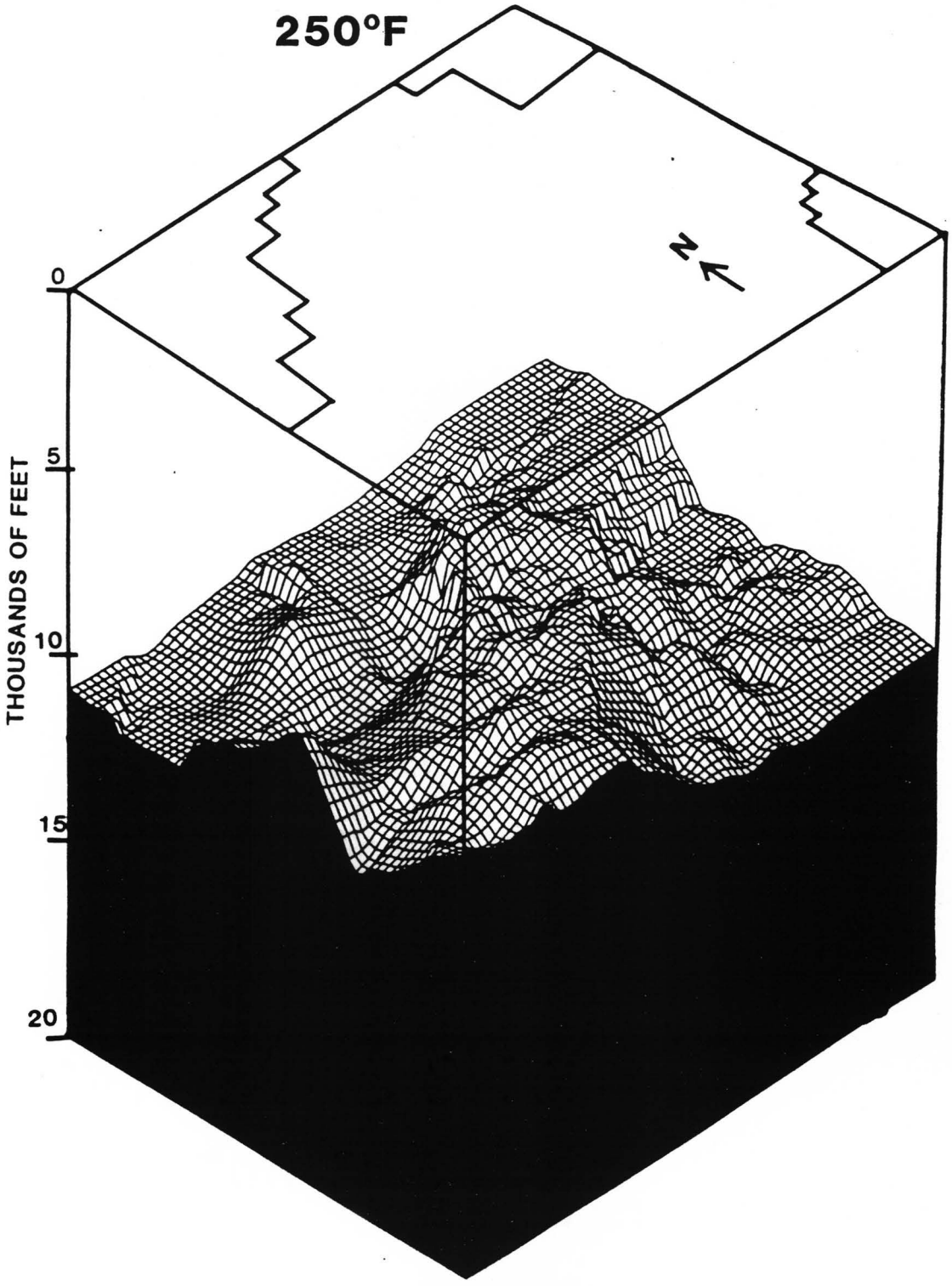


**Figure 1.7a:** Isotherm from corrected and Kriged BHT data with study area projected above.

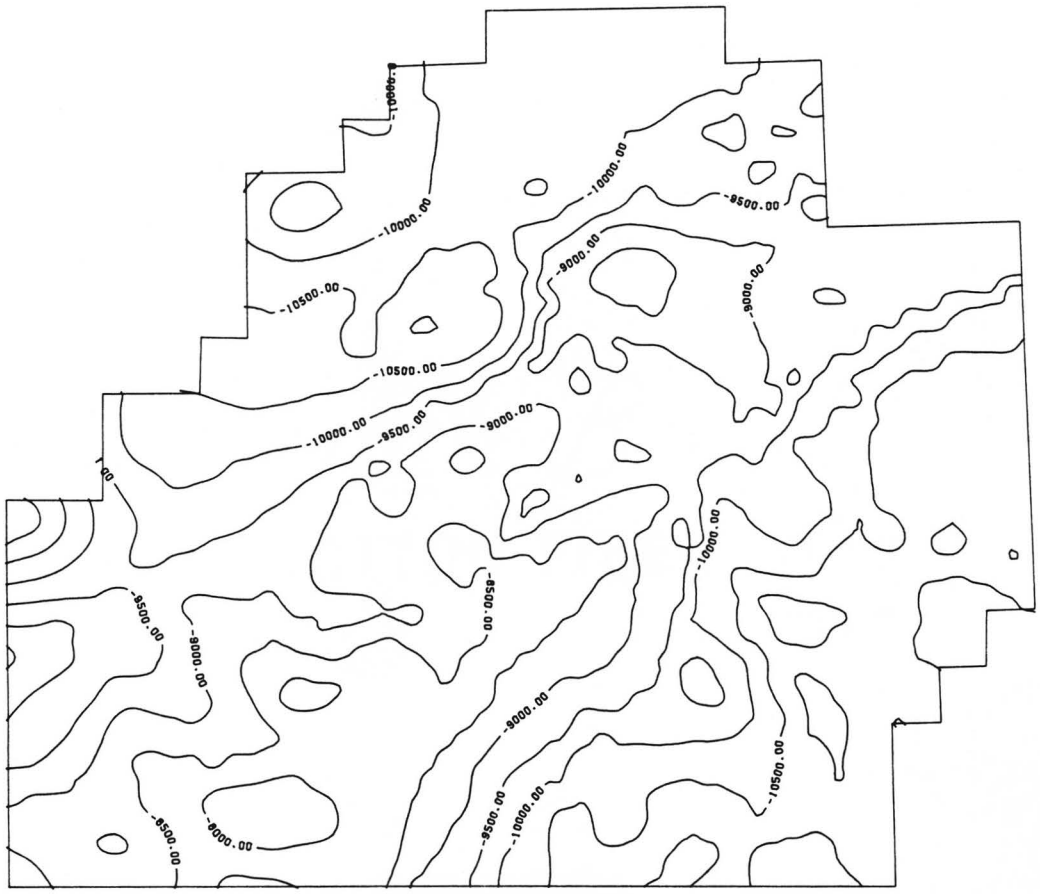


**Figure 1.7b**: Contoured 250°F isotherm within the study area.

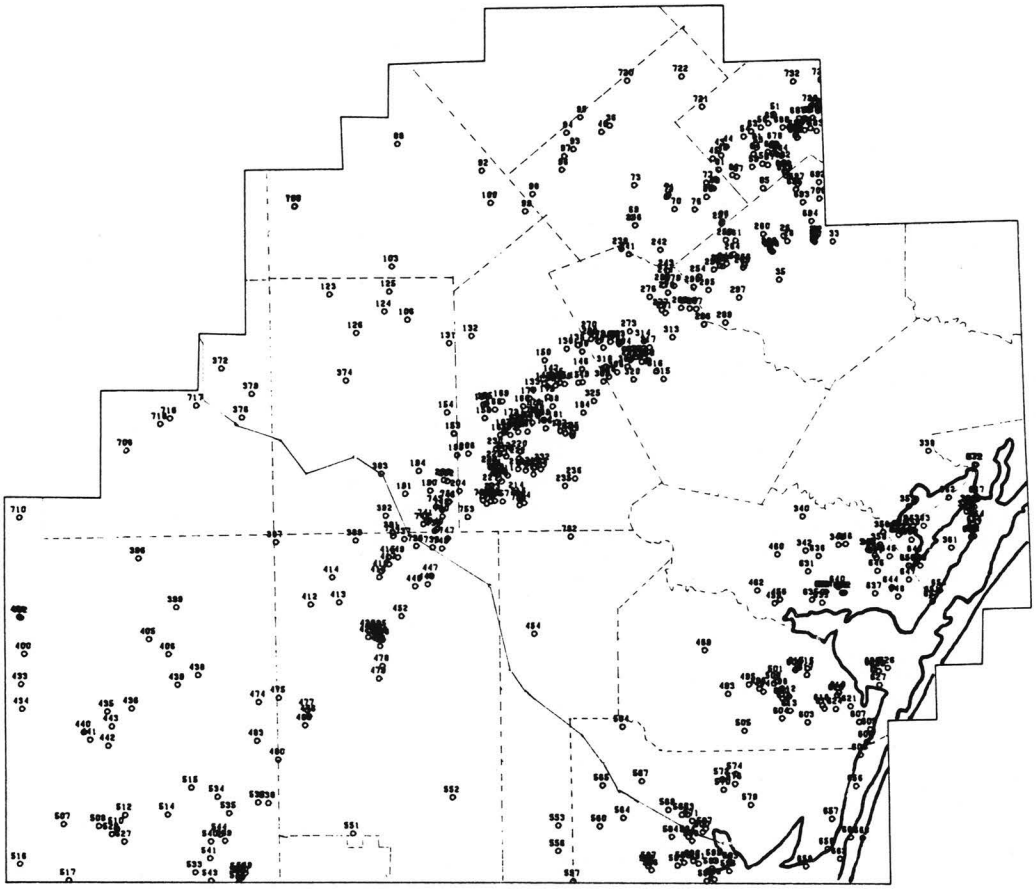

**Figure 1.7c**: Well locations for the 250°F isotherm.

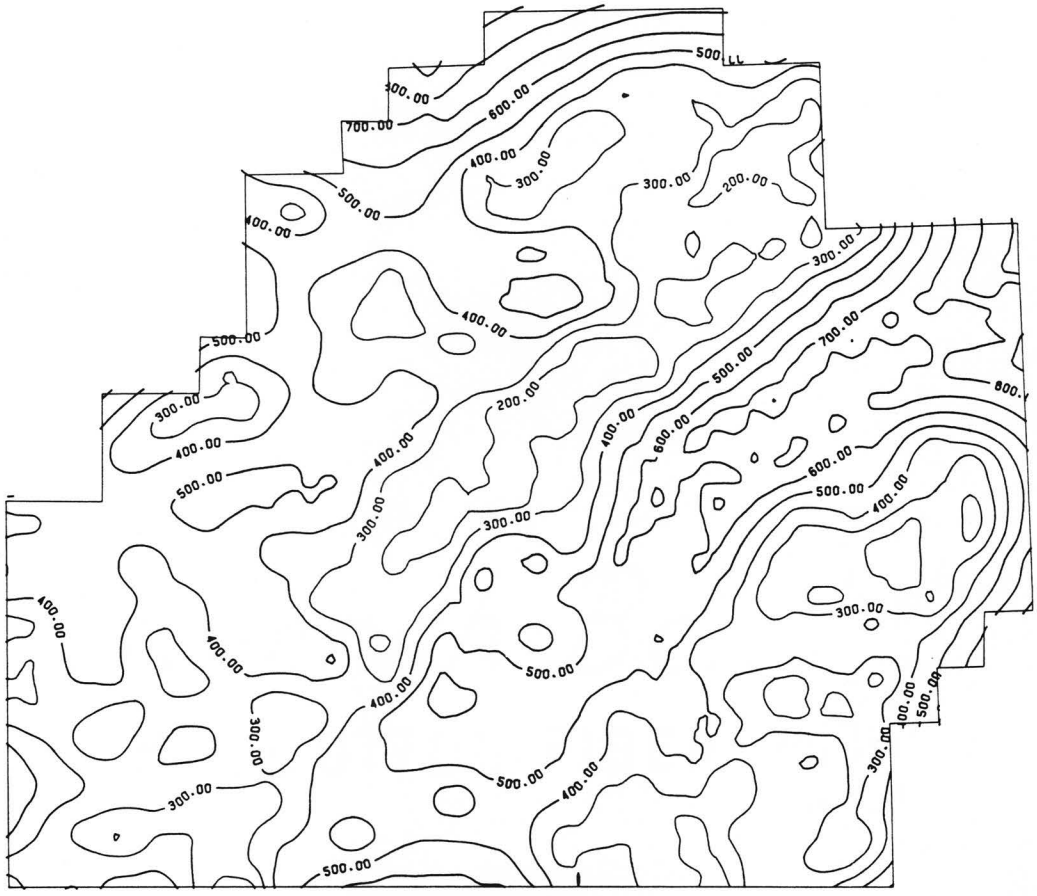


**Figure 1.7d**: Standard Deviation of contoured 250°F isotherm (computed by Kriging).

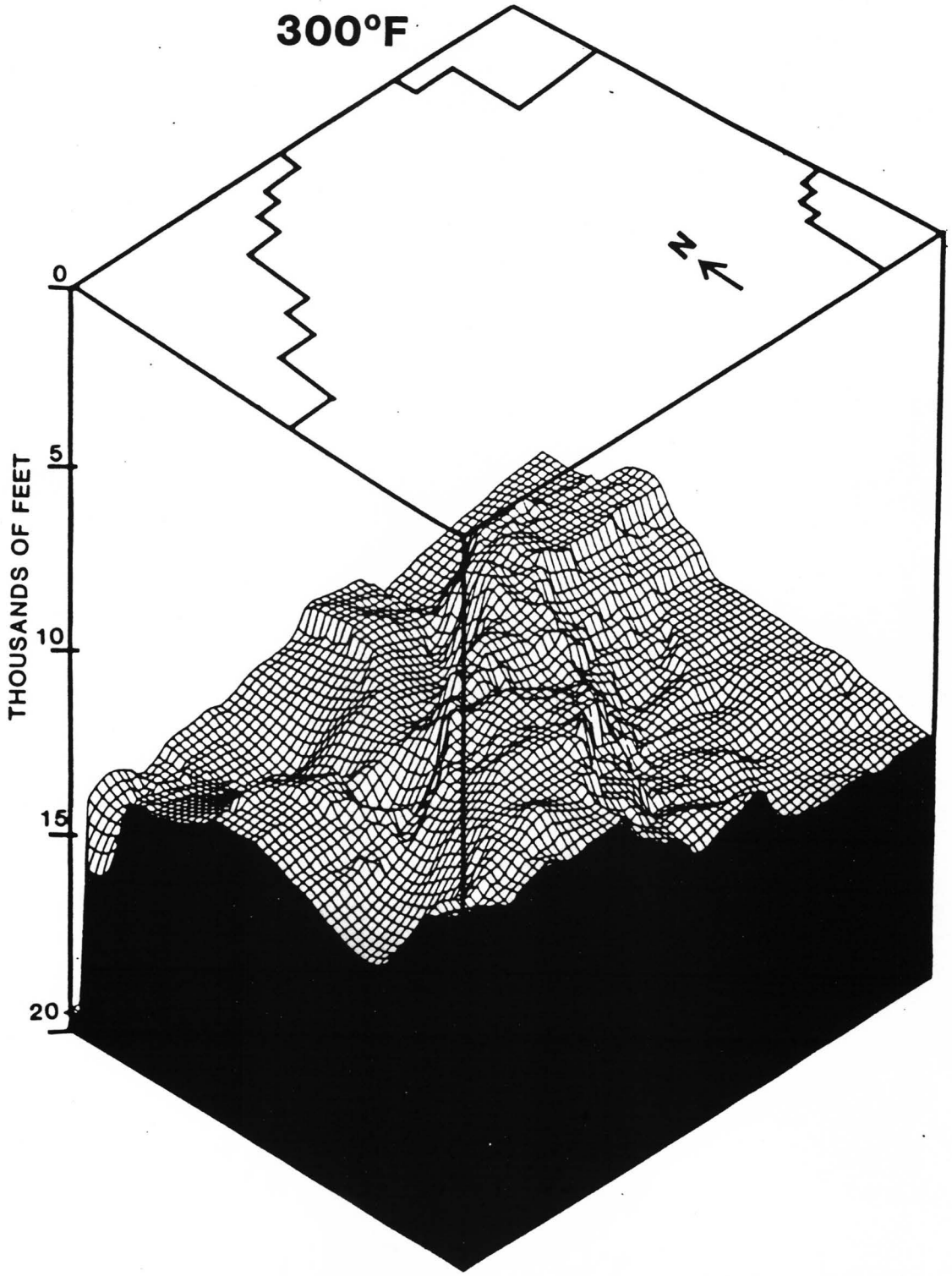


**Figure 1.8a**: Isotherm from corrected and Kriged BHT data with study area projected above.

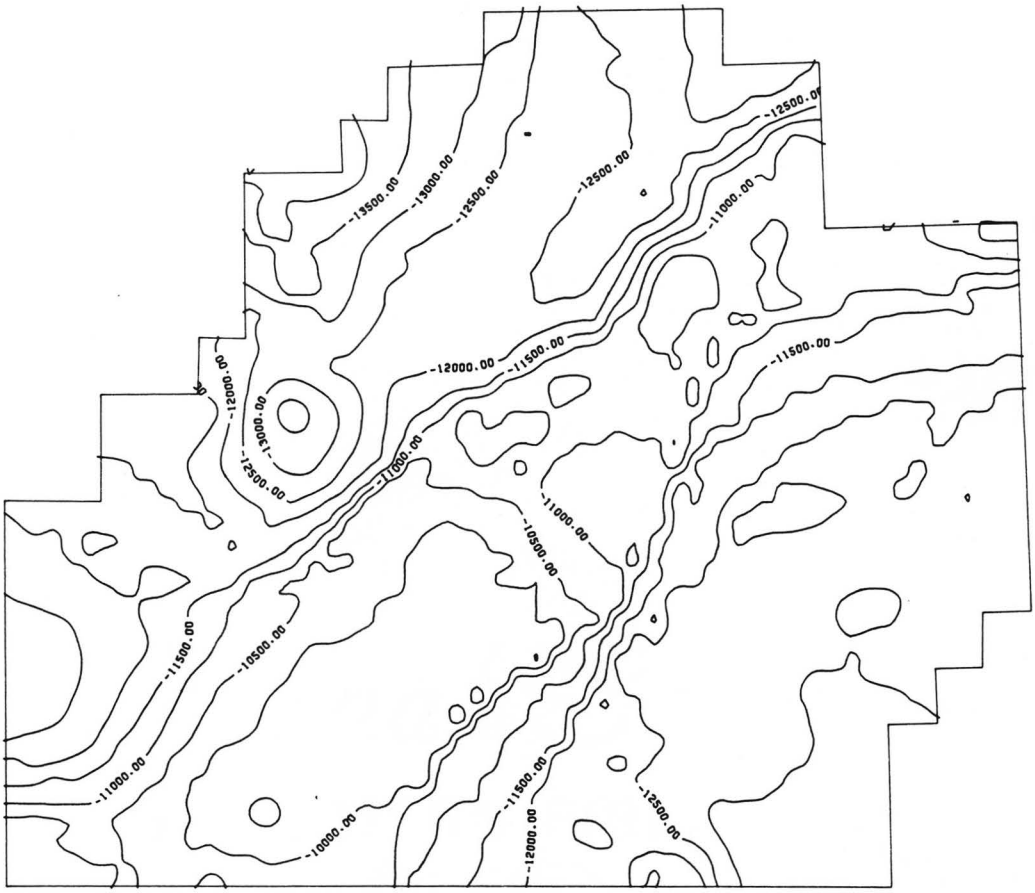


**Figure 1.8b**: Contoured 300°F isotherm within the study area.

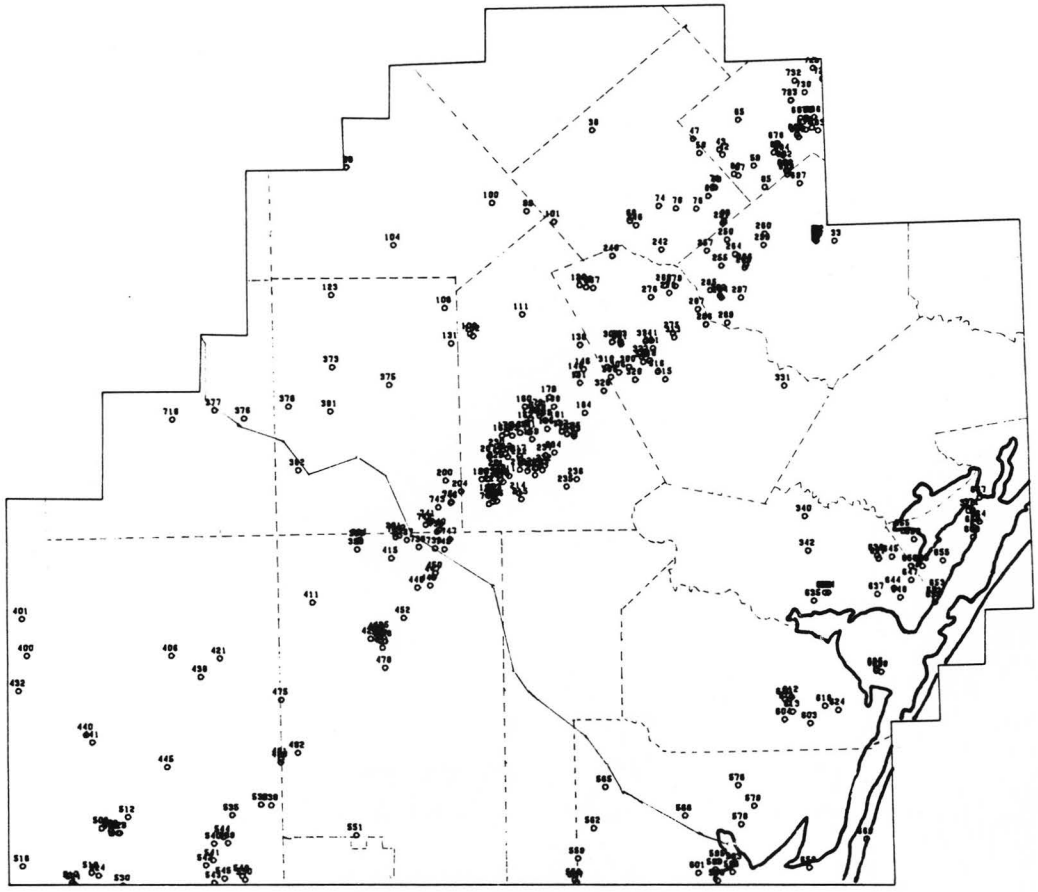

**Figure 1.8c**: Well locations for the 300°F isotherm.

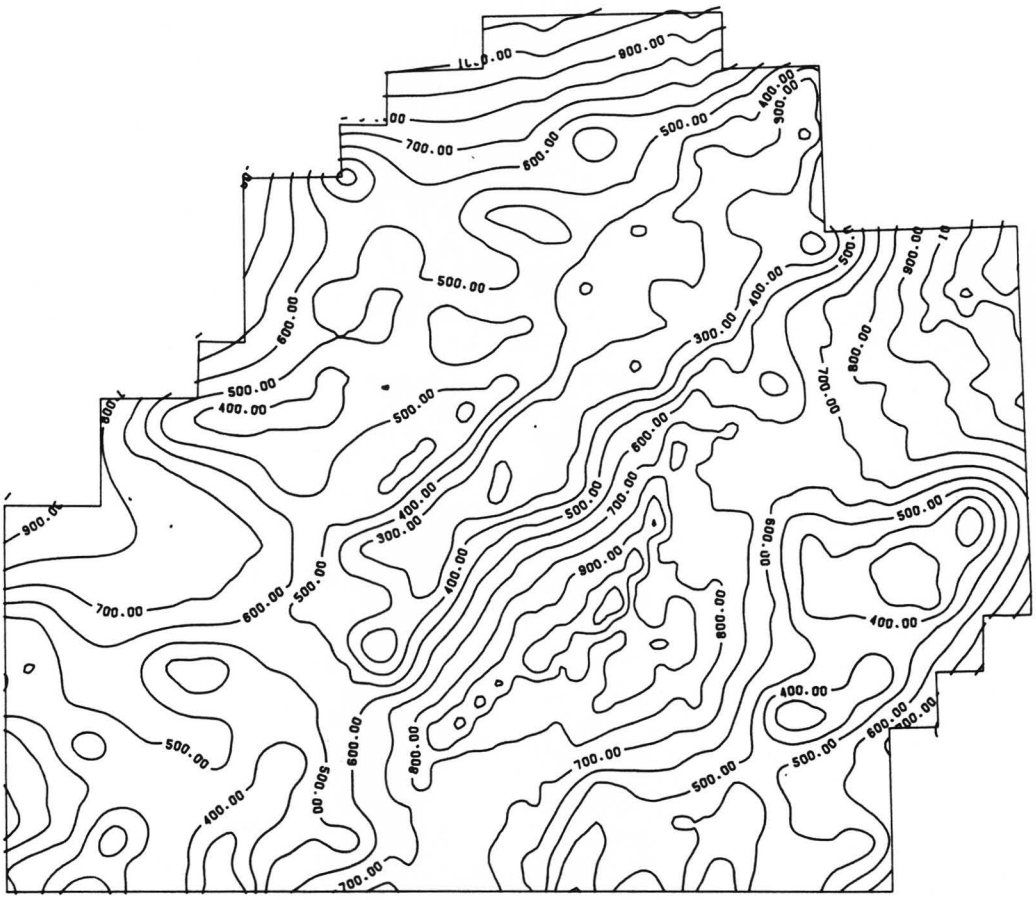


**Figure 1.8d**: Standard Deviation of contoured 300°F isotherm (computed by Kriging).

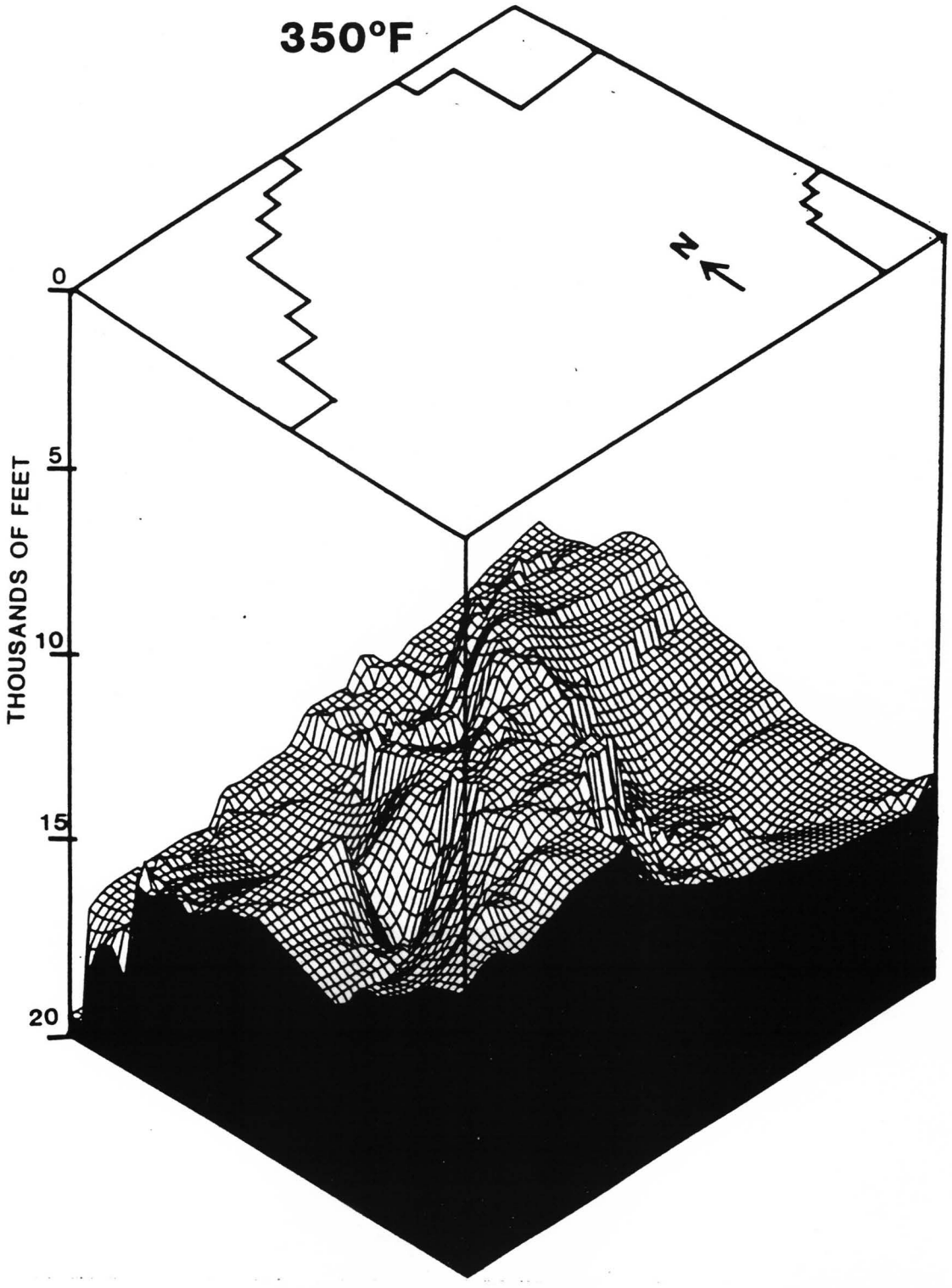


**Figure 1.9a**: Isotherm from corrected and Kriged BHT data with study area projected above.

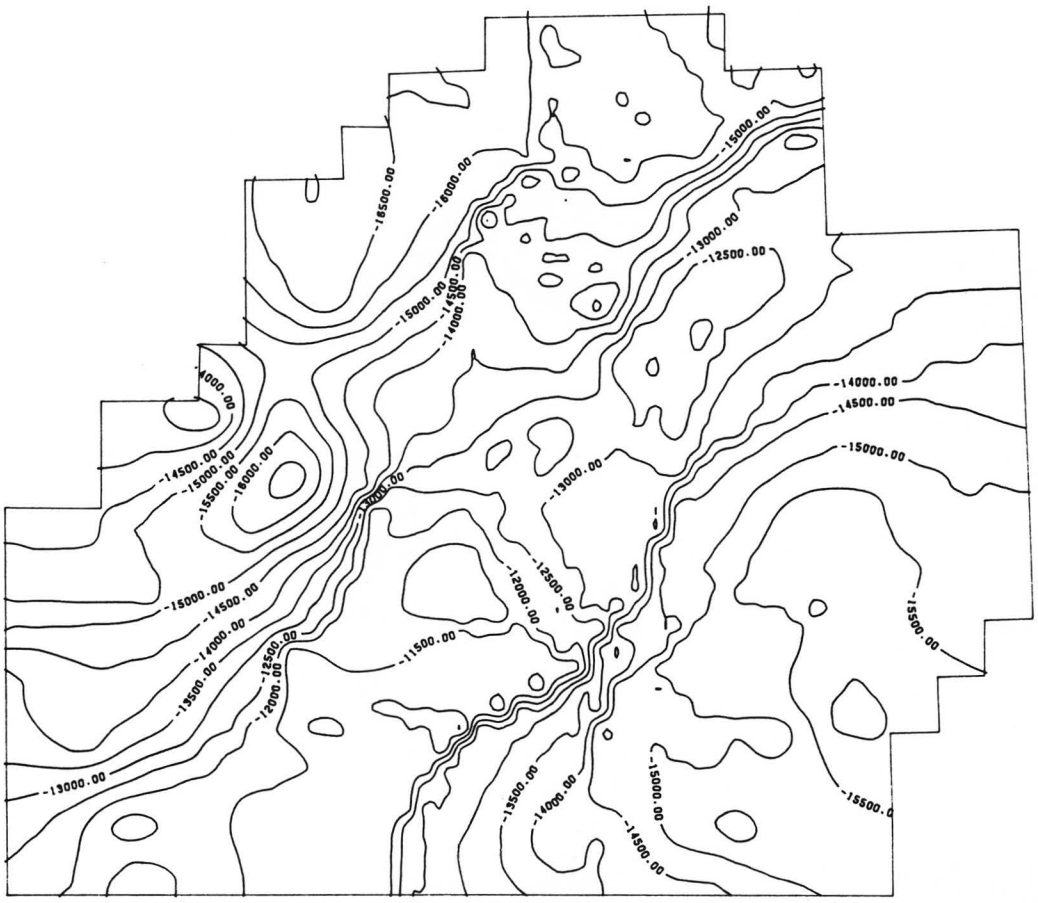


**Figure 1.9b**: Contoured 350°F isotherm within the study area.

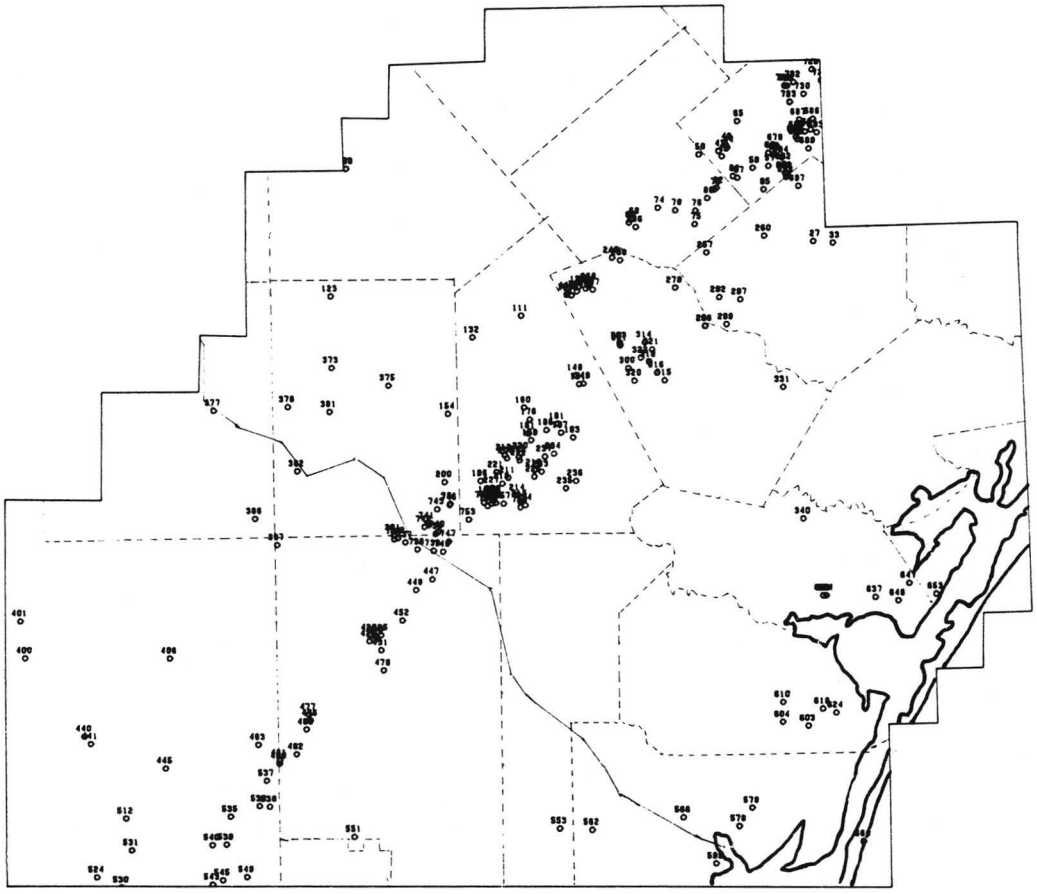

**Figure 1.9c**: Well locations for the 350°F isotherm.

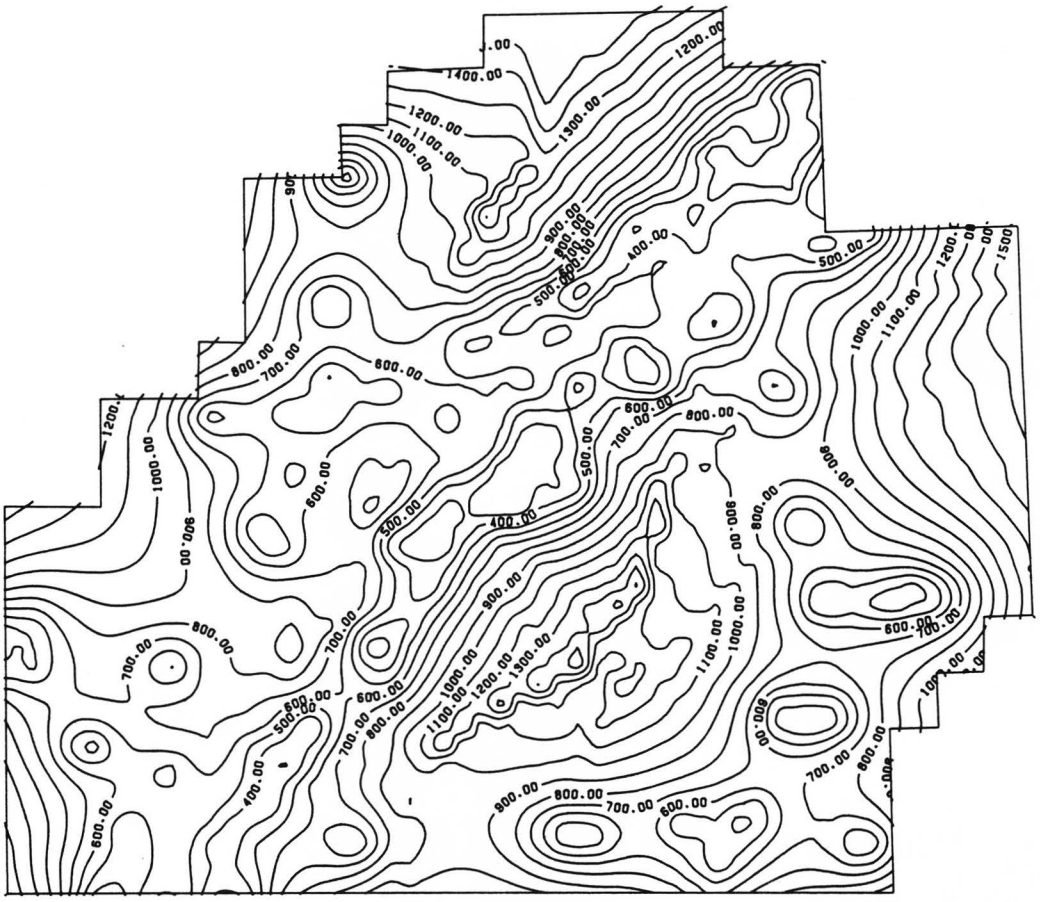


**Figure 1.9d**: Standard Deviation of contoured 350°F isotherm (computed by Kriging).

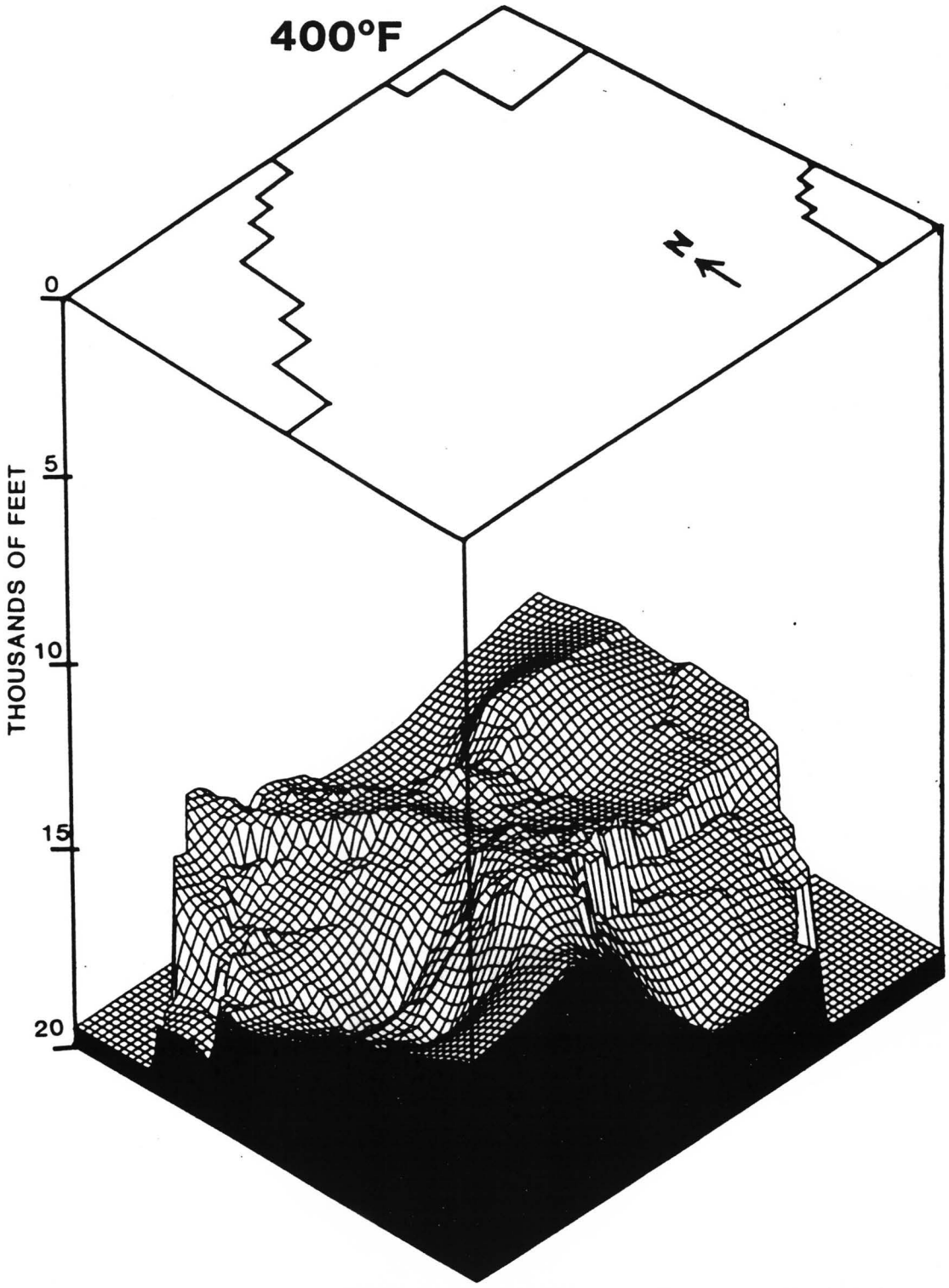


**Figure 1.10a:** Isotherm from corrected and Kriged BHT data with study area projected above.

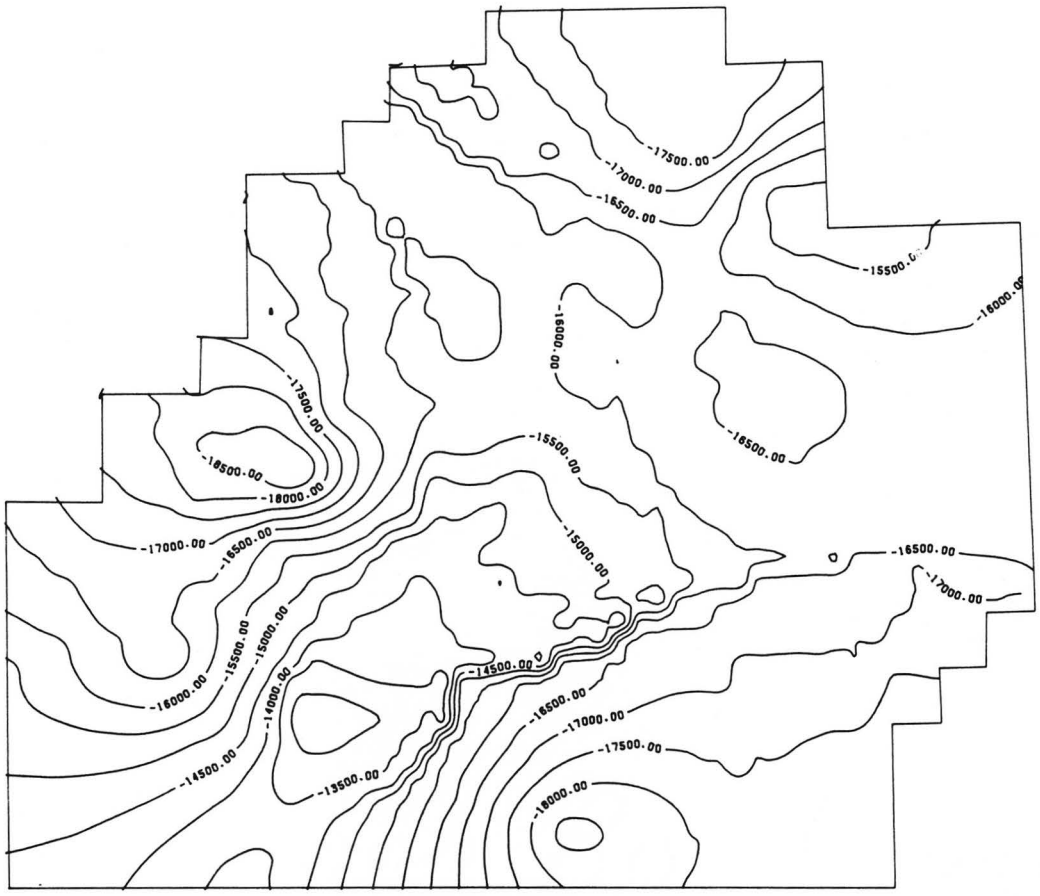


**Figure 1.10b**: Contoured 400°F isotherm within the study area.

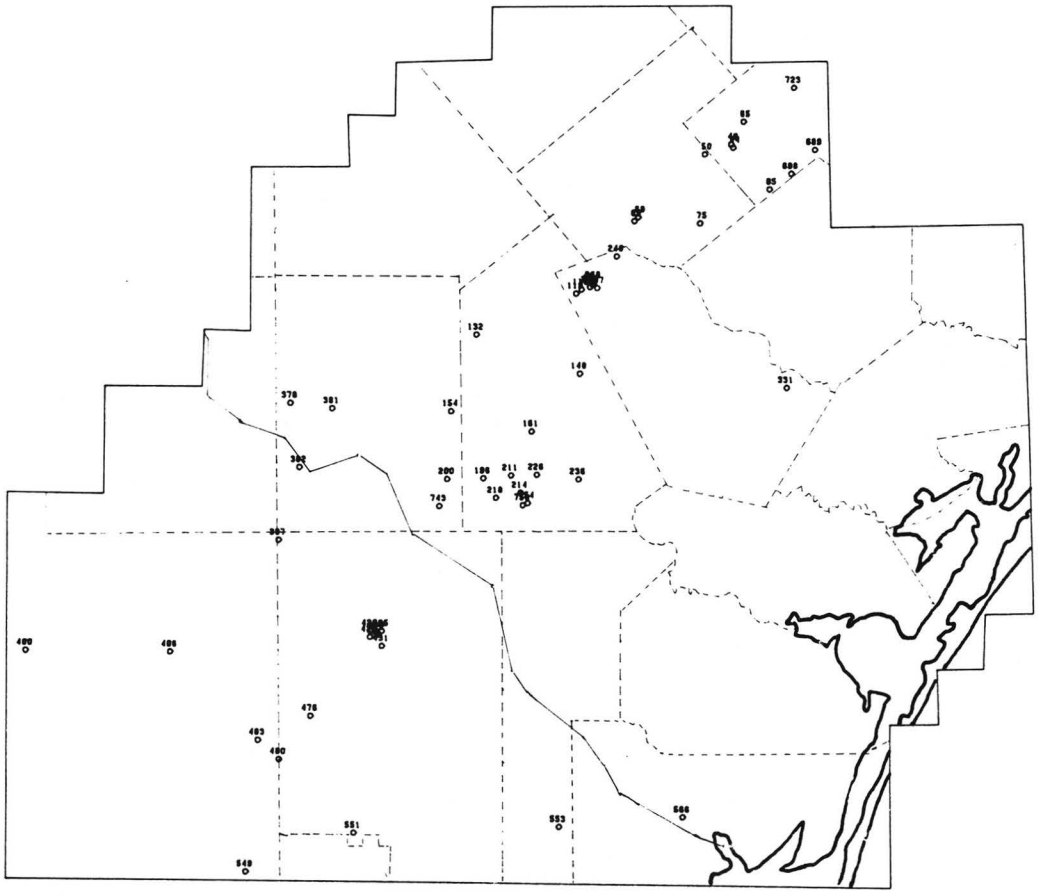

**Figure 1.10c**: Well locations for the 400°F isotherm.

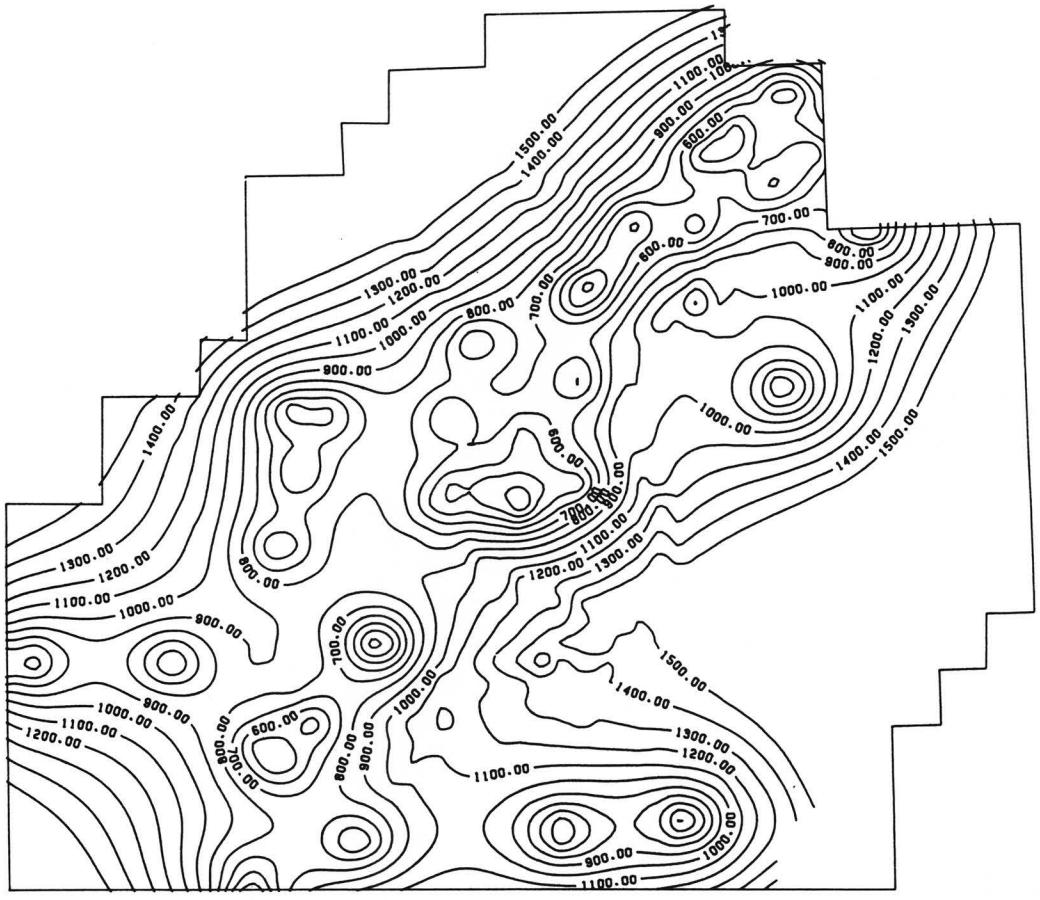


**Figure 1.10d**: Standard Deviation of contoured 400°F isotherm (computed by Kriging).

ridge trending SW subparallel to the coast. This ridge corresponds to the Wilcox growth fault zone shown in Fig 1.11. It indicates that high temperatures occur shallower near the fault zone than in the surrounding areas and that this effect begins at about 10,000 feet (3048m) and becomes more pronounced at increasing depths.

The isothermal surfaces are informative but they obscure the actual data points. Another way to observe the thermal trends is via a series of charts plotting depth versus temperature for the actual corrected BHT measurements. For this purpose, the study area was divided into 12 subareas, shown in figure 1.11. The subareas were drawn to correspond to the Wilcox growth fault trend (subareas 1 through 5), the Vicksburg/Frio growth fault trend (subareas 10, 11 and 12), and the remaining outlying areas. These temperature profiles appear in numeric order from figure 1.12 to 1.23. On this plot, the slope of a line corresponds to a thermal gradient. The steeper the slope, the lower the gradient. The dashed line on each plot indicates what is generally considered the normal earth gradient of 1.64 °F/100 Ft (30 °C/km) The + signs indicate individual corrected BHT measurements. The solid line is a linear regression for the data. The correlation coeficients among the regressions were all above .90. Fig. 1.24 summarizes all the regression lines and also tabulates the gradients represented by each regression line for each subarea. Not surprisingly, the Wilcox growth fault zone is characterized by the highest gradients, which far exceed normal gradients. Fairly high gradients are also found in the Vicksburg/Frio

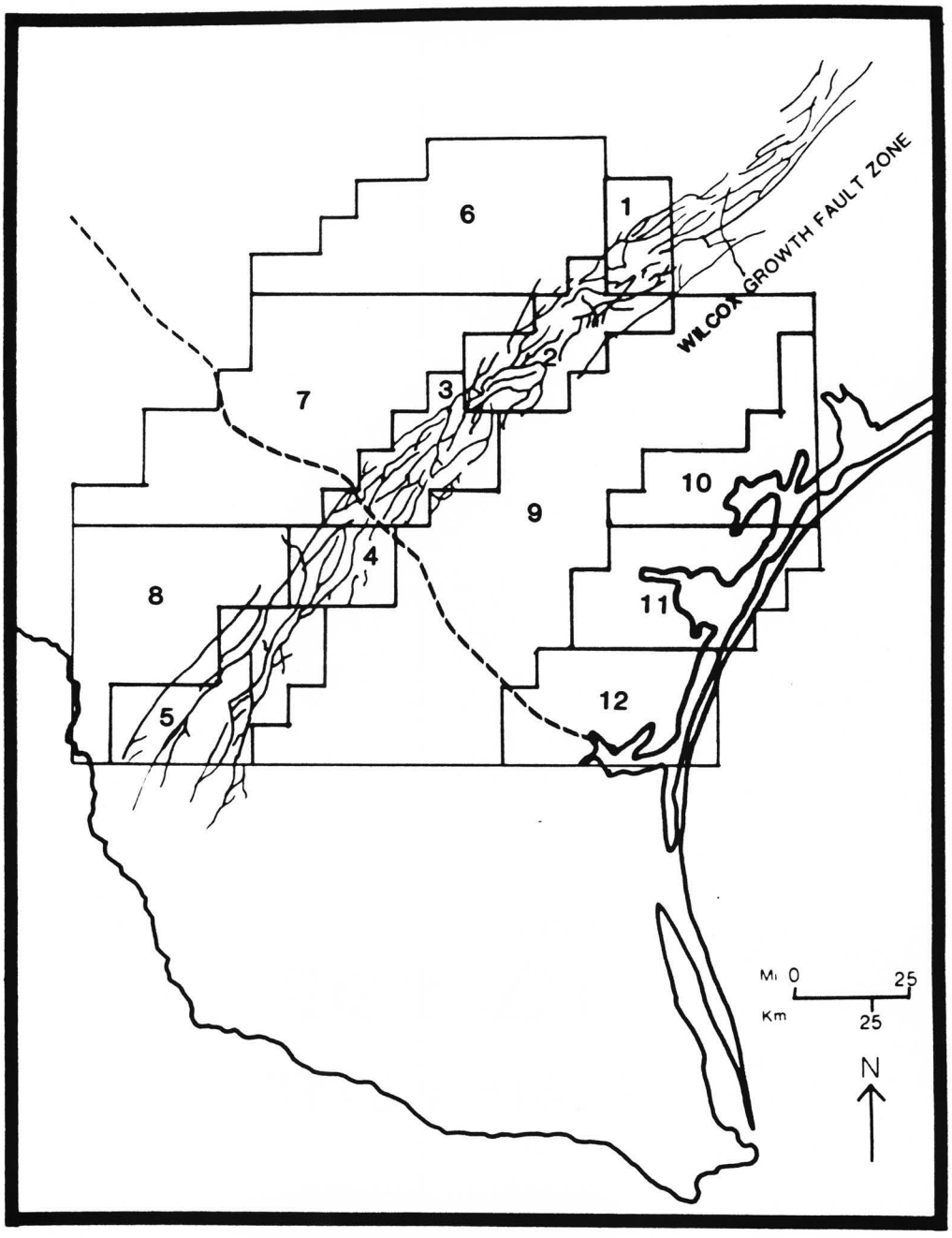


**Figure 1.11**: Study area showing the twelve subareas and the distribution of the Wilcox growth faults. Dashed line shows the location of the type cross section (Figure 1.2).

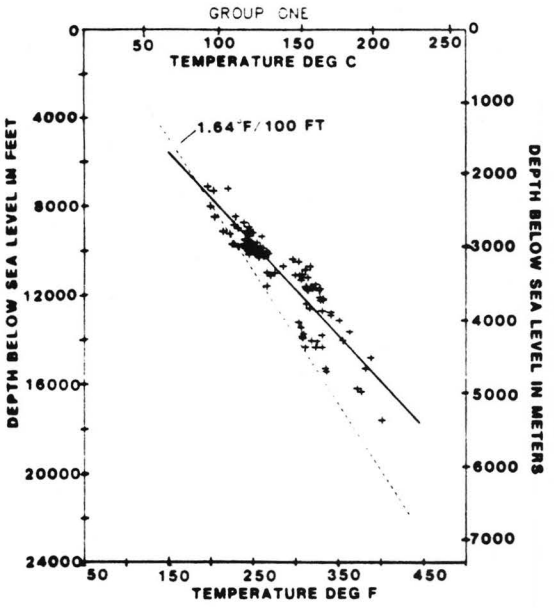


Figure 1.12

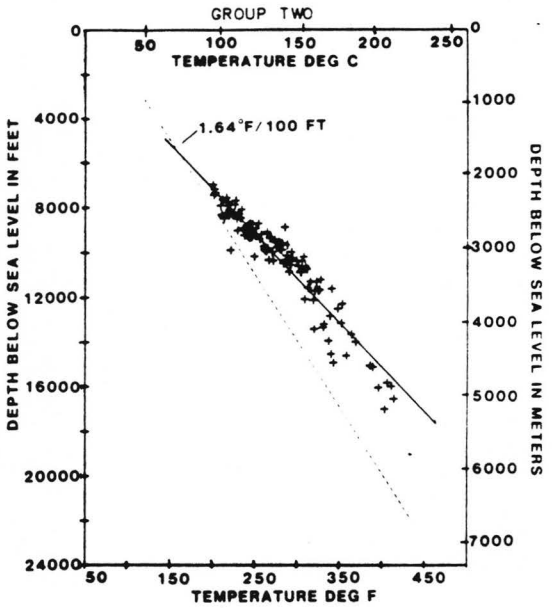


Figure 1.13

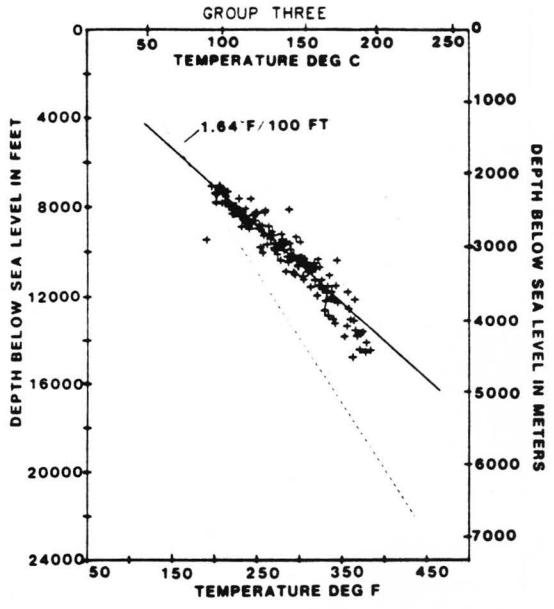


Figure 1.14

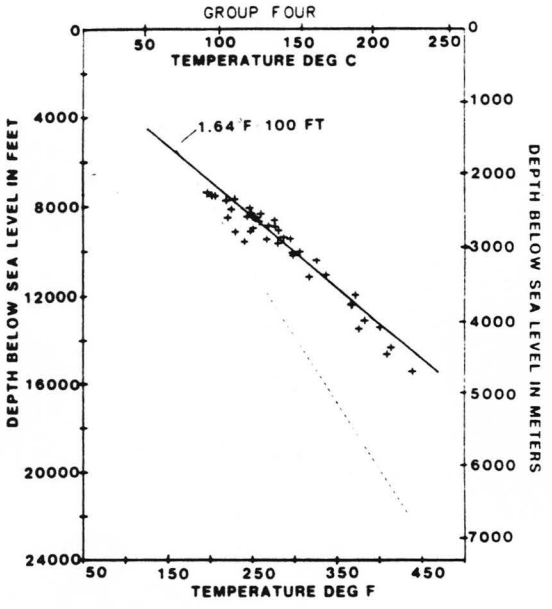


Figure 1.15

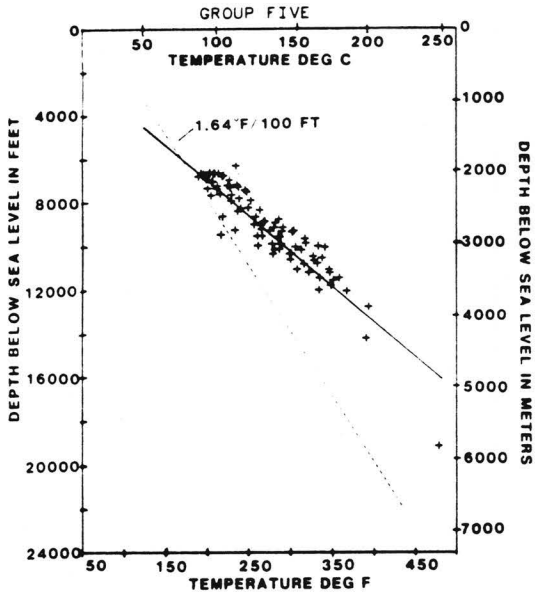


Figure 1.16

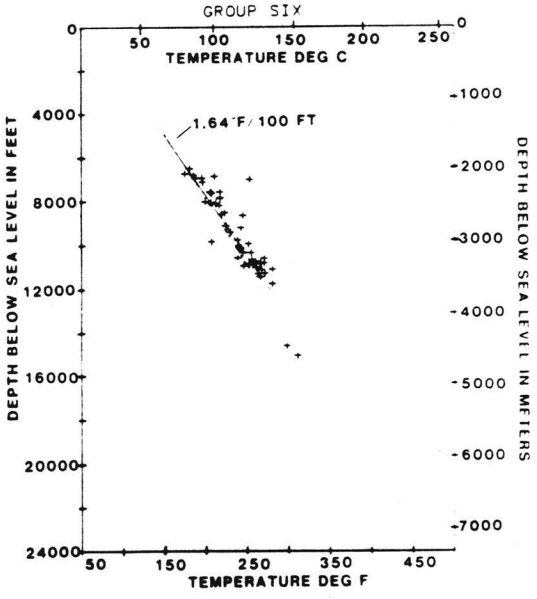


Figure 1.17

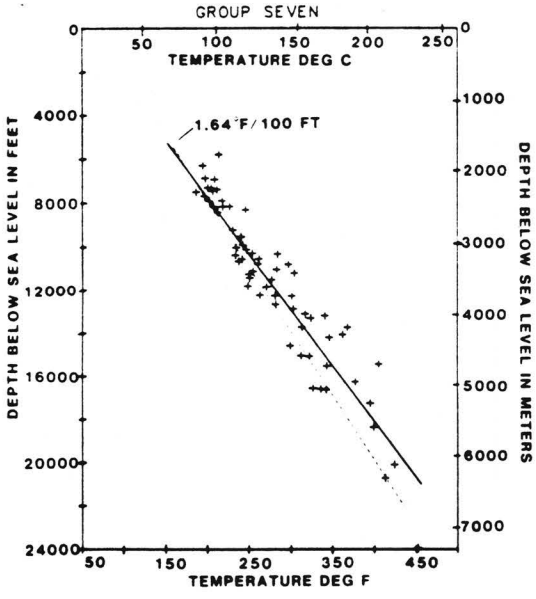


Figure 1.18

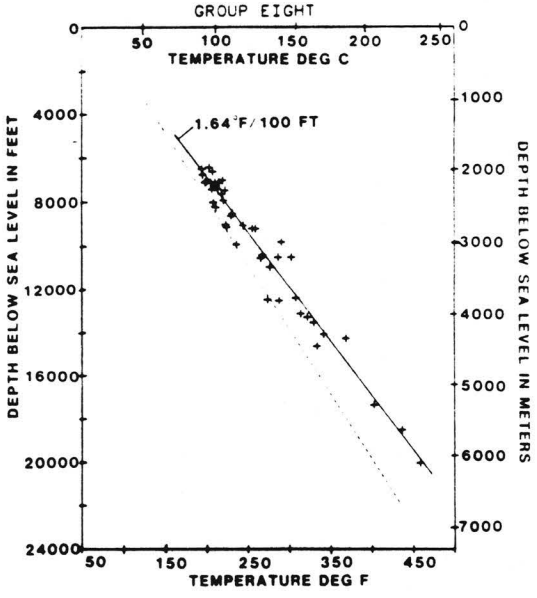


Figure 1.19

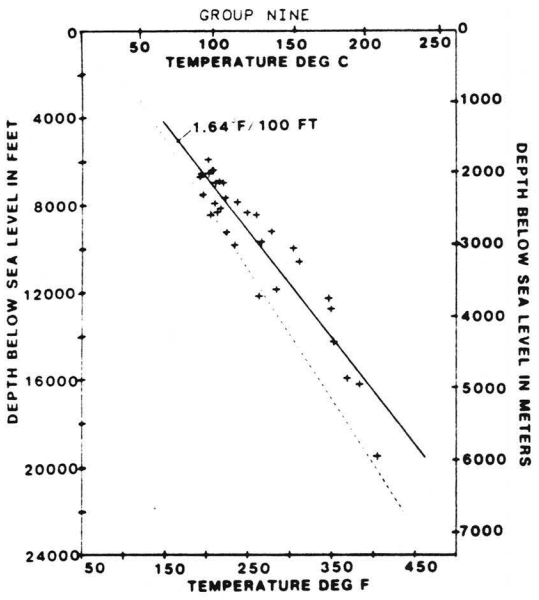


Figure 1.20

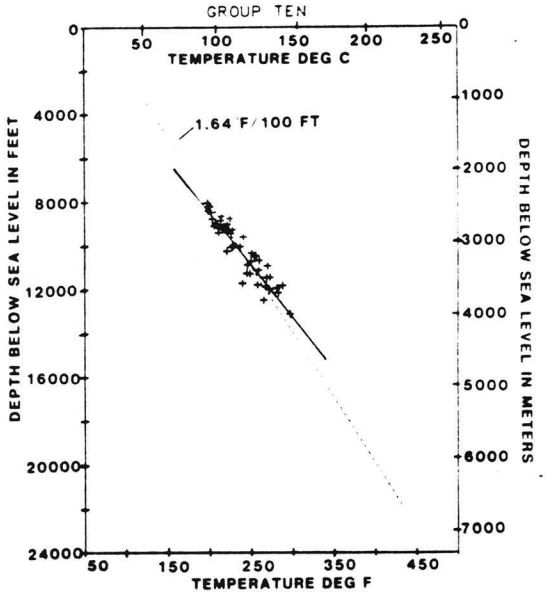


Figure 1.21

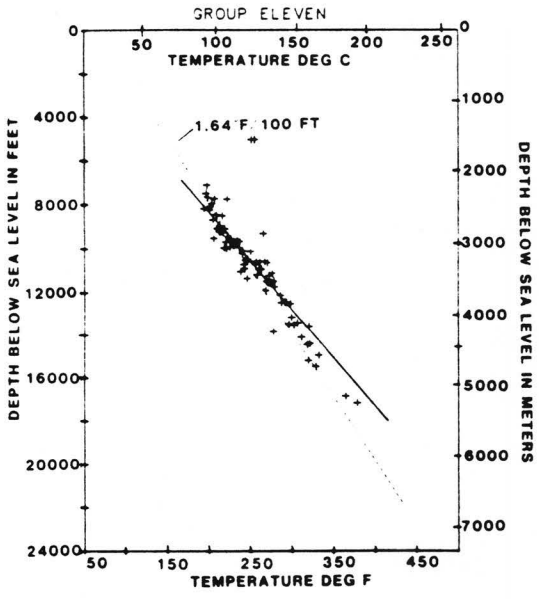


Figure 1.22

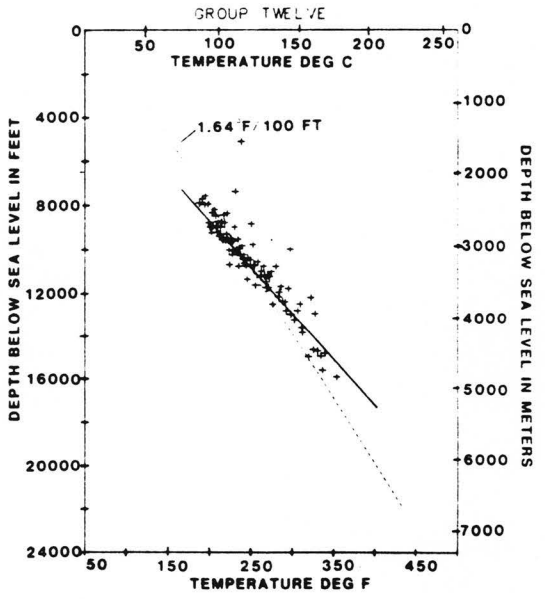


Figure 1.23

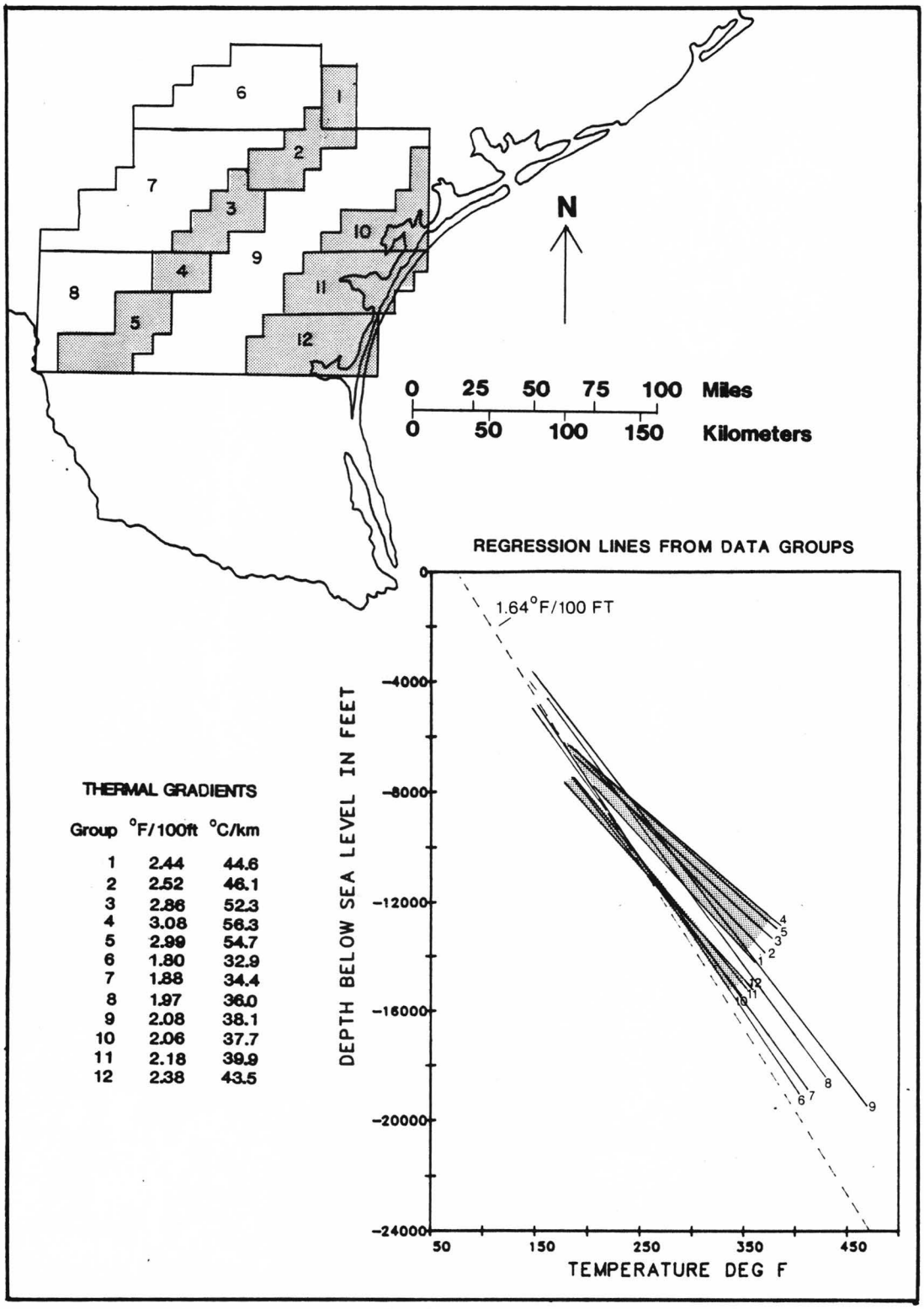


**Figure 1.24:** South Texas showing subareas where temperature data were collected and their corresponding geothermal gradients, generated by linear regression.

fault zone. The summary of regression lines also reveals a trend of higher gradients toward the southwest.

## 1.4 GROUNDWATER FLOW

One of the most frequently invoked scenarios to explain anomalously high temperatures in the Gulf Coast was first described by Lewis and Rose (1970) who called on overpressuring as a major contributing factor. The correlation between overpressuring and abrupt increases in thermal gradients is hard to deny. On the temperature profiles of figures 1.12 through 1.23 the departure of the data trend from the normal gradient (dashed line) corresponds closely with the top of geopressuring indicated by the hachured line in figure 1.2 (derived from mud weights). The Lewis and Rose model attributes this to decreased thermal conductivity of the overpressured zone (i.e., the ability of this zone to conduct heat is diminished), giving it insulating properties relative to the surrounding sediments. The decreased conductivity results from the higher porosity and consequent water content of these overpressured sediments. Water has a lower thermal conductivity than mineral grains.

This scenario is not completely consistent with the known configuration of the basin and the temperature data. Since overpressuring largely results from a compactional disequilibrium, its presence correlates to the presence of extensive marine shale bodies whose low permeability causes the disequilibrium. According to the scenario, these same areas should exhibit a temperature build up because

of their insulating characteristics, and the more extensive the shales are, the larger the thermal insulating effect should be. But, in fact, the marine shales are more extensive on either side of the Wilcox fault zone than in the zone itself, which features significant sand accumulation (see Fig. 1.2). Yet the thermal anomaly is greatest within the growth fault zone and declines sharply on either side. Increased thermal gradients are also noted in the other major growth-faulted regions, the Vicksburg and Frio zones, where marine shales are least prevalent. One must therefore conclude that simple thermal conductivity variation is not sufficient to explain the observed patterns. Furthermore, the presence of the growth faults is clearly associated with the development of high-temperature anomalies within geopressure, so that fluid movement along the faults is an attractive mechanism for heat transfer. For reasons stated in section 1.1.3, isolated regions of high basement heat flux were ruled out as a possilbe factor.

### 1.4.1 EVIDENCE FOR VERTICALLY MOVING FLUIDS

There is much circumstantial evidence that fluids move upward along growth faults. Galloway (1984) and Smith and others (1982) described evidence in Uranium deposits in the Oakville Sandstone (Miocene) for pulses of deep-basinal fluids from adjoining growth faults. Similar findings from temperature and salinity data were reported by Mumme and Ferrel (1979) for growth faults in Louisiana, and by Kingston (1985) for Oakville associated growth faults. Furthermore, the occurences of oil often suggests involvement of faults in migration.

Philippi (1965) discusses chemical evidence from shallow oil fields indicating its similarity to deep-dispersed oil, again suggesting vertical migration of fluids.

Petrographers have been confounded by the abundance of cements in Gulf Coast sediments, which imply that large volumes of water have been flushed through the system. Oxygen isotopes suggest that the fluids responsible for this cementation were from high temperature regions, as is also suggested by the presence of sphalerite (K. L. Milliken, personal communication, 1985), and sphene and laumontite (Boles, 1980; Richman and others, 1980) in minor cements. Again, the evidence points toward fluids upwelling from great depths.

Therefore it is not unreasonable that growth faults could act as conduits for upwelling fluids. The result of fluid movement of this type would be transport of heat from the compactional or thermobaric zones toward the surface. This could cause a thermal ridge like the one associated with the Wilcox growth faults. If so, the temperatures observed in this zone suggest that flow is occurring at depths even greater than 20,000 feet (6096 m), steadily diminishing to10,000 feet (3048 m). This is indicated by the initial prominence and steady dissipation of the thermal ridge through this depth range.

A similar, albeit more subdued pattern is evident in the temperature profiles from the Vicksburg/Frio fault trend. The above-average gradients occur at greater depths because the geopressure system is likewise deeper. The lithology in the Vicksburg/Frio trend is more complex than in the Wilcox trend, and its flow regime may

therefore involve more than the simple vertical flow proposed for the Wilcox growth faults. For example, free convection has been proposed for the extensive normally pressured sand packages in the Frio (Blanchard and Sharp, 1985; Bodner and others, 1985). Free convection would cause temperatures to exceed normal values at the top of the convection cell, while causing below normal temperatures at its base. Hence the low temperatures near the top of geopressuring which are indicated in the temperature profiles 1.21-1.23 may result from the lower portion of a convection cell. The mechanism of the moving boundary effect (Sharp and Domenico, 1976) could also be invoked. When sediment accumlations are sufficiently rapid, deposited material remains cool relative to its burial depth unitl it can thermally equilibrate. The low temperatues near the top of geopressuring could be explained in this way. Without the shallow temperature data, possible flow mechanisms in this region are conjectural.

It should be noted that free-convection may also be occuring on a regional scale in the basin. Petrologists and sedimentary geochemists have estimated that large volumes of water are needed to account for the volume of cements in the basin ( Bjorlykke, 1983; Wood and Hewett, 1982; Land and Dutton, 1979; Sibley and Blatt, 1976). The flow volumes indicated are so large that the recirculation of basinal fluids is the only reasonable means by which they can be supplied. Convection cells might integrate growth faults in their circulation, which presumably would be

confined to the compactional system since fluids could not freely convect downward across the geopressure transition.

### 1.4.2 REGIONAL TRENDS

An interesting trend is observable in figure 1.24. The summary of regression lines from each subarea shows a strong relationship between geothermal gradient and proximity to the Mexican border. The further southwest the subarea is located, the higher its geothermal gradient tends to be. This is observed in regressions lines 1-5, 6-7,and 10-12. The explanation for this phenomena is unknown. A possible cause is increased heat flux across the basement towards the southwest. Why such a variation in heat flux should occur is unkown. Other possibilities include a systematic regional gradation of lithology. Such a gradation seems unlikely because the trend is perpendicular to the progradation of facies and is therefore correlated to the location of deposition, and not the type of deposition. If regional free convection is somehow integrated into the flow pattern of the major fault trends, one might speculate that the regional variations in the three-dimensional shape of the basin might affect large scale convection cells, which could inturn produce regional variations in geothermal gradients.

## 1.5 SUMMARY

Data collected for this research consists of bottom-hole temperatures from 750 wells. It is clear that a high-temperature ridge exists in the overpressured portion of the Wilcox growth fault zone. The

anomaly begins to emerge at 10,000 feet (3048 m) and becomes more pronounced at increasing depths. Although high porosities associated with geopressures have been linked to lower thermal conductivities and higher geothermal gradients, this mechanism alone does not explain why the temperatures and gradients are highest in the fault zones, and lower in adjacent areas with similar geopressures. Instead, the fault zones themselves seem to be important, serving as conduits for vertical flow. The Wilcox faults correspond to greater temperatures than do the Vicksburg/Frio faults, perhaps due to the greater geopressuring in the Wilcox faults or other differences in their configuration and location. In addition, thermal gradients increase to the southwest for unknown reasons. The increase may be linked to increasing basement heat flux, but is not understood. Free convection may also be integrated into the flow pattern of the faults on a regional or local scale. The gradients in the Frio/Vicksburg trend, for example, may in part be caused by a shallow, local convection cell. The regional variation of thermal gradients may likewise by tied to a changing configuration of regional convection cells.

The evidence presented in this section is empirical. Although it presents a clear indication that vertical fluid movement in growth fault zones might be occurring, such an approach falls short of quantifying the flow. Variables such as thermal conductivy, hydraulic permeability, porosity, and the interplay between the meteoric, geopressured, and thermobaric zones, must be considered, and can be treated better by a quantitative model.

# PART 2-THE MODEL

The temperature data discussed in the previous section support the hypothesis that vertical fluid movement is concentrated along fault-zones in the Gulf Coast Basin. However, because of the many different influences on heat distribution within the basin, it is difficult to distill empirically from these thermal patterns a definitive model of the deep-basinal flow regime. In order to account for the many complicating factors in an integrated and realistic manner, a computer model is used to analyze the relative importance of certain factors vis-á-vis the others. This approach is termed a sensitivity analysis. In the case of observed thermal patterns, a model can, for example, help determine whether or not the concentrated vertical movement of fluids is an essential condition for producing the known temperature field.

I have adopted a computer model for this purpose. This chapter is devoted to the modeling phase of research, and encompasses all its aspects, from the design of the program itself, to its

implementation, and the subsequent conclusions. For clarity, the computer code which performs the modeling operations shall henceforth be referred to as the *program*, and the design of the mesh and its various parameters to which the program is applied shall be termed the *model*.

## 2.1 MODEL SPECIFICATIONS

The overall goal of modeling was to determine the role of the groundwater flow regime in determining the basin's thermal regime. Using temperature distribution as the primary data, a model was implimented to inversely solve for fluid flow. A two-dimensional program by Smith (1984) was obtained for the study. It features coupled heat/fluid flow at steady-state conditions and calculates densities and viscosities as temperature and pressure dependent variables.

Since the model was two-dimensional, only cross-sections could be modeled. For this purpose, a detailed cross-section compiled from well-logs by W. E. Galloway (written communication, 1985) was chosen as the type section. This particular section was one of the best available and also traversed the study area from which the thermal data was collected. Fig. 2.1 shows its location in the study area and Fig. 1.2 shows a modified version of the cross-section. A second cross-section by Wesselman (1983) which traverses a nearby area was also used as a cross reference. This cross-section also showed temperature data, which generally agreed with my data, but were

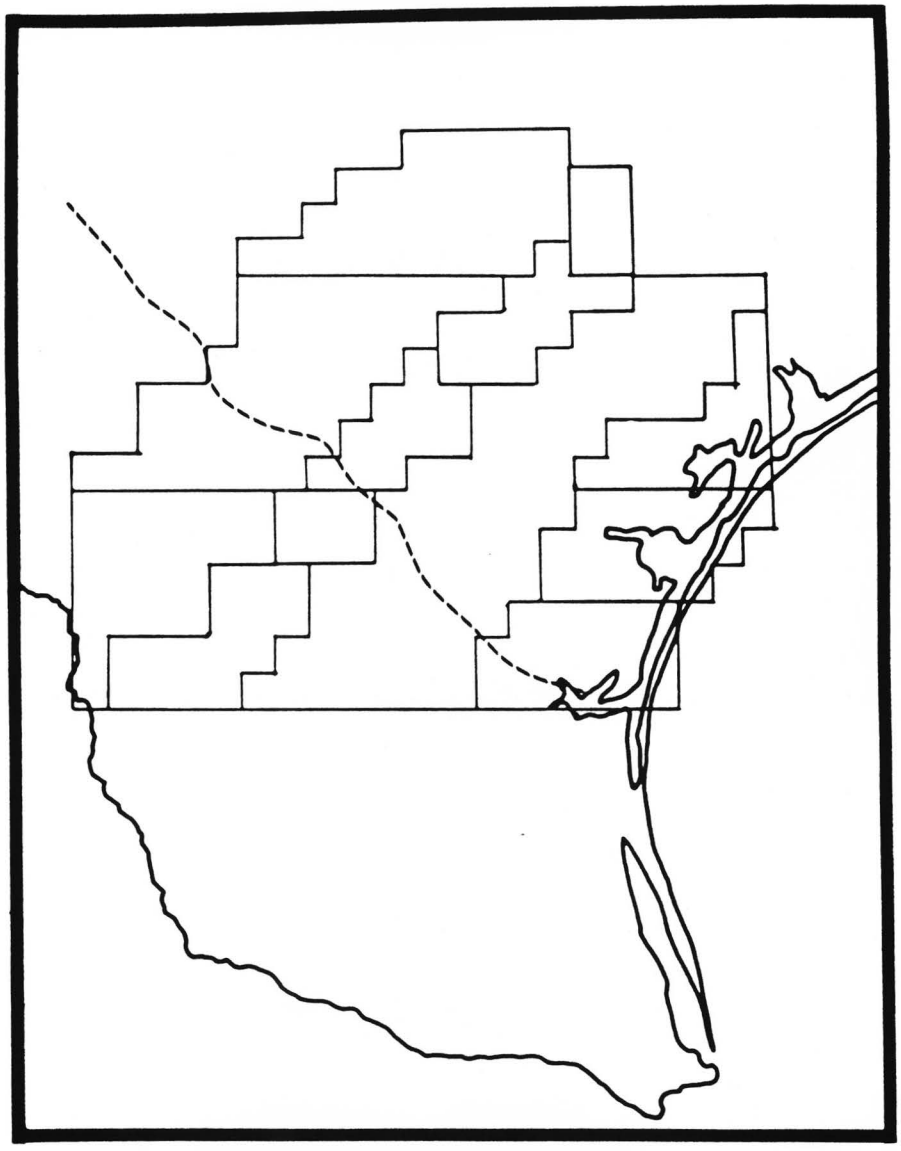

**Figure 2.1**: Dashed line indicates location of the type cross section (Figure 1.2) in the study area.

derived from fewer points and were not statistically treated. The cross-section also provided pressure data, which also correlated well with pressure data taken from mud-weights. These data consist of contours of the geopressure transition zone and were used to position the top of the geopressure zone on the cross-section.

## 2.2 FEATURES OF THE MODEL

The first part of the following discussion covers the mathematical basis of the modeling program including its underlying assumptions. The mathematics are covered in greater detail by Smith (1984). A second section deals with the boundary conditions and assumptions.

### 2.2.1 EQUATIONS OF HEAT AND FLUID FLOW

The building blocks of any computer model are the equations on which it operates. Smith's model uses two general equations, one describing fluid flow, and the other heat flow. The fluid flow equation can be further subdivided into two parts, one for describing the driving forces for flow, and the other to state the conservation of mass at steady-state conditions. The former is of the form:

$$q_i = \frac{-k_{ij}\rho_o g}{\mu}\left[\frac{\partial h_j}{\partial x_j} + \rho_r \frac{\partial z}{\partial x_j}\right] \qquad \text{where } \rho_r = \frac{\rho_f}{\rho_o} - 1 \qquad (1)$$

where $q_i$ is the specific discharge in the coordinate direction $i$, $k_{ij}$ is the

intrinsic permeability tensor of the porous medium, $\mu$ is the dynamic viscosity of the fluid, $g$ is the gravitational constant, $h$ is the hydraulic head, $\rho_0$ is a reference density of water, and $\rho_r$ is a relative density of water derived from $\rho_0$ and $\rho_f$, the nodal density of the fluid. Taken together, the permeability tensor, density, gravitational constant, and viscosity terms form the hydraulic conductivity $K$. The equation can be seen as a version of Darcy's law $q = K * I$ where $I$, the hydraulic gradient, is reduced to two components, the pressure head plus the elevation head. The elevation head is modified in this case by the relative density term which adjusts for buoyancy affects.

The flow equation must be combined with a continuity equation. The continuity equation is simply the mathematical statement that fluid mass is conserved, ie., in any given portion of the modeled area, the amount of fluid flowing in is equal to the amount flowing out. This equation is of the form:

$$\frac{\partial}{\partial x}[\rho r q_x] + \frac{\partial}{\partial z}[\rho r q_z] = 0 \qquad (2)$$

**fluid continuity equation**

The equation is set equal to zero to specify steady-state conditions. One equation is obtained from the two by substituting the expression for q from (1) into equation (2), this step being omitted here for clarity.

The heat transport equation is composed of three basic terms, set equal to zero (steady-state). The equation is:

$$\frac{\partial}{\partial x}\left[(n\lambda_{xx}^{f} + (1-n)\lambda_{xx}^{s})\frac{\partial T}{\partial x} + (n\lambda_{xz}^{f} + (1-n)\lambda_{xz}^{s})\frac{\partial T}{\partial z}\right]$$

**(x direction heat conduction and dispersion in the solid-fluid composite)**

$$+ \frac{\partial}{\partial z}\left[(n\lambda_{zx}^{f} + (1-n)\lambda_{zx}^{s})\frac{\partial T}{\partial x} + (n\lambda_{zz}^{f} + (1-n)\lambda_{zz}^{s})\frac{\partial T}{\partial z}\right]$$

**(z direction heat conduction and dispersion in the solid-fluid composite)**

$$- \rho_f C_f \left[ q_x \frac{\partial T}{\partial x} + q_z \frac{\partial T}{\partial z} \right] = 0 \qquad (3)$$

**(advection of heat with fluid)**

where T is temperature, $C_f$ is the specific heat of the fluid, n is the porosity, $\lambda_f$ is the conduction-dispersion tensor for fluid, $\lambda_s$ is the heat conduction tensor for solid. The assigned longitudinal and horizontal thermal dispersivities were 100 and 10 meters respectively. The first two terms of the equation account for thermal conduction and dispersion in the saturated medium. The third term accounts for the advection of heat with the fluid.

For the above series of equations, viscosity and density are both figured as functions of temperature and pressure. For density, an iterative proceedure is used, based on equations given by Keenan and others, (1978). The basic equation which is solved for density $\rho$ is:

$$p=\rho RT\left[1+\rho Q+\rho^2\left(\frac{\partial Q}{\partial \rho}\right)_\tau\right] \qquad (4)$$

where p is pressure, R is the gas constant, T is temperature on the Kelvin scale, $\tau$ is 1000/T and Q is defined as:

$$Q=(\tau-\tau_c)\sum_{j=1}^{7}(\tau-\tau_{aj})^{j-2}\left[\sum_{i=1}^{8}A_{ij}(\rho-\rho_{aj})^{i-j}+e^{-E\rho}\sum_{i=9}^{10}A_{ij}\rho^{i-9}\right] \qquad (5)$$

where $\tau_c \equiv 1000/T_{critical}$ and $\tau_{aj}=\tau_c$ (if j=1) or =2.5 (if j>1) and $\rho_{aj}$= 0.634 (if j=1) or = 1.0 (if j>1). $A_{ij}$ are coefficients which are tabulated in the appendix of Keenan and others (1978).

Viscosity is determined from a set of equations presented by Watson and others (1980). The domain of validity for the equations is given by (0< Temp (Deg C) <900) for (0< Pres (MPa) <300). The viscosity equation is:

$$\mu=\mu_o(T)\exp\left[\rho^*\left[\sum\sum a_{ij}X^iY^j\right]\right] \qquad (6)$$

where $\mu$ is viscosity, T is temperature on the Kelvin Scale; $\rho^* = \rho/\rho_r$ where $\rho$ is the denisty, $\rho_r$ is a reference density; $X=T^{*-1}$ where $T^*=T/T_r$, $T_r$ being a reference temperature; $Y=\rho^*-1$; $a_{ij}$ are coefficients tabulated in Watson and others (1980); and $\mu_0$ is given by the equation:

$$\frac{\mu o(T)}{10\text{-}6 Pa.s} = \sqrt{T^*}\left[\sum_{k=0}^{3}\left(\frac{a_k}{T^*}\right)\right]^{-1} \qquad (7)$$

where $a_k$ are coefficients which are also tabulated in the reference.

The two dimensional model features anisotropic permeability, and temperature/pressure dependent density and viscosity. It employs the Galerkin finite-element method using linear basis functions applied to triangular elements. The reader is referred to the the works of Wang and Anderson (1982) and Pinder and Gray (1977) for a complete development of this method. For more about the application of finite-elements in heat transport problems see Mercer and others (1975), Andrews and Anderson (1979) and Li (1980).

To use the model, a finite-element mesh is designed to conform to the area being studied. The mesh is a series of polygons, each being an element. At the corners of each polygon are nodes. Fig. 2.2 shows the mesh used for this study. The following procedure was used to couple the heat and fluid flow equations: A purely conductive thermal regime is initially assumed and the temperature field is calculated by the heat transport equation (3), setting the advective term to zero. Appropriate viscosities and densities at the initial temperatures and pressures are then calculated for each element. These are entered into the fluid-flow equation (1)+(2) to obtain a set of heads at the nodal points. The specific discharge $q$ is then calculated for each node (1). These are plugged back into the advective term of the heat-flow equation (3), and the whole equation is then

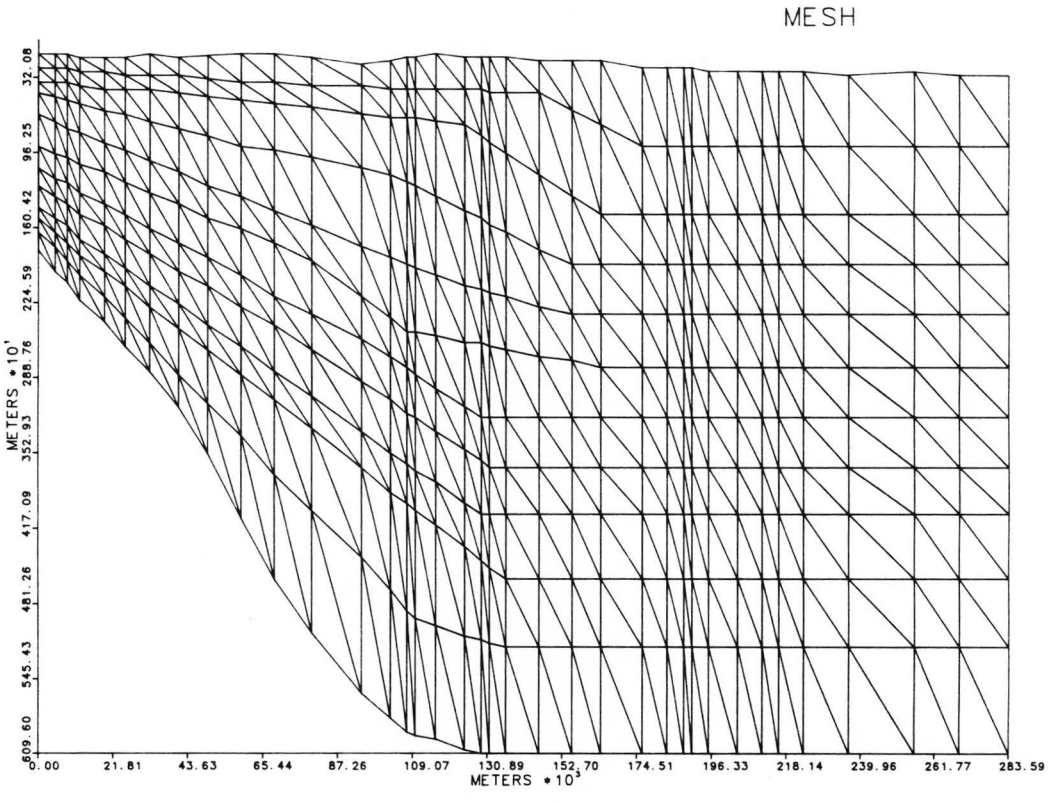


**Figure 2.2**: The finite element mesh used to model the type section (Figure 1.2), shown at a vertical exaggeration of 40.

recalculated, entering into an iterative sequence. The iterations are halted when the maximum change in nodal temperatures is less than a given tolerance. The tolerance was set at .5°C.

### 2.2.2 BOUNDARY CONDITIONS,ASSUMPTIONS AND LIMITATIONS

The basic boundaries of the model are the four sides of the mesh, representing the bottom, surface, northwest and southeast edges of the cross section.

Basal Boundary. The basal boundary is treated by the program as impermeable with a fixed heat flux value across it. It was assumed that the temperature perturbations of the basin are not the result of any basal heat source or sink, such as a pluton or a tectonic feature. Thus the basal heat flux was treated as uniform across the width of the mesh. The value used was 60 mW/sq m, which is a typical value for stable continental interiors (Reiter 1982, Epp and others, 1970, Smith, written communication, 1985). The Cretaceous boundary was taken as the basement of the basin, and although it is not impermeable, its permeability is probably very low. Note that the northwestern portion of the mesh slopes abruptly downward from shallow depths. This is intended to correspond with the position of the ancestral cretaceous shelf edges of the Stuart City and Sligo reefs. Further southeast, the boundary of the mesh is drawn horizontal at a constant depth of about 19,000 feet (5790 m). The actual depth to the Cretaceous here is not accurately known, but is perhaps as deep as 40,000 feet (12200 m). However, it was impractical to include greater

depths in the model because of the lack of well control and temperature data.

Surface Boundary. The upper boundary of the mesh is a constant head boundary with a fixed temperature at 20°C. Because the temperature is fixed, the model can not account for any local heating at the water table due to upwelling fluids nor can it account for possible thermal springs. Since the meteoric system is not the prime focus of this investigation, these limitations are inconsequential.

Lateral (Vertical) Boundaries. The sides of the mesh are treated as impermeable (no flow) and are also thermally nonconductive. This is a somewhat unrealistic configuration. The mesh does not extend to the outcrop of many of the lower formations, nor does it go far offshore. Fluid and heat transfer could occur across both boundaries in nature. To resolve this problem, fluid flux terms were added to selected nodes on each of these boundaries.

Flux Nodes. Several flux nodes were assigned to the lateral boundaries. Two on the northwest boundary near the outcrop belt of the Wilcox formation were assigned a combined flux of -0.00014 Kg/s, which is about 1/2 ml per hour. The negative sign signifies injection of fluid. On the other side of the mesh were placed three constant flux nodes which withdrew fluid at the equal but opposite rate of +0.00014 Kg/ms. This arrangement simulated the passage of fluid into the section from outcrop, and also from the section into the Gulf. These fluxes proved to be rather unimportant in their effect on the pressure and temperature fields, and consequently their assigned values could be

varied considerably without appreciable influence. Aside from the two negative flux nodes on the outcrop side of the mesh, other recharge of the meteoric zone was ignored.

Because the model is steady-state and noncompacting, flux nodes were needed to simulate compaction-driven fluid in the geopressured zone. The model was first designed without such nodes and the result was a complete absence of geopressuring. Several distributions of these flux nodes were tried, and it was determined that fluxes assigned just to the basal nodes worked best.

Mathematical Assumptions. As mentioned above, the program calculates appropriate densities and viscosities as functions of both temperature and pressure (equations 4 -7). The subroutines which handle these calculations are equipped to treat pure water in fluid, steam, or supercritical phases. However, multiphase flow is not allowed. In addition, the fluid is required to be in thermal equilibrium with the medium at all times. Thermal conductivity of the rock is assumed to be constant, although in reality is varies slightly as a function of temperature. Thermal conductivity of water is treated as a function of temperature. Porosity is also assumed to be nontransient.

Chemistry. Chemical processes are extremely difficult to couple with groundwater models because of the numerous calculations which even simple chemical models require. Including such calculations in an iterative sequence across an entire mesh would result in unmanageable computation times. As a result, both density and fluid flow calculations are somewhat handicapped. Fluid samples

collected from Tertiary formations in the Gulf (Fisher 1982, Land, personal communication, 1985) indicate that the salinity (ppm) of formation waters is significantly correlated to its in-situ density. The modeling program assumes only pure water. In an attempt to circumvent the problem, a reference density corresponding to a 50,000 ppm solution at standard state (1.053 gm/cm$^2$) was substituted for the reference density of pure water in one test run. This had no affect on the modeled temperatures, and only a subtle affect on the modeled pressures, mainly in the meteoric zone. In the modeling program, the meteroic zone can not be assigned a separate reference density from the geopressured section. Likewise, viscosity and density subroutines were writen for pure water only. Hence, high ppm pore fluids could not be realistically considered in the study. Additionally, clay dehydration reactions may contribute a significant quantity of fluid at particular horizons. Some simulation runs of the model were conducted using assigned fluid flux nodes in areas of critical temperatures and pressures to simulate such fluid release, but this failed to produce correct temperatures or heads (simulating the process in this way did not take into account the heats of reaction).

Assessing Thermal Conductivity. The model requires the assignment of both a thermal conductivity and porosity field. The thermal conductivity is assigned to the solid portion of each element, and the porosity is therefore used to determine the fraction of the element that is assigned the thermal conductivity of fresh water at the appropriate temperature and pressure. Unfortunately, there has been

very little research into the thermal conductivities of the solid portion of rocks. Instead, there have been studies which list thermal conductivities for typical rock-types. These values are given without regard to porosity, water content, or pressure. Pressure is important because an important factor in the thermal conductivity of the solid matrix is the nature of the grain to grain contacts, which may vary as a function of pressure. Of course, the mineral composition of the sediment grains is also quite important because different minerals have widely different conductivities. Therefore, the thermal conductivity of the solid matrix should be dependant upon rock type. Because of the lack of research in this field, the only guide to thermal conductivities at present are the values for typical rock types. The porosity field modifies these values.

Limitations of Scale. The mesh and all the output related to the mesh have been printed at a vertical exaggeration of forty. At true scale, the actual cross section represented by the mesh is very wide relative to its depth as shown in Fig. 2.3. Since the parameters in the design of the model are assigned on a per element basis, and the width of each element is at least several kilometers, many details of the cross section were omitted. A finer mesh could have been used to increase resolution, but this would have caused longer run times and an increased complexity in the set up and calibration of the model. Of course, an important consideration in the design of the mesh was the quality of the data.

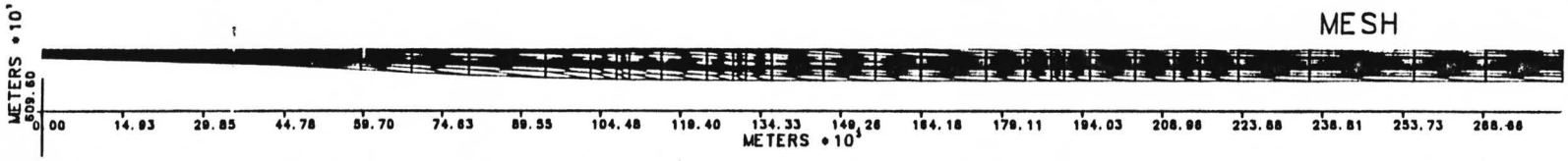


**Figure 2.3**: The finite element mesh shown at true scale.

Generally, most of the loss of detail was forfeited in the shallow meteoric portions of the basin. The deeper areas are apparently simpler lithologically although there are fewer well-logs available to document this fact. Because of scale, faults were treated as zones rather than as discrete discontinuities, and these zones thus reflect an averaged behavior. Modeled fluid velocities may therefore be less than the actual velocities that may exist in discrete portions of the fault zone. Likewise, much of the anisotropy caused by the small scale interlayering of muds and sands was averaged by assigning anisotropic permeabilies to the grid elements.

## 2.3 DESIGN

### 2.3.1 CALIBRATION

Calibrating adjusts the model to accurately simulate the actual system. It involves repeatedly running the model, checking the output, making revisions, and then rerunning it. In an ideally calibrated model, all of the independent variables are known. The model is adjusted so that these are all accurately reproduced by the model, and the dependent variables are then computed. Such ideal cases are rarely realized.

The primary calibration tool for this investigation was the temperature data. Other constraints were the stratigraphy and the top of geopressure plus a general knowledge of the shape of the pressure-versus-depth profile. In addition were crude estimates on the magnitude of overall vertical flow from the deep basin (section 2.4.2).

The modeling procedure was as follows: 1) Four fields were assigned for vertical and horizontal intrinsic permeability, thermal conductivity, and porosity. For each field a code map was constructed where each element is represented by a coded number which is assigned a value for the particular parameter. 2) Flow rates were assigned to constant flux nodes, keeping the total flux as low as possible. 3) These parameters were then run with the program.

The output from the model includes plotted isotherms and hydraulic heads. The isothermal plot was superimposed on the isothermal plots compiled from temperature data and any discrepancies were noted. The same was done for the head plot. Adjustments were made to the various design aspects on a priority of permeability fields first, then if necessary flow rates, followed by conductivities and finally porosities. Initially, several parameters were adjusted between each run. As the model came closer to meeting the calibration critera, only one or two changes were made per run.

### 2.3.2 THE MESH

The mesh (Fig 2.2) corresponds to a cross-sectional width of 176 miles (283 km) and a depth of 20,000 ft (6096 meters). In this program, four-sided polygons are each divided into two triangular elements. All rows and columns of nodes are continuous. A general rule in designing the elements is to avoid any elements with obtuse angles. For mathematical reasons, obtuse angles will lead to erroneous values and convergence problems. Convergence problems may also result from

extreme differences in assigned parameter values in adjacent elements. As a further consideration, to compensate for some of the scale problems mentioned earlier, nodes were concentrated in areas of greatest interest, such as in the growth fault zones.

### 2.3.3 THE CODE MAPS

Porosity Field. The data used to code for porosity was mostly taken from Loucks and others (1979), Bonham (1980) and Fyfe and others (1978). In general, porosity was treated as a function of depth, ranging from 35% at the surface to 5% at the greatest depths. Additionally, this decline with depth was suspended in the geopressured transition zone. Changes made to the porosity field proved to have very little effect on the modeling results. Porosity is only used in the conduction terms of the heat transfer equation (3), and its low sensitivity seems to indicate that saturated porosity is perhaps not as significant a factor in basinal thermal patterns as has been suggested by Lewis and Rose (1970).

Thermal Conductivity. The thermal conductivity values were assigned using as a guide a table from Reiter and Tovar (1982) which lists thermal conductivities for various rock types. The conductivities were assigned to the mesh according to the rock types shown on the type-section. Somewhat lower conductivities were found to be necessary for the deep marine shales than the values listed in the table for shales, but this is justifiable in that much of the marine shale occurring under geopressures has been found to be more like a "dense

clay" than lithified rock (Weaver & Beck, 1971). The values chosen were consequently intermediate between shale and clay. Additionally, the deepest marine shales were assigned higher conductivities because they are presumably more dense and consequently more conductive.

Permeability. The data presented in Loucks and others (1979) was used for permeability values. This data consisted mostly of whole core analysis plotted against depth. A major draw-back with this type of measurement is that it ignores large scale permeabilities created by faults and fractures. These are perhaps more important in determining hydrologic characteristics of a large area. Additionally, permeability is not only a function of depth but also of rock type, pressure and chemical reactions. The whole core analyses are relative to atmospheric pressure. Nonetheless, the range of values for each depth was quite great, which provided room for adjustments in the calibration process. Permeability was the most sensitive of the input parameters.

A matter of some speculation is the contribution to permeability made by hydraulic fracturing, also known as mircofracturing. According to Fyfe and others (1978), microfractures are theorized to originate in flaws, which grow when pore-fluid pressure exceeds the least principal stress by an amount equal to the tensile strength of the rock. The stresses on rock can be resolved into three vectors, one for each dimension, x,y, and z. These are called the principal stresses, the smallest of which is called the least principal stress. In undeformed rock these stresses are usually compressional. Pore pressures tend to oppose compressional stresses equally in all

directions by forcing pore spaces open. When pore pressures exceed the least compressional force by an amount greater than the matrix can tolerate (the tensile strength), the rock ruptures, causing a fracture. Fracturing will occur in the direction perpendicular to the least principal stress. In a compacting basin the least principal stress is usually horizontal, while the greatest principal stress, resulting from the weight of sediments above, is vertical. Microfractures are usually oriented vertically (Jaeger & Cook, 1979). Stronger rocks are more susceptible because they tend to have greater stress differentials (the difference between least and greatest principal stresses). The strongest rocks should be those in the deeper basin, owing to their degree of consolidation. On the other hand, stress differentials decrease with depth. How these opposing factors control the occurence of hydrofacturing is currently unstudied, but faulted areas may be particularly susceptible owing to an abundance of suitably oriented flaws.

## 2.4 RESULTS

The investigation was broken down into three simulations, each testing a basic type of flow regime. The first considered the affects of evenly dispersed advection while the second concentrated the advecting fluids along faults. The third was a special case of the second, adding a speculative region of high thermal and hydraulic conductivity in order to more closely meet the constraints.

Several criteria were employed to calibrate the model. They were fluid flux, fluid pressure, and temperature. The degree to which model output matches the calibrating critera is a measure of how well the design of the model depicts the actual system. The same criteria where used for each simulation, and the following discussion systematically compares them to the model's output. The implications of the results are covered in the discussion section 2.5.

### 2.4.1 SIMULATION ONE - CONDUCTION DOMINATED

The object of this simulation was to test the hypothesis that thermal patterns are basically controlled by the movement of dispersed (as opposed to fault-concentrated) compactional fluids coupled with geopressure-dominated thermal conductivities.

Flux Nodes. Fluid flux nodes were needed to simulate the release of compaction fluids, thus establishing a geopressured zone. These fluxes were evenly distributed across the base of the section. Because fluid fluxes must be assigned to nodes, which are point sources, the basal elements were given artificially high horizontal permeabilities. If this were not done, all nodes, being separated by several kilometers, would produce high pressure plumes. By assigning high horizontal permeabilities to the basal elements, a permeable avenue was created which permitted the simulation of a diffuse upward flow that would be typical of a hydraulically homogeneous compacting basin. Fig. 2.4 shows the flux distribution along the basal boundary. During calibration, very low fluxes were initially assigned. After

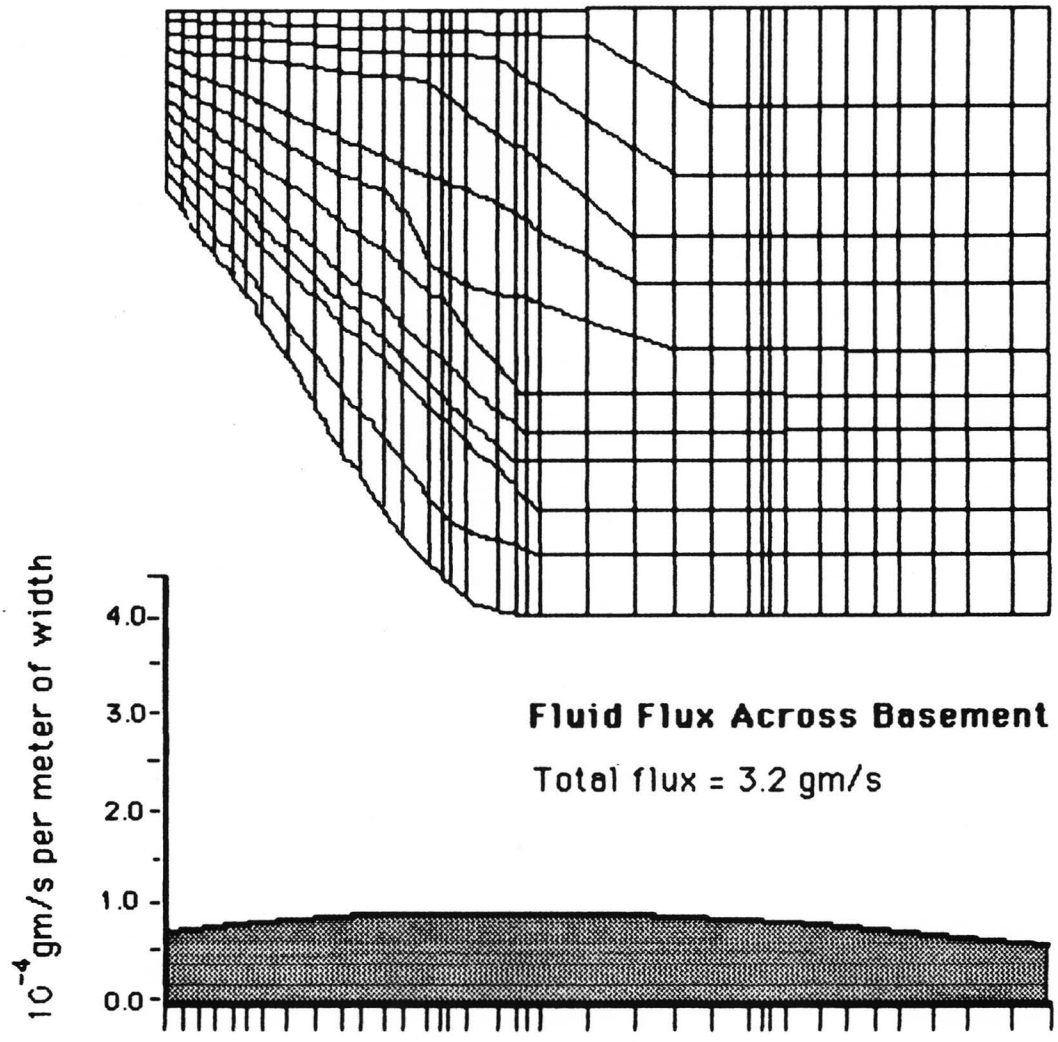


**Figure 2.4:** Fluid flux assigned to the basement nodes of the mesh for Simulation One.

permeabilities and thermal conductivities were optimized, remaining calibration discrepancies were addressed by conservatively incrementing the fluxes. This procedure was repeated until a "best fit" was obtained. The overall average was $8.91 \times 10^{-8}$ kg/s for each meter across the section; the total flux for the entire section being $3.2 \times 10^{-3}$ kg/s.

Permeability Codes. Figs. 2.5 through 2.8 show the coded mesh for horizontal and vertical permeability, porosity and thermal conductivity. The permeability fields were kept simple by assuming faults to have no influence. The geopressured zone was assigned the lowest permeabilities, with a rapid increase in permeability at the transition to normal pressures. The southeastern or right portion of the mesh corresponds to the sands of the Frio Formation and consequently higher permeabilities.

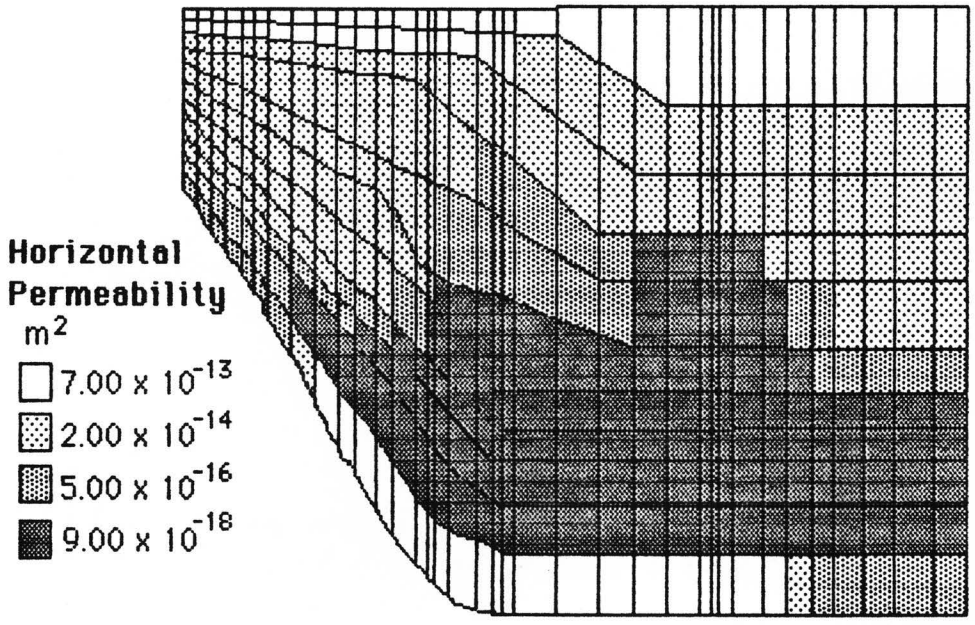


Figure 2.5

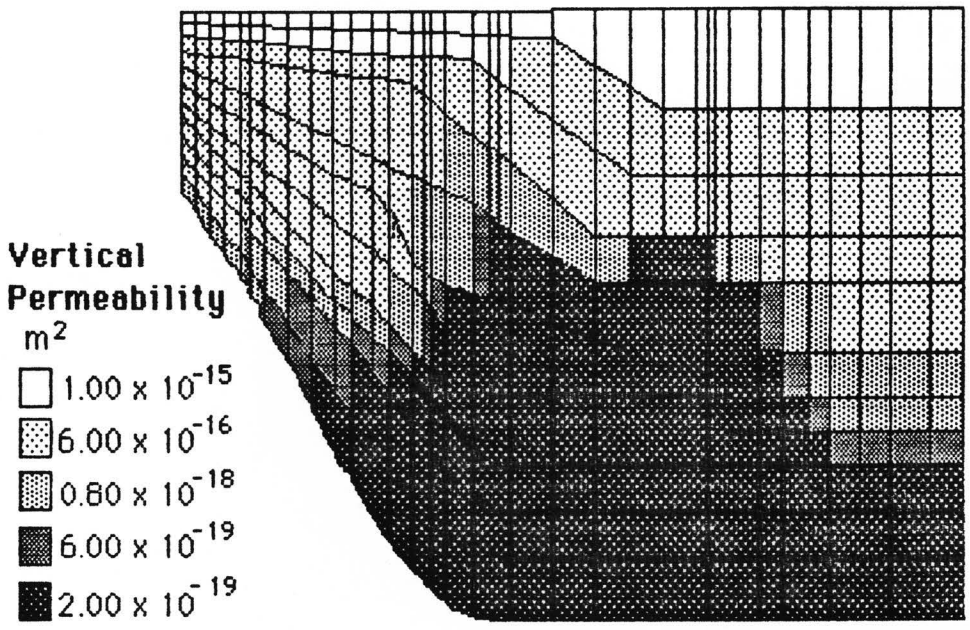


Figure 2.6

Porosity Code. The porosity mesh was also simply designed. Porosity decreases from a maximum of 35% at the surface to 5% at 20,000 feet (6096 m). Porosity is held constant at 21% across the pressure transition to geopressuring. Fig. 2.7 shows the coding for the porosity mesh.

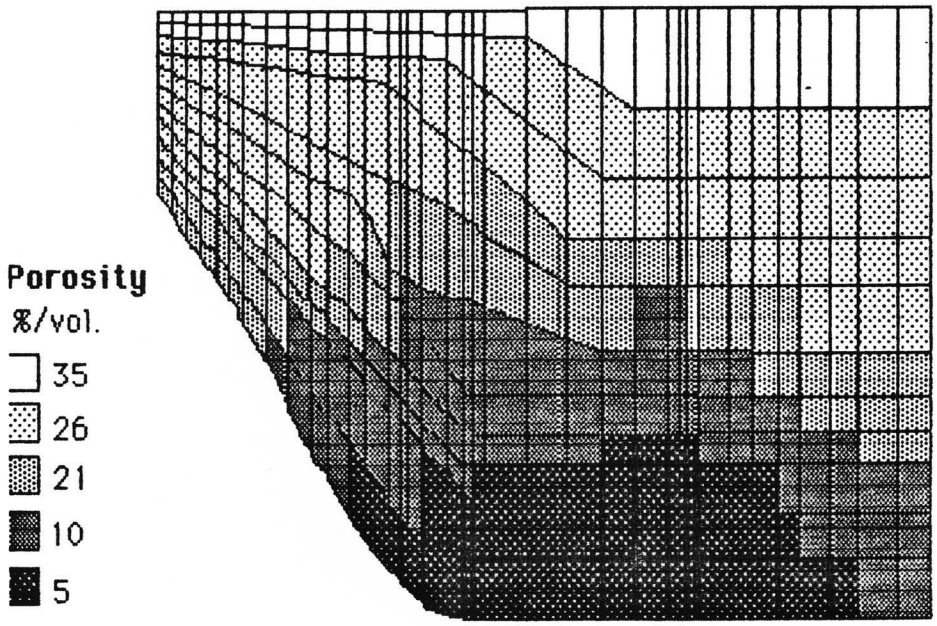


Figure 2.7

Thermal Conductivity Code. The Thermal Conductivity mesh is comparatively complex (Fig. 2.8), particularly in the portions above the top of geopressure, because the lithology is most variable there. Sandy units typically have higher conductivities than clays and shales (Reiter and Tovar, 1982). Thus, higher conductivity units were assigned in the Frio formation on the right portion of the mesh. The lowest conductivities were assigned to the shallow geopressured section because the least consolidated thickly bedded clays were presumed to occur there. The more unconsolidated the sediments are, the more poorly they conduct heat. An isolated high conductivity unit was placed in the deep geopressured Wilcox to correspond with a large sand body which is indicated on the type-section.

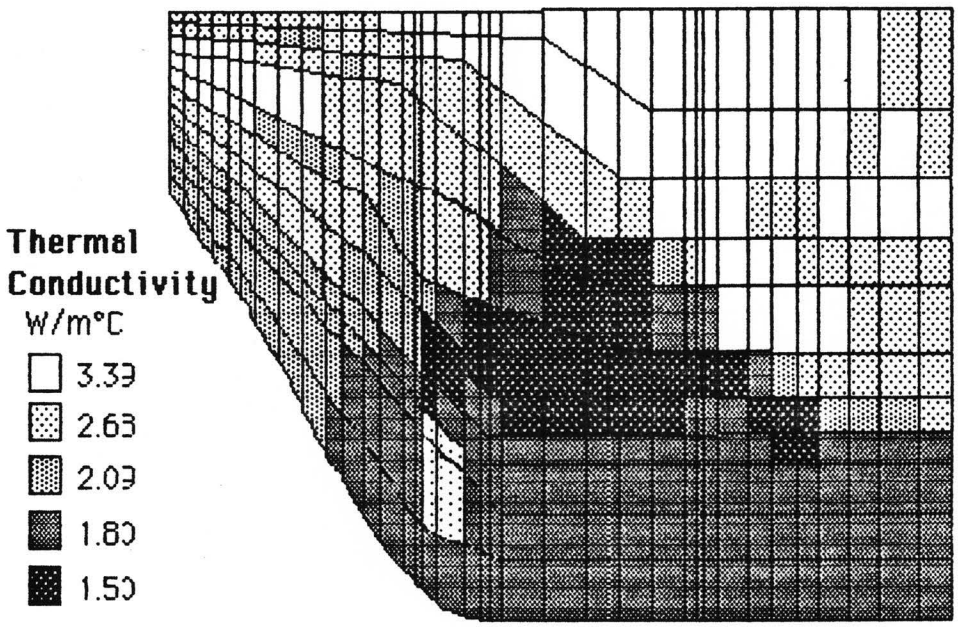


Figure 2.8

2.4.2 SIMULATION ONE-RESULTS.

Fluid Flux. As mentioned above, the average fluid flux assigned across the geopressured section was $8.91 \times 10^{-8}$ kg/ms for each meter across the section. An estimate for comparison was provided by Lynton Land (personnel communication, 1985). The estimate is based on the chloride concentration of Gulf Coast rivers and streams whose watersheds do not drain Pennsylvannian or Permian evaporites. Possible sources of chloride in surface waters are aerosols (mostly in the form of rain), halite from evaporites, and discharge of deep-basinal brines. The average value for river-borne chloride was 8 grams of chloride per square meter of land surface per year. Of this, only 1.2 grams can be accounted for by aerosols. The 6.8 gram deficit which remains is assumed to be due to the contribution from deep-basinal discharge.

Figuring the flux assigned in the model provides 2.81 kg or about 2.8 liters per square meter per year, this implies a chloride concentration in the upwelling deep-basinal fluids of 243 parts per thousand. This is well within the realm of halite saturation which is about 400 parts per thousand at 100°C, and is also very similar to concentrations reported from brines in the Edwards Formation of the basin. This estimate thus provides an indication that the flux rates chosen are quite reasonable.

On the other hand, a volumetric calculation yields a very different result. Using the same 2.8 kg/ms flow rate, an estimate of the initial height of a one meter square column of compacting sediment needed to produce this flow rate was obtained. Assuming a period of 40 million years and an initial porosity of 35%, a column of sediment 320,000 meters high would have to be compacted to 0% porosity to maintain this flow rate. Since the depth of the basin is probably no more than 13,000 meters, the flow rate appears from this calculation to be more than an order a magnitude too high, indicating that simple compaction is inadequate to account for the postulated flow rate. Bruce (1984) claims that the smectite-illite clay transition can supply as much as three times more fluid than compaction in the depth range of 7000-11000 feet (2134-3353 m). However, this is only for a 5% volume reduction from 14%to 9% porosity. Though potentially important, the transition alone does not account for all the fluid needed, nor does is account for fluids sourced from depths greater than 11000 feet (3353m).

Fluid Pressure. Fig. 2.9 shows the pressure contours generated by the model. The contours are meters of excess hydraulic head relative

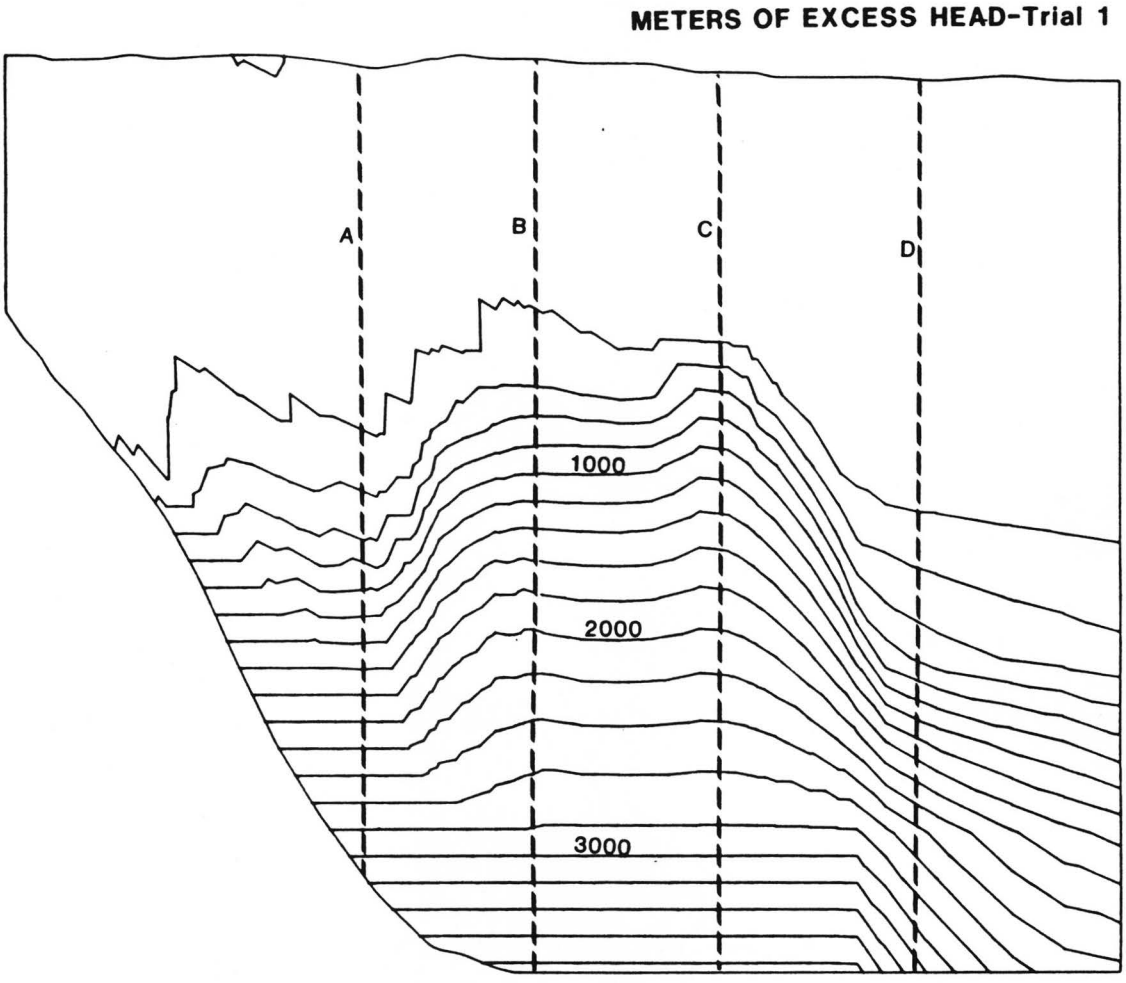


**Figure 2.9**: Hydraulic head generated by the model for Simulation One. Dashed lines show location of pressure profiles in Figure 2.10.

to the highest topographic elevation of the section. The contour interval is 200 meters. Since the contours are excess heads, they mark the geopressured zone. The first several contours should therefore correspond to the top of geopressuring as indicated by the hatchured line in the cross section of Fig. 1.2. Fig. 2.10 shows pressure profiles taken along four transects of the section indicated on Fig. 2.9. Here the agreement with other data (shown on the figure) is not good. The pressures modeled at each of the four transects are within reason but are generally low compared to the generalized pressure trends, which are taken from Neogene deposits of South Texas (line 1) and recent to Miocene in Louisiana (line 2). But missing from the modeled pressures is the characteristic shape of the pressure profile, namely the inflection in the line caused by the transition from increasing pressure gradients at shallow geopressures to a constant pressure gradient at continued depths. The profiles are instead relatively linear, with little variation in the pressure gradient. The pressures therefore can not be considered well calibrated.

Temperature. Fig. 2.11 shows the isotherms produced by the model (dotted lines) superimposed on those from the BHT data (solid line). The gray shaded areas are the error ranges for the BHT data. These were taken from the contoured variances (from Kriging) shown in Figs. 1.6-1.10d. The match of the 200°C isotherm is quite good, but discrepancies increase at higher temperatures, and are especially large between the 350°C and 400°C isotherms. The largest discrepancies

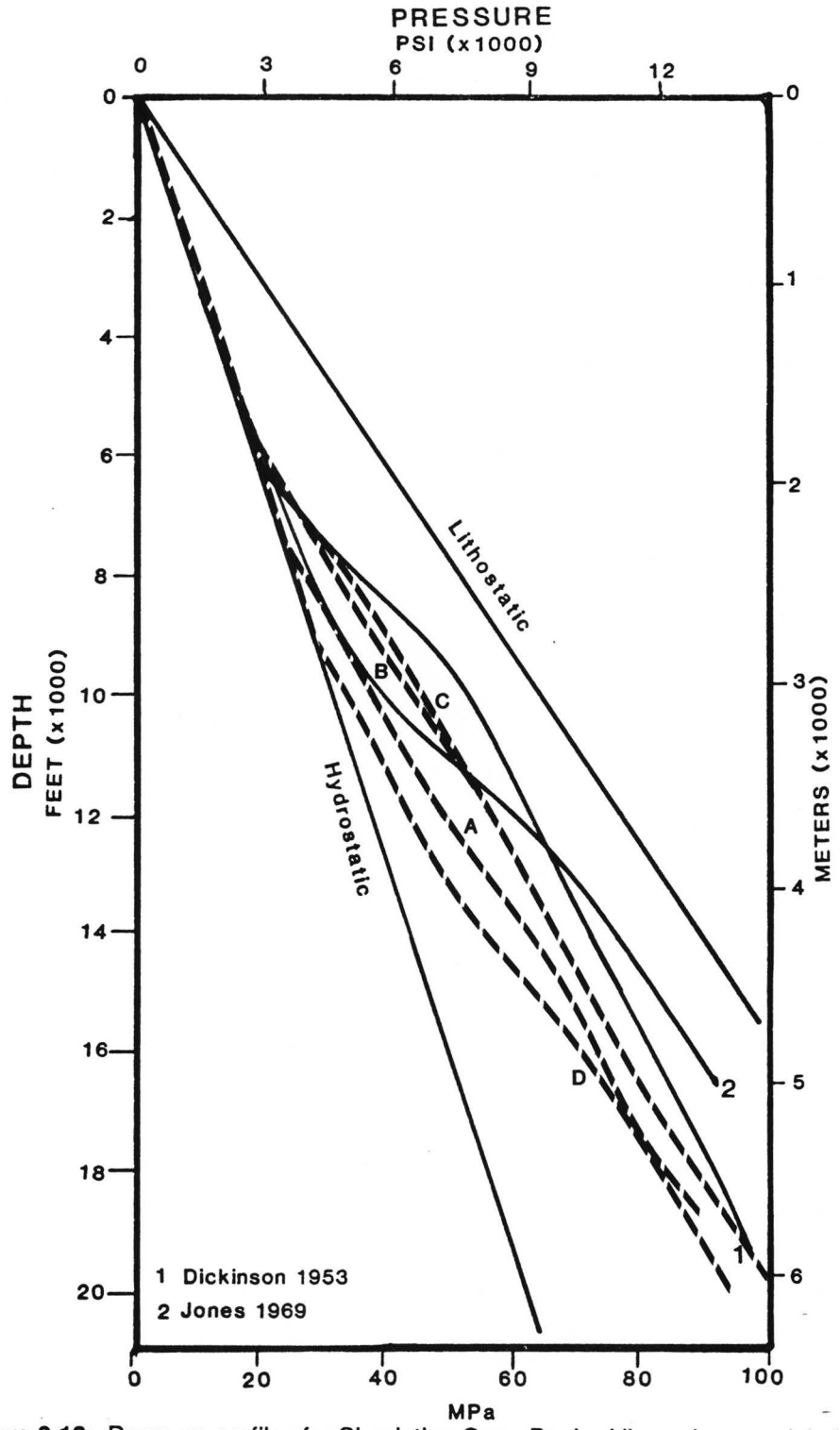


**Figure 2.10**: Pressure profiles for Simulation One. Dashed lines show modeled pressure profiles keyed in Figure 2.9. Solid lines 1 & 2 show generalized profiles for Gulf Coast.

occur at the Wilcox growth fault zone, where modeled temperatures are much lower than the data indicate.

Four temperature profiles where constructed from selected transects of Fig. 2.11 and these where superimposed on the temperature profiles from the corresponding subareas presented in Figs. 1.18, 1.14, 1.20, and 1.23. The advantage of this comparison is the ability to view the actual BHT measurements in conjunction with the modeled temperatures. Figs. 2.12 through 2.15 show these profiles. Once again, the matches are generally poor. In all but the group nine area, in fact, modeled temperature gradients are below average, whereas the data show that gradients in all areas are above average.

The Flow Regime. Fig. 2.16 is of the fluid velocity vector field. The arrows in the figure are vectors, meaning that their length is proportional to the fluid velocity at the point of the arrow's origin, and the direction of the arrow indicates the flow direction. The direction is corrected to account for the vertical exaggeration of the figure. The vectors are placed at element centers. Since many of the flow rates are extremely low, they appear only as the head of the arrow. Wide differences may still exist between these velocities, though not apparent from the figure. Appendix F lists the flow rates for each element. Readily apparent from the figure is the break from geopressured to meteroic regimes. The meterioc system is characterized by much higher flow rates as well as more variable, topographically controlled directions.

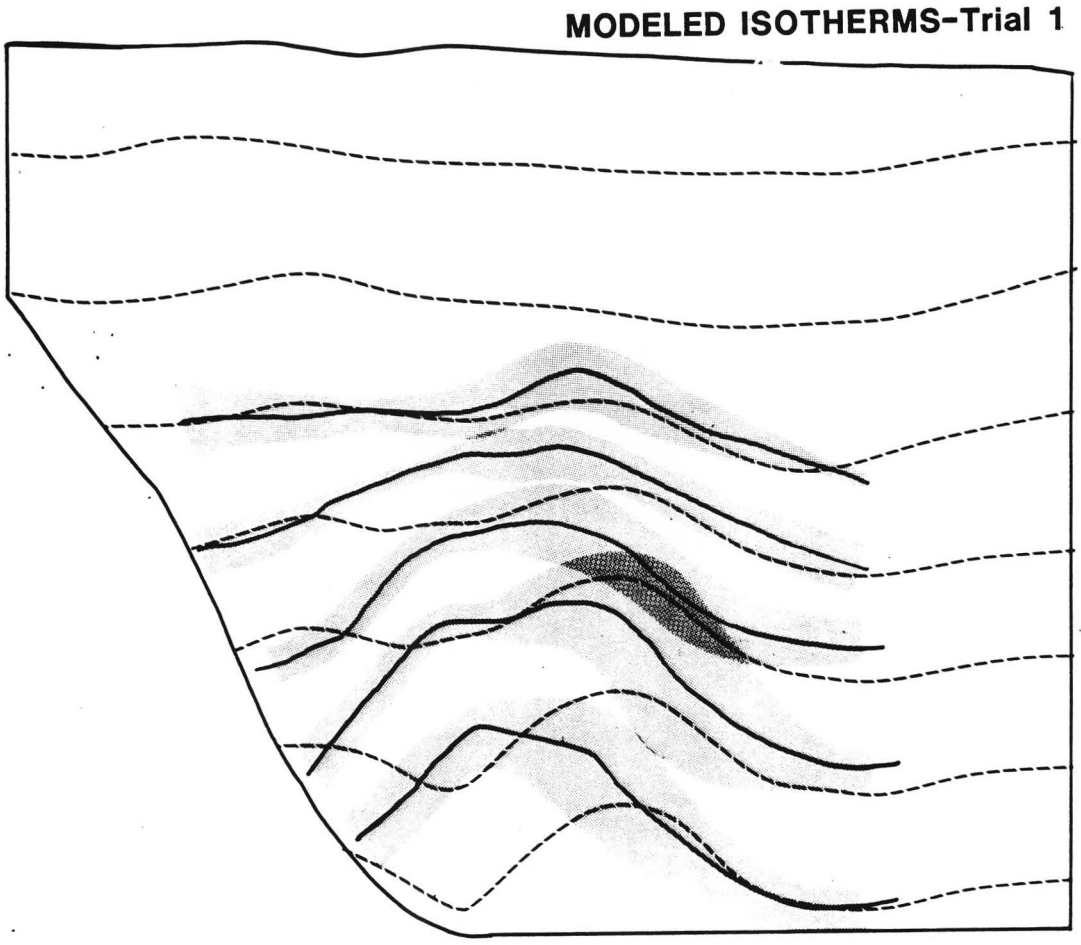


**Figure 2.11**: Modeled isotherms for Simulation One shown by the dashed lines; solid lines indicate isotherms from kriged BHT data with the grey shaded areas showing their standard deviations.

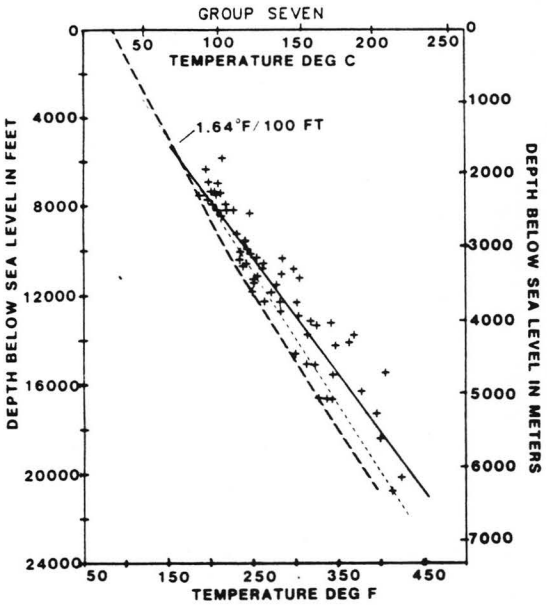


Figure 2.12

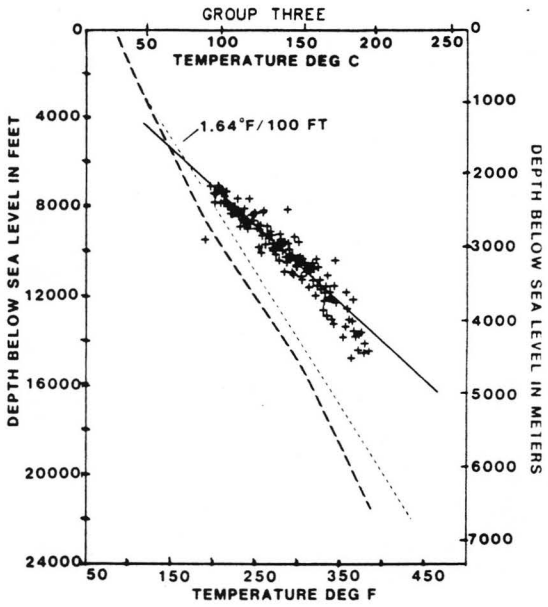


Figure 2.13

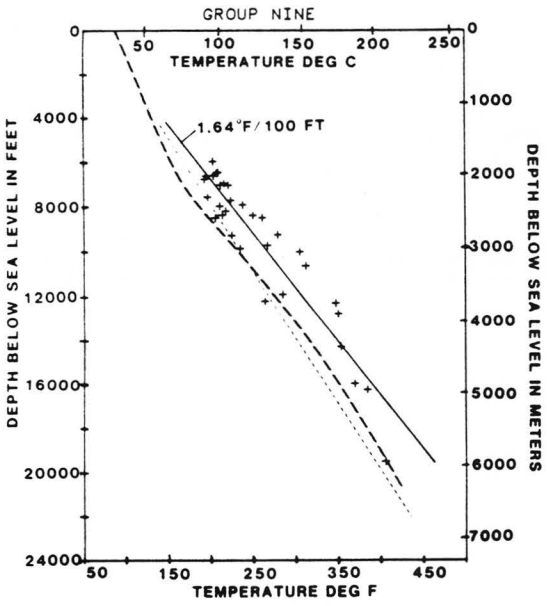


Figure 2.14

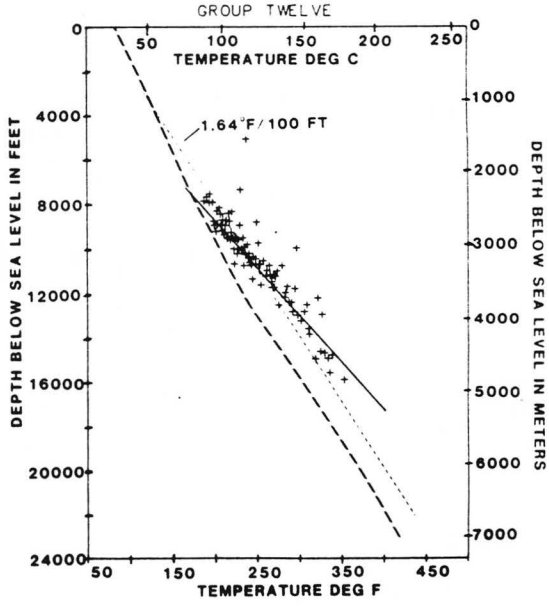


Figure 2.15

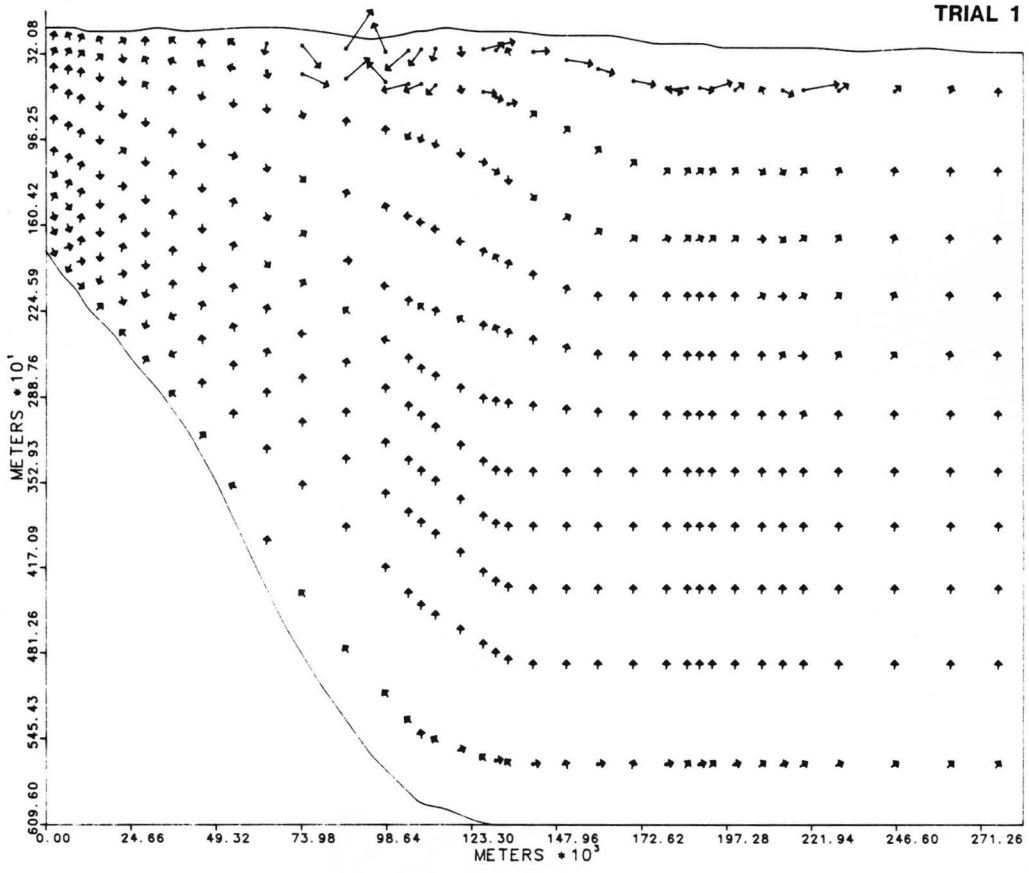


**Figure 2.16**: Simulation One flow velocity vectors.

## 2.4.3 SIMULATION TWO - CONCENTRATED FLOW

Flux Nodes. The second simulation employed areas of concentrated vertical flow to model the basin. The same overall flux used in the first simulation was maintained in Simulation Two, but it was redistributed in such a way as to concentrate most of the flux along the Wilcox growth-fault zone. Fig. 2.17 shows this distribution.

Permeability Codes. Figs. 2.18 and 2.19 show the permeability codes. These are much more complex than in the previous simulation. Relatively high horizontal permeabilities were assigned to the basal row of elements to avoid pressure plumes around each node, but these values were much lower than those used previously in order to avoid widely dispersed fluxes across the basement.(Fig. 2.4). Elsewhere, horizontal permeability was decreased with depth, and in response to the new flux conditions, the horizontal permeability field was refined in the upper geopressured section. Specifically, values were increased in order to disperse the concentrated flux below the pressure transition, a condition necessary to calibrate the isotherms. The justification for this alteration is that although vertical permeability in the marine shales is certainly very restricted, horizontal permeability can increase near the top of geopressure because of high porosity and a relatively unconsolidated, laminar structure.

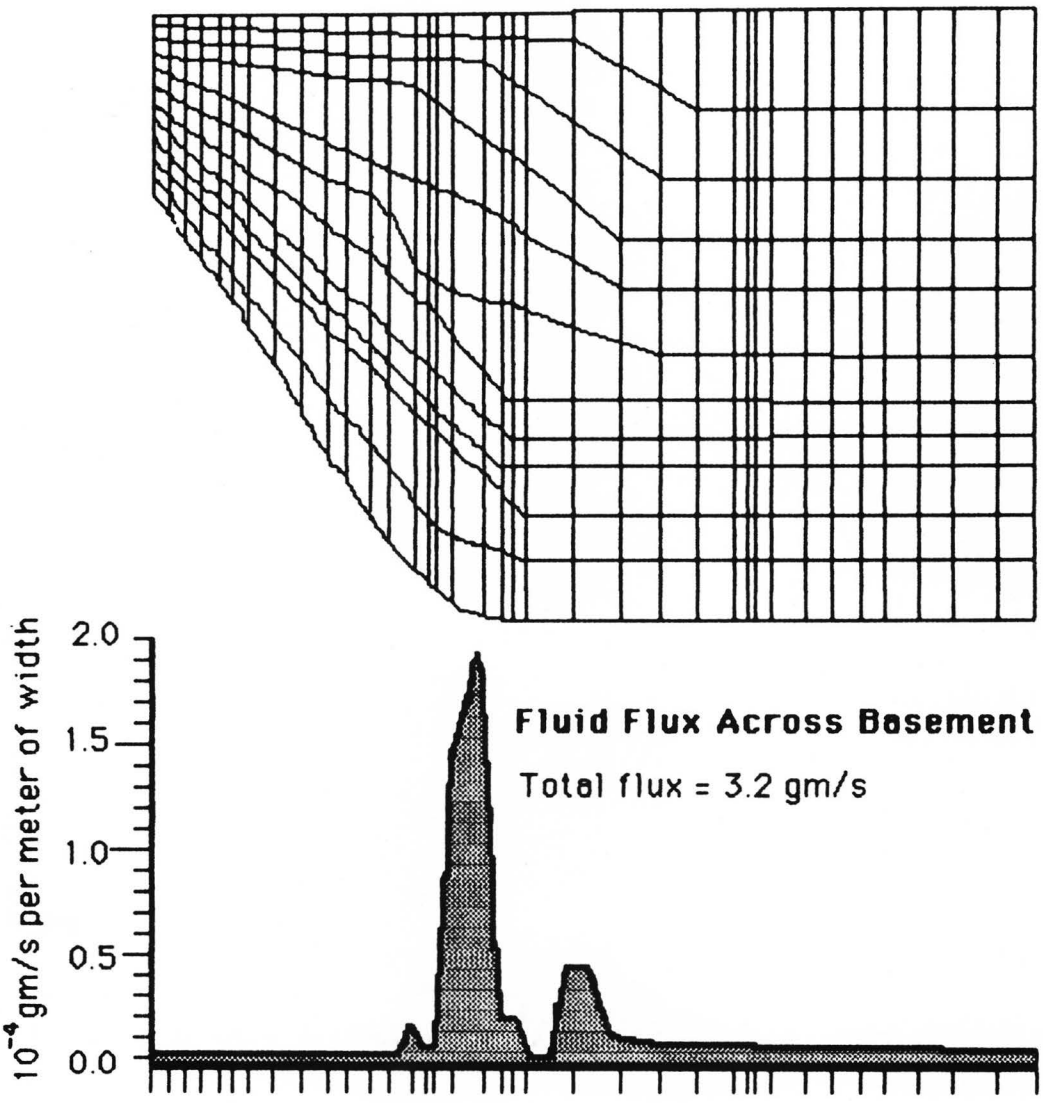


**Figure 2.17**: Fuid flux assigned to the basement nodes of the mesh for Simulation Two.

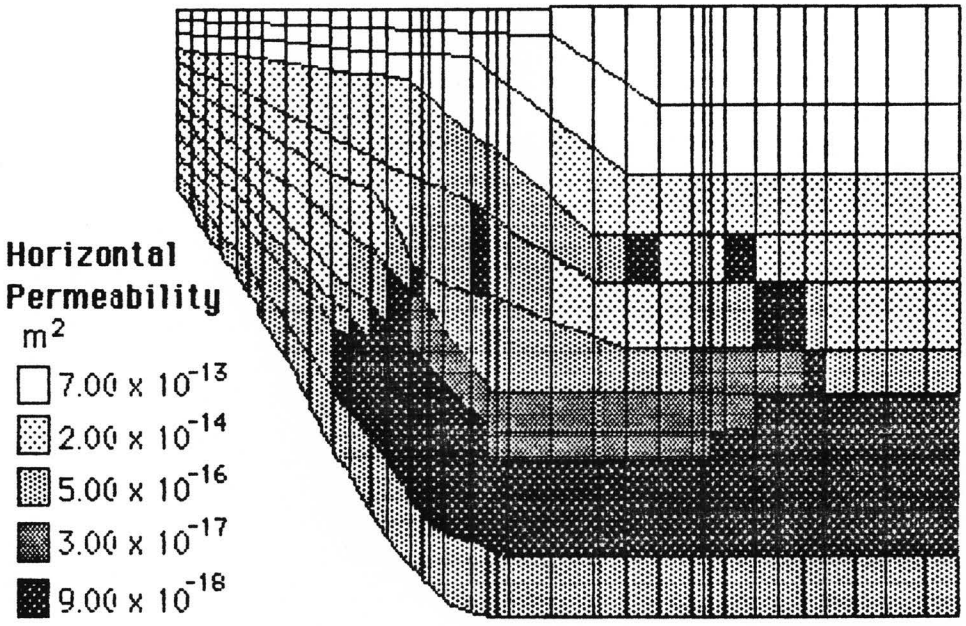


**Figure 2.18**

The vertical permeability mesh has a different configuration. Its values were assigned as a function of depth except where vertical conduits for flow were hypothesized. Two portions were modeled as such, the deeper parts of the Wilcox growth faults, and the geopressured portion of faults in the Catahoula Fm.

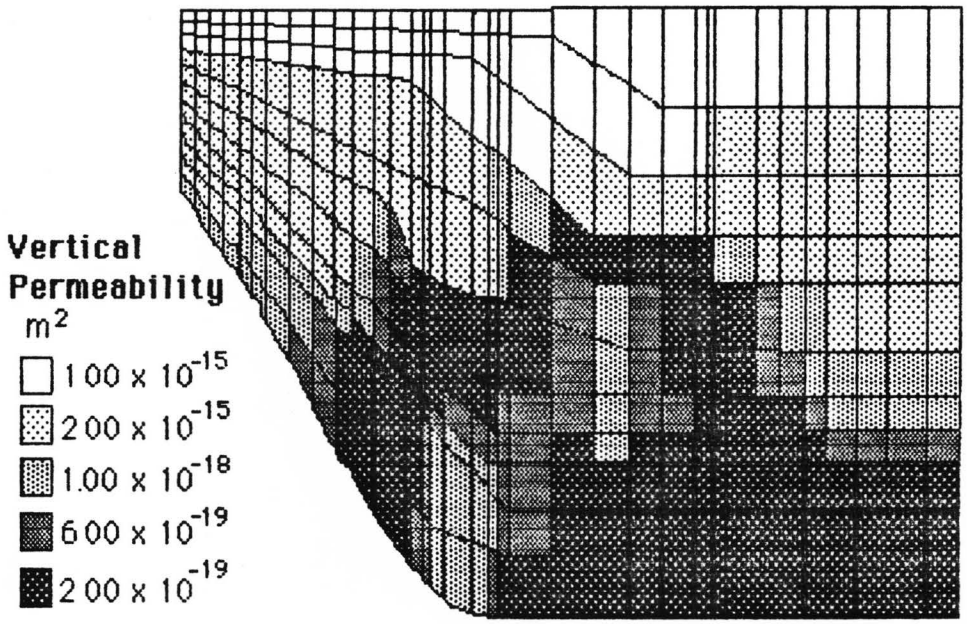


**Figure 2.19**

Porosity & Thermal Conductivity Codes. The porosity field is unchanged from the first simulation (Fig 2.7). Slight modifications were made to the thermal-conductivity mesh (Fig 2.20). The conductive sand body in the deep basin was removed, and the elements of least conductivity were redistributed, adding more in the Wilcox growth-fault zone. These refinements were needed to calibrate the model given the new fluid flux conditions, being careful to keep values within ranges supported by the available data.

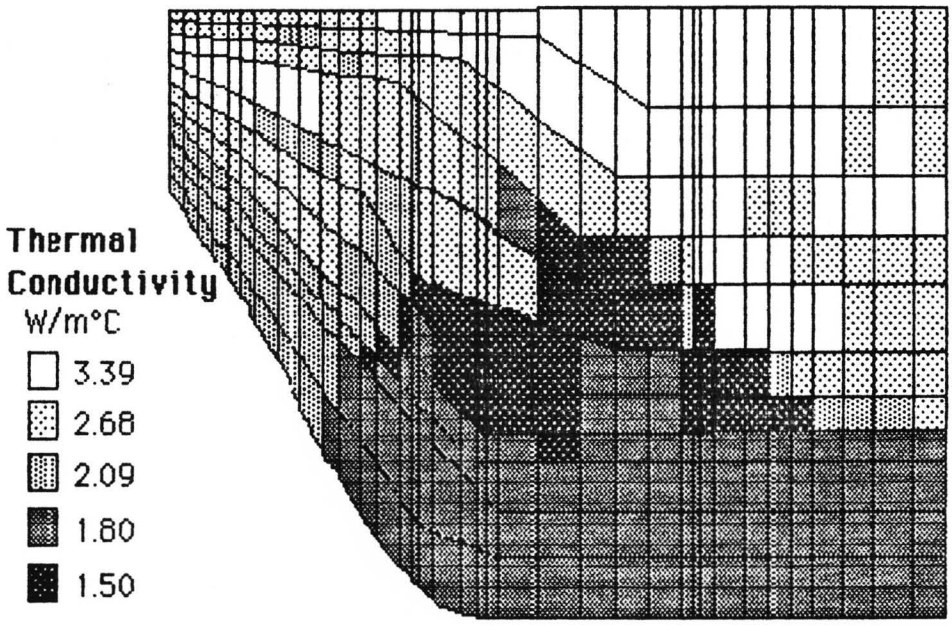


Figure 2.20

2.4.4 SIMULATION TWO-RESULTS.

Fluid Pressure. Fig. 2.21 shows the pressure contours for Simulation Two. Unlike the previous simulation, a plume indicative of concentrated upwelling is apparent in this figure. The pressure vs. depth profiles derived from this diagram and given in Fig. 2.22 show much better agreement with the two other data sources shown. Line B from the growth fault zone shows near perfect agreement with Dickinson's data, reproducing the characteristic inflection point. The fact that the actual top of geopressure (indicated by the first deviation away from the hydrostatic line) does not match is not significant because Dickinson's data is from a different location, and the depth to the top of geopressuring is variable across the basin. Line D,

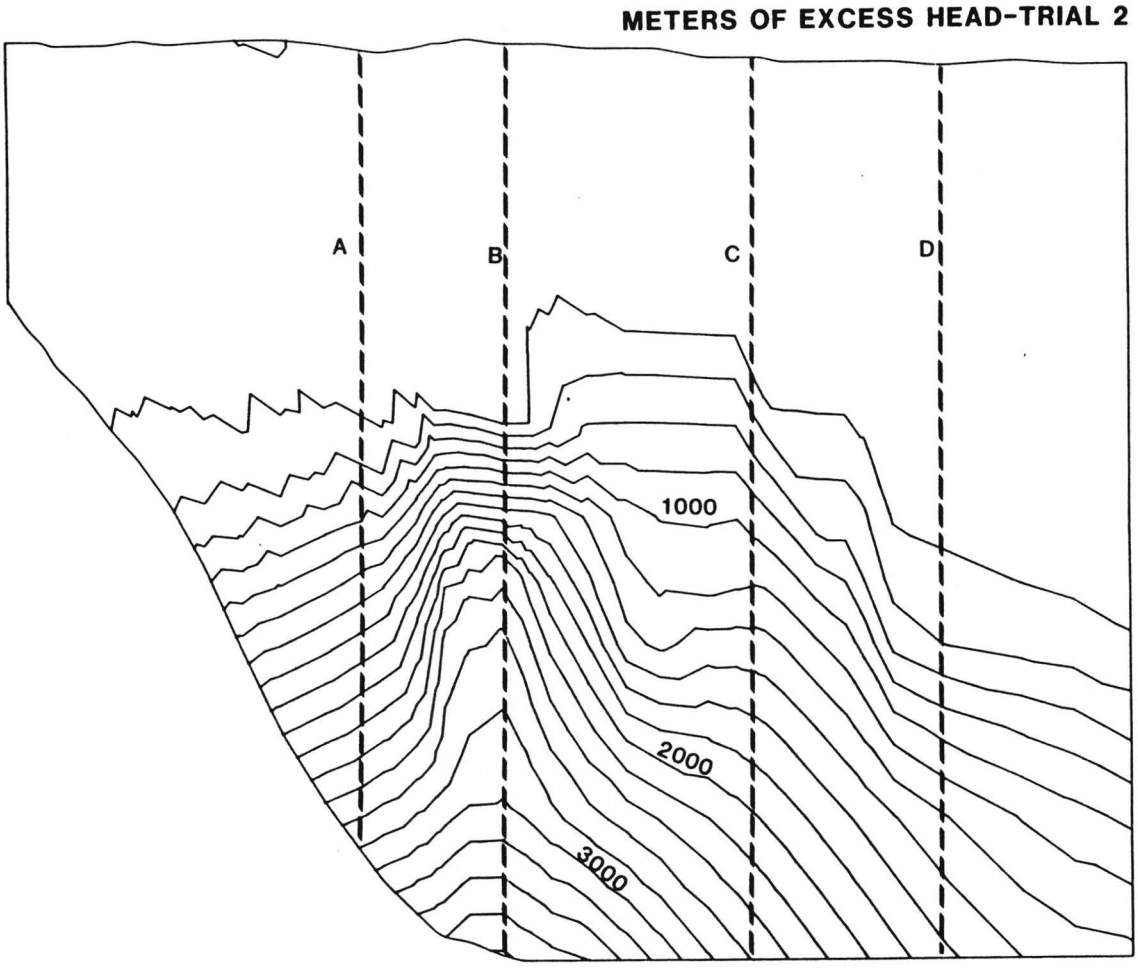


**Figure 2.21**: Hydraulic head generated by the model for Simulation Two. Dashed lines show location of pressure profiles in Figure 2.22.

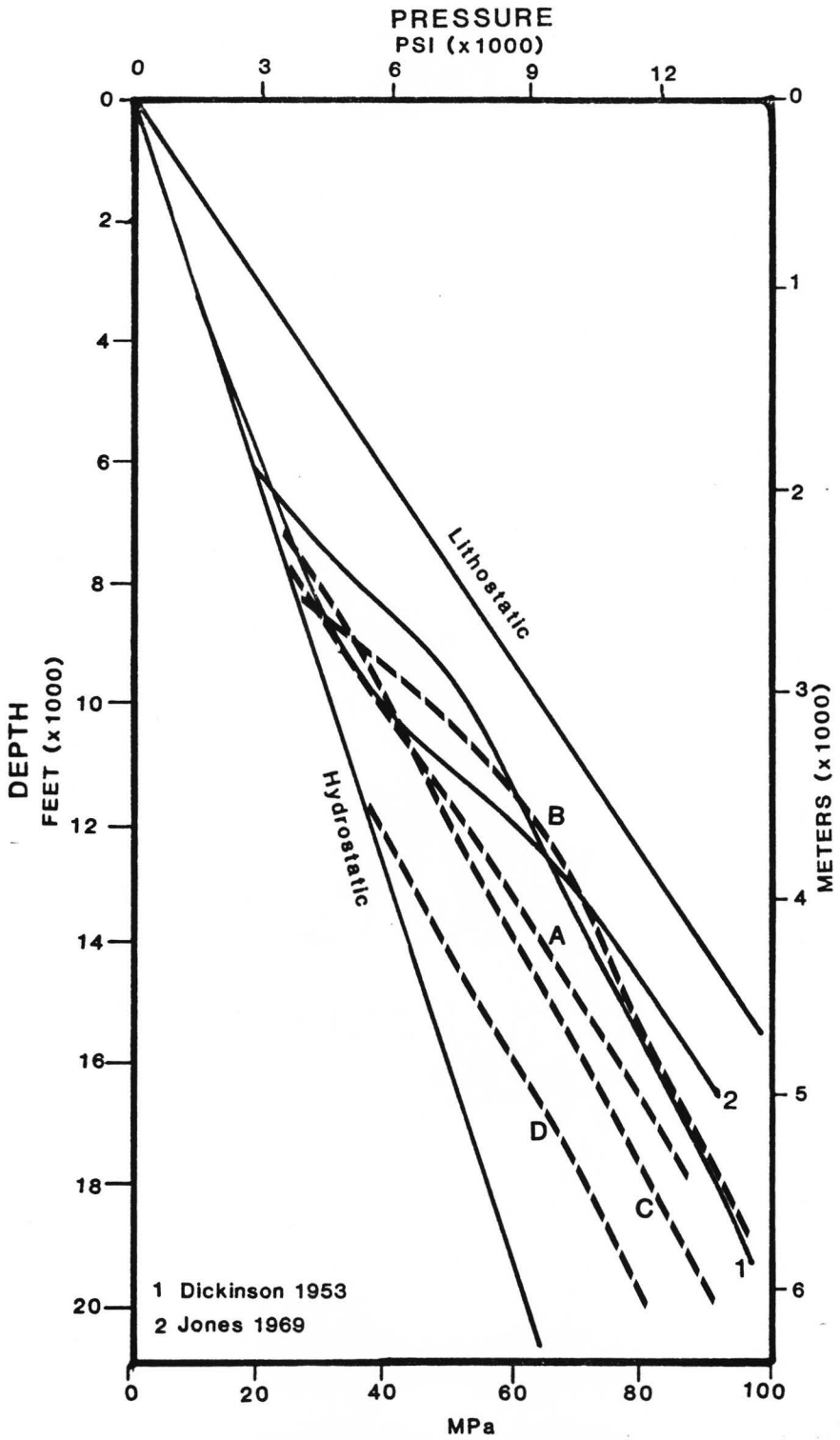


**Figure 2.22**: Pressure profiles for Simulation Two. Dashed lines show modeled pressure- profiles keyed in Figure 2.21. Solid lines 1 & 2 show generalized profiles for Gulf Coast.

corresponding to the Frio Formation, shows lower overpressures, as would be expected in an area of higher sand content and permeability.

Temperature. The temperature contours modeled in Simulation Two are shown in Fig. 2.23. The match with the data is better here as well. The modeled isotherms stay within the error margins in most places. Some discrepancies appear along the 350 and 400°C isotherms just southeast (right) of the Wilcox growth-fault zone, where temperatures are once again somewhat cool relative to the data. This trend is also evident in the temperature-vs.-depth profiles of Figs. 2.24 through 2.27, where the modeled temperatures fall consistently below the general trend indicated by the BHT measurements. No manner of fluid flux could lessen these decrepancies without disrupting the rest of the cross-section.

The Flow Regime. Fig. 2.28 differs little in appearance from Fig. 2.16. In each, the direction and magnitude of fluid movement appear quite similar. However, as previously mentioned, the flow rates are so low in the geopressured zone that differences within this zone do not show on the diagram. Appendix F lists the velocities from this figure. The highest values for the meteoric zone are on the order of $10^{-8}$ m/s. In the geopressured zone where fluids are concentrated, velocities are about $10^{-11}$ m/s, and drop off elsewhere in the geopressured zone to as low as $10^{-14}$ m/s.

## 2.4.5 SIMULATION THREE - MIXED CONDITIONS

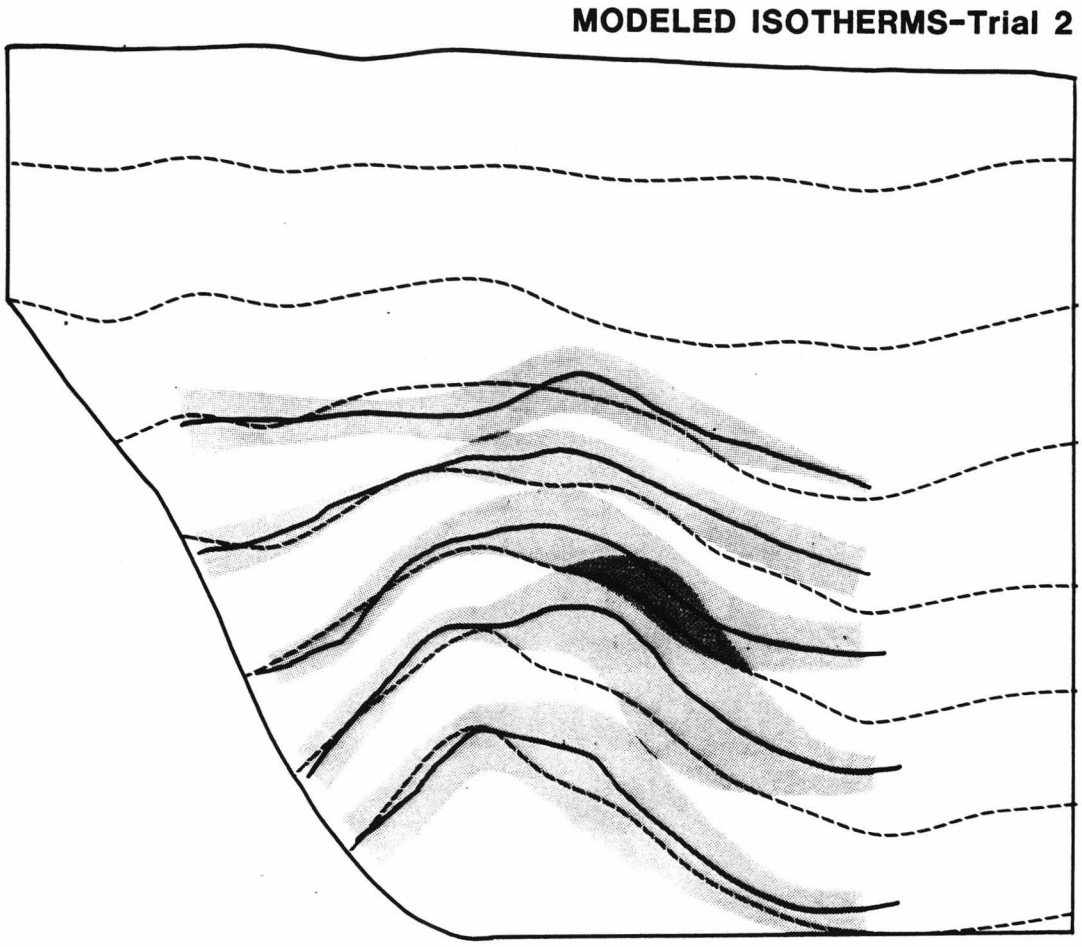


**Figure 2.23**: Modeled isotherms for Simulation Two shown by the dashed lines; solid lines indicate isotherms from kriged BHT data with the grey shaded areas showing their standard deviations.

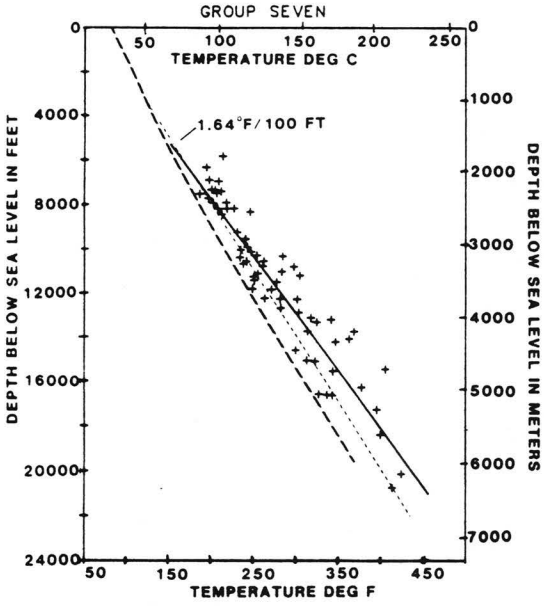


Figure 2.24

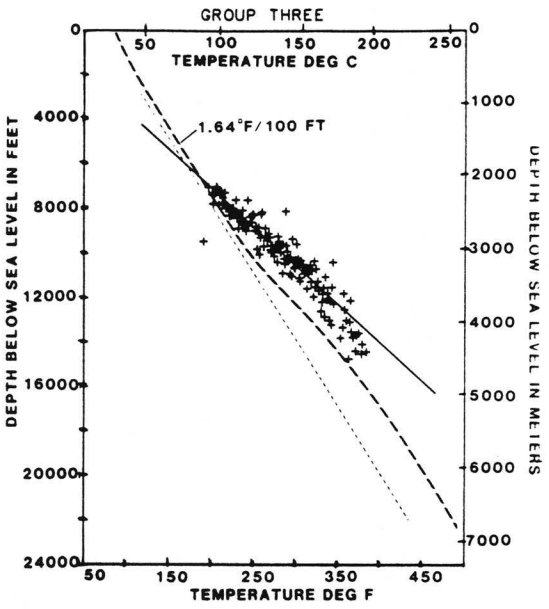


Figure 2.25

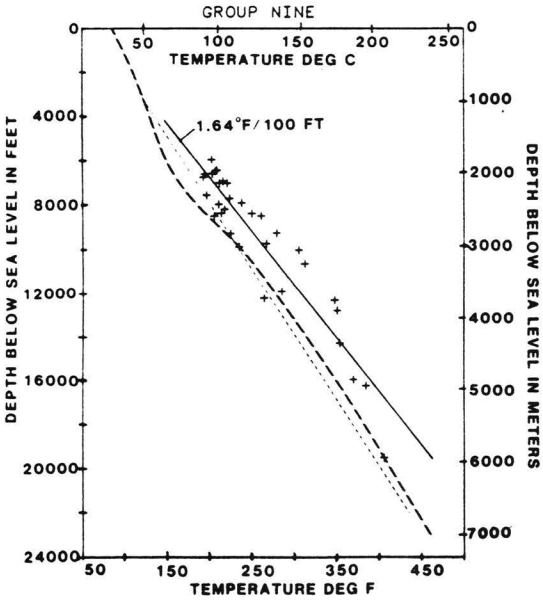


Figure 2.26

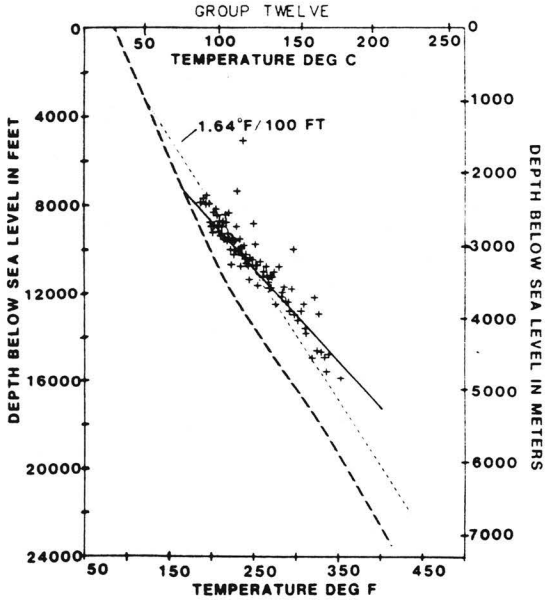


Figure 2.27

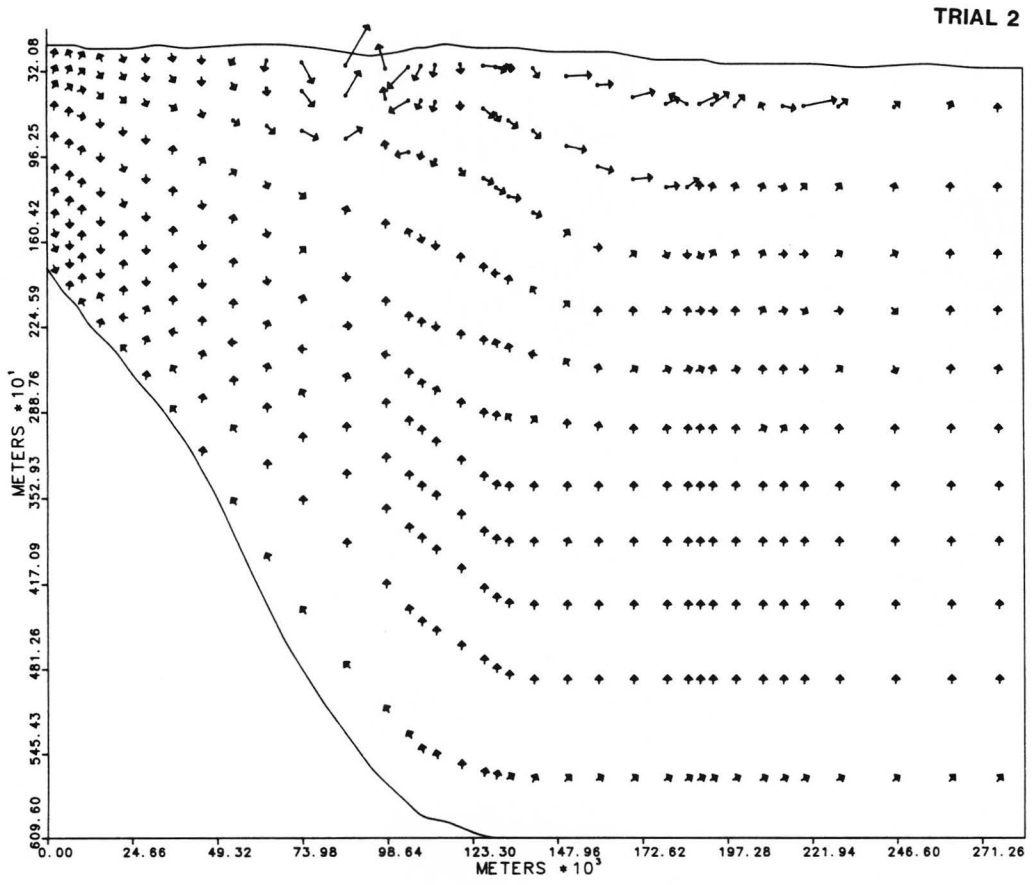


**Figure 2.28**: Simulation Two flow velocity vectors.

Simulation Three evolved from Simulation Two after successive refinements. The suite of code maps are shown in figs. 2.29 through 2.32. Porosity and fluid fluxes are essentially unchanged and the permeabilities are also very similar, excepting the addition of a speculative zone of high thermal and hydraulic conductivity located southeast (right) of the Wilcox growth-faults, which was added to simulate the isotherms more closely than in Simulation Two. The differences in the code maps between Simulation Two and Three are centered around the addition of this body. In conjunction, the depth of influence of the Carrizo-associated fault was decreased as indicated in Fig. 2.30.

## 2.4.6 SIMULATION THREE - RESULTS

Fluid Pressure. The fluid pressures are quite similar in this simulation to those from Simulation Two as illustrated in Fig. 2.33. The pressure profiles (Fig. 2.34) are consequently also quite similar and agree well with the available data.

Temperature. Simulation Three produced temperature isotherms which correspond very closely to the data, as seen in Fig. 2.35. The major discrepancies which appeared in Fig. 2.23 from Simulation Two were largely eliminated in this simulation. An even better indication of the success of this simulation are the Temperature-vs.-Depth profiles in Figs. 2.36 through 2.39. The correlation of the model to the data is nearly perfect for all four profiles.

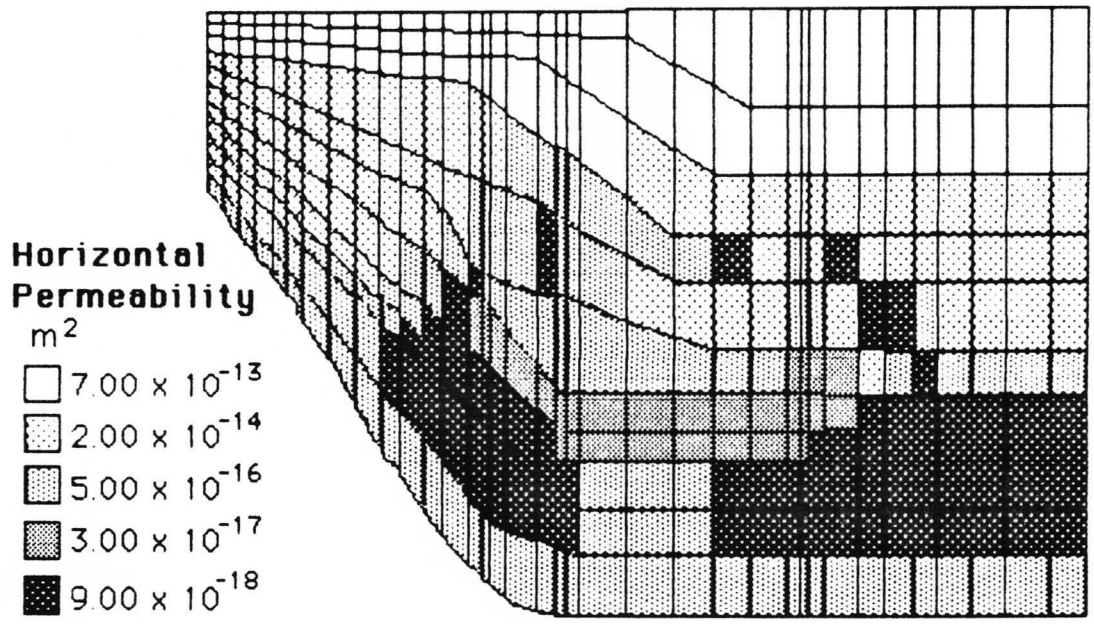


Figure 2.29

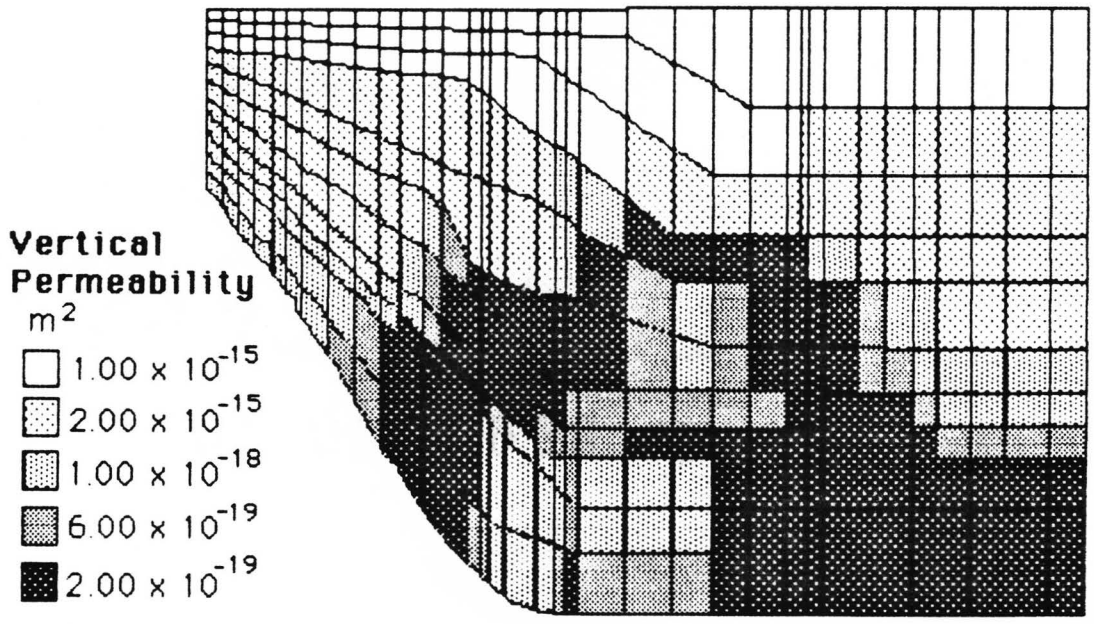


Figure 2.30

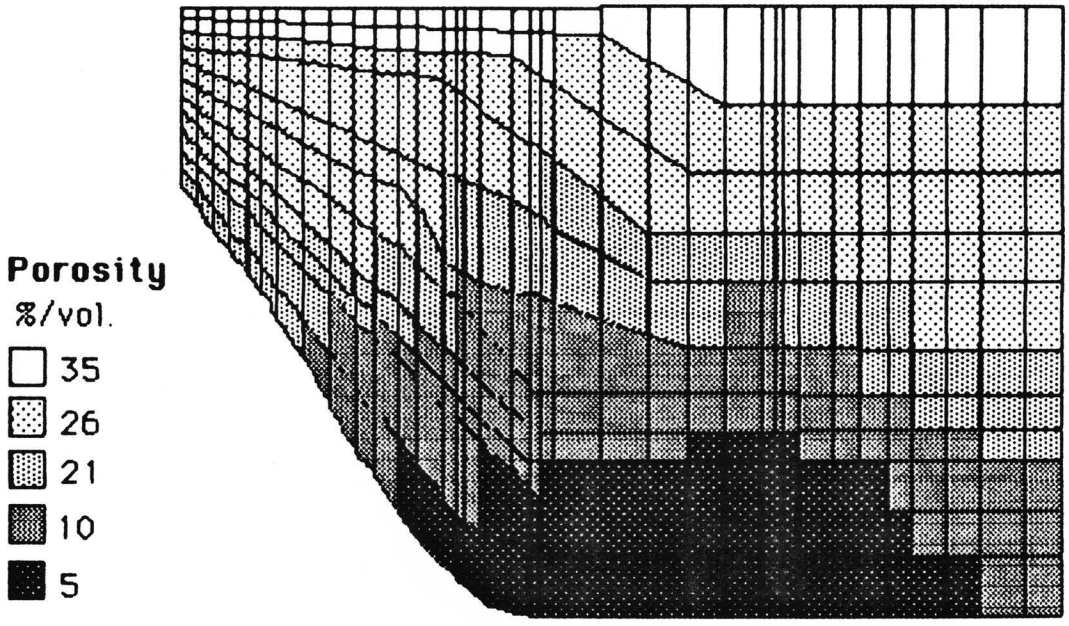


Figure 2.31

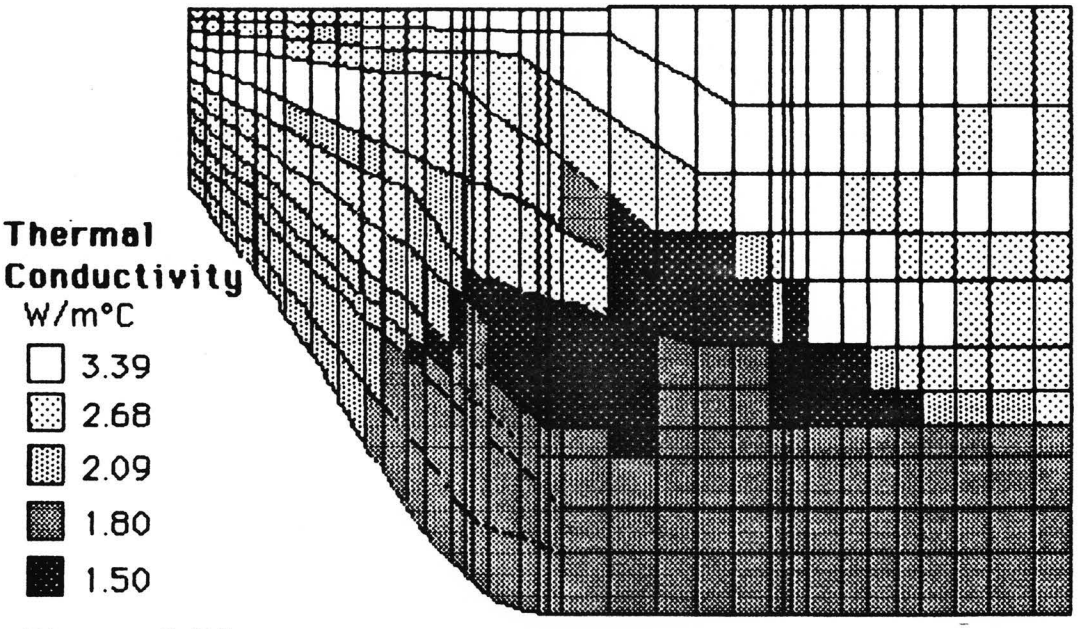


Figure 2.32

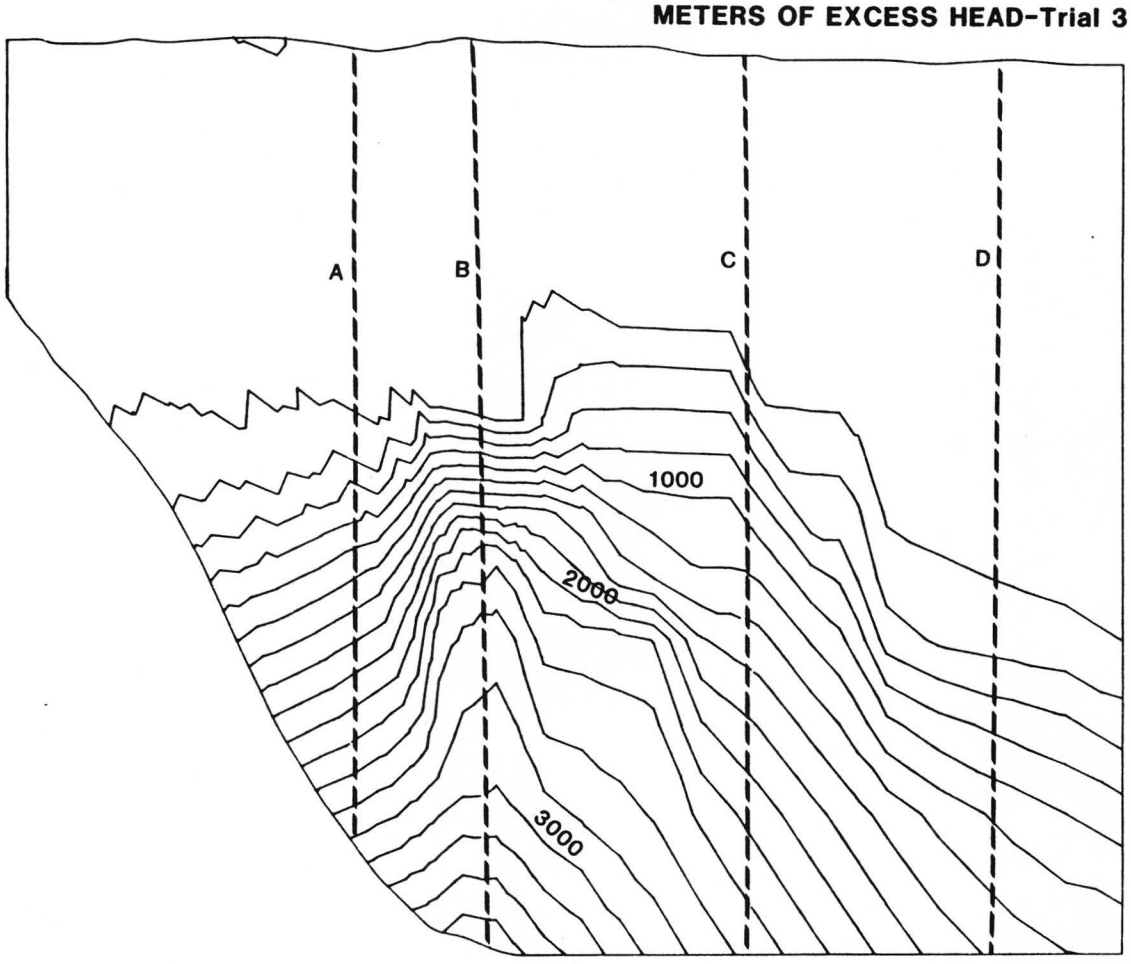


**Figure 2.33**: Hydraulic head generated by the model for Simulation Three. Dashed lines show location of pressure profiles in Figure 2.34.

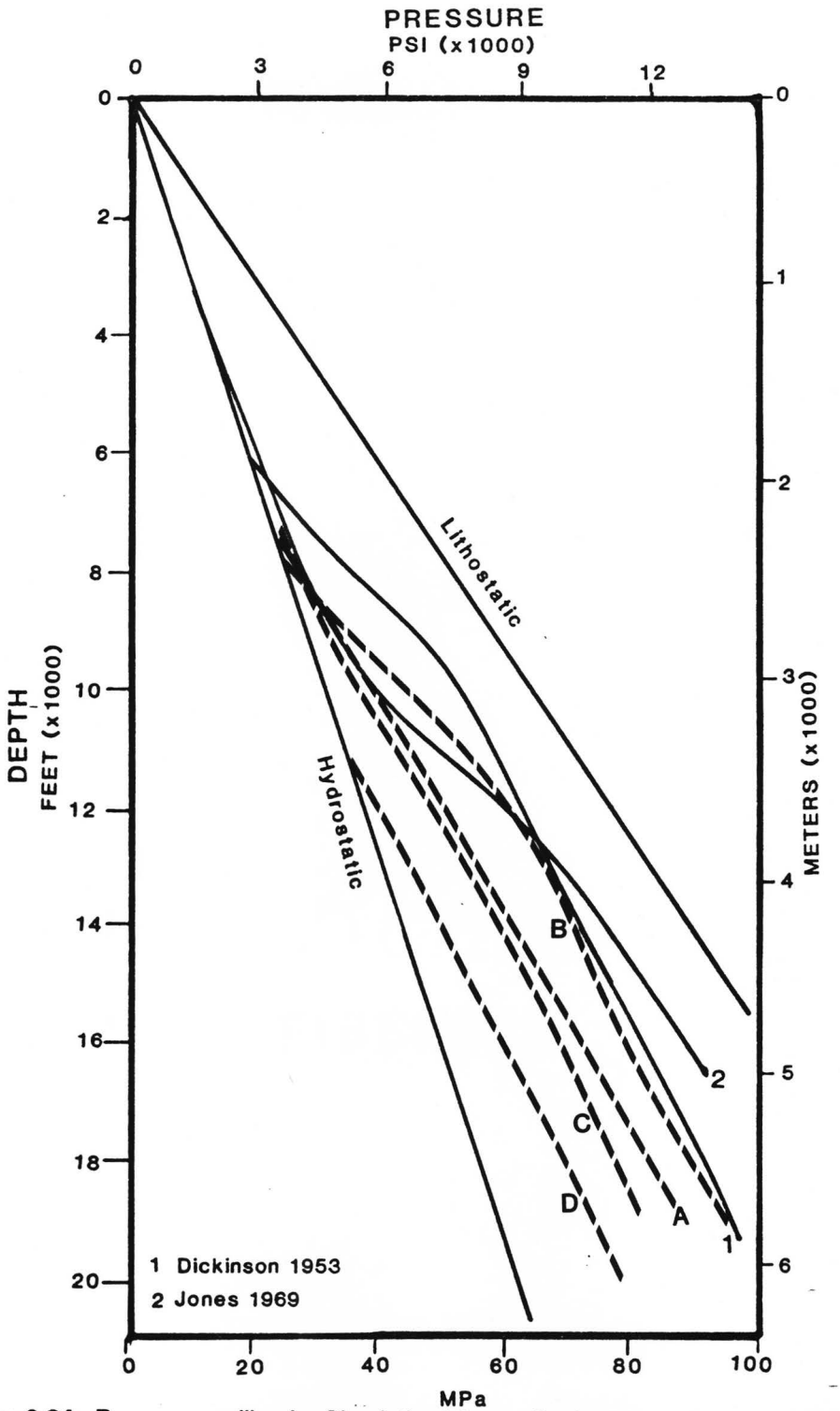


**Figure 2.34**: Pressure profiles for Simulation Three. Dashed lines show modeled pressure- profiles keyed in Figure 2.33. Solid lines 1 & 2 show generalized profiles for Gulf Coast.

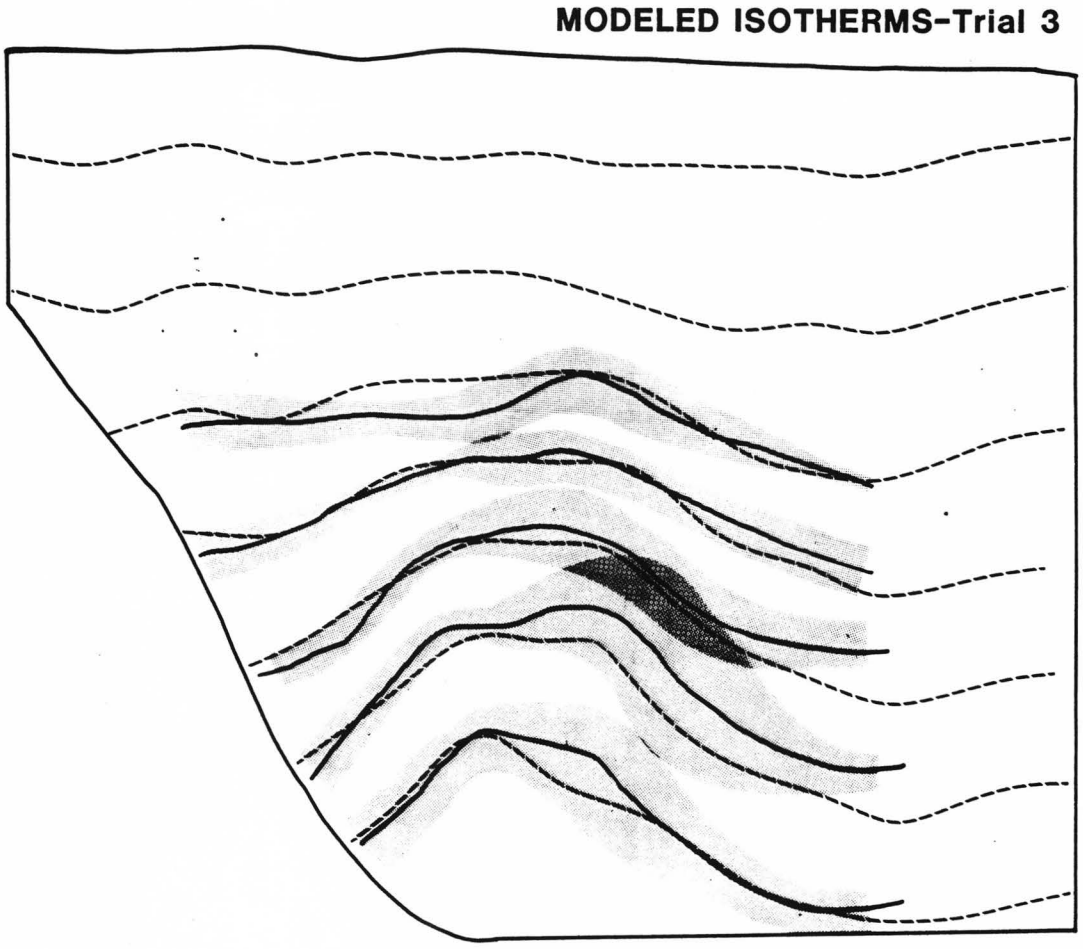


**Figure 2.35**: Modeled isotherms for Simulation Three shown by the dashed lines; solid lines indicate isotherms from kriged BHT data with the grey shaded areas showing their standard deviations.

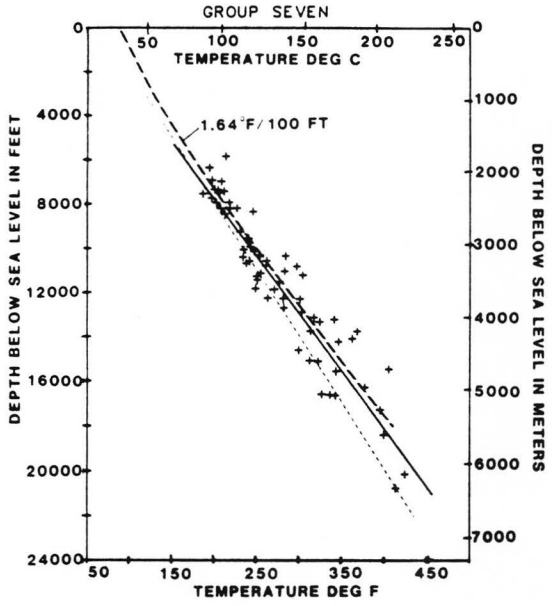


Figure 2.36

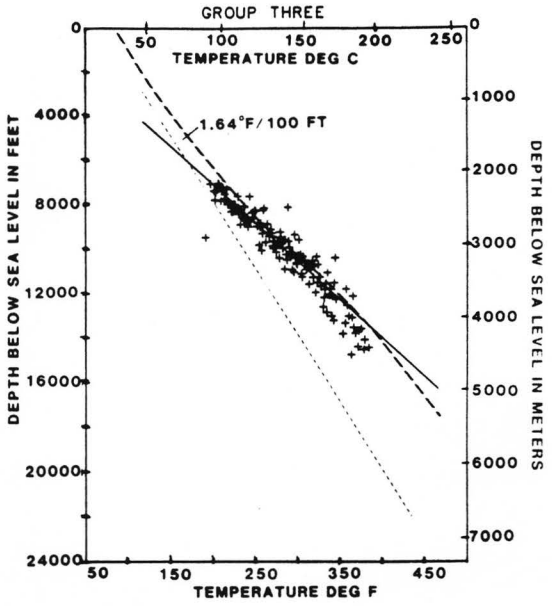


Figure 2.37

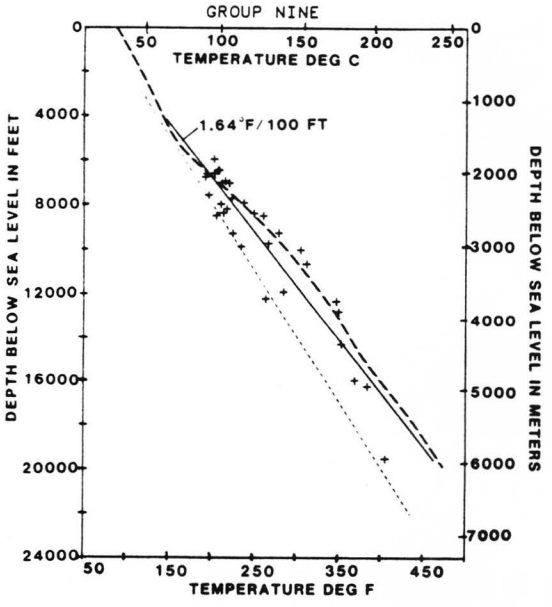


Figure 2.38

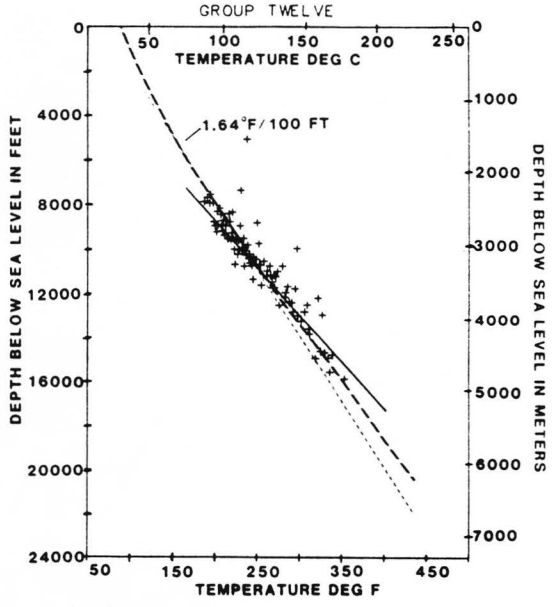


Figure 2.39

The Flow Regime. Once again, the fluid velocity vector plot (Fig. 2.40) is nearly identical to the other simulations, and is especially similar to simulation two, as would be expected, since conditions governing the basic flow regime were essentially unchanged between simulations Two and Three. Appendix F lists the velocities for each element.

## 2.5 DISCUSSION

As a result of the three simulations, I conclude that dispersed advection coupled with geopressure-dominated conduction is an inappropriate model for the Gulf Coast Basin of South Texas. Simulation One tested this hypothesis and failed to simulate either the basinal temperatures or the pressure data. Markedly better results were obtained in Simulation Two where concentrated flow was introduced in the growth-faulted zone associated with the Wilcox Group. The third simulation evolved from refinements to Simulation Two and achieved a close match to the calibrating criteria. The major adjustment was the addition of a hypothetical area of high thermal and hydraulic conductivity placed just coastward of the Wilcox growth faults.

### 2.5.1 IMPLICATIONS OF THE MODEL

Although the digital model cannot provide a unique solution, the simulations do provide insights into the operative geological processes.

The flux of fluids were all assigned along the basal boundary at a depth of 20,000 feet (6096 m) because the sensitivity analysis showed

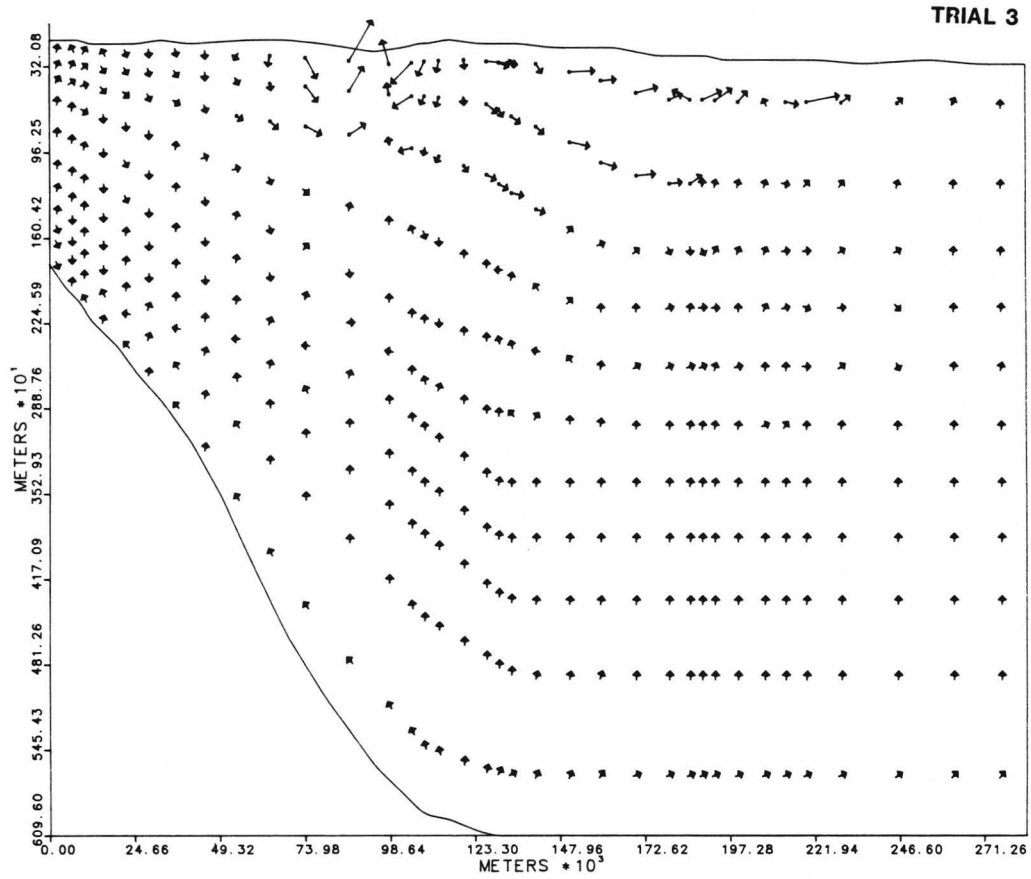


**Figure 2.40**: Simulation Three flow velocity vectors.

that this was the best placement of the flux nodes. Compactional fluids should be supplied diffusely throughout most of the section, predominantly by consolidating clays and shales, which are abundant above as well as below the basal boundary. The model, however, implies that most compactional fluids are from sediments below the basal boundary at 20,000 feet (6096 m), contradicting a study by Magara (1976) which places the maximum cumulative volume of expulsed fluids at about 11,000 feet (3353 m). (Magara calculated this assuming fluid release resulting only from the steady consolidation of a typical Gulf Coast sediment-pile.) Furthermore, not only were the fluxes sourced from the basal boundary, but in Simulations Two and Three, the fluxes were also concentrated along the boundary under the growth faults, implying that not only are the fluids supplied from great depths, but that they have been focussed at these depths.

The treatment of fault permeabilites opens other avenues of speculation. The deepest portion of the Wilcox growth fault zone was assigned higher vertical permeability ($1.0 \times 10^{-18}$ $m^2$) than the surrounding rock. At intermediate depths still within geopressure, the higher permeabilities were discontinued. In a test simulation without this termination, fluids escaped the geopressured zone, leaving a large temperature plume penetrating the meteoric zone, with little geopressuring left at depth. The configuration presented thus supports the premise that faults leak fluid, but do not do so along their entire length. How faults might become sealed at intermediate depths is open to speculation. Perhaps the shales become more consolidated and more

brittle at depth, healing the faults more easily at intermediate depths, but leaving the faults open further below. There might also be greater fault movement in the deep basin. Finally, there is an unassessed potential for hydraulic fracturing. The fault zone may be particularly susceptible to microfracturing because of the existing faults and associated structural flaws . Furthermore, since the occurrence of microfracturing is dependent on high fluid pressure, suitable conditions may exist at greater depths. In short, it is not difficult to formulate several ways in which the configuration of the growth fault zone modeled in Simulation Two and Three might be produced in nature.

Shallower faults in the Catahoula Formation were modeled in a similar way, with higher permeabilities terminated just below the top of geopressure. Uranium deposits in the meteoric portions of these faults, similar to those studied by Galloway (1982), indicate that pulses of fluid have periodically moved up these faults. Therefore, probably during periods of fault movement, higher permeability did extend up through the top of geopressure. This was apparently a temporary situation. The faults may have become plugged near the geopressure boundary, as configured. Causes could be rapid cementation or the fast healing of poorly consolidated sediments, especially aided by high differential stresses at these shallow depths. W. E. Galloway (personal communication, 1985) states that there is little indication, at least at shallow depths, of extensive plugging due to cementation.

The most puzzling aspect of Simulation Three is the speculation of a zone of high hydraulic and thermal conductiviy. Despite

that fact that the temperature contours most closely linked to this hypothesis also exhibit the largest standard deviations, comparison with the data points plotted on the temperature-vs-depth profiles argue persuasively that the temperature trends are real and that Simulation Three offers a possilbe solution to the temperature distribution. This region, if it exists, could best be explained by the presence of salt diapirs, the salt itself being virtually impermeable but of high thermal conductivity, while the diapirism can lead to overlying faulting and good vertical permeability. S. Seni and W. Mullican (personal communication, 1985) confirm that salt is present in this portion of the basin at the depths corresponding to the hypothetical zone. This salt may be in the form of salt pillows at various stages of maturity, and perhaps also diapiric structures. Several shallower salt structures in the form of salt domes have been identified in the region, including the Moca Dome, the Palangana Dome, and the Gyp Hill Dome, although W. E. Galloway (personal communication, 1985) suggests that the overall presence of salt in this region may not be very extensive.

Thus far, we have assumed that the model is useful in providing insights into the processes within the study area. However, unknowns preclude a unique solution. One of these is the problem of fluid flux. The estimate using chloride concentrations shows that the fluxes modeled are reasonable for present day conditions. However, these values are not volumetrically possible if they have been maintained over the history of the basin. They are in fact, more than an order of magnitude too large for this. Other flow estimates have been made based on various

observations such as the volume of cementation in the basin (Land, 1984, Table 2). These estimates have consistently been above flow rates that are volumetrically reasonable. My simulation adds one more high estimate to the pile.

A host of alternatives can be invoked to explain this discrepancy. One possibility is that the temperature data are seriously skewed. This is unlikely because the data base is large and the consistency of the data is good. Recall from Part One that the correlation coefficients for the thermal profiles were all above 90%. The steady-state assumption of the model is another possible contributing source of error. The flow rates may indeed be correct, but are transient, and have not persisted for a significant geologic period of time. Finally, error may have been introduced in the method employed to simulate compactional fluid flux. In reality, the volume of fluid moving out of the basin as a result of consolidation must be about equal to the volume loss of the consolidating sediments. Since the model does not compact, this inverse relationship does not occur. It is not know how significant this limitation is, but for the purpose of this investigation it was assumed to be insignificant.

If the flow rates are correct, then perhaps there are other sources for the fluids besides compaction. A source from outside the modeled portion of the basin or from the Cretaceous sediments cannot not be ruled out, nor can the possible occurrence of some type of free convection, in which fluids flow in recirculating cells. Because fluids recirculate, much more flow can be generated for a given volume of fluid.

Convection cells might occur on a small scale, such as within a local sediment package or sand-body, or they might also exist on a much grander scale, where faults function as the vertical portion of the cell, and horizontal bedding planes and cross-bedding flow function to complete the cycle. Descending legs of the cells may be located off-shore and also northwest of the cross section, in the shallower Cretaceous.

A limitation of the model is the inability to account for the dependence of fluid density on dissolved chemical species. The model uses pure water as the fluid. But the deep-basinal brines may be more dense than pure water and would therefore require greater fluxes or other forces to concentrate them into upwelling plumes. However, if fluids released by consolidating clays are fresher than these brines, (Kharaka and others,1980; Price,1976; Russell,1971), then these fluids would also be less dense than the brines. Consequently, upon release, if mixing were limited, these fluids would be buoyed upward, creating upwelling plumes of fluids where conditions were appropriate, and requiring less fluid flux from below to drive the flow. In this way, a sufficient upward flow could be sustained to account for the temperature distribution while requiring smaller overall fluid fluxes. Such an explanation would unfortunately unbalance the chloride concentration calculation.

Clearly, much work remains in deciphering the hydraulic and thermal regimes of the Gulf Coast Basin. This research has hopefully provided a spring-board for further research and insight into the complex

nature of this system.

# CONCLUSIONS

Having compiled and assembled sufficient data to characterize the thermal distributions in a portion of the Tertiary rocks of the South Texas Gulf Coast Basin, it is evident that regional-scale processes are at work modifying the heat flux above the Cretaceous boundary. The most prominent feature of the temperature distributions is an arc-shaped region of high temperatures which correspond to the growth fault zone of the Wilcox Group. The anomaly begins to emerge at 10,000 feet (3048m) and becomes increasingly pronounced toward 20,000 feet (6096m), beyond which depth there are no data. Although high porosities associated with geopressures have been linked to lower thermal conductivities and higher geothermal gradients, this mechanism does not explain why the temperatures and gradients are highest in the faults zones, and lower in adjacent areas with similar geopressures. Instead, the fault zones themselves seem to be important, perhaps serving as conduits for vertical flow. The configuration of the thermal

ridge implies upwelling from below the 20,000 foot (6096m) extent of data.

This largely empirical method of deciphering the cause for the observed temperatures is limited because of the complexity of the problem. It is complex because many factors can influence temperature, including the nature of the heat source, thermal properties of the sediments, the thermal properties of the fluids which saturate the sediments, the hydraulic properties of the entire system through which the fluids move and advect heat, and the chemical behavior and interaction of the sediments and the fluids. Numeric modeling provides a way of accounting for these factors in a coordinated and quantitative way.

The modeling effort provided additional support for the hypothesis that upwelling fluids are the major cause of the thermal anomaly in the Wilcox trend. For example, it was determined that the optimum placement of flux nodes was along the basal boundary of the model, with the flux concentrated along the Wilcox fault zone. This configuration supports the initial inference that upwelling occurs from below 20,000 feet (6096m), implying in addition, that the flow is focussed at these depths. Permeabilities configured for the model allow flow pathways along the growth fault zone, but only within the deeper portions of the zone. The model calls for a sealing of the fault zone at intermediate depths nearing the top of geopressure. Speculative plugging mechanisms include cementation, differential healing of faults, differential fault movement and displacement, and depth constrained

microfacturing. A puzzling aspect of the model is the call for a zone of high hydraulic and thermal conductivity coastward of the deep Wilcox growth faults. This region, if it exists, could be explained by the presence of salt diapirs, the salt itself being virtually impermeable but of high thermal conductivity, while diapirism can lead to faulting and good vertical permeability.

The model leaves unsolved a problem common to numerous other studies involving fluid movement in the basin. Namely, that the fluid fluxes called for are beyond what can be supplied from compactional processes alone. Studies of dissolution and cementation call for fluxes that are even greater. For this reason, the occurrence of free convection has been suggested. It may occur on both a local and regional scale. Regionally, growth faults may be integrated into the circulation of convection cells, a circulation which would presumably be confined to the compactional system since fluids could not freely convect downward across the geopressure transition.

There is clearly much work still needed to decipher the hydraulic and thermal regimes of the Gulf Coast Basin. This research has hopefully provided a spring-board for further research and insight into the complex nature of this system.

# APPENDIX A - DATA

This appendix contains first a complete listing of the names of the well-data base, followed by the file of all the data which is associated with each well. They can be cross referenced using the well number.

| Township Range | Well No. | Well Name |
|---|---|---|
| 11S 21E | 26 | Harkins,#B-1 Fimbel |
| 11S 21E 1 | 27 | Assoc O&G et al,#1Van Dohlen |
| 11S 21E 3 | 28 | Hewitt,#1 Baker |
| 11S 21E 9 | 29 | Plymouth,#1 Thompson |
| 11S 21E 1 | 30 | Hewitt,#1 Hall |
| 11S 21E 1 | 31 | Assic O&G et al, #1 Cunningham |
| 11S 21E 1 | 32 | Texas O&G,#1 "A" Richter |
| 11S 22E 3 | 33 | Texas O&G,#1 Earp |
| 11S 22E 1 | 34 | Shell,#1-A Bego |
| 12S 21E | 35 | Plymouth,#1 Thompson |
| 9S 17E 1 | 36 | Standard,#1 Rzeppa |
| 9S 17E 2 | 37 | Standard,#1 Moczygemba |
| 9S 17E 3 | 38 | Mortimer et al,#1 Dzuik |
| 9S 17E 2 | 39 | Coastal States,#1 Kowalik |
| 9S 17E 2 | 40 | Standard,#1 Pollok |
| 9S 18E 7 | 41 | Standard,#1 Pace |
| 9S 19E 7 | 42 | Tex East. Trans.,#1 Garbe |
| 9S 19E | 43 | Tex East. Trans.,#1 Mugge |
| 9S 19E | 44 | Tex East. Trans.,#2 Voelkel |
| 9S 19E 7 | 45 | Tex East. Trans.,#1 Woskow |
| 9S 19E 8 | 46 | Standard,#1 Tipton |
| 9S 19E | 47 | Mustang,#1 Yanta |
| 9S 19E | 48 | Occidental,#1 Osterloh et al. |
| 9S 19E 6 | 49 | Hunt Est.,#1 Schuenemann |
| 9S 19E 8 | 50 | #1 Flenniken |
| 19S 20E | 51 | Southland,#1 Responder |
| 19S 20E | 52 | Ranger,#1 Clark |
| 19S 20E | 53 | Tidewater,#1 Musselman |
| 19S 20E 5 | 54 | Hamon,#1 Roeder |
| 19S 20E 8 | 55 | Hanson et al.,#1 Altman |
| 19S 20E 1 | 56 | Southland,#1 Gips |
| 19S 20E 7 | 57 | McCulloch,#1 Franke |
| 19S 20E 7 | 58 | Monsanto et al.,#1 Green |
| 19S 20E 8 | 59 | Monsanto et al,#1 Kolodzeg |
| 19S 20E 7 | 60 | Monsanto et al.,#1 Estrella |
| 19S 20E 5 | 61 | Tidewater,#1 Korth |
| 19S 20E 1 | 62 | Harper-Smith,#2 Gips |
| 19S 20E 2 | 63 | Hamon & Ehman,#1 Kleberg |
| 19S 20E 8 | 64 | Murphy Baxter,#1 Hilgartner |
| 19S 20E 3 | 65 | Untex,#1 Warwas |
| 19S 20E 7 | 66 | McCulloch,#1 Hurst et al. |
| 10S 17E 9 | 67 | Delta Am, #1 Sahm |
| 10S 17E 7 | 68 | General Crude,#1 Gunewald |
| 10S 18E 9 | 69 | General Crude,#1 McDowell |
| 10S 18E 7 | 70 | Atlantic Ref.,#1 Pullin et al. |
| 10S 18E 6 | 71 | General Crude,#1 Wessendorff |
| 10S 18E | 72 | Bruns,#1 Tips |
| 10S 18E 3 | 73 | Harrison,#1 Hysaw et al. |
| 10S 18E 5 | 74 | Hunt,#1 Huckman |
| 10S 19E 9 | 75 | Shell,#1-R Atkinson |
| 10S 19E 8 | 76 | Hunt,#1 Zavesky |
| 10S 19E 2 | 77 | Argo,#1-A Dittmer Est |
| 10S 19E 5 | 78 | Cities,#1 Stanchos "A" |
| 10S 19E 6 | 79 | Cities,#1-A Janssen |
| 10S 19E 5 | 80 | Cities,#1-A Pargmann |
| 10S 19E 1 | 81 | Kirk & Neeb,#1 Mueller Est. |
| 10S 19E 1 | 82 | Cities,#1-A Gaus |
| 10S 19E 7 | 83 | Nat. Explor. Co.,#1 Effenberger |
| 10S 20E 8 | 84 | Continental,#42 Pettus |
| 10S 20E 6 | 85 | Lone Star,#1 Jank |
| 10S 20E 3 | 86 | Getty,#11 Nordheim |
| 10S 20E 3 | 87 | Southland,#1 Fuhrken |
| 9S 13E 4 | 88 | Continental,#1 Taylor & Brow |
| 9S 13E 7 | 89 | Corthay Land,#1 Brite |
| 9S 14E 1 | 90 | Exxon,#1 Heinen |
| 9S 14E 3 | 91 | Sorelle & Sorelle,#1 Heinen |
| 9S 14E 7 | 92 | Smith,#1 Westland |
| 9S 16E 6 | 93 | Seaboard,#2 Gabrysch |
| 9S 16E 2 | 94 | Coloma,#2 Dzuik |
| 9S 16E | 95 | Seaboard-Hamon,#1 Szalwinski |
| 9S 16E 8 | 96 | Viking,#1 Clark |
| 9S 16E | 97 | Renwar et al.,#1 Franklin |
| 10S 15E 6 | 98 | Burnwell,#1 Pfiel |
| 10S 15E 7 | 99 | Harkins,#1 Zunker |
| 10S 15E 4 | 100 | Continental,#1 Stienle |
| 10S 16E | 101 | Filon,#1 Sturcken |
| 10S 16E 8 | 102 | Hundt,#1 Hardt |
| 11S 13E 9 | 103 | Dougherty,#1 Henry |
| 11S 15E 1 | 104 | Steward,#1 Mcilvaine et al |
| 11S 15E 8 | 105 | Buzzini,#1 Seale |
| 12S 13E 8 | 106 | Continental,#1 Horton |
| 12S 13E 6 | 107 | Tenneco,#1 Jamber |
| 12S 14E 4 | 108 | Chiles,#1 Morril |
| 12S 14E 8 | 109 | Tex East.Trans,#1-A Atkinson |
| 12S 15E 4 | 110 | Glasscock,#1 Terrel |
| 12S 15E 7 | 111 | Tenneco,#1 Schulz |
| 12S 16E 2 | 112 | Pickens,#1 Meyer |
| 12S 16E 8 | 113 | Vreeland,#1 Probst |
| 12S 16E 8 | 114 | Burns,#1 Stidde |
| 12S 16E 1 | 115 | Shell,#2 Turner |
| 12S 16E 1 | 116 | Shell,#1 Overby |
| 12S 16E 7 | 117 | Texas O&G,#1-C Smith |
| 12S 16E 1 | 118 | Shell,#1 Leppard |
| 12S 16E 1 | 119 | Shell,#1 Currer |
| 12S 16E 2 | 120 | Shell,#2 O'Neal |

| Township Range | Well No. | Well Name |
|---|---|---|
| 12S 16E 1 | 121 | Shell,#1 Turner |
| 12S 16E 8 | 122 | Shell,#1 Braune |
| 12S 11E 1 | 123 | Pan Amer,#1 Franklin |
| 12S 12E 6 | 124 | Colo Oil,#1 Roark |
| 12S 12E 1 | 125 | Humble,#B-1 Gubbels |
| 12S 12E | 126 | Supron,#1 Henry |
| 9S 9E | 127 | Magnolia,#1 McKinley |
| 9S 12E 9 | 128 | Skelly,#1 Winkler |
| 10S 9E 5 | 129 | Pan Amer,#1 Oppenheimer |
| 10s 11E 4 | 130 | Gulf,#1 Reese |
| 13S 14E 3 | 131 | Standard,#1 Calliham |
| 13S 14E 1 | 132 | Standard,#1 Isaacks |
| 13S 15E 7 | 133 | Kilroy,#2 McClelland |
| 13S 16E 9 | 134 | Western Nat.,#1 Harris |
| 13S 16E 8 | 135 | Carrl,#1 Smith |
| 13S 16E 2 | 136 | Peet,#1 Goebel |
| 13S 16E 2 | 137 | Coloma,#1-A Dove |
| 13S 16E 1 | 138 | Hanson et al,#1 Maguglin |
| 13S 16E 8 | 139 | Coastal St,#1 Morrison |
| 13S 16E 1 | 140 | Texas O&G,#1 Maguglin |
| 13S 16E 1 | 141 | Sinclair,#3 Dilworth |
| 13S 16E 9 | 142 | Shoreline,#1 Bartlett |
| 13S 16E 4 | 143 | Texas O&G,#10 McClelland |
| 13S 16E 8 | 144 | Love et al,#1 McMurray |
| 13S 16E 8 | 145 | Jones et al,#1 Martin |
| 13S 16E | 146 | Newman,#1 Edwards |
| 13S 16E 9 | 147 | Huisache,#1 Allen |
| 13S 16E 7 | 148 | Texas O&G,#1-A Dunn |
| 13S 16E 7 | 149 | Continental,#1 McKinney |
| 13S 16E 4 | 150 | Neumin,#1 Hinton et al |
| 13S 16E 7 | 151 | Nat. Explo,#1 McKinney et al |
| 14S 14E 8 | 152 | Meeker,#1 Lebman |
| 14S 14E 9 | 153 | Kilroy,#1 Hays-Ezzell |
| 14S 14E 4 | 154 | Texam,#1 Hays-Ezzell |
| 14S 14E 1 | 155 | Kilroy,#1 Herring |
| 14S 14E 1 | 156 | Kilroy,#2 Herring |
| 14S 14E 9 | 157 | Kilroy,#2 Hays-Ezzell |
| 14S 14E 6 | 158 | Tenneco,#1 Stephens |
| 14S 15E 7 | 159 | Getty,#1 Christenson |
| 14S 15E 1 | 160 | Pen Oreille,#3 Nelson Tr |
| 14S 15E 7 | 161 | Limes,#1 Houdmann |
| 14S 15E 6 | 162 | Hanson,#1 Prosen |
| 14S 15E 8 | 163 | LaGloria,#1 Bush |
| 14S 15E 8 | 164 | Kilroy,#1 Beirwith |
| 14S 15E 9 | 165 | Atlantic Rich,#12 Lyne |
| 14S 15E 6 | 166 | So Petro,#1 West |
| 14S 15E 9 | 167 | Warren,#1 Whitley-Johnson |
| 14S 15E 3 | 168 | Inter. Amer.,#2 Herring |
| 14S 15E 3 | 169 | Venus,#1 Schreiner |
| 14S 15E 9 | 170 | Mesa,#1 Johnson |
| 14S 15E 1 | 171 | Coastal St.,#1 Lukas et al |
| 14S 15E 5 | 172 | Atlantic Rich,#2 Richter |
| 14S 15E 1 | 173 | Hanover,#1 Fair |
| 14S 15E 5 | 174 | Hamon-Carl,#1 Katzfey |
| 14S 15E 5 | 175 | Hamon-Carl,#1 Ybaney |
| 14S 15E 6 | 176 | Argo,#1 Braslau |
| 14S 15E 6 | 177 | Hughes,#1-A W Townsite |
| 14S 15E 6 | 178 | Crow-Muslow,#1 Smith |
| 14S 16E 3 | 179 | Pam Amer,#1 Scogin |
| 14S 16E 4 | 180 | Hughes-Hughes,#2 Kendall |
| 14S 16E | 181 | Hanson,#1 Perkins |
| 14S 16E 8 | 182 | Atlantic,#1 Riser |
| 14S 16E 7 | 183 | Atlantic,#1 Baker |
| 14S 16E 6 | 184 | Brown,#1 Hayes |
| 14S 16E 7 | 185 | Smith,#1 Cravens |
| 14S 16E 9 | 186 | Abercrombie,#1 West et al |
| 14S 16E 8 | 187 | Pan Am,#1 Randall |
| 14S 16E 3 | 188 | Gulf, #1 Lee |
| 14S 16E 4 | 189 | Kilroy,#1-A Crocker |
| 15S 13E 7 | 190 | Argo,#1-A Edrington Est |
| 15S 13E 9 | 191 | Appell,#1 Atkinson |
| 15S 13E 5 | 192 | Steward-Quigley,#1 Rhode |
| 15S 13E 1 | 193 | Mobil,#1 Wheeler |
| 15S 13E 5 | 194 | Southland et al,#1 Coron |
| 15S 13E 5 | 195 | Peet,#1 Rhode |
| 15S 14E 6 | 196 | Atlantic,#1 El Paso Nat |
| 15S 14E 5 | 197 | Hamon,#1 Dougherrty |
| 15S 14E 7 | 198 | Coastal St,#1 Lehmberg |
| 15S 14E 2 | 199 | Hurt MPS et al,#1 Riser |
| 15S 14E 4 | 200 | Arco,Rhode Sect.18 |
| 15S 14E 9 | 201 | Rutherford,#4-A Baker |
| 15S 14E 4 | 202 | Atlantic Rich,#3 Rhodes |
| 15S 14E 6 | 203 | Aninoil,#1 Ausa et al |
| 15S 14E 8 | 204 | Rutherfor,#2-A Baker et al |
| 15S 14E 1 | 205 | Davis,#2 Lyne |
| 15S 14E 2 | 206 | Kilroy,#1 Pettit et al |
| 15S 14E 1 | 207 | Davis,#3 Lyons |
| 15S 15E 2 | 208 | Hanson-Hurt,#1 Sparkman |
| 15S 15E 4 | 209 | Sohio,#A-2 Slick |
| 15S 15E 6 | 210 | Huber-Manco,#1 Tullis |
| 15S 15E 5 | 211 | Standard,#1 Burns |
| 15S 15E 2 | 212 | Stanolind,#1 Sparkman |
| 15S 15E 5 | 213 | Tidewater,#1 Burns |
| 15S 15E 8 | 214 | Placid,#1 Patterson |
| 15S 15E 8 | 215 | Tenneco,#1 Jones |
| 15S 15E 6 | 216 | Cities,#1 Bailey |

| Township Range | Well No. | Well Name |
|---|---|---|
| 15S 15E 2 | 217 | Atlantic Ref,#1 Burns |
| 15S 15E 9 | 218 | Cities,#1-B Hendrick |
| 15S 15E 4 | 219 | Coastal St,#1 Ferrell |
| 15S 15E 2 | 220 | Coastal St.,#2-A Lennox |
| 15S 15E 4 | 221 | Hunt Sands,#1 Dolan |
| 15S 15E 2 | 222 | McMoran,#1 Burns |
| 15S 15E 9 | 223 | Hamill,#1 McClure |
| 15S 15E 9 | 224 | Monsanto,#1 McCullough |
| 15S 15E 3 | 225 | Austral,#1 Lyne |
| 15S 15E 6 | 226 | Hilliard,#1 Bailey |
| 15S 15E 9 | 227 | Katz,#C-1 Slick |
| 15S 15E 4 | 228 | Constantin, #1 Dolan |
| 15S 15E 4 | 229 | Atlantic Ref,#2 Lyne |
| 15S 15E 3 | 230 | SRG,#1 Lyne |
| 15S 16E 2 | 231 | Lone Star,#1 Watson |
| 15S 16E 4 | 232 | Tidewater,}-A Hall Est |
| 15S 16E 4 | 237 | Highland,#1 Cocker |
| 15S 16E 3 | 234 | Hanson-McCormick,#1 Johnson |
| 15S 16E 8 | 235 | Austral,#1-A Hinnant |
| 15S 16E 6 | 236 | Anschutz,#1 Parker |
| 15S 16E 3 | 237 | Daniel,#1 Peter et al |
| 11S 17E | 238 | MGF,#1 Zuniga |
| 11S 17E | 239 | Apache et al,B-1 Tips |
| 11S 17E 5 | 240 | Shell,#1 Ruhmann |
| 11S 17E 6 | 241 | Spartan,#1 Tips |
| 11S 18E 5 | 242 | Union,#2 Burnell Spielhagen |
| 11S 18E 7 | 243 | Union,#84 Ray |
| 11S 18E 7 | 244 | Union,N Pettus Ray7 |
| 11S 18E 9 | 245 | Cox-Hering,#1 Copeland |
| 11S 18E 3 | 246 | Southland,#1 Mueller |
| 11S 19E 4 | 247 | Miller-Fox,#1 Lott |
| 11S 19E 7 | 248 | Amerada,#3 McFadden |
| 11S 19E 7 | 249 | Tex East Prod,#1 Hall |
| 11S 19E 1 | 250 | Haring-Alcoa,#1 Powell et al |
| 11S 19E 1 | 251 | Samedan,#1 Berckenhoff |
| 11S 19E 7 | 252 | Amerada,#3 McFadden |
| 11S 19E 4 | 253 | Miller-Fox,#1 Lott |
| 11S 19E 8 | 254 | Viking,#1 Ray Est |
| 11S 19E 7 | 255 | Brown,#1 Pereira |
| 11S 19E 7 | 256 | Coastal St,#1 McKinney |
| 11S 19E 5 | 257 | Fly,#1 Key Estate |
| 11S 20E 6 | 258 | Abel & Bancroft,#2 Neese |
| 11S 20E 6 | 259 | Abel & Bancroft,#2 Ramsey |
| 11S 20E 1 | 260 | McCormack,#25 Albrecht |
| 11S 20E 4 | 261 | Coastal St,#1 Ussery |
| 11S 20E 6 | 262 | Humble,#1 Neese |
| 11S 20E 6 | 263 | Normanly,#1 Nesse |
| 11S 20E 4 | 264 | General Crude,#1 Pettus |

| Township Range | Well No. | Well Name |
|---|---|---|
| 11S 20E 9 | 265 | Cattle Land,#1 Gantt |
| 11S 20E 9 | 266 | Relco,#1 Gantt |
| 12S 17E 3 | 267 | Shell,#1 Alvarado et al |
| 12S 17E 3 | 268 | Shell,#1 Ford |
| 12S 17E 7 | 269 | Mosbacker-Century,#1 Lytle |
| 12S 17E 9 | 270 | South Tex,#1 Mckinley |
| 12S 17E 3 | 271 | Shell,#1 Tomasek et al |
| 12S 17E 3 | 272 | Shell,#1 O'Neal |
| 12S 17E 7 | 273 | Gasoline,#C-1 Holzmark |
| 12S 18E 8 | 274 | Atlantic Rich,#2 Dougherty Est |
| 12S 18E 7 | 275 | Coastal St,#1-A Scott |
| 12S 18E 2 | 276 | Harris,#2 West Tuleta-Hall |
| 12S 18E 5 | 277 | Skelly,#2 Hill |
| 12S 18E 1 | 278 | Hughes et al,#2 McKinney |
| 12S 18E 1 | 279 | Tex O & G,#1-A McKinney |
| 12S 18E 2 | 280 | Ellsworth-Stapp,#1 McKinney |
| 12S 18E 6 | 281 | Skelly,#1 Zook |
| 12S 18E 2 | 282 | Fly,#2 Ray |
| 12S 18E 1 | 283 | Hughes et al,#3 McKinney |
| 12S 18E 6 | 284 | Hanson et al,#1 Harris |
| 12S 19E 3 | 285 | Haring et al,#1 Ray |
| 12S 19E 8 | 286 | Coastal St,#1 Farish |
| 12S 19E 4 | 287 | Miller,#1 Farish |
| 12S 19E 4 | 288 | Tidewater,#1 Kidd |
| 12S 19E 7 | 289 | El Paso et al,#1 Hardison |
| 12S 19E 4 | 290 | Kissinger,#1 Kidd |
| 12S 19E 8 | 291 | Coastal St,#1 Farish |
| 12S 19E 1 | 292 | Coastal St,#3 McCord |
| 12S 19E 6 | 293 | Coastal St,#1 McCord |
| 12S 19E 6 | 294 | Coastal St,#4 McCord |
| 12S 19E 2 | 295 | Forest,#1 First V Ntl Bank |
| 12S 19E 3 | 296 | Forest,#1 Ray |
| 12S 19E 4 | 297 | Magnolia,#2 Irby |
| 13S 17E 3 | 298 | Chorchran Zoch,#1 Lippard |
| 13S 17E 6 | 299 | Carl,#1 Gillette |
| 13S 17E 6 | 300 | Carle,#1Turnbow |
| 13S 17E 1 | 301 | Hughes et al,#1 Pouloit "A" |
| 13S 17E 2 | 302 | Tex Co.,#1 Ragsdale |
| 13S 17E 1 | 303 | Hughes et al,#1 Macdon et al |
| 13S 17E 1 | 304 | Viking et al,#1 Williams |
| 13S 17E 3 | 305 | Cities,#B-1 Beck |
| 13S 17E 7 | 306 | N Central et al,#1 Bomar |
| 13S 17E 2 | 307 | Hamon,#1 Ragsdale |
| 13S 17E 8 | 308 | Argo,#1 Huegler |
| 13S 17E 8 | 309 | Colorado,#1 Choate |
| 13S 17E 5 | 310 | Colorado,#1 Tindal |
| 13S 18E 2 | 311 | Carrl-Leahy,#1 Littlejohn |
| 13S 18E 4 | 312 | Tidewater,#1 Taylor |

| Township Range | Well No. | Well Name |
|---|---|---|
| 13S 18E 1 | 313 | Coastal,#1 Scott |
| 13S 18E 3 | 314 | Dougherty et al,#1 Johnson |
| 13S 18E 8 | 315 | Sunray D-X,#1 May |
| 13S 18E 8 | 316 | Tamarack,#1 Humberson |
| 13S 18E 3 | 317 | Texaco,#1 Littlejohn |
| 13S 18E 4 | 318 | Tidewater,#1 Taylor |
| 13S 18E 4 | 319 | Tidewater,#1 Algea |
| 13S 18E 9 | 320 | Mitchell et al,#B-1 Robertson |
| 13S 18E 2 | 321 | Dougherty,#2 Perez |
| 13S 18E 4 | 322 | White Shield,#1 Martin |
| 13S 18E 4 | 323 | McCormick,#1 Littlejohn |
| 13S 18E 4 | 324 | McCormick,#1 Kearns |
| 14S 17E 3 | 325 | Shenandoah,#1 Good |
| 14S 17E 2 | 326 | Pend Oreille,#1 Womack |
| 14S 17E 7 | 327 | Humble,#B-9 Thompson |
| 16S 17E 9 | 328 | Max Pray,#3 Banker |
| 16S 20E 8 | 329 | Morgan,#3 Dodson Van Way |
| 16S 20E 8 | 330 | Morgan,#1 Johnson |
| 13S 21E 9 | 331 | Pure Oile,#1-B O'Brien |
| 14S 22E 8 | 332 | Kelly-Brock,#1 Snyder |
| 14S 24E 7 | 333 | Cities,#D-1 Tatton |
| 15S 21E 6 | 334 | Cities,#1-A Rooke |
| 15S 22E 9 | 335 | 4-B Trust,#1 Rooke |
| 15S 23E 8 | 336 | Sunray et al,#1 Hartman |
| 15S 23E 7 | 337 | Storm,St. Tr. #53,#1 |
| 15S 23E 3 | 338 | Contenental,#34 St Charles |
| 15S 23E 7 | 339 | Prairie,St Tr 12 #1 |
| 16S 21E 5 | 340 | Superior,#27 Welder |
| 16S 21E 9 | 341 | Smith,#1 Cage et al |
| 16S 21E 8 | 342 | Atlantic Rich,#1 Fite |
| 16S 22E 7 | 343 | Cities,#1 Elzner |
| 16S 22E 7 | 344 | Fox,#1 Wendland |
| 16S 22E 7 | 345 | Fox,#1 Netek |
| 16S 22E 8 | 346 | Texaco,#3 Ritchie |
| 16S 22E 1 | 347 | Gloria,#A-1 Welder |
| 16S 22E 6 | 348 | Hurt,#1 Ritchie |
| 16S 22E 9 | 349 | Cherryville,p Sweatt |
| 16S 23E 7 | 350 | Hamon,#1 Banker Mort |
| 16S 23E 2 | 351 | Cities,St Tr 86 #1 |
| 16S 23E 8 | 352 | Hunt Trust,#65-1 Banker M |
| 16S 23E 1 | 353 | Aluminum Co,St Tr 84 #2 |
| 16S 23E 6 | 354 | Shenandoah,St Tr 120 #1 |
| 16S 23E 5 | 355 | Amerada,#1 Bankers Mort |
| 16S 23E 9 | 356 | Graham,et al, Bible #2 |
| 16S 23E 6 | 357 | Midwest,St Tr 122,#1 |
| 16S 23E 9 | 358 | Amer Petrofina,#1 Ray et al |
| 16S 23E | 359 | State Tract 128 #1 |
| 16S 24E 6 | 360 | Getty-Mission,St Tr 125 #1 |
| 16S 24E 8 | 361 | Amerada,St Tr 191 #1 |
| 16S 24E 2 | 362 | Phillips,#1 Pano |
| 16S 24E 4 | 363 | Chevron,St Tr 125 #1 |
| 16S 24E 1 | 369 | Getty,St Tr 94 #1 |
| 16S 24E 1 | 370 | Getty,St Tr 119 #1 |
| 16S 24E 6 | 371 | Getty,St Tr 118, #1 |
| 13S 9E 5 | 372 | Gulf,#1 Naylor & Jones |
| 13S 11E 6 | 373 | Exxon,#13 Dilworth |
| 13S 12E 9 | 374 | Standard,#1 Henry |
| 13S 12E 7 | 375 | Pan Am,#1 McClaugherty |
| 14S 9E 6 | 376 | Phillips,#1 La Salle |
| 14S 9E 3 | 377 | Pan Am,#1 Foerster |
| 14S 10E 1 | 378 | Texas O & G,C-1 Washburn |
| 14S 10E 3 | 379 | Sutton,So Tex Syn #1 |
| 14S 10E 1 | 380 | Pam Am,#1-A Alamo Ntl Bank |
| 14S 11E 6 | 381 | Amerada,#1 Grines |
| 15S 11E 4 | 382 | Phillips,#1-A Nueces |
| 15S 12E 6 | 383 | Ridley Wheeler,#1 Rives |
| 15S 12E 7 | 384 | Tex Co,#1 Atkinson |
| 16S 9E 9 | 385 | Smyth,#1 Withers |
| 16S 10E 3 | 386 | Texaco,#1 Canales |
| 16S 10E 8 | 387 | Gulf,#1 Friedrichs |
| 16S 11E 1 | 388 | Mid Century,#1 Hubbend |
| 16S 12E 9 | 389 | Altantic,#1 Hagist |
| 16S 12E 8 | 390 | Marion,#1 Heirs |
| 16S 12E 6 | 391 | Rutherford,#1 Pursch |
| 16S 12E 1 | 392 | Cox,#1 Atkinson |
| 16S 12E 9 | 393 | Atlantic Rich,#44 Foster |
| 16S 12E 9 | 394 | Arco,#2 Hagist |
| 17S 5E 5 | 395 | Burns Corp,#1148 Matrix |
| 17S 7E 1 | 396 | Southwest Petro,#1 Olmitos |
| 17S 7E 8 | 397 | Mobil,#5 Callaghan |
| 17S 7E 3 | 398 | Haynes-UT,#1 Olmitos |
| 17S 7E 8 | 399 | Southern Un,#4 Williams et al |
| 18S 5E 8 | 400 | Lamar Hunt,#1 Benavides |
| 18S 5E 3 | 401 | Lamar Hunt,#1 Hachar |
| 18S 5E 3 | 402 | MGF,#2-C Hachar |
| 18S 6E 7 | 403 | Mobil,#1 Gretchen et al |
| 18S 7E 7 | 404 | Gulf,#1 Hirsch |
| 18S 7E 5 | 405 | Sunray Mid,#1 Lincoln |
| 18S 8E 8 | 406 | Hunt,#1 Walker |
| 17S 9E 9 | 407 | Dougherty et al,#1 Nicholson |
| 17S 9E 6 | 408 | Appell,#1 Adami |
| 17S 10E 5 | 409 | Rowe,#1 Hendrickson |
| 17S 10E 1 | 410 | Blair-Vreeland,#1 Harlson |
| 17S 11E 9 | 411 | Mobil,#9 DCRC Sec 80 |
| 17S 11E 9 | 412 | Magnolia,#79 DCRC |
| 17S 11E 7 | 413 | Marine,#1 Hahl Weiderkehr |

| Township Range | Well No. | Well Name |
|---|---|---|
| 17S 11E 6 | 414 | Horizon,#1 Lundell 364 |
| 17S 12E | 415 | Atlantic Rich,#1 Arco et al |
| 17S 12E 1 | 416 | Texaco,Hugo State #1 |
| 17S 12E 1 | 417 | Argo,#1 Gorman |
| 17S 12E 6 | 418 | Ramada,Welder Heirs 2-217 |
| 18S 9E 5 | 419 | McDermott,#A-1 Mclean |
| 18S 9E 7 | 420 | The Tex Co,#B-1 Moos |
| 18S 9E 8 | 421 | Conoco,#2 Hughes est |
| 18S 12E 5 | 422 | Shell,A-3 Weatherby |
| 18S 12E 5 | 423 | Shell,#2 Lloyd |
| 18S 12E 5 | 424 | Shell,#1-B Hubberd |
| 18S 12E 6 | 425 | Shell,#1-A Weatherby |
| 18S 12E 6 | 426 | Shell,#2 Weatherby |
| 18S 12E 6 | 427 | Shell,#1 Hubberd |
| 18S 12E 6 | 428 | Socony Mobil,#1 Weatherby |
| 18S 12E 5 | 429 | Shell,#1 Penwell |
| 18S 12E 5 | 430 | Shell,#1-B Hubberd |
| 18S 12E 6 | 431 | Shell,#3Wenecke |
| 19S 5E 4 | 432 | Lamar Hunt,#1 Reuthinger |
| 19S 5E 3 | 433 | General Crude,#1 Ruethinger |
| 19S 5E 3 | 434 | General Crude,#1 Killam-Hurd |
| 19S 7E 9 | 435 | Mobil,B-1 Garza |
| 19S 7E 8 | 436 | North Cent,#1 Webb Co Schl |
| 19S 8E 8 | 437 | Delange et al,#1 Walker |
| 19S 8E 1 | 438 | Forest,#1 Russel-Winch |
| 19S 8E 5 | 439 | Good Hope,#1 Carr |
| 20S 6E 2 | 440 | Ginther et al,#1-A Killam |
| 20S 6E 6 | 441 | Ginther et al,#1 Killam |
| 20S 7E 4 | 442 | Ginther et al,#1 Benavides |
| 20S 7 E 3 | 443 | Ginther et al,#1 Benavides |
| 20S 8E 7 | 444 | Bright-Schiff,#1-24 Atlantic |
| 20S 8E 9 | 445 | Good Hope,#3 Frost Ntl Bank |
| 17S 13E 6 | 446 | Pan Am,#1-E Farmers Life |
| 17S 13E 6 | 447 | El Paso,#1-B Yates |
| 17S 13E 5 | 448 | Davis,#1 Bravo Land |
| 17S 13E 3 | 449 | Texas Crude,#1 Farmers Life |
| 17S 13E 1 | 450 | El Paso,#2-B Farmers |
| 17S 15E 7 | 451 | Kidd,#1 Trejo |
| 18S 13E 3 | 452 | Cherryville,#1 Reyes |
| 18S 15E 2 | 453 | Esunas et al,#1 Hawkins |
| 18S 15E 6 | 454 | Howell,#1 Moos |
| 17S 19E 9 | 455 | Northern Pump,#1 Ocker |
| 17S 20E 7 | 456 | Sinclair,#1 Doney Jr |
| 17S 20E 5 | 457 | Renwar,#1 Peeks |
| 17S 20E 4 | 458 | Union,#1 Parker |
| 17S 20E 7 | 459 | Hamon,#8-1 Odem |
| 17S 20E 1 | 460 | Trans Cont,#1 Taft Morrow |
| 17S 20E 6 | 461 | Diamond Sham,#1 Cleo Pianta |
| 17S 20E 8 | 462 | Southern Min,#1 Griffith |
| 18S 18E 6 | 463 | Southern Min,#1 Stone et al |
| 18S 18E 2 | 464 | Bell et al,#1 Franks Est |
| 18S 18E 8 | 465 | Hughes et al,#4 Shulze |
| 18S 18E 4 | 466 | Amer Petrofina,#1 Kaiser |
| 18S 18E 1 | 467 | Gillring,#2 Dix |
| 18S 18E 6 | 468 | Dominion,#1 Charba |
| 18S 19E 8 | 469 | Chicago et al,#1 Lewis |
| 18S 20E 4 | 470 | Barnsdall,#1 Merritt |
| 18S 20E 2 | 471 | Gulf,#1 Mcgregor |
| 19S 9E 5 | 472 | Sundance,#1 Frost |
| 19S 9E 3 | 473 | Forest,#4 Winch-State |
| 19S 10E 4 | 474 | Houston,#1 Billings |
| 19S 10E 5 | 475 | Rowe,#1 Peal Est |
| 19S 11E 9 | 476 | Eason,#1 Peters Est |
| 19S 11E 9 | 477 | Eason-Harper,#1-160 Peters |
| 19S 12E 1 | 478 | Aluminum,#1 Hoffman et al |
| 19S 12E 1 | 479 | Maguire,#1 Braslau |
| 20S 10E 8 | 480 | Mobil,#1 Dinn |
| 20S 10E 5 | 481 | Hamon,#1 Leal |
| 20S 10E 6 | 482 | Morgan,#3-B Richardson |
| 20S 10E 4 | 483 | Shell,#1 Benavides |
| 20S 11E 8 | 484 | Argo,#A-21 Bennett |
| 20S 11E 3 | 485 | Amerada,#1 Gruy |
| 19S 14E 5 | 486 | Aluminum,#1 Oliveira |
| 19S 15E 1 | 487 | Delta Gulf,#1 Kalinec |
| 20S 13E 7 | 488 | Hiawatha,#B-1 |
| 20S 13E 9 | 489 | Morris et al,#1 Southland |
| 19S 18E 9 | 490 | Hawley,#1 Treybig |
| 19S 18E 3 | 491 | #3 Ingram |
| 19S 18E 5 | 492 | Outline,#1 Hoepfner |
| 19S 19E 6 | 493 | Atlantic Ref,#1 Womack |
| 19S 20E 5 | 494 | Midwest,#1 Walton |
| 19S 20E 4 | 495 | Hamon,#1 Hoepfner |
| 19S 20E 5 | 496 | Southern Un,#1 Bevly |
| 19S 20E 2 | 497 | Hoover,#1 Baker |
| 19S 20E 6 | 498 | Sabine,#1 Doughty |
| 19S 20E 3 | 499 | Fisher-Davidson,#1 Klosterman |
| 19S 20E 6 | 500 | Inexco,#1 Bevly |
| 19S 20E | 501 | Coastal St,#1 Cudding Airport |
| 19S 20E 9 | 502 | Anderman et al,#1 Ocker |
| 19S 20E 3 | 503 | May,#1 Merritt |
| 20S 17E 1 | 504 | Champlin,#127 Wardner |
| 20S 20E 3 | 505 | Texaco,#55 Loby |
| 20S 20E 7 | 506 | Humble,#39 King Rch |
| 21S 5E | 507 | Gulf,#A-2 Martin |
| 21S 6E 5 | 508 | Chevron,#1 Martin |
| 21S 7E 9 | 509 | Gulf,#A-10 BMT |

| Township Range | Well No. | Well Name |
|---|---|---|
| 21S 7E 9 | 510 | Gulf,#A-11 BMT |
| 21S 7E 9 | 511 | Gulf,#A-2 BMT |
| 21S 7E | 512 | Northern Natural,#1 BMT |
| 21S 8E 9 | 513 | Tex East,#1 Brunie Est |
| 21S 8E 8 | 514 | Skelly,#6 Martin |
| 21S 8E 1 | 515 | Gulf,#1 Villarreal |
| 22S 5E 4 | 516 | Consol O&G et al,#2 Zachry |
| 22S 6E 9 | 517 | Chevron,#1 Briones |
| 22S 6E 7 | 518 | Tex O&G,#4 Hein |
| 22S 6E 1 | 519 | Moore et al,#G-1 Hubbard |
| 22S 6E 5 | 520 | Good Hope,#2 Bruni Rch |
| 22S 6E 8 | 521 | Chevron,#1 McCann |
| 22S 6E 7 | 522 | HNG,#1 Hein Est |
| 22S 6E 6 | 523 | Tex O&G,#E-1 BMT |
| 22S 6E 7 | 524 | El Pason,#1 Hein Trust |
| 22S 7E 3 | 525 | Gulf,#A-11 BMT |
| 22S 7E 2 | 526 | Good Hope,#9 BMT |
| 22S 7E 2 | 527 | Good Hope,#1 Saldivar |
| 22S 7E 3 | 528 | Gulf,#A-16 BMT |
| 22S 7E 3 | 529 | Gulf,#A-4 BMT |
| 22S 7E 8 | 530 | Gas Prod,#1 Bartera |
| 22S 7E 2 | 531 | Mobil,#1 Bonugli |
| 22S 8E 3 | 532 | Coastal,#1 Martin et al |
| 22S 8E 7 | 533 | Superior,#1 McGrath |
| 21S 9E 5 | 534 | Pauley,#1 Laurel Fee |
| 21S 9E | 535 | Hughes et al,#1-A Laurel |
| 21S 10E 4 | 536 | McCulloch,#1 Cuellar et al |
| 21S 10E 2 | 537 | Brown,#1 Benavides |
| 21S 10E 5 | 538 | Getty,#1 Benavides |
| 22S 9E 2 | 539 | Coastal St,#1 Puig |
| 22S 9E 3 | 540 | Atlantic Ref,#1 Puig |
| 22S 9E 4 | 541 | Pickens,#1 Brunie |
| 22S 9E 4 | 542 | Hamon,#1 Ramirez |
| 22S 9E 9 | 543 | Atlantic Ref,#A-1 Hinnant |
| 22S 9E 2 | 544 | Atlantic Ref,#1 Garcia |
| 22S 9E 8 | 545 | Mosbacher,#1 Fulbright |
| 22S 9E 7 | 546 | Austral,#2 Mclean |
| 22S 9E 7 | 547 | Atlantic Ref,#3 Mclean |
| 22S 9E 7 | 548 | Atlantic Ref,#1 Stroman |
| 22S 9E 7 | 549 | Atlantic Rich,#2 Stroman |
| 22S 9E 7 | 550 | Austal,#1 Mclean |
| 22S 12E | 551 | Lone Star,#1 Miller |
| 21S 14E 4 | 552 | Jocelyn-varn,#1 Palacios |
| 21S 16E 8 | 553 | Sun,#117 Canales |
| 22S 13E 1 | 554 | Harkins,#1 Leal |
| 22S 13E 7 | 555 | Tex. Co,#1 Denman |
| 22S 16E 5 | 556 | Mobil,B-3 Blucher |
| 22S 16E | 557 | Sun,#9 Sullivan |
| 22S 16E 8 | 558 | Sun,#1 Wright |
| 22S 16E 6 | 559 | Sun,#21 Canales |
| 21S 17E 9 | 560 | Morgan,#1 Hill |
| 21S 17E 1 | 561 | Southern Min,#1 Werneck |
| 21S 17E 9 | 562 | Exxon,#A-34 King Rch |
| 21S 17E 6 | 563 | Meeker Haas,#1 Burris |
| 21S 17E 7 | 564 | Meeker Haas,#1 Conner |
| 21S 17E 3 | 565 | Humble,#ME-1 Bornegos |
| 21S 18E 7 | 566 | Lone Star,#1 Muil |
| 21S 18E 3 | 567 | Fly,#1 Fisher |
| 21S 18E 5 | 568 | Sun, #1 Dietz |
| 21S 19E 9 | 569 | Mokeen,#1 May |
| 21S 19E 1 | 570 | Exxon,#15 King Rch Madero |
| 21S 19E 9 | 571 | Mokeen,#1 Salazar |
| 21S 19E 9 | 573 | Viking et al,#1 Muil |
| 21S 20E 3 | 574 | Exxon,#303 Alazon |
| 21S 20E 5 | 575 | Exxon,#308 Alazon |
| 21S 20E 3 | 576 | Exxon,#306 Alazon |
| 21S 20E 5 | 577 | Humble,#245 Alazon |
| 21S 20E 9 | 578 | Humble,#267 Alazon |
| 21S 20E 5 | 579 | Humble, #266 Alazon |
| 22S 17E 3 | 580 | Humble,#31 King Rch Canelo |
| 22S 18E 7 | 581 | Arkans Conroe,#1 Kaufer |
| 22S 18E 4 | 582 | Exxon,#6 Rincon |
| 22S 18E 7 | 583 | Arkanxax McKeen,#1 Womack |
| 22S 18E 1 | 584 | Hill et al,#1 Brookshire |
| 22S 18E 6 | 585 | Cities,#1 Poteet |
| 22S 18E 9 | 586 | Humble,#4 Rincon |
| 22S 18E 4 | 587 | Exxon,#5 Rincon |
| 22S 19E 8 | 588 | Humble,#B-23 East |
| 22S 19E 8 | 589 | Sun,#1 Laguna Olmos |
| 22S 19E 4 | 590 | Forest,#1 Alvarado |
| 22S 19E 9 | 591 | Davis Chiles,#1 Koch |
| 22S 19E 8 | 592 | Humble,#B-25 East |
| 22S 19E 6 | 593 | Carre et al,St Tr 70 #1 |
| 22S 19E 3 | 594 | Cities,#1 Yaklin |
| 22S 19E 5 | 595 | Cosden,#1 Hubert |
| 22S 19E 7 | 596 | Carrll Hawn,St Tr 68 #1 |
| 22S 19E 2 | 597 | Pan Am,Cayo Del Grullo 84 #1 |
| 22S 19E 3 | 598 | McMormick,#1 King Rnch |
| 22S 19E 4 | 599 | Arkansas,#1 Huff |
| 22S 19E 2 | 600 | Morgan,#1 Matilda Limp |
| 22S 19E 9 | 601 | Tex O&G,#1-B Martin |
| 20S 21E 6 | 602 | King Ranch G-38 |
| 20S 21E 2 | 603 | Marion #1 Heirs |
| 20S 21E 1 | 604 | Mobil #B-9 Chapman |
| 20S 22E 1 | 605 | Humble, ST Tr 173 #1 |
| 20S 22E 6 | 606 | McMoran, ST Tr 171 #1 |

| Township Range | Well No. | Well Name |
|---|---|---|
| 20S 22E 2 | 607 | Hill, #1 Richardson |
| 20S 22E 8 | 608 | Am Petrofina, St Tr 169 #2 |
| 19S 21E 1 | 609 | Nor Am, #1 Vision |
| 19S 21E 4 | 610 | Socony Mobil,#1 Russel |
| 19S 21E 9 | 611 | Morgan Ent, #1 Zdansky |
| 19S 21E 4 | 612 | Getty, #1 Bevly |
| 19S 21E 9 | 613 | Clinton,Sims 1-V Trust |
| 19S 21E 7 | 614 | Davis,#1 Gwynn |
| 19S 21E 3 | 615 | Nor Am, #1 Peterson Prop |
| 19S 21E 2 | 616 | Hamon, #1 Pulliam |
| 19S 21E 2 | 617 | Hamon, #1 Sikora |
| 19S 21E 7 | 618 | Heard BDK, Guaranty Nat'l Bk |
| 19S 22E 4 | 619 | Mitrchell et al, #1 Nugent |
| 19S 22E 4 | 620 | Atlantic Ref, #1 Pearse |
| 19S 22E 8 | 621 | Coastal St.#1 Dunn et al |
| 19S 22E 2 | 622 | Anadarko,St Tr 181 #1 |
| 19S 22E 2 | 623 | Cities, St Tr 96 #2 |
| 19S 22E 9 | 624 | Marion, #1 Peterson |
| 19S 22E 1 | 625 | Cherryville, St Tr 81 #1 |
| 19S 22E 3 | 626 | State Tract 88, #1 |
| 19S 22E 4 | 627 | McMoran, StTr 37 #1 |
| 19S 22E 3 | 628 | McMoran, ST Tr 97 #2 |
| 19S 22 | 629 | McMoran, St Tr 97 #1 |
| 19S 22E 4 | 630 | Coastal St, St Tr 83 #1 |
| 17S 21E 6 | 631 | Phillips, #1 Flinn |
| 17S 21E 7 | 632 | Galaxy, #1 Moore |
| 17S 21E 7 | 633 | Houston Natrl,#1 Campbell |
| 17S 21E 7 | 634 | Galaxy, #1 Cities |
| 17S 21E 8 | 635 | Marathon, #2 Kellog |
| 17S 21E 1 | 636 | Hiawatha,#1 Green est |
| 17S 22E 7 | 637 | Am Petrofina,#1 Green Est |
| 17S 22E 1 | 638 | TerO&G,Ray "b" #1-A |
| 17S 22E 9 | 639 | Republic Natrl,#1 Floerke |
| 17S 22E 4 | 640 | Lawbar, Hunt Dugat #2 |
| 17S 22E 1 | 641 | Hamon,#3 Harvey |
| 17S 22E 9 | 642 | Stark #1 |
| 17S 23E 1 | 643 | Pennzoil,#1 Grant |
| 17S 23E 9 | 644 | Midwest, #3 McCampbell |
| 17S 23E 3 | 645 | Pan Am,#1 Banker's Mort |
| 17S 23E 4 | 646 | Hamon Sinclair, #1 Guettler |
| 17S 23E 5 | 647 | Getty,#1 McCampbell |
| 17S 23E 8 | 648 | McCampbell #1-A |
| 17S 23E 1 | 649 | Bass.,Atlantic-Porterfield |
| 17S 23E 2 | 650 | Tenneco,#1 Barry Est |
| 17S 24E 9 | 651 | Mobil,St Tr 284 #1 |
| 17S 24E 9 | 652 | Mobil, St Tr 310 #1 |
| 17S 24E 9 | 653 | Getty,St Tr 275 #1 |
| 17S 24E 9 | 654 | Tamarack, St Tr 274 #1 |
| 17S 24E 2 | 655 | Skelly, #1 Schnitz |
| 21S 22E 2 | 656 | Stnrd,#1 Dunn McCampbell |
| 21S 22E 9 | 657 | Humbel,St Tr 196 #1 |
| 21S 21E 6 | 658 | Shell,St Tr 206 #1 |
| 21S 21E 8 | 659 | Samedan et al,St Tr 6 #1 |
| 21S 22E 2 | 660 | Cherryvill,St Tr 978-S #1 |
| 21S 22E 2 | 661 | Sun,#1 Dunn-McCampbell |
| 21S 22E 4 | 662 | Sun,#3-A Dunn-McCampbell |
| 21S 22E 6 | 663 | Humble,#3 King Ranch et al |
| 16S 25E 4 | 664 | Hanson,St Tr 129 #1 |
| 16S 25E 3 | 665 | Sunray, St Tr 96 #1 |
| 16S 25E 4 | 666 | Getty, St Tr 142 #1 |
| 16S 25E 3 | 667 | St Tr 77 #1 |
| 16S 25E 4 | 668 | St Tr 143 #1 |
| 16S 25E 9 | 669 | Exxon,Nine Mi Pt, #12 |
| 16S 25E 3 | 670 | Getty, St Tr 95 #1 |
| 16S 25E 9 | 671 | Phillips,St Tr 163 #1 |
| 15S 25E 4 | 672 | Union,#15 Tatton |
| 15S 25E 4 | 673 | Union,#16 Tatton |
| 15S 25E 6 | 674 | Continental,#46 St Charles |
| 12S 25E 5 | 675 | Tenneo,#1 Schultz |
| 9S 21E 4 | 676 | Hanson, #1 Gips est |
| 9S 21E 4 | 678 | Skelly #1 Menn |
| 9S 21E 5 | 679 | Texaco,#2 Broughton |
| 9S 21E 3 | 680 | Musselman,#1 Danysh |
| 9S 21E 5 | 681 | Texaco,#1 Feller |
| 9S 21E 9 | 682 | Lone Star, #1 Gips |
| 9S 21E 6 | 683 | Brazos,#1 Sievers |
| 9S 21E 9 | 684 | Atlantic,#1 Kerlick |
| 9S 21E 5 | 685 | Houchins #2 |
| 9S 21E 1 | 686 | Austral,#1 Schroeter |
| 9S 21E 2 | 687 | Monsanto Et Al,#1 Boldt |
| 9S 21E 2 | 688 | Quintana,#1 Jochen |
| 9S 21E 6 | 689 | Hamilton,#1 Harter |
| 9S 21E 5 | 690 | Monsanto,#3 Kulawik |
| 9S 21E 1 | 691 | Mosbacher,#1 Spies |
| 10S 21E 1 | 692 | Normandy,#1 Fromme |
| 10S 21E 5 | 693 | Cummings et al,#1 Urban |
| 10S 21E 7 | 694 | Houston,#1 Fromme |
| 10S 21E 5 | 695 | Burns,#1 Norrel |
| 110S 21E 3 | 696 | Lone Start,#1 Dohlmann |
| 10S 21E 2 | 697 | Mitchell,#1 Dohlman |
| 10S 21E 3 | 698 | Lone Star,#1 Haynes |
| 10S 21E 3 | 699 | Humble, #2 McMillan |
| 10S 21E 6 | 700 | Kirkwood,#1 Hoff |
| 7S 16E 3 | 701 | Sohio,#1 Southern |
| 8S 13E 6 | 702 | Petro Tex, #1 Garcia |
| 9S 12E 9 | 703 | Skelly #1 Winkler |

| Township Range | Well No. | Well Name |
|---|---|---|
| 10S 10E 3 | 704 | Stanolind,#1 Garcia |
| 10S 11E 4 | 705 | Gulf,#1 Morris Reese |
| 15S 7E 2 | 706 | Shell,#1 Martin |
| 15S 7E 6 | 707 | W Artesia Trans, #1 Koehne |
| 15S 8E 8 | 708 | Flamingo Vent.et al, #1 Coquat |
| 16S 5E 1 | 709 | Stampede,#3 Burkholder |
| 16S 5E 3 | 710 | Stampede,#6 Dawson |
| 16S 5E 6 | 711 | Mengden,#1 Carr |
| 16S 6E 5 | 712 | Mengden,#1 Schletze |
| 17S 6E 6 | 713 | Royal O&G,#1 Dellano et al |
| 16S 7E 1 | 714 | General Crude,#1 Miller |
| 14S 7E 1 | 715 | Bass,#1 Johnson |
| 14S 8E 5 | 716 | Stanolind,#1 Cooke |
| 14S 8E 1 | 717 | Suttons,#1 Hillje |
| 14S 8E 4 | 718 | Pan Am,#C-1 Cooke |
| 7S 18E 8 | 719 | Sun,#1 Patton |
| 8S 17E 6 | 720 | Morgan,#1 Pawelek |
| 8S 19E 8 | 721 | Geochem Sur,#1 Tam Jr |
| 8S 19E 3 | 722 | Wiatrek #1 |
| 8S 21E 4 | 723 | Shell,#1 Brown |
| 8S 21E 6 | 724 | Superior,#1 Blackwell |
| 8S 21E 1 | 725 | Gulf,#1 Mueller |
| 8S 21E 7 | 726 | CommonWealth,#1 Richards |
| 8S 21E 9 | 727 | Shell, #1 Roehl |
| 8S 21E 7 | 728 | Howell,#1 Gansow |
| 8S 21E 7 | 729 | Am Petrofina,#1 Boldt |
| 8S 21E 5 | 730 | Highland,#1 Wood Jr |
| 8S 21E 4 | 731 | Esparanza,#1 Gohmert |
| 8S 21E 5 | 732 | Atlantic,#1 Smith |
| 8S 21E 9 | 733 | Shell,#1 Roehl |
| 16S 13E 9 | 734 | Harkins,Ragsdale Sec 120#1 |
| 16S 13E 7 | 735 | Siegfried,#1 Lowe |
| 16S 13E 8 | 736 | Mobil,Labbe Rnch 413#1 |
| 16S 13E 9 | 737 | Inland Ocian,#1 Roos |
| 16S 13E 7 | 738 | Petro-Lewis#1 Bindewald |
| 16S 13E 6 | 739 | Sunray,#1 Amer Nat Ins |
| 16S 13E 6 | 740 | Texaco,#1 Hughes |
| 16S 13E 6 | 741 | Sun Dx,#4 Stella Penn |
| 16S 13E 4 | 742 | Harkins,#1-112 Murphy est |
| 16S 13E 1 | 743 | Atlantic #1 Rhodes 54 |
| 16S 13E 5 | 744 | Texaco,#27 Gouyer |
| 16S 14E 1 | 745 | Kilroy et al,#1 Dunn |
| 16S 14E 3 | 746 | Atlantic,#1 Glasscock |
| 16S 14E 9 | 747 | #1 Eubanks |
| 16S 14E 3 | 748 | Centura,#1 Roos |
| 16S 14E 9 | 749 | Austral,#1 Baker |
| 16S 14E 3 | 750 | Argo,#1 Dearman |
| 16S 14E 3 | 751 | Atlantic,#4 Baker |
| 16S 14E 1 | 752 | Skelly,Weil "A" #1 |
| 16S 14E 2 | 753 | Mitchell,#1 Brookshire |
| 16S 14E 1 | 754 | Tenneco,#1 Patterson |
| 16S 14E 6 | 755 | Kilroy, et al,#1 Passmore |
| 16S 14E 3 | 756 | Hamon,#1 Hefner |
| 16S 14E 3 | 757 | Energy Soures,#1 Hinnant |
| 16S 14E 2 | 758 | Sanchez-O'Brien,#1 Jones |
| 16S 16E 3 | 759 | Humble, McCaslin #12 |
| 16S 16E 1 | 760 | Tex O&G,Hinnant #5 |
| 16S 16E 2 | 761 | Hughes & Hughes,Wilson#1 |
| 16S 16E 7 | 762 | Tidewater/Skelly,NoSH-22 |

Temperature and Elevation Corrected Data-Base

Each line represents one well. The well numbers are approximately sequential in the order that the file was created. However, some editing of the data was done after numbers were assigned (due to duplicate entries, lack of elevation data, etc.), so certain well numbers are skipped.

| ID | UTM COORDINATES | | DEPTH/TEMP PAIRS.... | | | | | | | | | | | | | | | |
|---|---|---|---|---|---|---|---|---|---|---|---|---|---|---|---|---|---|---|
| 26 | 3177887.0 | 648361.1 | 9219 | 238 | 0 | 0 | 0 | 0 | 0 | 0 | 0 | 0 | 0 | 0 | | | | |
| 27 | 3176823.0 | 655861.1 | 9184 | 250 | 10900 | 304 | 0 | 0 | 0 | 0 | 0 | 0 | 0 | 0 | | | | |
| 28 | 3176547.0 | 649312.5 | 8867 | 246 | 0 | 0 | 0 | 0 | 0 | 0 | 0 | 0 | 0 | 0 | | | | |
| 30 | 3176406.8 | 656315.2 | 9334 | 244 | 9985 | 291 | 0 | 0 | 0 | 0 | 0 | 0 | 0 | 0 | | | | |
| 31 | 3177516.5 | 655821.0 | 9265 | 240 | 10206 | 284 | 0 | 0 | 0 | 0 | 0 | 0 | 0 | 0 | | | | |
| 32 | 3177551.0 | 656539.1 | 8806 | 241 | 10298 | 288 | 0 | 0 | 0 | 0 | 0 | 0 | 0 | 0 | | | | |
| 33 | 3176462.4 | 660931.6 | 8819 | 242 | 12316 | 323 | 0 | 0 | 0 | 0 | 0 | 0 | 0 | 0 | | | | |
| 34 | 3181243.9 | 669796.8 | 8835 | 241 | 13100 | 347 | 13925 | 369 | 0 | 0 | 0 | 0 | 0 | 0 | | | | |
| 35 | 3166752.7 | 647218.9 | 11243 | 290 | 8789 | 223 | 0 | 0 | 0 | 0 | 0 | 0 | 0 | 0 | | | | |
| 36 | 3205702.1 | 604327.8 | 10820 | 268 | 0 | 0 | 0 | 0 | 0 | 0 | 0 | 0 | 0 | 0 | | | | |
| 38 | 3204547.3 | 599632.4 | 11101 | 282 | 0 | 0 | 0 | 0 | 0 | 0 | 0 | 0 | 0 | 0 | | | | |
| 40 | 3204069.3 | 602225.9 | 10740 | 261 | 0 | 0 | 0 | 0 | 0 | 0 | 0 | 0 | 0 | 0 | | | | |
| 42 | 3198193.7 | 632631.9 | 9900 | 237 | 13887 | 329 | 0 | 0 | 0 | 0 | 0 | 0 | 0 | 0 | | | | |
| 43 | 3199494.9 | 631792.8 | 9355 | 240 | 11655 | 283 | 13652 | 326 | 0 | 0 | 0 | 0 | 0 | 0 | | | | |
| 44 | 3200374.2 | 633968.9 | 8018 | 252 | 14147 | 350 | 0 | 0 | 0 | 0 | 0 | 0 | 0 | 0 | | | | |
| 45 | 3197338.1 | 630425.1 | 9090 | 226 | 0 | 0 | 0 | 0 | 0 | 0 | 0 | 0 | 0 | 0 | | | | |
| 47 | 3202248.5 | 625171.8 | 13033 | 292 | 0 | 0 | 0 | 0 | 0 | 0 | 0 | 0 | 0 | 0 | | | | |
| 49 | 3201216.0 | 633440.2 | 16174 | 383 | 16816 | 344 | 18178 | 370 | 0 | 0 | 0 | 0 | 0 | 0 | | | | |
| 50 | 3198612.0 | 626772.3 | 12912 | 316 | 15594 | 318 | 17919 | 404 | 20673 | 432 | 0 | 0 | 0 | 0 | | | | |
| 51 | 3208560.0 | 646006.2 | 9812 | 241 | 0 | 0 | 0 | 0 | 0 | 0 | 0 | 0 | 0 | 0 | | | | |
| 53 | 3200137.4 | 641620.6 | 9153 | 215 | 10150 | 269 | 0 | 0 | 0 | 0 | 0 | 0 | 0 | 0 | | | | |
| 54 | 3202902.3 | 638338.7 | 8480 | 230 | 0 | 0 | 0 | 0 | 0 | 0 | 0 | 0 | 0 | 0 | | | | |
| 56 | 3205227.2 | 642711.2 | 9672 | 249 | 0 | 0 | 0 | 0 | 0 | 0 | 0 | 0 | 0 | 0 | | | | |
| 57 | 3195754.0 | 644462.9 | 9831 | 233 | 11609 | 267 | 12171 | 333 | 0 | 0 | 0 | 0 | 0 | 0 | | | | |
| 58 | 3196039.0 | 643095.9 | 9759 | 243 | 0 | 0 | 0 | 0 | 0 | 0 | 0 | 0 | 0 | 0 | | | | |
| 59 | 3195259.8 | 640472.3 | 9716 | 226 | 11659 | 318 | 12259 | 330 | 0 | 0 | 0 | 0 | 0 | 0 | | | | |
| 60 | 3199015.1 | 644453.5 | 9890 | 242 | 12179 | 333 | 0 | 0 | 0 | 0 | 0 | 0 | 0 | 0 | | | | |
| 61 | 3200900.9 | 641396.9 | 8864 | 228 | 9829 | 259 | 0 | 0 | 0 | 0 | 0 | 0 | 0 | 0 | | | | |
| 62 | 3206257.7 | 644601.1 | 9732 | 240 | 0 | 0 | 0 | 0 | 0 | 0 | 0 | 0 | 0 | 0 | | | | |
| 63 | 3204194.4 | 640225.0 | 9009 | 233 | 0 | 0 | 0 | 0 | 0 | 0 | 0 | 0 | 0 | 0 | | | | |
| 64 | 3198453.2 | 640835.1 | 9547 | 241 | 10216 | 264 | 0 | 0 | 0 | 0 | 0 | 0 | 0 | 0 | | | | |
| 65 | 3206978.0 | 636547.3 | 13474 | 307 | 15441 | 337 | 16183 | 373 | 0 | 0 | 0 | 0 | 0 | 0 | | | | |
| 66 | 3198629.7 | 645602.8 | 9988 | 248 | 11635 | 312 | 0 | 0 | 0 | 0 | 0 | 0 | 0 | 0 | | | | |
| 67 | 3180931.9 | 599445.4 | 8039 | 200 | 0 | 0 | 0 | 0 | 0 | 0 | 0 | 0 | 0 | 0 | | | | |
| 68 | 3181523.3 | 609050.6 | 14794 | 329 | 15606 | 382 | 0 | 0 | 0 | 0 | 0 | 0 | 0 | 0 | | | | |
| 69 | 3182473.4 | 609980.3 | 10722 | 259 | 14480 | 333 | 15798 | 383 | 0 | 0 | 0 | 0 | 0 | 0 | | | | |
| 70 | 3184590.0 | 620738.3 | 8162 | 217 | 9187 | 246 | 9442 | 254 | 10794 | 300 | 0 | 0 | 0 | 0 | | | | |
| 71 | 3188217.7 | 619105.3 | 9844 | 252 | 0 | 0 | 0 | 0 | 0 | 0 | 0 | 0 | 0 | 0 | | | | |
| 72 | 3187690.2 | 618802.4 | 8753 | 227 | 0 | 0 | 0 | 0 | 0 | 0 | 0 | 0 | 0 | 0 | | | | |

| ID | UTM COORDINATES | | DEPTH/TEMP PAIRS.... | | | | | | | | | | | |
|---|---|---|---|---|---|---|---|---|---|---|---|---|---|---|
| 73 | 3190591.5 | 610511.1 | 8459 | 227 | 0 | 0 | 0 | 0 | 0 | 0 | 0 | 0 | 0 | 0 |
| 74 | 3185179.6 | 616367.4 | 13631 | 308 | 0 | 0 | 0 | 0 | 0 | 0 | 0 | 0 | 0 | 0 |
| 75 | 3181082.5 | 625728.2 | 15718 | 387 | 17923 | 414 | 19207 | 436 | 21483 | 452 | 0 | 0 | 0 | 0 |
| 76 | 3184486.2 | 625905.5 | 9408 | 239 | 10369 | 272 | 12745 | 339 | 0 | 0 | 0 | 0 | 0 | 0 |
| 77 | 3191196.2 | 628847.3 | 8800 | 220 | 9713 | 247 | 0 | 0 | 0 | 0 | 0 | 0 | 0 | 0 |
| 78 | 3189997.6 | 630154.0 | 8990 | 242 | 10540 | 295 | 0 | 0 | 0 | 0 | 0 | 0 | 0 | 0 |
| 79 | 3189773.5 | 630656.1 | 9202 | 252 | 10051 | 270 | 11370 | 304 | 0 | 0 | 0 | 0 | 0 | 0 |
| 80 | 3187643.6 | 628903.3 | 9254 | 245 | 9826 | 266 | 12119 | 319 | 0 | 0 | 0 | 0 | 0 | 0 |
| 81 | 3194513.7 | 631982.8 | 9374 | 241 | 0 | 0 | 0 | 0 | 0 | 0 | 0 | 0 | 0 | 0 |
| 82 | 3190196.6 | 631319.5 | 12247 | 337 | 0 | 0 | 0 | 0 | 0 | 0 | 0 | 0 | 0 | 0 |
| 83 | 3181402.0 | 632873.0 | 8616 | 252 | 8989 | 252 | 9981 | 282 | 0 | 0 | 0 | 0 | 0 | 0 |
| 84 | 3182122.0 | 640803.1 | 7328 | 204 | 0 | 0 | 0 | 0 | 0 | 0 | 0 | 0 | 0 | 0 |
| 85 | 3189859.4 | 643255.8 | 9756 | 249 | 11109 | 305 | 13152 | 352 | 13643 | 364 | 0 | 0 | 0 | 0 |
| 86 | 3193157.0 | 635451.8 | 9651 | 249 | 10985 | 267 | 11628 | 313 | 0 | 0 | 0 | 0 | 0 | 0 |
| 87 | 3192759.7 | 636619.5 | 9914 | 242 | 11697 | 321 | 0 | 0 | 0 | 0 | 0 | 0 | 0 | 0 |
| 88 | 3200982.4 | 550461.1 | 6735 | 175 | 7006 | 254 | 0 | 0 | 0 | 0 | 0 | 0 | 0 | 0 |
| 89 | 3197379.5 | 560162.8 | 8102 | 213 | 0 | 0 | 0 | 0 | 0 | 0 | 0 | 0 | 0 | 0 |
| 90 | 3202721.4 | 563484.5 | 6936 | 188 | 7569 | 206 | 7830 | 218 | 0 | 0 | 0 | 0 | 0 | 0 |
| 91 | 3205872.0 | 562677.9 | 6494 | 181 | 6802 | 186 | 6856 | 211 | 0 | 0 | 0 | 0 | 0 | 0 |
| 92 | 3194224.2 | 571801.3 | 9130 | 226 | 0 | 0 | 0 | 0 | 0 | 0 | 0 | 0 | 0 | 0 |
| 93 | 3199639.5 | 595163.4 | 8050 | 207 | 8591 | 220 | 9401 | 231 | 10146 | 244 | 10327 | 246 | 10592 | 272 |
| 94 | 3203800.3 | 593409.5 | 11013 | 262 | 0 | 0 | 0 | 0 | 0 | 0 | 0 | 0 | 0 | 0 |
| 95 | 3207720.9 | 596926.9 | 9931 | 253 | 10342 | 256 | 10881 | 258 | 11304 | 265 | 11445 | 267 | 0 | 0 |
| 96 | 3194420.8 | 592163.3 | 10762 | 258 | 0 | 0 | 0 | 0 | 0 | 0 | 0 | 0 | 0 | 0 |
| 97 | 3197870.6 | 592808.0 | 10680 | 257 | 10835 | 262 | 11120 | 269 | 0 | 0 | 0 | 0 | 0 | 0 |
| 98 | 3188303.6 | 584694.1 | 10588 | 240 | 10942 | 247 | 0 | 0 | 0 | 0 | 0 | 0 | 0 | 0 |
| 99 | 3183972.1 | 582832.2 | 10810 | 272 | 0 | 0 | 0 | 0 | 0 | | | | | |
| 100 | 3186090.6 | 574043.8 | 10111 | 242 | 11279 | 273 | 0 | 0 | 0 | 0 | 0 | 0 | 0 | 0 |
| 101 | 3181242.4 | 589788.0 | 11756 | 282 | 0 | 0 | 0 | 0 | 0 | 0 | 0 | 0 | 0 | 0 |
| 102 | 3183125.1 | 591814.5 | 7631 | 208 | 0 | 0 | 0 | 0 | 0 | 0 | 0 | 0 | 0 | 0 |
| 103 | 3170111.2 | 549018.3 | 10137 | 243 | 0 | 0 | 0 | 0 | 0 | 0 | 0 | 0 | 0 | 0 |
| 104 | 3175592.3 | 549018.3 | 12014 | 297 | 0 | 0 | 0 | 0 | 0 | 0 | 0 | 0 | 0 | 0 |
| 105 | 3167266.9 | 578808.7 | 7761 | 208 | 0 | 0 | 0 | 0 | 0 | 0 | 0 | 0 | 0 | 0 |
| 106 | 3156696.1 | 552911.5 | 11816 | 249 | 0 | 0 | 0 | 0 | 0 | 0 | 0 | 0 | 0 | 0 |
| 107 | 3159136.0 | 558521.0 | 6319 | 195 | 0 | 0 | 0 | 0 | 0 | 0 | 0 | 0 | 0 | 0 |
| 108 | 3159735.2 | 561906.1 | 11038 | 283 | 0 | 0 | 0 | 0 | 0 | 0 | 0 | 0 | 0 | 0 |
| 109 | 3153183.4 | 568374.0 | 7399 | 212 | 12543 | 282 | 12841 | 282 | 0 | 0 | 0 | 0 | 0 | 0 |
| 110 | 3158882.0 | 573225.8 | 7506 | 187 | 0 | 0 | 0 | 0 | 0 | 0 | 0 | 0 | 0 | 0 |
| 111 | 3158060.6 | 581614.3 | 8233 | 218 | 13134 | 317 | 13704 | 343 | 0 | 0 | 0 | 0 | 0 | 0 |
| 112 | 3164898.0 | 590526.4 | 8235 | 217 | 0 | 0 | 0 | 0 | 0 | 0 | 0 | 0 | 0 | 0 |
| 113 | 3153733.0 | 589302.1 | 6925 | 206 | 0 | 0 | 0 | 0 | 0 | 0 | 0 | 0 | 0 | 0 |
| 114 | 3156703.9 | 591134.6 | 6966 | 206 | 0 | 0 | 0 | 0 | 0 | 0 | 0 | 0 | 0 | 0 |
| 115 | 3163381.9 | 593201.1 | 13843 | 334 | 0 | 0 | 0 | 0 | 0 | 0 | 0 | 0 | 0 | 0 |
| 116 | 3164141.1 | 595781.1 | 15211 | 359 | 0 | 0 | 0 | 0 | 0 | 0 | 0 | 0 | 0 | 0 |
| 117 | 3154198.0 | 593224.3 | 7426 | 210 | 0 | 0 | 0 | 0 | 0 | 0 | 0 | 0 | 0 | 0 |
| 118 | 3163857.7 | 593603.9 | 13844 | 346 | 0 | 0 | 0 | 0 | 0 | 0 | 0 | 0 | 0 | 0 |
| 119 | 3163139.1 | 594417.5 | 13895 | 353 | 0 | 0 | 0 | 0 | 0 | 0 | 0 | 0 | 0 | 0 |
| 120 | 3165319.5 | 596256.3 | 13697 | 329 | 0 | 0 | 0 | 0 | 0 | 0 | 0 | 0 | 0 | 0 |

| ID | UTM COORDINATES | | DEPTH/TEMP PAIRS.... | | | | | | | | | | | |
|---|---|---|---|---|---|---|---|---|---|---|---|---|---|---|
| 121 | 3163369.9 | 593195.3 | 14110 | 335 | 0 | 0 | 0 | 0 | 0 | 0 | 0 | 0 | 0 | 0 |
| 122 | 3155095.9 | 500172.7 | 6988 | 212 | 0 | 0 | 0 | 0 | 0 | 0 | 0 | 0 | 0 | 0 |
| 123 | 3163081.6 | 533221.1 | 10385 | 234 | 13960 | 303 | 15097 | 322 | 16601 | 336 | 0 | 0 | 0 | 0 |
| 124 | 3158748.1 | 547124.7 | 10844 | 262 | 0 | 0 | 0 | 0 | 0 | 0 | 0 | 0 | 0 | 0 |
| 125 | 3163773.5 | 548354.6 | 7346 | 207 | 8793 | 213 | 9689 | 243 | 10306 | 254 | 10823 | 261 | 0 | |
| 126 | 3153383.6 | 539984.7 | 10272 | 262 | 0 | 0 | 0 | 0 | 0 | 0 | 0 | 0 | 0 | 0 |
| 127 | 3199115.0 | 501743.1 | 9612 | 246 | 11020 | 238 | 11434 | 251 | 0 | 0 | 0 | 0 | | |
| 128 | 3195146.6 | 537211.5 | 9839 | 208 | 14594 | 299 | 15061 | 312 | 0 | 0 | 0 | 0 | 0 | 0 |
| 129 | 3188466.9 | 508119.5 | 9242 | 231 | 0 | 0 | 0 | 0 | 0 | 0 | 0 | 0 | 0 | 0 |
| 130 | 3185210.9 | 524491.0 | 7572 | 218 | 8657 | 246 | 0 | 0 | 0 | 0 | 0 | 0 | 0 | 0 |
| 131 | 3150797.8 | 563501.2 | 7314 | 201 | 11510 | 277 | 11951 | 271 | 12024 | 271 | 12194 | 301 | | |
| | | | 12361 | 303 | | | | | | | | | | |
| 132 | 3152597.5 | 569174.7 | 7284 | 198 | 12247 | 263 | 12395 | 301 | 12573 | 313 | 13610 | 362 | 0 | |
| 133 | 3139142.1 | 584843.4 | 7978 | 228 | 8281 | 232 | 0 | 0 | 0 | 0 | 0 | 0 | 0 | 0 |
| 134 | 3139950.8 | 588502.0 | 8296 | 211 | 8575 | 224 | 0 | 0 | 0 | 0 | 0 | 0 | 0 | 0 |
| 135 | 3141647.2 | 590931.0 | 9008 | 230 | 0 | 0 | 0 | 0 | 0 | 0 | 0 | 0 | 0 | 0 |
| 136 | 3149363.6 | 593391.1 | 8542 | 229 | 0 | 0 | 0 | 0 | 0 | 0 | 0 | 0 | 0 | 0 |
| 137 | 3148839.7 | 593392.7 | 7309 | 216 | 0 | 0 | 0 | 0 | 0 | 0 | 0 | 0 | 0 | 0 |
| 138 | 3150280.4 | 596291.4 | 8459 | 216 | 10183 | 246 | 11144 | 287 | 0 | 0 | 0 | 0 | 0 | 0 |
| 139 | 3140528.1 | 592861.1 | 7929 | 234 | 9001 | 240 | 9392 | 239 | 0 | 0 | 0 | 0 | 0 | 0 |
| 140 | 3148686.6 | 597314.0 | 8262 | 249 | 8699 | 255 | 0 | 0 | 0 | 0 | 0 | 0 | 0 | 0 |
| 141 | 3151050.5 | 596387.0 | 7448 | 217 | 0 | 0 | 0 | 0 | 0 | 0 | 0 | 0 | 0 | 0 |
| 142 | 3140647.0 | 587636.9 | 8412 | 226 | 0 | 0 | 0 | 0 | 0 | 0 | 0 | 0 | 0 | 0 |
| 144 | 3140132.1 | 590538.2 | 7803 | 227 | 8793 | 240 | 0 | 0 | 0 | 0 | 0 | 0 | 0 | 0 |
| 145 | 3140862.2 | 591664.4 | 7499 | 212 | 9040 | 241 | 0 | 0 | 0 | 0 | 0 | 0 | 0 | 0 |
| 146 | 3144243.1 | 597229.4 | 9631 | 249 | 10042 | 292 | 0 | 0 | 0 | 0 | 0 | 0 | 0 | 0 |
| 147 | 3142527.6 | 589652.9 | 8905 | 258 | 0 | 0 | 0 | 0 | 0 | 0 | 0 | 0 | 0 | 0 |
| 148 | 3143046.2 | 595494.0 | 10649 | 312 | 11607 | 341 | 13828 | 348 | 14610 | 358 | 0 | 0 | 0 | 0 |
| 149 | 3141000.7 | 597411.9 | 9743 | 249 | 11363 | 267 | 13194 | 332 | 13818 | 339 | 0 | 0 | 0 | 0 |
| 150 | 3146522.4 | 587726.6 | 7623 | 223 | 0 | 0 | 0 | 0 | 0 | 0 | 0 | 0 | 0 | 0 |
| 151 | 3140843.5 | 596295.0 | 10367 | 262 | 11200 | 328 | 0 | 0 | 0 | 0 | 0 | 0 | 0 | 0 |
| 152 | 3126331.7 | 567243.4 | 7115 | 206 | 0 | 0 | 0 | 0 | 0 | 0 | 0 | 0 | 0 | 0 |
| 153 | 3128140.0 | 564643.3 | 8195 | 225 | 0 | 0 | 0 | 0 | 0 | 0 | 0 | 0 | 0 | 0 |
| 154 | 3133455.6 | 562901.7 | 7220 | 212 | 8224 | 209 | 10264 | 257 | 13228 | 342 | 14763 | 363 | 0 | |
| 155 | 3135647.5 | 572847.9 | 8200 | 222 | 0 | 0 | 0 | 0 | 0 | 0 | 0 | 0 | 0 | 0 |
| 156 | 3135385.8 | 572160.2 | 8163 | 220 | 0 | 0 | 0 | 0 | 0 | 0 | 0 | 0 | 0 | 0 |
| 157 | 3128109.9 | 564656.3 | 8168 | 237 | 0 | 0 | 0 | 0 | 0 | 0 | 0 | 0 | 0 | 0 |
| 158 | 3132043.2 | 572473.2 | 8313 | 226 | 0 | 0 | 0 | 0 | 0 | 0 | 0 | 0 | 0 | 0 |
| 159 | 3126826.1 | 584014.8 | 6808 | 197 | 10231 | 297 | 11172 | 310 | 0 | 0 | 0 | 0 | 0 | 0 |
| 160 | 3134992.5 | 582259.4 | 8337 | 222 | 11732 | 291 | 12730 | 330 | 0 | 0 | 0 | 0 | 0 | 0 |
| 161 | 3128587.4 | 583341.1 | 8157 | 237 | 10619 | 270 | 12241 | 338 | 13701 | 356 | 0 | 0 | 0 | 0 |
| 162 | 3130907.2 | 582591.9 | 7774 | 215 | 9165 | 269 | 9679 | 291 | 0 | 0 | 0 | 0 | 0 | 0 |
| 163 | 3127711.7 | 578983.7 | 7535 | 209 | 8904 | 264 | 9107 | 268 | 9750 | 281 | 0 | 0 | 0 | 0 |
| 164 | 3128471.0 | 580992.5 | 7584 | 247 | 8114 | 288 | 0 | 0 | 0 | 0 | 0 | 0 | 0 | 0 |
| 165 | 3127715.6 | 576345.6 | 7225 | 214 | 9209 | 269 | 9710 | 277 | 0 | 0 | 0 | 0 | 0 | 0 |
| 166 | 3130874.3 | 584591.0 | 7530 | 223 | 8035 | 230 | 9232 | 266 | 0 | 0 | 0 | 0 | 0 | 0 |
| 167 | 3128963.2 | 577458.3 | 7294 | 197 | 8222 | 233 | 8706 | 240 | 0 | 0 | 0 | 0 | 0 | 0 |
| 168 | 3134164.2 | 575061.7 | 7793 | 222 | 0 | 0 | 0 | 0 | 0 | 0 | 0 | 0 | 0 | 0 |
| 169 | 3136248.2 | 576938.3 | 6935 | 206 | 8383 | 227 | 0 | 0 | 0 | 0 | 0 | 0 | 0 | 0 |

| ID | UTM COORDINATES | | DEPTH/TEMP PAIRS.... | | | | | | | | | | | |
|---|---|---|---|---|---|---|---|---|---|---|---|---|---|---|
| 170 | 3128374.3 | 577534.6 | 7217 | 211 | 9568 | 271 | 0 | 0 | 0 | 0 | 0 | 0 | 0 | 0 |
| 171 | 3136935.1 | 583853.4 | 8307 | 224 | 0 | 0 | 0 | 0 | 0 | 0 | 0 | 0 | 0 | 0 |
| 172 | 3131543.1 | 579425.5 | 7721 | 213 | 9201 | 238 | 0 | 0 | 0 | 0 | 0 | 0 | 0 | 0 |
| 173 | 3134555.8 | 583263.9 | 7854 | 219 | 0 | 0 | 0 | 0 | 0 | 0 | 0 | 0 | 0 | 0 |
| 174 | 3130318.9 | 581065.9 | 7813 | 223 | 8350 | 247 | 9010 | 253 | 9692 | 269 | 0 | 0 | 0 | 0 |
| 175 | 3130020.6 | 580610.7 | 7602 | 226 | 9236 | 265 | 0 | 0 | 0 | 0 | 0 | 0 | 0 | 0 |
| 176 | 3132026.0 | 583671.4 | 7610 | 217 | 8235 | 237 | 8344 | 279 | 9334 | 301 | 9834 | 301 | 0 | 0 |
| 177 | 3133528.1 | 585892.2 | 8158 | 231 | 8824 | 296 | 9281 | 262 | 9708 | 270 | 0 | 0 | 0 | 0 |
| 178 | 3134038.8 | 585153.9 | 7750 | 227 | 9325 | 285 | 0 | 0 | 0 | 0 | 0 | 0 | 0 | 0 |
| 179 | 3137327.9 | 588613.4 | 9170 | 272 | 9202 | 270 | 0 | 0 | 0 | 0 | 0 | 0 | 0 | 0 |
| 180 | 3132687.3 | 585889.9 | 8467 | 223 | 9625 | 281 | 0 | 0 | 0 | 0 | 0 | 0 | 0 | 0 |
| 181 | 3130928.1 | 590828.1 | 8080 | 234 | 9882 | 291 | 10370 | 308 | 0 | 0 | 0 | 0 | 0 | 0 |
| 182 | 3128101.7 | 592937.1 | 9263 | 240 | 9765 | 279 | 10733 | 271 | 10829 | 273 | 0 | 0 | 0 | 0 |
| 183 | 3127521.1 | 594725.1 | 8885 | 232 | 10393 | 278 | 11654 | 293 | 12197 | 331 | 0 | 0 | 0 | 0 |
| 184 | 3133351.5 | 597514.9 | 8552 | 236 | 9847 | 285 | 0 | 0 | 0 | 0 | 0 | 0 | 0 | 0 |
| 185 | 3128191.4 | 594731.9 | 7770 | 213 | 8996 | 234 | 9933 | 291 | 0 | 0 | 0 | 0 | 0 | 0 |
| 186 | 3129395.5 | 587907.4 | 7852 | 216 | 9002 | 280 | 9543 | 271 | 10201 | 282 | 10714 | 305 | 0 | |
| 187 | 3128738.2 | 591653.2 | 8686 | 248 | 9786 | 291 | 10800 | 309 | 0 | 0 | 0 | 0 | 0 | 0 |
| 188 | 3134929.8 | 589626.6 | 8777 | 230 | 9925 | 273 | 10895 | 284 | 11472 | 297 | 0 | 0 | 0 | 0 |
| 189 | 3131496.1 | 587395.5 | 8523 | 219 | 9803 | 254 | 10153 | 292 | 0 | 0 | 0 | 0 | 0 | 0 |
| 190 | 3113723.8 | 558600.1 | 8005 | 229 | 0 | 0 | 0 | 0 | 0 | 0 | 0 | 0 | 0 | 0 |
| 191 | 3112932.6 | 552200.9 | 8120 | 220 | 0 | 0 | 0 | 0 | 0 | 0 | 0 | 0 | 0 | 0 |
| 192 | 3116198.6 | 557027.8 | 7062 | 216 | 0 | 0 | 0 | 0 | 0 | 0 | 0 | 0 | 0 | 0 |
| 193 | 3124752.3 | 560702.7 | 7665 | 214 | 0 | 0 | 0 | 0 | 0 | 0 | 0 | 0 | 0 | 0 |
| 194 | 3118704.8 | 555693.2 | 7745 | 250 | 0 | 0 | 0 | 0 | 0 | 0 | 0 | 0 | 0 | 0 |
| 195 | 3117076.0 | 558237.3 | 7321 | 203 | 0 | 0 | 0 | 0 | 0 | 0 | 0 | 0 | 0 | 0 |
| 196 | 3116647.0 | 571197.3 | 7710 | 214 | 11072 | 303 | 11790 | 305 | 13100 | 364 | 14410 | 371 | 0 | |
| 197 | 3116048.5 | 566962.0 | 7100 | 207 | 7849 | 219 | 0 | 0 | 0 | 0 | 0 | 0 | 0 | 0 |
| 198 | 3112544.2 | 572801.3 | 7722 | 209 | 10621 | 310 | 0 | 0 | 0 | 0 | 0 | 0 | 0 | 0 |
| 199 | 3122639.1 | 565364.9 | 7776 | 260 | 8253 | 259 | 0 | 0 | 0 | 0 | 0 | 0 | 0 | 0 |
| 200 | 3116392.0 | 562039.4 | 7739 | 221 | 10924 | 297 | 13574 | 366 | 0 | 0 | 0 | 0 | 0 | 0 |
| 201 | 311448.6 | 564566.5 | 6777 | 201 | 7759 | 217 | 8526 | 260 | 10067 | 298 | 10560 | 299 | 11059 | 314 |
| 202 | 3116097.3 | 562943.2 | 8020 | 226 | 0 | 0 | 0 | 0 | 0 | 0 | 0 | 0 | 0 | 0 |
| 203 | 3116684.6 | 572782.6 | 10123 | 292 | 0 | 0 | 0 | 0 | 0 | 0 | 0 | 0 | 0 | 0 |
| 204 | 3113610.9 | 565973.0 | 7487 | 201 | 8987 | 221 | 9966 | 294 | 0 | 0 | 0 | 0 | 0 | 0 |
| 205 | 1.0 | 1.0 | -513 | -1 | -513 | -1 | -513 | -1 | 0 | 0 | 0 | 0 | 0 | 0 |
| 206 | 3122999.8 | 568247.6 | 7234 | 229 | 0 | 0 | 0 | 0 | 0 | 0 | 0 | 0 | 0 | 0 |
| 207 | 3122449.0 | 573189.4 | 7359 | 212 | 9976 | 297 | 0 | 0 | 0 | 0 | 0 | 0 | 0 | 0 |
| 208 | 3122323.9 | 577891.4 | 8527 | 249 | 10234 | 295 | 11838 | 333 | 0 | 0 | 0 | 0 | 0 | 0 |
| 209 | 3116540.8 | 576039.5 | 8653 | 230 | 10308 | 282 | 11014 | 299 | 0 | 0 | 0 | 0 | 0 | 0 |
| 210 | 3118718.1 | 582834.9 | 8550 | 235 | 11045 | 291 | 0 | 0 | 0 | 0 | 0 | 0 | 0 | 0 |
| 211 | 3117459.3 | 578224.5 | 8623 | 225 | 11165 | 298 | 12207 | 323 | 14093 | 379 | 14445 | 384 | 0 | |
| 212 | 3123077.4 | 577290.4 | 8669 | 227 | 9639 | 289 | 10269 | 303 | 0 | 0 | 0 | 0 | 0 | 0 |
| 213 | 3119044.7 | 580894.2 | 8758 | 242 | 9809 | 280 | 10486 | 287 | 10968 | 294 | 0 | 0 | 0 | 0 |
| 214 | 3113098.3 | 580689.5 | 8754 | 240 | 10389 | 282 | 11545 | 321 | 12620 | 341 | 13596 | 375 | 0 | |
| 215 | 3111570.4 | 581275.7 | 9775 | 256 | 10827 | 316 | 12483 | 330 | 0 | 0 | 0 | 0 | 0 | 0 |
| 216 | 3119349.5 | 584905.3 | 8587 | 234 | 10053 | 258 | 11098 | 312 | 0 | 0 | 0 | 0 | 0 | 0 |
| 217 | 3122556.9 | 580860.0 | 10208 | 293 | 11716 | 295 | 12394 | 304 | 0 | 0 | 0 | 0 | 0 | 0 |

| ID | UTM COORDINATES | | DEPTH/TEMP PAIRS.... | | | | | | | | | | | |
|---|---|---|---|---|---|---|---|---|---|---|---|---|---|---|
| 218 | 3111722.5 | 574469.8 | 9595 | 281 | 10737 | 323 | 12540 | 358 | 0 | 0 | 0 | 0 | 0 | 0 |
| 219 | 3115964.5 | 576694.6 | 8665 | 230 | 10365 | 302 | 11865 | 337 | 0 | 0 | 0 | 0 | 0 | 0 |
| 220 | 3123498.9 | 581489.9 | 7151 | 214 | 7624 | 222 | 11505 | 333 | 0 | 0 | 0 | 0 | 0 | 0 |
| 221 | 3118823.7 | 575187.6 | 8491 | 231 | 11620 | 323 | 0 | 0 | 0 | 0 | 0 | | | |
| 222 | 3121734.6 | 581065.0 | 8607 | 253 | 11671 | 321 | 12867 | 334 | 0 | 0 | 0 | 0 | 0 | 0 |
| 223 | 3112711.0 | 574611.6 | 8870 | 255 | 10311 | 306 | 10991 | 319 | 0 | 0 | 0 | 0 | 0 | 0 |
| 224 | 3112013.4 | 574078.2 | 11293 | 333 | 0 | 0 | 0 | 0 | 0 | 0 | 0 | 0 | 0 | 0 |
| 225 | 3120805.1 | 575099.4 | 8579 | 250 | 9182 | 256 | 9950 | 290 | 0 | 0 | 0 | 0 | 0 | 0 |
| 226 | 3117684.2 | 584778.7 | 9771 | 236 | 12410 | 327 | 13692 | 372 | 0 | 0 | 0 | 0 | 0 | 0 |
| 227 | 3114903.9 | 574101.7 | 8752 | 242 | 10290 | 300 | 10817 | 304 | 11825 | 332 | 0 | 0 | 0 | 0 |
| 228 | 3117630.5 | 575632.1 | 8746 | 244 | 10442 | 299 | 0 | 0 | 0 | 0 | 0 | 0 | 0 | 0 |
| 229 | 3119500.6 | 573849.1 | 8527 | 256 | 8830 | 252 | 9086 | 258 | 9628 | 276 | 10128 | 274 | 10236 | 286 |
| 230 | 3124110.9 | 575267.3 | 7303 | 205 | 9160 | 247 | 9766 | 277 | 0 | 0 | 0 | 0 | 0 | 0 |
| 231 | 3123191.6 | 590376.0 | 7691 | 219 | 0 | 0 | 0 | 0 | 0 | 0 | 0 | 0 | 0 | 0 |
| 232 | 3120092.1 | 587298.4 | 7511 | 203 | 9589 | 266 | 10111 | 272 | 11212 | 295 | 0 | 0 | 0 | 0 |
| 233 | 3118948.7 | 586626.7 | 7967 | 230 | 10678 | 317 | 0 | 0 | 0 | 0 | 0 | 0 | 0 | 0 |
| 234 | 3123402.3 | 589783.5 | 7843 | 201 | 11283 | 318 | 0 | 0 | 0 | 0 | 0 | 0 | 0 | 0 |
| 235 | 3114763.1 | 592816.7 | 8901 | 238 | 11587 | 313 | 12318 | 337 | 13031 | 340 | 13509 | 366 | 14533 | 378 |
| 236 | 3116634.8 | 595418.1 | 7839 | 225 | 9751 | 252 | 12653 | 321 | 13829 | 353 | 0 | 0 | 0 | 0 |
| 237 | 3122715.0 | 587481.6 | 7783 | 202 | 10618 | 312 | 11418 | 327 | 0 | 0 | 0 | 0 | 0 | 0 |
| 238 | 3171969.5 | 606718.5 | 13391 | 332 | 0 | 0 | 0 | 0 | 0 | 0 | 0 | 0 | 0 | 0 |
| 239 | 3174374.9 | 607268.1 | 8002 | 244 | 8186 | 254 | 0 | 0 | 0 | 0 | 0 | 0 | 0 | 0 |
| 240 | 3172611.0 | 604689.5 | 12915 | 284 | 13484 | 361 | 0 | 0 | 0 | 0 | 0 | 0 | 0 | 0 |
| 241 | 3173029.5 | 609132.6 | 7610 | 226 | 0 | 0 | 0 | 0 | 0 | 0 | 0 | 0 | 0 | 0 |
| 242 | 3174143.1 | 617140.3 | 9076 | 271 | 0 | 0 | 0 | 0 | 0 | 0 | 0 | 0 | 0 | 0 |
| 243 | 3168825.1 | 618871.3 | 7663 | 226 | 0 | 0 | 0 | 0 | 0 | 0 | 0 | 0 | 0 | 0 |
| 244 | 3167146.7 | 618689.3 | 8259 | 243 | 8587 | 268 | 0 | 0 | 0 | 0 | 0 | 0 | 0 | 0 |
| 245 | 3167308.5 | 612416.8 | 7177 | 203 | 0 | 0 | 0 | 0 | 0 | 0 | 0 | 0 | 0 | 0 |
| 246 | 3180316.9 | 610716.6 | 8688 | 270 | 13277 | 309 | 0 | 0 | 0 | 0 | 0 | 0 | 0 | 0 |
| 247 | 3175205.6 | 622980.1 | 6975 | 201 | 0 | 0 | 0 | 0 | 0 | 0 | 0 | 0 | 0 | 0 |
| 248 | 3170599.3 | 633974.7 | 10739 | 250 | 0 | 0 | 0 | 0 | 0 | 0 | 0 | 0 | 0 | 0 |
| 249 | 3169351.5 | 632847.8 | 7652 | 217 | 0 | 0 | 0 | 0 | 0 | 0 | 0 | 0 | 0 | 0 |
| 250 | 3176634.3 | 633737.9 | 8917 | 236 | 10323 | 288 | 0 | 0 | 0 | 0 | 0 | 0 | 0 | 0 |
| 251 | 3180798.7 | 632688.3 | 8805 | 223 | 9660 | 270 | 9975 | 278 | 0 | 0 | 0 | 0 | 0 | 0 |
| 252 | 3169914.5 | 633003.9 | 8148 | 221 | 10739 | 250 | 0 | 0 | 0 | 0 | 0 | 0 | 0 | 0 |
| 253 | 3175205.5 | 622974.0 | 6965 | 201 | 0 | 0 | 0 | 0 | 0 | 0 | 0 | 0 | 0 | 0 |
| 254 | 3167344.2 | 626985.6 | 8939 | 249 | 0 | 0 | 0 | 0 | 0 | 0 | 0 | 0 | 0 | 0 |
| 255 | 3170092.2 | 632257.8 | 9017 | 270 | 0 | 0 | 0 | 0 | 0 | 0 | 0 | 0 | 0 | 0 |
| 256 | 3169106.0 | 630694.4 | 9130 | 247 | 0 | 0 | 0 | 0 | 0 | 0 | 0 | 0 | 0 | 0 |
| 257 | 3173858.0 | 628606.2 | 10161 | 300 | 0 | 0 | 0 | 0 | 0 | 0 | 0 | 0 | 0 | 0 |
| 258 | 3174070.8 | 645232.0 | 9452 | 269 | 0 | 0 | 0 | 0 | 0 | 0 | 0 | 0 | 0 | 0 |
| 259 | 3175231.5 | 642990.5 | 8873 | 286 | 0 | 0 | 0 | 0 | 0 | 0 | 0 | 0 | 0 | 0 |
| 260 | 3178118.2 | 643294.5 | 9033 | 239 | 10693 | 302 | 0 | 0 | 0 | 0 | 0 | 0 | 0 | 0 |
| 261 | 3176470.3 | 636208.2 | 8430 | 233 | 0 | 0 | 0 | 0 | 0 | 0 | 0 | 0 | 0 | 0 |
| 262 | 3174397.7 | 645093.0 | 7767 | 212 | 8823 | 274 | 9272 | 280 | 9575 | 282 | 9734 | 281 | 10244 | 287 |
| 263 | 3173657.1 | 645683.0 | 9768 | 269 | 0 | 0 | 0 | 0 | 0 | 0 | 0 | 0 | 0 | 0 |

| ID | UTM COORDINATES | DEPTH/TEMP PAIRS.... | | | | | | | | | | | | |
|---|---|---|---|---|---|---|---|---|---|---|---|---|---|---|
| 264 | 3172996.3 | 635748.5 | 7900 | 210 | 8898 | 252 | 10995 | 271 | 0 | 0 | 0 | 0 | 0 | 0 |
| 265 | 3169615.1 | 638230.4 | 9546 | 275 | 10100 | 280 | 0 | 0 | 0 | 0 | 0 | 0 | 0 | 0 |
| 266 | 3170331.7 | 638475.6 | 9851 | 271 | 0 | 0 | 0 | 0 | 0 | 0 | 0 | 0 | 0 | 0 |
| 267 | 3164584.2 | 599783.3 | 14045 | 309 | 14917 | 343 | 15624 | 337 | 16537 | 414 | 0 | 0 | 0 | 0 |
| 268 | 3165979.2 | 598945.9 | 15174 | 331 | 15817 | 406 | 15974 | 411 | 0 | 0 | 0 | 0 | 0 | 0 |
| 269 | 3153496.8 | 606049.1 | 7651 | 212 | 0 | 0 | 0 | 0 | 0 | 0 | 0 | 0 | 0 | 0 |
| 270 | 3153292.4 | 599331.1 | 7589 | 227 | 0 | 0 | 0 | 0 | 0 | 0 | 0 | 0 | 0 | 0 |
| 271 | 3165384.7 | 598711.1 | 13040 | 348 | 13985 | 369 | 15047 | 386 | 0 | 0 | 0 | 0 | 0 | 0 |
| 272 | 3164806.5 | 597945.9 | 13417 | 320 | 14531 | 340 | 15124 | 389 | 16033 | 396 | 16988 | 403 | 0 | |
| 273 | 3153583.1 | 609368.7 | 7904 | 220 | 9074 | 265 | 0 | 0 | 0 | 0 | 0 | 0 | 0 | 0 |
| 274 | 1.0 | 1.0 | -441 | -1 | -441 | -1 | 0 | 0 | 0 | 0 | 0 | 0 | 0 | 0 |
| 275 | 3153204.7 | 619891.6 | 9660 | 289 | 0 | 0 | 0 | 0 | 0 | 0 | 0 | 0 | 0 | 0 |
| 276 | 3162256.1 | 614381.5 | 8353 | 245 | 9801 | 288 | 0 | 0 | 0 | 0 | 0 | 0 | 0 | 0 |
| 277 | 3158927.1 | 617502.5 | 7626 | 224 | 8318 | 267 | 0 | 0 | 0 | 0 | 0 | 0 | 0 | 0 |
| 278 | 3163276.4 | 619033.7 | 8073 | 235 | 9851 | 292 | 0 | 0 | 0 | 0 | 0 | 0 | 0 | 0 |
| 279 | 3165012.7 | 620634.6 | 7364 | 219 | 7680 | 228 | 10632 | 310 | 0 | 0 | 0 | 0 | 0 | 0 |
| 280 | 3165148.8 | 617927.1 | 8155 | 239 | 9750 | 295 | 0 | 0 | 0 | 0 | 0 | 0 | 0 | 0 |
| 281 | 3158154.3 | 618385.4 | 7909 | 218 | 8172 | 249 | 8824 | 262 | 0 | 0 | 0 | 0 | 0 | 0 |
| 285 | 3165434.3 | 623165.5 | 8911 | 216 | 0 | 0 | 0 | 0 | 0 | 0 | 0 | 0 | 0 | 0 |
| 286 | 3155337.1 | 628236.7 | 8693 | 248 | 9903 | 280 | 10919 | 292 | 11236 | 309 | 11516 | 313 | 0 | |
| 287 | 3159214.2 | 626235.2 | 8268 | 243 | 9221 | 269 | 10170 | 292 | 0 | 0 | 0 | 0 | 0 | 0 |
| 288 | 3159445.4 | 622395.5 | 8149 | 219 | 8995 | 258 | 0 | 0 | 0 | 0 | 0 | 0 | 0 | 0 |
| 289 | 3155741.1 | 633657.9 | 8799 | 256 | 9981 | 287 | 10382 | 306 | 11305 | 323 | 0 | 0 | 0 | 0 |
| 290 | 3159309.5 | 624574.9 | 9880 | 222 | 0 | 0 | 0 | 0 | 0 | 0 | 0 | 0 | 0 | 0 |
| 291 | 3155331.2 | 628249.0 | 8692 | 248 | 9902 | 280 | 10918 | 292 | 11235 | 309 | 11515 | 313 | 0 | |
| 292 | 3162633.2 | 631803.3 | 11395 | 316 | 0 | 0 | 0 | 0 | 0 | 0 | 0 | 0 | 0 | 0 |
| 294 | 3162079.2 | 632245.2 | 10127 | 292 | 0 | 0 | 0 | 0 | 0 | 0 | 0 | 0 | 0 | 0 |
| 295 | 3163972.4 | 629366.8 | 9171 | 283 | 9421 | 279 | 0 | 0 | 0 | 0 | 0 | 0 | 0 | 0 |
| 296 | 3164686.0 | 625562.1 | 8826 | 269 | 0 | 0 | 0 | 0 | 0 | 0 | 0 | 0 | 0 | 0 |
| 297 | 3162060.2 | 637148.7 | 8995 | 234 | 9207 | 251 | 9788 | 263 | 10524 | 302 | 0 | 0 | 0 | 0 |
| 298 | 3151711.8 | 599562.4 | 7510 | 232 | 0 | 0 | 0 | 0 | 0 | 0 | 0 | 0 | 0 | 0 |
| 299 | 3146403.1 | 609538.8 | 9675 | 243 | 10299 | 262 | 0 | 0 | 0 | 0 | 0 | 0 | 0 | 0 |
| 300 | 3144760.3 | 608714.5 | 9564 | 279 | 9934 | 287 | 10327 | 304 | 0 | 0 | 0 | 0 | 0 | 0 |
| 301 | 3150460.9 | 606692.1 | 8585 | 239 | 10032 | 280 | 11617 | 313 | 0 | 0 | 0 | 0 | 0 | 0 |
| 302 | 3150938.5 | 604476.7 | 8466 | 214 | 9612 | 279 | 10118 | 292 | 0 | 0 | 0 | 0 | 0 | 0 |
| 303 | 3151036.1 | 606563.8 | 9090 | 247 | 10634 | 267 | 11218 | 284 | 11703 | 325 | 0 | 0 | 0 | 0 |
| 304 | 3149147.5 | 608043.2 | 8693 | 246 | 0 | 0 | 0 | 0 | 0 | 0 | 0 | 0 | 0 | 0 |
| 305 | 3151091.1 | 601482.0 | 8646 | 224 | 0 | 0 | 0 | 0 | 0 | 0 | 0 | 0 | 0 | 0 |
| 306 | 3143388.4 | 606169.0 | 8906 | 249 | 9762 | 277 | 10038 | 284 | 0 | 0 | 0 | 0 | 0 | 0 |
| 307 | 3149545.3 | 602690.2 | 7427 | 202 | 8452 | 229 | 0 | 0 | 0 | 0 | 0 | 0 | 0 | 0 |
| 308 | 3142234.9 | 604112.6 | 8403 | 245 | 9515 | 281 | 10028 | 283 | 10500 | 287 | 0 | 0 | 0 | 0 |
| 309 | 3141070.7 | 602699.8 | 10004 | 256 | 0 | 0 | 0 | 0 | 0 | 0 | 0 | 0 | 0 | 0 |
| 310 | 3144725.9 | 603263.5 | 9143 | 278 | 0 | 0 | 0 | 0 | 0 | 0 | 0 | 0 | 0 | 0 |
| 311 | 3151293.6 | 614446.6 | 10161 | 287 | 0 | 0 | 0 | 0 | 0 | 0 | 0 | 0 | 0 | 0 |
| 312 | 3146334.7 | 614007.7 | 9084 | 242 | 10827 | 293 | 11883 | 348 | 0 | 0 | 0 | 0 | 0 | 0 |
| 313 | 3152090.5 | 620210.4 | 8187 | 227 | 9566 | 281 | 9984 | 294 | 0 | 0 | 0 | 0 | 0 | 0 |
| 314 | 3151184.8 | 612954.5 | 8543 | 226 | 9607 | 293 | 10226 | 300 | 10610 | 309 | 0 | 0 | 0 | 0 |
| 315 | 3141700.9 | 617941.9 | 9700 | 258 | 10310 | 290 | 10640 | 305 | 11162 | 3 | | | | |
| 316 | 3143578.8 | 616068.0 | 8750 | 248 | 10440 | 295 | 10829 | 312 | 0 | 0 | 0 | 0 | 0 | 0 |

| ID | UTM COORDINATES | | DEPTH/TEMP PAIRS.... | | | | | | | | | | | |
|---|---|---|---|---|---|---|---|---|---|---|---|---|---|---|
| 317 | 3149574.2 | 614327.4 | 9986 | 250 | 0 | 0 | 0 | 0 | 0 | 0 | 0 | 0 | 0 | 0 |
| 318 | 3146383.1 | 613988.9 | 9085 | 242 | 10820 | 293 | 11879 | 348 | 0 | 0 | 0 | 0 | 0 | 0 |
| 319 | 3146005.8 | 612378.6 | 9026 | 232 | 10093 | 274 | 10913 | 292 | 10959 | 293 | 11647 | 327 | 11925 | 339 |
| 320 | 3141573.4 | 610270.0 | 9722 | 261 | 10704 | 300 | 0 | 0 | 0 | 0 | 0 | 0 | 0 | 0 |
| 321 | 3149385.5 | 614797.1 | 10127 | 282 | 11497 | 331 | 11922 | 348 | 0 | 0 | 0 | 0 | 0 | 0 |
| 322 | 3147293.8 | 611956.5 | 9936 | 264 | 10189 | 308 | 0 | 0 | 0 | 0 | 0 | 0 | 0 | 0 |
| 323 | 3147226.9 | 610919.3 | 10116 | 268 | 0 | 0 | 0 | 0 | 0 | 0 | 0 | 0 | 0 | 0 |
| 324 | 3146183.6 | 613554.2 | 10010 | 262 | 0 | 0 | 0 | 0 | 0 | 0 | 0 | 0 | 0 | 0 |
| 325 | 3136184.7 | 600220.3 | 10129 | 262 | 0 | 0 | 0 | 0 | 0 | 0 | 0 | 0 | 0 | 0 |
| 326 | 3138850.3 | 602307.3 | 10348 | 282 | 0 | 0 | 0 | 0 | 0 | 0 | 0 | 0 | 0 | 0 |
| 327 | 3127470.3 | 644451.6 | 5883 | 190 | 0 | 0 | 0 | 0 | 0 | 0 | 0 | 0 | 0 | 0 |
| 328 | 3097920.8 | 601046.0 | 7400 | 207 | 0 | 0 | 0 | 0 | 0 | 0 | 0 | 0 | 0 | 0 |
| 329 | 3101577.1 | 642244.8 | 7850 | 194 | 0 | 0 | 0 | 0 | 0 | 0 | 0 | 0 | 0 | 0 |
| 330 | 3101505.4 | 641039.2 | 7924 | 198 | 0 | 0 | 0 | 0 | 0 | 0 | 0 | 0 | 0 | 0 |
| 331 | 3139980.6 | 648027.4 | 11887 | 285 | 14274 | 353 | 16213 | 384 | 0 | 0 | 0 | 0 | 0 | 0 |
| 332 | 3126250.5 | 665199.7 | 8961 | 210 | 0 | 0 | 0 | 0 | 0 | 0 | 0 | 0 | 0 | 0 |
| 333 | 3127752.4 | 695443.8 | 8400 | 199 | 9078 | 206 | 9589 | 216 | 0 | 0 | 0 | 0 | 0 | 0 |
| 334 | 3117404.9 | 657458.1 | 7971 | 201 | 0 | 0 | 0 | 0 | 0 | 0 | 0 | 0 | 0 | 0 |
| 335 | 3113962.2 | 661286.5 | 8480 | 202 | 0 | 0 | 0 | 0 | 0 | 0 | 0 | 0 | 0 | 0 |
| 336 | 3114345.1 | 676840.7 | 8031 | 198 | 8971 | 208 | 0 | 0 | 0 | 0 | 0 | 0 | 0 | 0 |
| 337 | 3112958.8 | 681620.4 | 9000 | 219 | 0 | 0 | 0 | 0 | 0 | 0 | 0 | 0 | 0 | 0 |
| 338 | 3123604.8 | 685364.9 | 8707 | 215 | 9792 | 226 | 11108 | 259 | 11937 | 240 | 12576 | 249 | 13109 | 297 |
| 339 | 3117032.9 | 693444.8 | 8666 | 214 | 0 | 0 | 0 | 0 | 0 | 0 | 0 | 0 | 0 | 0 |
| 340 | 3107094.2 | 653178.5 | 8570 | 234 | 11468 | 279 | 13481 | 296 | 15457 | 328 | 16827 | 364 | 17142 | 378 |
| 341 | 3098328.5 | 650707.1 | 8454 | 215 | 0 | 0 | 0 | 0 | 0 | 0 | 0 | 0 | 0 | 0 |
| 342 | 3098431.1 | 653946.4 | 9391 | 240 | 11112 | 276 | 0 | 0 | 0 | 0 | 0 | 0 | 0 | 0 |
| 343 | 3099146.7 | 667568.0 | 7718 | 194 | 9958 | 219 | 0 | 0 | 0 | 0 | 0 | 0 | 0 | 0 |
| 344 | 3098610.6 | 670395.2 | 10167 | 230 | 0 | 0 | 0 | 0 | 0 | 0 | 0 | 0 | 0 | 0 |
| 345 | 3098610.4 | 669979.6 | 9980 | 229 | 0 | 0 | 0 | 0 | 0 | 0 | 0 | 0 | 0 | 0 |
| 346 | 3100108.7 | 664222.4 | 9321 | 225 | 9694 | 231 | 0 | 0 | 0 | 0 | 0 | 0 | 0 | 0 |
| 347 | 3107454.3 | 669618.5 | 8989 | 210 | 9183 | 216 | 0 | 0 | 0 | 0 | 0 | 0 | 0 | 0 |
| 348 | 3105751.1 | 668517.5 | 7680 | 209 | 8757 | 215 | 8984 | 219 | 0 | 0 | 0 | 0 | 0 | 0 |
| 349 | 3099900.5 | 662382.1 | 9193 | 215 | 9475 | 220 | 0 | 0 | 0 | 0 | 0 | 0 | 0 | 0 |
| 350 | 3101154.7 | 681013.6 | 9135 | 215 | 11500 | 273 | 12140 | 283 | 0 | 0 | 0 | 0 | 0 | 0 |
| 351 | 3108768.3 | 678948.1 | 9232 | 206 | 0 | 0 | 0 | 0 | 0 | 0 | 0 | 0 | 0 | 0 |
| 352 | 3102449.5 | 677759.4 | 9380 | 215 | 10485 | 250 | 0 | 0 | 0 | 0 | 0 | 0 | 0 | 0 |
| 353 | 3109638.2 | 680320.6 | 9644 | 222 | 9982 | 229 | 0 | 0 | 0 | 0 | 0 | 0 | 0 | 0 |
| 354 | 3104569.3 | 679733.7 | 10009 | 211 | 10116 | 215 | 10328 | 251 | 0 | 0 | 0 | 0 | 0 | 0 |
| 355 | 3103330.9 | 678288.4 | 9042 | 208 | 10251 | 221 | 11996 | 281 | 0 | 0 | 0 | 0 | 0 | 0 |
| 356 | 3103137.0 | 673779.3 | 8411 | 222 | 9057 | 237 | 9469 | 241 | 0 | 0 | 0 | 0 | 0 | 0 |
| 357 | 3104648.5 | 681407.2 | 8807 | 211 | 9027 | 216 | 10666 | 260 | 0 | 0 | 0 | 0 | 0 | 0 |
| 358 | 3100010.8 | 672988.7 | 9990 | 249 | 0 | 0 | 0 | 0 | 0 | 0 | 0 | 0 | 0 | 0 |
| 359 | 3103698.2 | 681505.7 | 8752 | 225 | 10567 | 245 | 0 | 0 | 0 | 0 | 0 | 0 | 0 | 0 |
| 360 | 3106582.8 | 694751.5 | 9060 | 204 | 9814 | 215 | 0 | 0 | 0 | 0 | 0 | 0 | 0 | 0 |
| 361 | 3099161.6 | 691145.6 | 8422 | 201 | 9481 | 215 | 11021 | 237 | 0 | 0 | 0 | 0 | 0 | 0 |
| 362 | 3111898.4 | 690485.5 | 8995 | 215 | 10878 | 246 | 12479 | 265 | 0 | 0 | 0 | 0 | 0 | 0 |

| ID | UTM COORDINATES | | DEPTH/TEMP PAIRS.... | | | | | | | | | | | | | |
|---|---|---|---|---|---|---|---|---|---|---|---|---|---|---|---|---|
| 363 | 3104760.8 | 684086.2 | 9034 | 206 | 12324 | 268 | 0 | 0 | 0 | 0 | 0 | 0 | 0 | 0 | | |
| 364 | 3109754.5 | 695764.4 | 9069 | 210 | 11379 | 268 | 0 | 0 | 0 | 0 | 0 | 0 | 0 | 0 | | |
| 365 | 1.0 | 1.0 | -21 | -1 | -21 | -1 | 0 | 0 | 0 | 0 | 0 | 0 | 0 | 0 | | |
| 366 | 1.0 | 1.0 | -21 | -1 | -21 | -1 | 0 | 0 | 0 | 0 | 0 | 0 | 0 | 0 | | |
| 367 | 1.0 | 1.0 | -21 | -1 | -21 | -1 | 0 | 0 | 0 | 0 | 0 | 0 | 0 | 0 | | |
| 368 | 1.0 | 1.0 | -21 | -1 | -21 | -1 | 0 | 0 | 0 | 0 | 0 | 0 | 0 | 0 | | |
| 369 | 1.0 | 1.0 | -21 | -1 | -21 | -1 | 0 | 0 | 0 | 0 | 0 | 0 | 0 | 0 | | |
| 370 | 3108382.2 | 695037.9 | 9056 | 219 | 10447 | 256 | 10918 | 270 | 0 | 0 | 0 | 0 | 0 | 0 | | |
| 371 | 3108589.9 | 696040.8 | 9178 | 220 | 11808 | 288 | 0 | 0 | 0 | 0 | 0 | 0 | 0 | 0 | | |
| 372 | 3144552.5 | 505813.6 | 7920 | 203 | 10578 | 242 | 0 | 0 | 0 | 0 | 0 | 0 | 0 | 0 | | |
| 373 | 3144945.4 | 533340.2 | 11617 | 297 | 13326 | 324 | 14217 | 346 | 0 | 0 | 0 | 0 | 0 | 0 | | |
| 374 | 3141493.9 | 537278.6 | 11125 | 255 | 11261 | 250 | 0 | 0 | 0 | 0 | 0 | 0 | 0 | 0 | | |
| 375 | 3140475.1 | 547726.4 | 11733 | 303 | 0 | 0 | 0 | 0 | 0 | 0 | 0 | 0 | 0 | 0 | | |
| 376 | 3132261.9 | 510950.0 | 9539 | 241 | 11586 | 271 | 0 | 0 | 0 | 0 | 0 | 0 | 0 | 0 | | |
| 377 | 3134328.4 | 503489.9 | 8795 | 297 | 11210 | 304 | 12356 | 368 | 13220 | 341 | 16267 | 377 | 17262 | 395 | | |
| 378 | 3135182.6 | 522216.9 | 16572 | 326 | 18374 | 399 | 20124 | 424 | 0 | 0 | 0 | 0 | 0 | 0 | | |
| 379 | 3138194.4 | 513461.3 | 10344 | 238 | 0 | 0 | 0 | 0 | 0 | 0 | 0 | 0 | 0 | 0 | | |
| 381 | 3133944.8 | 532769.1 | 13557 | 303 | 14561 | 362 | 0 | 0 | 0 | 0 | 0 | 0 | 0 | 0 | | |
| 382 | 3119135.0 | 524606.3 | 7327 | 205 | 12273 | 281 | 14915 | 313 | 17372 | 343 | 20746 | 413 | 23937 | 452 | | |
| 383 | 3117932.8 | 546185.9 | 8156 | 227 | 0 | 0 | 0 | 0 | 0 | 0 | 0 | 0 | 0 | 0 | | |
| 384 | 3113012.3 | 545421.5 | 7601 | 207 | 0 | 0 | 0 | 0 | 0 | 0 | 0 | 0 | 0 | 0 | | |
| 385 | 3100124.8 | 500166.5 | 6130 | 198 | 0 | 0 | 0 | 0 | 0 | 0 | 0 | 0 | 0 | 0 | | |
| 386 | 3107292.1 | 513950.2 | 7712 | 208 | 16628 | 342 | 0 | 0 | 0 | 0 | 0 | 0 | 0 | 0 | | |
| 387 | 3100721.1 | 519488.4 | 9031 | 240 | 15136 | 368 | 15448 | 405 | 0 | 0 | 0 | 0 | 0 | 0 | | |
| 388 | 3107094.8 | 533128.4 | 7703 | 197 | 0 | 0 | 0 | 0 | 0 | 0 | 0 | 0 | 0 | 0 | | |
| 389 | 3101094.4 | 539628.7 | 9049 | 217 | 9549 | 279 | 0 | 0 | 0 | 0 | 0 | 0 | 0 | 0 | | |
| 390 | 3097179.5 | 542113.2 | 7522 | 217 | 0 | 0 | 0 | 0 | 0 | 0 | 0 | 0 | 0 | 0 | | |
| 391 | 3103091.0 | 549024.6 | 8354 | 246 | 10406 | 302 | 10907 | 314 | 11385 | 327 | 0 | 0 | 0 | 0 | | |
| 392 | 3107344.0 | 547252.9 | 8178 | 224 | 8994 | 241 | 0 | 0 | 0 | 0 | 0 | 0 | 0 | 0 | | |
| 393 | 3099061.9 | 539422.0 | 7868 | 214 | 9870 | 290 | 10968 | 295 | 0 | 0 | 0 | 0 | 0 | 0 | | |
| 394 | 3101425.7 | 540140.1 | 9572 | 280 | 0 | 0 | 0 | 0 | 0 | 0 | 0 | 0 | 0 | 0 | | |
| 395 | 3088406.3 | 458107.4 | 7921 | 219 | 0 | 0 | 0 | 0 | 0 | 0 | 0 | 0 | 0 | 0 | | |
| 396 | 3096639.9 | 484730.0 | 8639 | 230 | 9023 | 232 | 9405 | 237 | 0 | 0 | 0 | 0 | 0 | 0 | | |
| 397 | 3087825.8 | 483311.3 | 6567 | 195 | 0 | 0 | 0 | 0 | 0 | 0 | 0 | 0 | 0 | 0 | | |
| 398 | 3093120.7 | 492019.0 | 6770 | 196 | 0 | 0 | 0 | 0 | 0 | 0 | 0 | 0 | 0 | 0 | | |
| 399 | 3084194.8 | 494285.1 | 7482 | 223 | 0 | 0 | 0 | 0 | 0 | 0 | 0 | 0 | 0 | 0 | | |
| 400 | 3072431.2 | 455681.2 | 12486 | 274 | 14279 | 369 | 0 | 0 | 0 | 0 | 0 | 0 | 0 | 0 | | |
| 401 | 3081822.9 | 454480.3 | 11786 | 277 | 13555 | 330 | 14628 | 334 | 0 | 0 | 0 | 0 | 0 | 0 | | |
| 402 | 3081615.2 | 454869.0 | 8465 | 232 | 0 | 0 | 0 | 0 | 0 | 0 | 0 | 0 | 0 | 0 | | |
| 403 | 3071451.8 | 474529.7 | 6459 | 195 | 6837 | 201 | 0 | 0 | 0 | 0 | 0 | 0 | 0 | 0 | | |
| 404 | 3072069.5 | 486303.7 | 7441 | 214 | 0 | 0 | 0 | 0 | 0 | 0 | 0 | 0 | 0 | 0 | | |
| 405 | 3076104.9 | 487322.3 | 8248 | 212 | 9032 | 224 | 0 | 0 | 0 | 0 | 0 | 0 | 0 | 0 | | |
| 406 | 3072280.9 | 492281.6 | 9662 | 256 | 13300 | 322 | 14090 | 342 | 17360 | 403 | 18520 | 437 | 20055 | 459 | | |
| 407 | 3087274.1 | 500151.9 | 7144 | 206 | 0 | 0 | 0 | 0 | 0 | 0 | 0 | 0 | 0 | 0 | | |
| 408 | 3090578.0 | 510169.8 | 7103 | 204 | 0 | 0 | 0 | 0 | 0 | 0 | 0 | 0 | 0 | 0 | | |
| 409 | 3092037.4 | 517017.1 | 6637 | 208 | 0 | 0 | 0 | 0 | 0 | 0 | | | | | | |

| ID | UTM COORDINATES | | DEPTH/TEMP PAIRS.... | | | | | | | | | | | |
|---|---|---|---|---|---|---|---|---|---|---|---|---|---|---|
| 410 | 3093296.4 | 520945.6 | 5777 | 204 | 0 | 0 | 0 | 0 | 0 | 0 | 0 | 0 | 0 | 0 |
| 411 | 3085741.3 | 528048.9 | 7717 | 219 | 10467 | 298 | 0 | 0 | 0 | 0 | 0 | 0 | 0 | 0 |
| 412 | 3084824.1 | 528273.5 | 7489 | 202 | 8959 | 251 | 0 | 0 | 0 | 0 | 0 | 0 | 0 | 0 |
| 413 | 3085355.0 | 535497.7 | 7348 | 197 | 7510 | 206 | 9569 | 241 | 9700 | 248 | 0 | 0 | 0 | 0 |
| 414 | 3091738.1 | 533730.9 | 8111 | 225 | 8655 | 258 | 0 | 0 | 0 | 0 | 0 | 0 | 0 | 0 |
| 415 | 3096796.1 | 548057.4 | 8520 | 248 | 10065 | 297 | 0 | 0 | 0 | 0 | 0 | 0 | 0 | 0 |
| 416 | 3093238.3 | 546260.2 | 8485 | 221 | 0 | 0 | 0 | 0 | 0 | 0 | 0 | 0 | 0 | 0 |
| 417 | 3095001.9 | 548141.4 | 8857 | 269 | 0 | 0 | 0 | 0 | 0 | 0 | 0 | 0 | 0 | 0 |
| 418 | 3091719.8 | 545661.1 | 8316 | 260 | 0 | 0 | 0 | 0 | 0 | 0 | 0 | 0 | 0 | 0 |
| 419 | 3076905.3 | 507740.8 | 7125 | 199 | 0 | 0 | 0 | 0 | 0 | 0 | 0 | 0 | 0 | 0 |
| 420 | 3070891.9 | 510284.1 | 7111 | 215 | 7395 | 219 | 0 | 0 | 0 | 0 | 0 | 0 | 0 | 0 |
| 421 | 3071623.8 | 504621.8 | 8013 | 209 | 10515 | 287 | 0 | 0 | 0 | 0 | 0 | 0 | 0 | 0 |
| 422 | 3077077.3 | 544807.7 | 8099 | 247 | 9655 | 280 | 13645 | 376 | 0 | 0 | 0 | 0 | 0 | 0 |
| 423 | 3076493.1 | 542791.5 | 7990 | 247 | 9894 | 298 | 13294 | 376 | 0 | 0 | 0 | 0 | 0 | 0 |
| 424 | 3077622.3 | 544396.7 | 8411 | 250 | 10414 | 326 | 11061 | 337 | 12387 | 367 | 0 | 0 | 0 | 0 |
| 425 | 3078001.9 | 545787.6 | 8299 | 249 | 11147 | 317 | 11948 | 372 | 13400 | 401 | 14323 | 414 | | |
| | | | 15415 | 439 | | | | | | | | | | |
| 426 | 3076318.6 | 546096.0 | 8466 | 252 | 9466 | 267 | 0 | 0 | 0 | 0 | 0 | 0 | 0 | 0 |
| 427 | 3075906.6 | 545380.6 | 8442 | 244 | 8899 | 277 | 9447 | 295 | 0 | 0 | 0 | 0 | 0 | 0 |
| 428 | 3075803.9 | 546482.4 | 8602 | 276 | 9065 | 281 | 9361 | 287 | 0 | 0 | 0 | 0 | 0 | 0 |
| 429 | 3078026.8 | 542903.8 | 9119 | 230 | 11069 | 337 | 12349 | 368 | 12881 | 383 | 13274 | 383 | 0 | |
| 430 | 3077689.2 | 544390.2 | 8425 | 250 | 10398 | 326 | 11045 | 337 | 12373 | 367 | 0 | 0 | 0 | 0 |
| 431 | 3074181.6 | 545835.3 | 7654 | 229 | 10020 | 306 | 14631 | 409 | 0 | 0 | 0 | 0 | 0 | 0 |
| 432 | 3063536.9 | 453624.7 | 12536 | 288 | 0 | 0 | 0 | 0 | 0 | 0 | 0 | 0 | 0 | 0 |
| 433 | 3064689.3 | 454767.7 | 8936 | 232 | 0 | 0 | 0 | 0 | 0 | 0 | 0 | 0 | 0 | 0 |
| 434 | 3058498.9 | 455074.0 | 9152 | 225 | 0 | 0 | 0 | 0 | 0 | 0 | 0 | 0 | 0 | 0 |
| 435 | 3057797.1 | 476666.1 | 9212 | 260 | 0 | 0 | 0 | 0 | 0 | 0 | 0 | 0 | 0 | 0 |
| 436 | 3058535.3 | 482881.0 | 7650 | 232 | 8748 | 256 | 0 | 0 | 0 | 0 | 0 | 0 | 0 | 0 |
| 437 | 3059710.4 | 492140.5 | 7326 | 201 | 0 | 0 | 0 | 0 | 0 | 0 | 0 | 0 | 0 | 0 |
| 438 | 3066942.8 | 499776.6 | 7486 | 216 | 9285 | 277 | 9832 | 291 | 0 | 0 | 0 | 0 | 0 | 0 |
| 439 | 3064491.4 | 494565.9 | 7428 | 207 | 10462 | 237 | 10467 | 266 | 0 | 0 | 0 | 0 | 0 | 0 |
| 440 | 3052507.1 | 470702.0 | 7328 | 210 | 9070 | 245 | 10647 | 266 | 11808 | 277 | 13140 | 314 | 0 | |
| 441 | 3050633.5 | 472270.1 | 7379 | 214 | 10421 | 268 | 12412 | 308 | 0 | 0 | 0 | 0 | 0 | 0 |
| 442 | 3049128.9 | 476948.7 | 7023 | 220 | 0 | 0 | 0 | 0 | 0 | 0 | 0 | 0 | 0 | 0 |
| 443 | 3054017.5 | 477829.2 | 7927 | 221 | 0 | 0 | 0 | 0 | 0 | 0 | 0 | 0 | 0 | 0 |
| 444 | 3045008.0 | 499617.8 | 6783 | 216 | 0 | 0 | 0 | 0 | 0 | 0 | 0 | 0 | 0 | 0 |
| 445 | 3044392.8 | 491212.7 | 7106 | 211 | 10517 | 303 | 0 | 0 | 0 | 0 | 0 | 0 | 0 | 0 |
| 446 | 3089863.8 | 557919.5 | 7919 | 214 | 9469 | 275 | 0 | 0 | 0 | 0 | 0 | 0 | 0 | 0 |
| 447 | 3092013.1 | 558844.8 | 8756 | 250 | 9487 | 296 | 9800 | 302 | 0 | 0 | 0 | 0 | 0 | 0 |
| 448 | 3089345.3 | 554733.2 | 9014 | 236 | 9868 | 302 | 0 | 0 | 0 | 0 | 0 | 0 | 0 | 0 |
| 449 | 3096708.7 | 550364.2 | 8771 | 228 | 0 | 0 | 0 | 0 | 0 | 0 | 0 | 0 | 0 | 0 |
| 450 | 3092981.1 | 559308.7 | 8050 | 291 | 9005 | 287 | 9500 | 291 | 9636 | 292 | 0 | 0 | 0 | 0 |
| 451 | 3087740.6 | 583209.5 | 6703 | 195 | 0 | 0 | 0 | 0 | 0 | 0 | 0 | 0 | 0 | 0 |
| 452 | 3081731.3 | 551215.5 | 8355 | 250 | 9230 | 279 | 9993 | 305 | 0 | 0 | 0 | 0 | 0 | 0 |
| 453 | 3080694.5 | 578229.0 | 6470 | 195 | 0 | 0 | 0 | 0 | 0 | 0 | 0 | 0 | 0 | 0 |
| 454 | 3077197.1 | 584977.6 | 7116 | 212 | 7888 | 238 | 0 | 0 | 0 | 0 | 0 | 0 | 0 | 0 |
| 455 | 3091223.5 | 629616.0 | 7646 | 199 | 0 | 0 | 0 | 0 | 0 | 0 | 0 | 0 | 0 | 0 |
| 456 | 3085955.5 | 647405.4 | 9926 | 223 | 0 | 0 | 0 | 0 | 0 | 0 | 0 | 0 | 0 | 0 |
| 457 | 3091378.5 | 639370.6 | 8958 | 210 | 0 | 0 | 0 | 0 | 0 | 0 | 0 | 0 | 0 | 0 |

| ID | UTM COORDINATES | | DEPTH/TEMP PAIRS.... | | | | | | | | | | | |
|---|---|---|---|---|---|---|---|---|---|---|---|---|---|---|
| 458 | 3088934.9 | 636267.3 | 8250 | 204 | 8907 | 215 | 0 | 0 | 0 | 0 | 0 | 0 | 0 | 0 |
| 459 | 3085011.7 | 646035.2 | 9773 | 215 | 10303 | 221 | 0 | 0 | 0 | 0 | 0 | 0 | 0 | 0 |
| 460 | 3097412.7 | 646726.8 | 9210 | 216 | 9543 | 241 | 10106 | 255 | 0 | 0 | 0 | 0 | 0 | 0 |
| 461 | 3089382.0 | 643630.8 | 9888 | 211 | 0 | 0 | 0 | 0 | 0 | 0 | 0 | 0 | 0 | 0 |
| 462 | 3088273.2 | 641650.6 | 8643 | 202 | 9287 | 223 | 9942 | 229 | 0 | 0 | 0 | 0 | 0 | 0 |
| 463 | 3079223.7 | 621053.7 | 8454 | 214 | 8704 | 216 | 0 | 0 | 0 | 0 | 0 | 0 | 0 | 0 |
| 464 | 3080015.8 | 616917.2 | 7085 | 198 | 0 | 0 | 0 | 0 | 0 | 0 | 0 | 0 | 0 | 0 |
| 466 | 3078906.6 | 614409.8 | 7450 | 213 | 0 | 0 | 0 | 0 | 0 | 0 | 0 | 0 | 0 | 0 |
| 467 | 3079312.2 | 621852.5 | 8416 | 219 | 0 | 0 | 0 | 0 | 0 | 0 | 0 | 0 | 0 | 0 |
| 468 | 3078827.3 | 622840.1 | 8461 | 214 | 0 | 0 | 0 | 0 | 0 | 0 | 0 | 0 | 0 | 0 |
| 469 | 3073118.3 | 628284.7 | 8420 | 223 | 0 | 0 | 0 | 0 | 0 | 0 | 0 | 0 | 0 | 0 |
| 470 | 3079016.5 | 637902.9 | 8018 | 217 | 0 | 0 | 0 | 0 | 0 | 0 | 0 | 0 | 0 | 0 |
| 471 | 3082494.4 | 641351.2 | 8897 | 210 | 0 | 0 | 0 | 0 | 0 | 0 | 0 | 0 | 0 | 0 |
| 472 | 3064407.6 | 508085.3 | 7629 | 213 | 0 | 0 | 0 | 0 | 0 | 0 | 0 | 0 | 0 | 0 |
| 473 | 3067547.0 | 501449.2 | 7610 | 216 | 0 | 0 | 0 | 0 | 0 | 0 | 0 | 0 | 0 | 0 |
| 474 | 3060053.2 | 515116.6 | 7924 | 228 | 8995 | 257 | 0 | 0 | 0 | 0 | 0 | 0 | 0 | 0 |
| 475 | 3061145.2 | 520208.0 | 6302 | 235 | 9309 | 291 | 0 | 0 | 0 | 0 | 0 | 0 | 0 | 0 |
| 476 | 3056381.0 | 527891.8 | 7507 | 248 | 10487 | 352 | 0 | 0 | 0 | 0 | 0 | 0 | 0 | 0 |
| 477 | 3057931.8 | 527454.3 | 7424 | 238 | 10521 | 339 | 0 | 0 | 0 | 0 | 0 | 0 | 0 | 0 |
| 478 | 3069106.6 | 546437.1 | 6964 | 227 | 8136 | 241 | 9335 | 303 | 0 | 0 | 0 | 0 | 0 | 0 |
| 479 | 3065921.8 | 545596.9 | 7413 | 229 | 0 | 0 | 0 | 0 | 0 | 0 | 0 | 0 | 0 | 0 |
| 480 | 3045527.6 | 520023.2 | 6743 | 220 | 10526 | 329 | 11038 | 347 | 11425 | 359 | 12741 | 394 | 0 | |
| 481 | 3046327.0 | 520060.8 | 11105 | 328 | 11275 | 349 | 0 | 0 | 0 | 0 | 0 | 0 | 0 | 0 |
| 482 | 3047865.6 | 524347.2 | 8912 | 283 | 10316 | 302 | 11085 | 317 | 12285 | 349 | 0 | 0 | 0 | 0 |
| 483 | 3050300.9 | 514701.3 | 9011 | 241 | 12600 | 352 | 14197 | 391 | 19126 | 479 | 21639 | 507 | | |
| | | | 22973 | 526 | | | | | | | | | | |
| 484 | 3045329.0 | 532070.4 | 6986 | 207 | 0 | 0 | 0 | 0 | 0 | 0 | 0 | 0 | 0 | 0 |
| 485 | 3054160.8 | 526869.7 | 7190 | 226 | 9841 | 254 | 10694 | 333 | 0 | 0 | 0 | 0 | 0 | 0 |
| 486 | 3063936.3 | 569076.8 | 6906 | 216 | 0 | 0 | 0 | 0 | 0 | 0 | 0 | 0 | 0 | 0 |
| 487 | 3068482.6 | 586230.5 | 8166 | 218 | 0 | 0 | 0 | 0 | 0 | 0 | 0 | 0 | 0 | 0 |
| 488 | 3045654.1 | 559059.1 | 8475 | 206 | 0 | 0 | 0 | 0 | 0 | 0 | 0 | 0 | 0 | 0 |
| 489 | 3046499.4 | 551449.2 | 5579 | 197 | 0 | 0 | 0 | 0 | 0 | 0 | 0 | 0 | 0 | 0 |
| 490 | 3059104.5 | 613624.1 | 7708 | 207 | 0 | 0 | 0 | 0 | 0 | 0 | 0 | 0 | 0 | 0 |
| 491 | 3068423.9 | 614560.5 | 7464 | 197 | 0 | 0 | 0 | 0 | 0 | 0 | 0 | 0 | 0 | 0 |
| 492 | 3064732.4 | 615753.8 | 7115 | 204 | 0 | 0 | 0 | 0 | 0 | 0 | 0 | 0 | 0 | 0 |
| 493 | 3062056.3 | 634241.4 | 8396 | 232 | 8921 | 265 | 9200 | 270 | 9432 | 261 | 9672 | 265 | 9926 | |
| | | | 267 | | | | | | | | | | | |
| 494 | 3062652.9 | 643215.2 | 8642 | 216 | 10120 | 251 | 0 | 0 | 0 | 0 | 0 | 0 | 0 | 0 |
| 495 | 3064428.5 | 639537.3 | 8929 | 214 | 9218 | 226 | 0 | 0 | 0 | 0 | 0 | 0 | 0 | 0 |
| 496 | 3063390.0 | 642228.5 | 8439 | 209 | 10486 | 247 | 0 | 0 | 0 | 0 | 0 | 0 | 0 | 0 |
| 497 | 3069936.8 | 640095.0 | 9129 | 215 | 0 | 0 | 0 | 0 | 0 | 0 | 0 | 0 | 0 | 0 |
| 498 | 3063199.2 | 647708.8 | 10246 | 240 | 0 | 0 | 0 | 0 | 0 | 0 | 0 | 0 | 0 | 0 |
| 499 | 3068053.3 | 635314.7 | 8232 | 201 | 0 | 0 | 0 | 0 | 0 | 0 | 0 | 0 | 0 | 0 |
| 500 | 3064705.7 | 645924.9 | 9593 | 237 | 9748 | 237 | 0 | 0 | 0 | 0 | 0 | 0 | 0 | 0 |
| 501 | 3066391.1 | 646604.4 | 9079 | 206 | 9849 | 217 | 10121 | 222 | 0 | 0 | 0 | 0 | 0 | 0 |
| 502 | 3060604.9 | 639515.0 | 8453 | 211 | 0 | 0 | 0 | 0 | 0 | 0 | 0 | 0 | 0 | 0 |
| 503 | 3068052.4 | 639561.3 | 8542 | 219 | 0 | 0 | 0 | 0 | 0 | 0 | | | | |
| 504 | 3053739.8 | 607427.5 | 7560 | 195 | 8797 | 234 | 10756 | 265 | 0 | 0 | 0 | 0 | 0 | 0 |
| 505 | 3052752.6 | 638416.3 | 10661 | 253 | 0 | 0 | 0 | 0 | 0 | 0 | 0 | 0 | 0 | 0 |

| ID | UTM COORDINATES | | DEPTH/TEMP PAIRS.... | | | | | | | | | | | |
|---|---|---|---|---|---|---|---|---|---|---|---|---|---|---|
| 506 | 3044810.6 | 645353.9 | 8474 | 213 | 0 | 0 | 0 | 0 | 0 | 0 | 0 | 0 | 0 | 0 |
| 507 | 3029388.6 | 465673.9 | 8389 | 237 | 0 | 0 | 0 | 0 | 0 | 0 | 0 | 0 | 0 | 0 |
| 508 | 3028939.7 | 474639.7 | 7491 | 213 | 9465 | 259 | 10500 | 280 | 0 | 0 | 0 | 0 | 0 | 0 |
| 509 | 3028273.0 | 477020.6 | 10199 | 280 | 0 | 0 | 0 | 0 | 0 | 0 | 0 | 0 | 0 | 0 |
| 510 | 3028264.4 | 479219.6 | 9898 | 267 | 0 | 0 | 0 | 0 | 0 | 0 | 0 | 0 | 0 | 0 |
| 511 | 3027716.5 | 478896.1 | 7400 | 207 | 10199 | 290 | 0 | 0 | 0 | 0 | 0 | 0 | 0 | 0 |
| 512 | 3031721.8 | 481270.2 | 9279 | 276 | 10037 | 342 | 0 | 0 | 0 | 0 | 0 | 0 | 0 | 0 |
| 513 | 3029299.5 | 490178.9 | 7241 | 207 | 0 | 0 | 0 | 0 | 0 | 0 | 0 | 0 | 0 | 0 |
| 514 | 3031806.8 | 492131.0 | 7638 | 230 | 8888 | 268 | 0 | 0 | 0 | 0 | 0 | 0 | 0 | 0 |
| 515 | 3038530.8 | 498071.6 | 6288 | 210 | 7800 | 239 | 0 | 0 | 0 | 0 | 0 | 0 | 0 | 0 |
| 516 | 3019222.8 | 454643.2 | 7206 | 225 | 9575 | 289 | 0 | 0 | 0 | 0 | 0 | 0 | 0 | 0 |
| 517 | 3015066.4 | 467125.5 | 6793 | 190 | 9208 | 265 | 9602 | 279 | 0 | 0 | 0 | 0 | 0 | 0 |
| 518 | 3017509.4 | 472037.8 | 7056 | 210 | 10146 | 288 | 0 | 0 | 0 | 0 | 0 | 0 | 0 | 0 |
| 519 | 3025489.6 | 471462.2 | 9459 | 217 | 9609 | 219 | 0 | 0 | 0 | 0 | 0 | 0 | 0 | 0 |
| 520 | 3022140.7 | 470325.4 | 7000 | 197 | 0 | 0 | 0 | 0 | 0 | 0 | 0 | 0 | 0 | 0 |
| 521 | 3014602.7 | 467746.2 | 7066 | 206 | 9566 | 286 | 0 | 0 | 0 | 0 | 0 | 0 | 0 | 0 |
| 522 | 3016279.7 | 471396.8 | 6596 | 197 | 0 | 0 | 0 | 0 | 0 | 0 | 0 | 0 | 0 | 0 |
| 523 | 3020146.2 | 472650.0 | 6612 | 207 | 0 | 0 | 0 | 0 | 0 | 0 | 0 | 0 | 0 | 0 |
| 524 | 3016788.6 | 473833.9 | 6824 | 207 | 10241 | 307 | 0 | 0 | 0 | 0 | 0 | 0 | 0 | 0 |
| 525 | 3027614.9 | 477202.6 | 6829 | 197 | 10159 | 282 | 0 | 0 | 0 | 0 | 0 | 0 | 0 | 0 |
| 526 | 3026325.1 | 481190.9 | 7346 | 201 | 0 | 0 | 0 | 0 | 0 | 0 | 0 | 0 | 0 | 0 |
| 527 | 3024991.2 | 481134.5 | 9972 | 262 | 0 | 0 | 0 | 0 | 0 | 0 | 0 | 0 | 0 | 0 |
| 528 | 3027685.7 | 479249.4 | 7180 | 199 | 10105 | 288 | 0 | 0 | 0 | 0 | 0 | 0 | 0 | 0 |
| 529 | 3026895.3 | 477969.3 | 9522 | 261 | 0 | 0 | 0 | 0 | 0 | 0 | 0 | 0 | 0 | 0 |
| 530 | 3014229.2 | 480062.3 | 7359 | 212 | 11039 | 309 | 0 | 0 | 0 | 0 | 0 | 0 | 0 | 0 |
| 531 | 3023734.7 | 482619.4 | 7674 | 205 | 11982 | 335 | 0 | 0 | 0 | 0 | 0 | 0 | 0 | 0 |
| 532 | 3025223.2 | 491228.0 | 6641 | 208 | 0 | 0 | 0 | 0 | 0 | 0 | 0 | 0 | 0 | 0 |
| 533 | 3017064.0 | 499198.1 | 6790 | 218 | 7829 | 259 | 0 | 0 | 0 | 0 | 0 | 0 | 0 | 0 |
| 534 | 3036224.0 | 504753.8 | 6588 | 213 | 7896 | 253 | 8338 | 264 | 0 | 0 | 0 | 0 | 0 | 0 |
| 535 | 3032123.2 | 507712.1 | 7133 | 238 | 10521 | 317 | 0 | 0 | 0 | 0 | 0 | 0 | 0 | 0 |
| 536 | 3034796.2 | 515050.3 | 6686 | 228 | 9280 | 305 | 9784 | 328 | 9980 | 334 | 0 | 0 | 0 | 0 |
| 537 | 3041222.5 | 516850.1 | 11432 | 336 | 0 | 0 | 0 | 0 | 0 | 0 | 0 | 0 | 0 | 0 |
| 538 | 3034638.5 | 517618.3 | 7247 | 236 | 9641 | 318 | 9849 | 319 | 0 | 0 | 0 | 0 | 0 | 0 |
| 539 | 3025112.8 | 506679.1 | 7416 | 246 | 8758 | 287 | 9803 | 307 | 10746 | 329 | 0 | 0 | 0 | 0 |
| 540 | 3024990.3 | 503137.6 | 7107 | 236 | 9151 | 267 | 10606 | 301 | 0 | 0 | 0 | 0 | 0 | 0 |
| 541 | 3020651.6 | 502925.5 | 10174 | 279 | 0 | 0 | 0 | 0 | 0 | 0 | 0 | 0 | 0 | 0 |
| 542 | 3019361.1 | 501094.2 | 6631 | 214 | 9139 | 281 | 0 | 0 | 0 | 0 | 0 | 0 | 0 | 0 |
| 543 | 3014925.4 | 503145.8 | 6595 | 203 | 9209 | 266 | 10155 | 314 | 0 | 0 | 0 | 0 | 0 | 0 |
| 544 | 3026731.2 | 505473.9 | 7822 | 229 | 9131 | 292 | 0 | 0 | 0 | 0 | 0 | 0 | 0 | 0 |
| 545 | 3016039.6 | 505780.5 | 7650 | 219 | 10342 | 300 | 11137 | 323 | 11240 | 323 | 0 | 0 | 0 | 0 |
| 546 | 3015724.1 | 510155.8 | 6655 | 204 | 7671 | 241 | 8840 | 265 | 0 | 0 | 0 | 0 | 0 | 0 |
| 547 | 3014300.2 | 510150.0 | 6662 | 196 | 8538 | 229 | 9246 | 234 | 0 | 0 | 0 | 0 | 0 | 0 |
| 548 | 3016661.2 | 510295.6 | 6660 | 199 | 8844 | 270 | 9561 | 290 | 0 | 0 | 0 | 0 | 0 | 0 |
| 549 | 3016825.9 | 511896.0 | 8228 | 250 | 10770 | 333 | 11188 | 348 | 12022 | 368 | 0 | 0 | 0 | 0 |
| 550 | 3015718.2 | 511007.8 | 6647 | 193 | 9636 | 275 | 10503 | 283 | 0 | 0 | 0 | 0 | 0 | 0 |
| 551 | 3026981.9 | 539027.7 | 8466 | 261 | 9710 | 267 | 10623 | 312 | 12282 | 347 | 12761 | 350 | 0 | |
| 552 | 3035985.7 | 564335.8 | 5935 | 203 | 6458 | 207 | 6873 | 212 | 7688 | 224 | 0 | 0 | 0 | 0 |
| 553 | 3028946.6 | 591216.8 | 8349 | 214 | 9269 | 225 | 9859 | 235 | 12199 | 264 | 15943 | 369 | 19492 | |

| ID | UTM COORDINATES | | DEPTH/TEMP PAIRS.... | | | | | | | | | | | |
|---|---|---|---|---|---|---|---|---|---|---|---|---|---|---|
| 554 | 3027843.8 | 559559.0 | 7541 | 197 | 0 | 0 | 0 | 0 | 0 | 0 | 0 | 0 | 0 | 0 |
| 555 | 3015206.0 | 558413.1 | 7943 | 211 | 0 | 0 | 0 | 0 | 0 | 0 | 0 | 0 | 0 | 0 |
| 556 | 3022447.0 | 591223.3 | 8072 | 210 | 10746 | 253 | 0 | 0 | 0 | 0 | 0 | 0 | 0 | 0 |
| 557 | 3014739.6 | 595005.8 | 9266 | 215 | 10110 | 250 | 12003 | 295 | 0 | 0 | 0 | 0 | 0 | 0 |
| 558 | 3015401.4 | 594523.3 | 8458 | 207 | 12393 | 291 | 0 | 0 | 0 | 0 | 0 | 0 | 0 | 0 |
| 559 | 3020855.9 | 595417.4 | 8180 | 206 | 11684 | 286 | 0 | 0 | 0 | 0 | 0 | 0 | 0 | 0 |
| 560 | 3028798.6 | 601789.1 | 9006 | 220 | 0 | 0 | 0 | 0 | 0 | 0 | 0 | 0 | 0 | 0 |
| 561 | 3040646.3 | 609512.0 | 7941 | 198 | 8337 | 204 | 8321 | 203 | 0 | 0 | 0 | 0 | 0 | 0 |
| 562 | 3028599.8 | 599466.3 | 8291 | 218 | 10766 | 280 | 11559 | 306 | 12187 | 322 | 0 | 0 | 0 | 0 |
| 563 | 3034835.6 | 608742.8 | 8428 | 217 | 0 | 0 | 0 | 0 | 0 | 0 | 0 | 0 | 0 | 0 |
| 564 | 3030885.5 | 607739.3 | 9133 | 228 | 0 | 0 | 0 | 0 | 0 | 0 | 0 | 0 | 0 | 0 |
| 565 | 3039015.9 | 602419.4 | 7687 | 191 | 9480 | 220 | 11161 | 270 | 0 | 0 | 0 | 0 | 0 | 0 |
| 566 | 3031685.4 | 622623.1 | 10149 | 221 | 12974 | 298 | 14929 | 334 | 15879 | 353 | 0 | 0 | 0 | 0 |
| 567 | 3040088.2 | 612386.6 | 8306 | 204 | 9004 | 214 | 9304 | 216 | 9437 | 226 | 0 | 0 | 0 | 0 |
| 568 | 3032908.6 | 619155.6 | 7951 | 194 | 8960 | 208 | 9519 | 215 | 9740 | 229 | 0 | 0 | 0 | 0 |
| 569 | 3029458.7 | 625589.5 | 9240 | 202 | 9318 | 204 | 9683 | 211 | 0 | 0 | 0 | 0 | 0 | 0 |
| 570 | 3037952.4 | 633180.4 | 10071 | 233 | 10437 | 240 | 0 | 0 | 0 | 0 | 0 | 0 | 0 | 0 |
| 571 | 3030164.1 | 625251.0 | 8900 | 216 | 9592 | 226 | 10286 | 237 | 0 | 0 | 0 | 0 | 0 | 0 |
| 572 | 3040552.9 | 632874.3 | 9373 | 218 | 10550 | 258 | 0 | 0 | 0 | 0 | 0 | 0 | 0 | 0 |
| 573 | 3031743.5 | 624073.6 | 9987 | 225 | 0 | 0 | 0 | 0 | 0 | 0 | 0 | 0 | 0 | 0 |
| 574 | 3041915.2 | 636254.5 | 9759 | 252 | 0 | 0 | 0 | 0 | 0 | 0 | 0 | 0 | 0 | 0 |
| 575 | 3034804.6 | 643162.2 | 8674 | 218 | 0 | 0 | 0 | 0 | 0 | 0 | 0 | 0 | 0 | 0 |
| 576 | 3039434.8 | 636067.0 | 9383 | 210 | 9513 | 219 | 10222 | 242 | 11947 | 284 | 0 | 0 | 0 | 0 |
| 577 | 3035699.6 | 640076.1 | 9172 | 211 | 0 | 0 | 0 | 0 | 0 | 0 | 0 | 0 | 0 | 0 |
| 578 | 3029529.5 | 636804.4 | 9846 | 211 | 9981 | 216 | 14954 | 319 | 15573 | 336 | 0 | 0 | 0 | 0 |
| 579 | 3034200.3 | 640116.8 | 9451 | 215 | 9944 | 239 | 13602 | 311 | 0 | 0 | 0 | 0 | 0 | 0 |
| 580 | 3026499.3 | 602746.6 | 8835 | 214 | 0 | 0 | 0 | 0 | 0 | 0 | 0 | 0 | 0 | 0 |
| 581 | 3018812.1 | 622245.2 | 7875 | 188 | 8979 | 208 | 9480 | 209 | 0 | 0 | 0 | 0 | 0 | 0 |
| 582 | 3018646.3 | 614019.4 | 10437 | 241 | 0 | 0 | 0 | 0 | 0 | 0 | 0 | 0 | 0 | 0 |
| 583 | 3018703.6 | 621487.7 | 9548 | 209 | 9982 | 223 | 10479 | 229 | 0 | 0 | 0 | 0 | 0 | 0 |
| 584 | 3026156.6 | 620003.7 | 9977 | 225 | 0 | 0 | 0 | 0 | 0 | 0 | 0 | 0 | 0 | 0 |
| 585 | 3019463.5 | 623170.6 | 10147 | 231 | 0 | 0 | 0 | 0 | 0 | 0 | 0 | 0 | 0 | 0 |
| 586 | 3017566.0 | 614867.5 | 10949 | 244 | 0 | 0 | 0 | 0 | 0 | 0 | 0 | 0 | 0 | 0 |
| 587 | 3019417.4 | 614414.7 | 9933 | 236 | 0 | 0 | 0 | 0 | 0 | 0 | 0 | 0 | 0 | 0 |
| 588 | 3015206.2 | 630837.1 | 9784 | 223 | 10370 | 246 | 10465 | 249 | 12249 | 288 | 14187 | 325 | | |
| | | | 14679 | 330 | | | | | | | | | | |
| 589 | 3017979.3 | 630297.6 | 9537 | 232 | 10215 | 250 | 11235 | 272 | 11724 | 271 | 0 | 0 | 0 | 0 |
| 590 | 3019929.8 | 625513.6 | 10254 | 230 | 10767 | 235 | 10871 | 242 | 0 | 0 | 0 | 0 | 0 | 0 |
| 591 | 3019203.3 | 626878.7 | 9473 | 213 | 10364 | 224 | 0 | 0 | 0 | 0 | 0 | 0 | 0 | 0 |
| 592 | 3014813.3 | 628936.2 | 9706 | 204 | 9910 | 227 | 11118 | 261 | 0 | 0 | 0 | 0 | 0 | 0 |
| 593 | 3019345.9 | 635183.7 | 10455 | 232 | 10549 | 244 | 11187 | 266 | 11748 | 274 | 12506 | 288 | | |
| | | | 15060 | 325 | | | | | | | | | | |
| 594 | 3026202.8 | 624308.4 | 9399 | 215 | 10014 | 221 | 10524 | 250 | 11031 | 254 | 0 | 0 | 0 | 0 |
| 595 | 3020072.3 | 630976.8 | 9985 | 221 | 11495 | 269 | 12495 | 309 | 0 | 0 | 0 | 0 | 0 | 0 |
| 596 | 3017363.4 | 634588.0 | 10092 | 228 | 11361 | 245 | 11915 | 283 | 13239 | 9 | | | | |
| 597 | 3028253.5 | 628643.8 | 8874 | 211 | 9337 | 215 | 10057 | 230 | 0 | 0 | 0 | 0 | 0 | 0 |
| 598 | 3025116.9 | 625187.0 | 10284 | 224 | 11984 | 269 | 0 | 0 | 0 | 0 | 0 | 0 | 0 | 0 |
| 599 | 3020222.1 | 623948.6 | 8776 | 199 | 9725 | 219 | 0 | 0 | 0 | 0 | 0 | 0 | 0 | 0 |
| 600 | 3027423.2 | 627945.8 | 9060 | 216 | 9902 | 223 | 11360 | 261 | 0 | 0 | 0 | 0 | 0 | 0 |

| ID | UTM COORDINATES | | DEPTH/TEMP PAIRS.... | | | | | | | | | | | |
|---|---|---|---|---|---|---|---|---|---|---|---|---|---|---|
| 601 | 3017173.8 | 625980.0 | 9980 | 297 | 0 | 0 | 0 | 0 | 0 | 0 | 0 | 0 | 0 | 0 |
| 602 | 3050293.6 | 660422.0 | 8371 | 214 | 0 | 0 | 0 | 0 | 0 | 0 | 0 | 0 | 0 | 0 |
| 603 | 3054948.8 | 654538.0 | 11413 | 224 | 12815 | 292 | 13582 | 306 | 0 | 0 | 0 | 0 | 0 | 0 |
| 604 | 3055925.8 | 648013.1 | 10255 | 274 | 11551 | 295 | 12939 | 327 | 0 | 0 | 0 | 0 | 0 | 0 |
| 605 | 3053177.7 | 670599.7 | 9364 | 220 | 10991 | 262 | 0 | 0 | 0 | 0 | 0 | 0 | 0 | 0 |
| 606 | 3050016.4 | 669717.7 | 9268 | 225 | 9514 | 239 | 10003 | 239 | 10430 | 254 | 10983 | 242 | 0 | |
| 607 | 3055031.0 | 667758.4 | 8744 | 209 | 10014 | 241 | 0 | 0 | 0 | 0 | 0 | 0 | 0 | 0 |
| 609 | 3046748.7 | 668079.4 | 9549 | 222 | 10256 | 234 | 0 | 0 | 0 | 0 | 0 | 0 | 0 | 0 |
| 609 | 3068184.8 | 651360.8 | 9551 | 250 | 10473 | 242 | 0 | 0 | 0 | 0 | 0 | 0 | 0 | 0 |
| 610 | 3060975.9 | 648091.9 | 10394 | 232 | 12444 | 293 | 14444 | 318 | 14933 | 332 | 0 | 0 | 0 | 0 |
| 611 | 3059929.6 | 648853.6 | 10149 | 216 | 11579 | 271 | 0 | 0 | 0 | 0 | 0 | 0 | 0 | 0 |
| 612 | 3061496.4 | 649804.6 | 10488 | 242 | 10900 | 240 | 11187 | 242 | 11355 | 246 | 13155 | 299 | 0 | |
| 613 | 3057879.4 | 650078.8 | 10300 | 218 | 11550 | 275 | 0 | 0 | 0 | 0 | 0 | 0 | 0 | 0 |
| 614 | 3058452.0 | 658792.8 | 9364 | 214 | 11155 | 258 | 0 | 0 | 0 | 0 | 0 | 0 | 0 | 0 |
| 615 | 3068673.4 | 651812.0 | 9657 | 226 | 10569 | 257 | 0 | 0 | 0 | 0 | 0 | 0 | 0 | 0 |
| 616 | 3068622.6 | 654373.7 | 9276 | 213 | 9601 | 218 | 9984 | 234 | 0 | 0 | 0 | 0 | 0 | 0 |
| 617 | 3066951.1 | 654237.9 | 9046 | 211 | 9938 | 223 | 11500 | 238 | 0 | 0 | 0 | 0 | 0 | 0 |
| 618 | 3059296.2 | 658235.5 | 10399 | 232 | 12441 | 293 | 14437 | 318 | 14933 | 332 | 0 | 0 | 0 | 0 |
| 619 | 3062508.3 | 662496.3 | 9484 | 231 | 0 | 0 | 0 | 0 | 0 | 0 | 0 | 0 | 0 | 0 |
| 620 | 3061824.7 | 662000.5 | 7466 | 202 | 8468 | 204 | 10452 | 247 | 0 | 0 | 0 | 0 | 0 | 0 |
| 621 | 3059006.7 | 665444.1 | 9321 | 210 | 10986 | 260 | 0 | 0 | 0 | 0 | 0 | 0 | 0 | 0 |
| 622 | 3069114.7 | 669836.9 | 9226 | 212 | 0 | 0 | 0 | 0 | 0 | 0 | 0 | 0 | 0 | 0 |
| 623 | 3068113.9 | 671338.0 | 9434 | 226 | 10811 | 256 | 11971 | 278 | 0 | 0 | 0 | 0 | 0 | 0 |
| 624 | 3058328.5 | 661653.3 | 9587 | 217 | 13836 | 277 | 14157 | 311 | 15176 | 319 | 0 | 0 | 0 | 0 |
| 625 | 3068538.7 | 671341.4 | 9402 | 214 | 11548 | 273 | 0 | 0 | 0 | 0 | 0 | 0 | 0 | 0 |
| 626 | 3068698.0 | 674978.9 | 9169 | 222 | 10509 | 244 | 0 | 0 | 0 | 0 | 0 | 0 | 0 | 0 |
| 627 | 3064370.8 | 672864.7 | 9329 | 220 | 10479 | 241 | 10872 | 267 | 0 | 0 | 0 | 0 | 0 | 0 |
| 628 | 3067903.6 | 672628.7 | 8455 | 209 | 9674 | 233 | 10569 | 256 | 0 | 0 | 0 | 0 | 0 | 0 |
| 629 | 3067830.3 | 672605.9 | 9599 | 223 | 10337 | 240 | 10891 | 260 | 11976 | 279 | 0 | 0 | 0 | 0 |
| 630 | 3064459.3 | 675708.8 | 9010 | 216 | 9384 | 219 | 0 | 0 | 0 | 0 | 0 | 0 | 0 | 0 |
| 631 | 3093173.6 | 654515.1 | 9158 | 216 | 9632 | 215 | 10139 | 255 | 0 | 0 | 0 | 0 | 0 | 0 |
| 632 | 3087972.2 | 658373.6 | 10821 | 243 | 13431 | 306 | 14546 | 340 | 0 | 0 | 0 | 0 | 0 | 0 |
| 633 | 3085171.2 | 658108.2 | 9624 | 213 | 10040 | 220 | 0 | 0 | 0 | 0 | 0 | 0 | 0 | 0 |
| 634 | 3087945.5 | 659147.6 | 10581 | 238 | 13584 | 320 | 14382 | 321 | 0 | 0 | 0 | 0 | 0 | 0 |
| 635 | 3085909.6 | 655504.6 | 10251 | 241 | 12276 | 286 | 0 | 0 | 0 | 0 | 0 | 0 | 0 | 0 |
| 636 | 3097035.2 | 657201.0 | 9695 | 216 | 10075 | 231 | 0 | 0 | 0 | 0 | 0 | 0 | 0 | 0 |
| 637 | 3087520.3 | 671678.5 | 10107 | 222 | 14137 | 311 | 0 | 0 | 0 | 0 | 0 | 0 | 0 | 0 |
| 638 | 3097258.4 | 671643.2 | 9680 | 230 | 10959 | 278 | 0 | 0 | 0 | 0 | 0 | 0 | 0 | 0 |
| 639 | 3087658.6 | 663276.8 | 8611 | 194 | 9523 | 213 | 9954 | 206 | 10666 | 250 | 11217 | 258 | 0 | |
| 640 | 3089166.7 | 662271.4 | 10407 | 214 | 11902 | 268 | 0 | 0 | 0 | 0 | 0 | 0 | 0 | 0 |
| 641 | 3096462.2 | 672025.0 | 9480 | 226 | 9730 | 229 | 10913 | 262 | 11469 | 270 | 12434 | 291 | 0 | |
| 642 | 3087664.3 | 663849.2 | 9906 | 222 | 10934 | 263 | 11683 | 261 | 0 | 0 | 0 | 0 | 0 | 0 |
| 643 | 3096783.2 | 682031.2 | 8991 | 211 | 9944 | 221 | 0 | 0 | 0 | 0 | 0 | 0 | 0 | 0 |
| 644 | 3089020.2 | 675917.2 | 9947 | 236 | 11260 | 271 | 12519 | 298 | 0 | 0 | 0 | 0 | 0 | 0 |
| 645 | 3096932.8 | 675371.2 | 9472 | 217 | 9686 | 221 | 10972 | 267 | 11228 | 270 | 0 | 0 | 0 | 0 |
| 646 | 3093209.4 | 672298.8 | 9970 | 230 | 10988 | 243 | 11479 | 269 | 0 | 0 | 0 | 0 | 0 | 0 |
| 647 | 3091034.4 | 680285.4 | 10020 | 225 | 11960 | 286 | 13974 | 311 | 0 | 0 | 0 | 0 | 0 | 0 |
| 648 | 3086701.6 | 677493.5 | 9949 | 226 | 11750 | 271 | 13528 | 302 | 0 | 0 | 0 | 0 | 0 | 0 |
| 649 | 3094529.0 | 683186.0 | 9383 | 230 | 11218 | 272 | 0 | 0 | 0 | 0 | 0 | 0 | 0 | 0 |

| ID | UTM COORDINATES | DEPTH/TEMP PAIRS.... | | | | | | | | | | | | | | | |
|---|---|---|---|---|---|---|---|---|---|---|---|---|---|---|---|---|---|
| 650 | 3094578.0 | 680231.0 | 9817 | 225 | 12472 | 287 | 0 | 0 | 0 | 0 | 0 | 0 | 0 | 0 | | | |
| 651 | 3086514.9 | 686505.2 | 8679 | 205 | 9825 | 258 | 10835 | 270 | 0 | 0 | 0 | 0 | 0 | 0 | | | |
| 652 | 3085396.2 | 686302.8 | 8997 | 212 | 9575 | 231 | 11983 | 281 | 0 | 0 | 0 | 0 | 0 | 0 | | | |
| 653 | 3088332.2 | 687211.0 | 9060 | 209 | 13005 | 308 | 0 | 0 | 0 | 0 | 0 | 0 | 0 | 0 | | | |
| 654 | 3088243.8 | 688248.2 | 9160 | 220 | 10610 | 262 | 0 | 0 | 0 | 0 | 0 | 0 | 0 | 0 | | | |
| 655 | 3095951.5 | 688400.7 | 9107 | 218 | 12963 | 297 | 0 | 0 | 0 | 0 | 0 | 0 | 0 | 0 | | | |
| 656 | 3038865.0 | 666856.8 | 8987 | 225 | 10191 | 238 | 0 | 0 | 0 | 0 | 0 | 0 | 0 | 0 | | | |
| 657 | 3030631.8 | 660720.0 | 10388 | 223 | 11481 | 268 | 0 | 0 | 0 | 0 | 0 | 0 | 0 | 0 | | | |
| 658 | 3022976.4 | 659607.9 | 8972 | 200 | 10474 | 230 | 0 | 0 | 0 | 0 | 0 | 0 | 0 | 0 | | | |
| 659 | 3018497.9 | 654034.1 | 10268 | 216 | 10574 | 227 | 12505 | 276 | 0 | 0 | 0 | 0 | 0 | 0 | | | |
| 660 | 3025817.5 | 668633.0 | 9964 | 229 | 10346 | 215 | 11620 | 255 | 12419 | 283 | 13271 | 306 | 0 | | | | |
| 661 | 3025933.0 | 665607.7 | 9043 | 209 | 10677 | 255 | 10989 | 262 | 0 | 0 | 0 | 0 | 0 | 0 | | | |
| 662 | 3020411.5 | 662845.3 | 8010 | 201 | 10803 | 257 | 0 | 0 | 0 | 0 | 0 | 0 | 0 | 0 | | | |
| 663 | 3035674.2 | 658590.3 | 8417 | 204 | 0 | 0 | 0 | 0 | 0 | 0 | 0 | 0 | 0 | 0 | | | |
| 664 | 3105642.3 | 697833.0 | 9213 | 217 | 11982 | 272 | 0 | 0 | 0 | 0 | 0 | 0 | 0 | 0 | | | |
| 665 | 3109420.7 | 696988.0 | 8473 | 204 | 8909 | 214 | 9718 | 241 | 10469 | 254 | 0 | 0 | 0 | 0 | | | |
| 666 | 3104290.2 | 697267.4 | 9117 | 217 | 9346 | 219 | 11505 | 240 | 11966 | 245 | 0 | 0 | 0 | 0 | | | |
| 667 | 3111727.6 | 697850.1 | 9080 | 226 | 11394 | 273 | 0 | 0 | 0 | 0 | 0 | 0 | 0 | 0 | | | |
| 668 | 3104251.9 | 696416.1 | 9141 | 216 | 11999 | 281 | 0 | 0 | 0 | 0 | 0 | 0 | 0 | 0 | | | |
| 669 | 3101751.6 | 696196.4 | 9258 | 228 | 11790 | 281 | 0 | 0 | 0 | 0 | 0 | 0 | 0 | 0 | | | |
| 670 | 3109153.9 | 696332.8 | 9155 | 220 | 11451 | 269 | 0 | 0 | 0 | 0 | 0 | 0 | 0 | 0 | | | |
| 671 | 3101971.4 | 696889.7 | 8959 | 214 | 10062 | 227 | 10964 | 250 | 11790 | 258 | 0 | 0 | 0 | 0 | | | |
| 672 | 3120033.6 | 697571.1 | 11076 | 255 | 0 | 0 | 0 | 0 | 0 | 0 | 0 | 0 | 0 | 0 | | | |
| 673 | 3120011.5 | 697148.6 | 11091 | 244 | 0 | 0 | 0 | 0 | 0 | 0 | 0 | 0 | 0 | 0 | | | |
| 674 | 3120217.9 | 705136.7 | -27 | -1 | 0 | 0 | 0 | 0 | 0 | 0 | 0 | 0 | 0 | 0 | | | |
| 675 | 3157330.8 | 705381.9 | -27 | -1 | 0 | 0 | 0 | 0 | 0 | 0 | 0 | 0 | 0 | 0 | | | |
| 676 | 3203165.3 | 647473.2 | -27 | -1 | 0 | 0 | 0 | 0 | 0 | 0 | 0 | 0 | 0 | 0 | | | |
| 677 | 1.0 | 1.0 | -27 | -1 | 0 | 0 | 0 | 0 | 0 | 0 | 0 | 0 | 0 | 0 | | | |
| 678 | 3200827.9 | 646557.6 | 9772 | 245 | 10272 | 263 | 10706 | 286 | 11802 | 315 | 0 | 0 | 0 | 0 | | | |
| 679 | 3204234.5 | 653825.6 | 9939 | 252 | 10112 | 254 | 12622 | 317 | 0 | 0 | 0 | 0 | 0 | 0 | | | |
| 680 | 3204910.3 | 648291.0 | 9870 | 243 | 0 | 0 | 0 | 0 | 0 | 0 | 0 | 0 | 0 | 0 | | | |
| 681 | 3204002.8 | 651961.4 | 9861 | 245 | 12243 | 333 | 12721 | 332 | 0 | 0 | 0 | 0 | 0 | 0 | | | |
| 682 | 3196016.2 | 648582.5 | 9813 | 255 | 10510 | 304 | 10858 | 312 | 12919 | 342 | 0 | 0 | 0 | 0 | | | |
| 683 | 3204015.0 | 656885.9 | 10162 | 266 | 11717 | 313 | 0 | 0 | 0 | 0 | 0 | 0 | 0 | 0 | | | |
| 684 | 3197787.6 | 647963.1 | 9100 | 247 | 9371 | 246 | 11079 | 308 | 12108 | 329 | 0 | 0 | 0 | 0 | | | |
| 685 | 3202899.3 | 651569.2 | 9911 | 252 | 11098 | 300 | 0 | 0 | 0 | 0 | 0 | 0 | 0 | 0 | | | |
| 686 | 3207411.1 | 655930.0 | 9723 | 241 | 10028 | 244 | 10190 | 246 | 11747 | 314 | 0 | 0 | 0 | 0 | | | |
| 687 | 3207207.9 | 652427.6 | 10102 | 256 | 11512 | 324 | 0 | 0 | 0 | 0 | 0 | 0 | 0 | 0 | | | |
| 688 | 3207273.9 | 653917.7 | 9903 | 262 | 10401 | 297 | 0 | 0 | 0 | 0 | 0 | 0 | 0 | 0 | | | |
| 689 | 3199985.7 | 654761.9 | 14808 | 389 | 15291 | 383 | 0 | 0 | 0 | 0 | | | | | | | |
| 690 | 3202304.6 | 651970.6 | 10062 | 252 | 11782 | 328 | 12776 | 342 | 0 | 0 | 0 | 0 | 0 | 0 | | | |
| 691 | 3204708.8 | 655338.1 | 9703 | 241 | 11213 | 315 | 11714 | 330 | 0 | 0 | 0 | 0 | 0 | 0 | | | |
| 692 | 3191127.0 | 657457.3 | 8752 | 240 | 0 | 0 | 0 | 0 | 0 | 0 | 0 | 0 | 0 | 0 | | | |
| 693 | 3186066.4 | 653357.0 | 9144 | 244 | 0 | 0 | 0 | 0 | 0 | 0 | 0 | 0 | 0 | 0 | | | |
| 694 | 3181288.2 | 655539.5 | 9232 | 245 | 9373 | 261 | 0 | 0 | 0 | 0 | 0 | 0 | 0 | 0 | | | |
| 695 | 3189282.1 | 651588.9 | 8960 | 246 | 0 | 0 | 0 | 0 | 0 | 0 | 0 | 0 | 0 | 0 | | | |
| 696 | 3193565.8 | 649032.7 | 10184 | 254 | 11013 | 276 | 12401 | 313 | 0 | 0 | 0 | 0 | 0 | 0 | | | |
| 697 | 3190595.5 | 652129.1 | 9218 | 251 | 10718 | 318 | 0 | 0 | 0 | 0 | 0 | 0 | 0 | 0 | | | |
| 698 | 3193852.7 | 648765.3 | 9729 | 251 | 10251 | 258 | 11646 | 313 | 14037 | 356 | 0 | 0 | 0 | 0 | | | |

| ID | UTM COORDINATES | DEPTH/TEMP PAIRS.... | | | | | | | | | | | | | |
|---|---|---|---|---|---|---|---|---|---|---|---|---|---|---|---|
| 699 | 3192824.3 | 649090.0 | 10202 | 264 | 11329 | 307 | 0 | 0 | 0 | 0 | 0 | 0 | 0 | 0 | |
| 700 | 3186965.0 | 657551.7 | 8504 | 205 | 9253 | 223 | 0 | 0 | 0 | 0 | 0 | 0 | 0 | 0 | |
| 701 | 3231943.0 | 587236.6 | 7126 | 197 | 0 | 0 | 0 | 0 | 0 | 0 | 0 | 0 | 0 | 0 | |
| 702 | 3213007.0 | 560232.7 | 8027 | 200 | 0 | 0 | 0 | 0 | 0 | 0 | 0 | 0 | 0 | 0 | |
| 703 | 3195033.5 | 537210.1 | 9839 | 208 | 14604 | 299 | 15057 | 312 | 0 | 0 | 0 | 0 | 0 | 0 | |
| 704 | 3191383.0 | 515670.8 | 6940 | 196 | 0 | 0 | 0 | 0 | 0 | 0 | 0 | 0 | 0 | 0 | |
| 705 | 3185204.0 | 524448.8 | 7572 | 218 | 8646 | 246 | 0 | 0 | 0 | 0 | 0 | 0 | 0 | 0 | |
| 706 | 3123907.1 | 481486.1 | 10764 | 261 | 0 | 0 | 0 | 0 | 0 | 0 | 0 | 0 | 0 | 0 | |
| 707 | 3119671.7 | 483848.3 | 8075 | 213 | 0 | 0 | 0 | 0 | 0 | 0 | 0 | 0 | 0 | 0 | |
| 708 | 3112902.5 | 494547.8 | 5809 | 214 | 0 | 0 | 0 | 0 | 0 | 0 | 0 | 0 | 0 | 0 | |
| 709 | 3110618.7 | 462051.3 | 7358 | 208 | 0 | 0 | 0 | 0 | 0 | 0 | 0 | 0 | 0 | 0 | |
| 710 | 3107029.6 | 454494.3 | 6682 | 246 | 0 | 0 | 0 | 0 | 0 | 0 | 0 | 0 | 0 | 0 | |
| 711 | 3101707.1 | 459794.9 | 6955 | 209 | 0 | 0 | 0 | 0 | 0 | 0 | 0 | 0 | 0 | 0 | |
| 712 | 3103245.8 | 469115.4 | 8110 | 219 | 0 | 0 | 0 | 0 | 0 | 0 | 0 | 0 | 0 | 0 | |
| 713 | 3102059.6 | 474832.5 | 8237 | 219 | 0 | 0 | 0 | 0 | 0 | 0 | 0 | 0 | 0 | 0 | |
| 714 | 1.0 | 1.0 | -478 | -1 | 0 | 0 | 0 | 0 | 0 | 0 | 0 | 0 | 0 | 0 | |
| 715 | 3134935.6 | 486014.2 | 7242 | 198 | 0 | 0 | 0 | 0 | 0 | 0 | 0 | 0 | 0 | 0 | |
| 716 | 3132072.7 | 492722.5 | 10049 | 235 | 10236 | 284 | 10446 | 284 | 0 | 0 | 0 | 0 | 0 | 0 | |
| 717 | 3135249.1 | 499432.1 | 10135 | 247 | 0 | 0 | 0 | 0 | 0 | 0 | 0 | 0 | 0 | 0 | |
| 718 | 3130637.3 | 490272.1 | 10114 | 240 | 0 | 0 | 0 | 0 | 0 | 0 | 0 | 0 | 0 | 0 | |
| 719 | 3224328.4 | 614288.5 | 7865 | 218 | 8190 | 217 | 0 | 0 | 0 | 0 | 0 | 0 | 0 | 0 | |
| 720 | 3216829.6 | 608870.2 | 9199 | 244 | 9759 | 240 | 10037 | 241 | 10840 | 267 | 0 | 0 | 0 | 0 | |
| 721 | 3210188.1 | 627926.9 | 8518 | 224 | 0 | 0 | 0 | 0 | 0 | 0 | 0 | 0 | 0 | 0 | |
| 722 | 3217890.2 | 622673.2 | 10853 | 254 | 0 | 0 | 0 | 0 | 0 | 0 | 0 | 0 | 0 | 0 | |
| 723 | 3215624.2 | 649304.7 | 15302 | 336 | 16334 | 378 | 17608 | 402 | 0 | 0 | 0 | 0 | 0 | 0 | |
| 724 | 3217049.5 | 658003.4 | 9650 | 255 | 11130 | 271 | 14358 | 332 | 0 | 0 | 0 | 0 | 0 | 0 | |
| 725 | 3219830.2 | 655621.5 | 13758 | 310 | 13952 | 309 | 0 | 0 | 0 | 0 | 0 | 0 | 0 | 0 | |
| 726 | 3209567.8 | 657716.0 | 9896 | 253 | 10314 | 257 | 0 | 0 | 0 | 0 | 0 | 0 | 0 | 0 | |
| 727 | 3211649.3 | 650013.1 | 13865 | 308 | 14355 | 324 | 0 | 0 | 0 | 0 | 0 | 0 | 0 | 0 | |
| 728 | 3209173.6 | 657324.5 | 10053 | 267 | 0 | 0 | 0 | 0 | 0 | 0 | 0 | 0 | 0 | 0 | |
| 729 | 3210365.7 | 655563.3 | 7228 | 221 | 0 | 0 | 0 | 0 | 0 | 0 | 0 | 0 | 0 | 0 | |
| 730 | 3213649.5 | 653510.7 | 13234 | 304 | 14063 | 319 | 14345 | 312 | 0 | 0 | 0 | 0 | 0 | 0 | |
| 731 | 3215745.3 | 648700.4 | 13810 | 332 | 0 | 0 | 0 | 0 | 0 | 0 | 0 | 0 | 0 | 0 | |
| 732 | 3216623.7 | 650998.6 | 9506 | 241 | 14084 | 326 | 0 | 0 | 0 | 0 | 0 | 0 | 0 | 0 | |
| 733 | 3211637.1 | 650013.3 | 14347 | 324 | 0 | 0 | 0 | 0 | 0 | 0 | 0 | 0 | 0 | 0 | |
| 734 | 3102095.4 | 549212.5 | 8527 | 248 | 10408 | 309 | 0 | 0 | 0 | 0 | 0 | 0 | 0 | 0 | |
| 735 | 3100349.4 | 559164.5 | 8179 | 221 | 8243 | 222 | 9465 | 191 | 0 | 0 | 0 | 0 | 0 | 0 | |
| 736 | 3099576.3 | 555084.5 | 8725 | 258 | 10181 | 308 | 10930 | 338 | 10997 | 343 | 0 | 0 | 0 | 0 | |
| 737 | 3101341.1 | 552016.8 | 9149 | 255 | 10364 | 292 | 11015 | 308 | 0 | 0 | 0 | 0 | 0 | 0 | |
| 738 | 3099209.4 | 559209.3 | 8335 | 252 | 9565 | 294 | 9671 | 296 | 10395 | 344 | 0 | 0 | 0 | 0 | |
| 739 | 3103396.3 | 559734.3 | 8010 | 225 | 8231 | 259 | 9022 | 269 | 9588 | 283 | 10136 | 304 | 0 | | |
| 740 | 3103869.9 | 560291.9 | 7648 | 236 | 10494 | 316 | 0 | 0 | 0 | 0 | 0 | 0 | 0 | 0 | |
| 741 | 3106076.7 | 557654.0 | 8402 | 230 | 10783 | 312 | 0 | 0 | 0 | 0 | 0 | 0 | 0 | 0 | |
| 742 | 3102412.8 | 550106.6 | 9360 | 303 | 10354 | 317 | 0 | 0 | 0 | 0 | 0 | 0 | 0 | 0 | |
| 743 | 3109557.9 | 560104.9 | 7832 | 256 | 9719 | 297 | 11370 | 343 | 13026 | 360 | 0 | 0 | 0 | 0 | |
| 744 | 3105138.1 | 556861.9 | 7478 | 224 | 7980 | 231 | 9850 | 257 | 10455 | 302 | 10779 | 302 | 0 | | |
| 745 | 3110296.1 | 572947.9 | 8606 | 236 | 10946 | 310 | 11517 | 327 | 0 | 0 | 0 | 0 | 0 | 0 | |
| 746 | 3110611.1 | 563274.3 | 7624 | 225 | 10126 | 302 | 0 | 0 | 0 | 0 | 0 | 0 | 0 | 0 | |

| ID | UTM COORDINATES | | DEPTH/TEMP PAIRS.... | | | | | | | | | | | |
|---|---|---|---|---|---|---|---|---|---|---|---|---|---|---|
| 747 | 3101499.1 | 563028.5 | 7968 | 249 | 9465 | 296 | 10431 | 319 | 10697 | 324 | 11804 | 357 | 12131 | |
| | | | 365 | | | | | | | | | | | |
| 748 | 3108758.1 | 561683.8 | 7748 | 237 | 10161 | 262 | 0 | 0 | 0 | 0 | 0 | 0 | 0 | |
| 749 | 3098945.9 | 561583.2 | 7998 | 238 | 8902 | 282 | 9421 | 296 | 10007 | 312 | 10339 | 322 | 0 | |
| 750 | 3107062.9 | 561683.8 | 7682 | 220 | 0 | 0 | 0 | 0 | 0 | 0 | 0 | 0 | 0 | |
| 751 | 3110880.7 | 563461.4 | 7629 | 243 | 9035 | 262 | 10036 | 297 | 10533 | 314 | 11220 | 341 | 0 | |
| 752 | 3111118.6 | 572002.9 | 8829 | 264 | 11560 | 338 | 12507 | 341 | 0 | 0 | 0 | 0 | 0 | 0 |
| 753 | 3106895.6 | 568136.5 | 7982 | 220 | 11060 | 335 | 0 | 0 | 0 | 0 | 0 | 0 | 0 | |
| 754 | 3110462.0 | 582508.2 | 10280 | 262 | 12468 | 338 | 13804 | 368 | 0 | 0 | 0 | 0 | 0 | 0 |
| 755 | 3110863.9 | 573907.3 | 8652 | 240 | 10899 | 319 | 11261 | 326 | 0 | 0 | 0 | 0 | 0 | 0 |
| 756 | 3111006.0 | 575022.2 | 6982 | 216 | 8942 | 273 | 10918 | 315 | 12183 | 343 | 0 | 0 | 0 | 0 |
| 757 | 3110873.8 | 576998.8 | 8552 | 250 | 12217 | 341 | 0 | 0 | 0 | 0 | 0 | 0 | 0 | |
| 758 | 3109922.9 | 581310.7 | 9402 | 223 | 12043 | 339 | 12271 | 345 | 12992 | 356 | 0 | 0 | 0 | 0 |
| 759 | 3108078.2 | 589397.5 | 6729 | 193 | 0 | 0 | 0 | 0 | 0 | 0 | 0 | 0 | 0 | |
| 760 | 3108444.9 | 598047.8 | 6419 | 209 | 0 | 0 | 0 | 0 | 0 | 0 | 0 | 0 | 0 | |
| 761 | 3108935.3 | 594147.8 | 6562 | 204 | 0 | 0 | 0 | 0 | 0 | 0 | 0 | 0 | 0 | |
| 762 | 3101966.7 | 594319.5 | 7007 | 221 | 0 | 0 | 0 | 0 | 0 | 0 | 0 | 0 | 0 | |

# APPENDIX B–THE KEHLE TEMPERATURE CORRECTION SCHEME

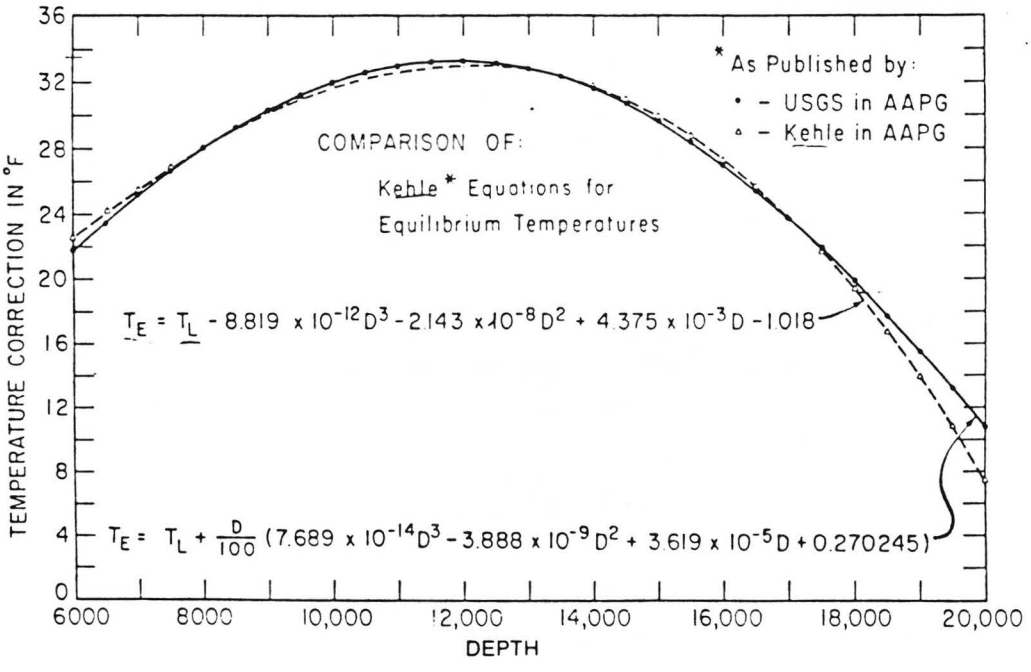

# APPENDIX C-CALCULATING ISOTHERMS

Program DBINTP

This program creates a data file (OUTPUT) for an isothermal surface. The program interactively asks for the temperature of the isothermal surface and the temperature range (± ILIM) of eligable data. The program reads CORCT which is the filename of the temperature corrected data base.

```
      PROGRAM DBINTP(CORCT,OUTPUT,TTY,TAPE5=CORCT,TAPE6=
     1OUTPUT,TAPE7=TTY)
        DIMENSION ITEMP(9)
        DIMENSION IDEPTH(9)
         NC=0
        WRITE(7,5)
5       FORMAT(1X,'WHAT TEMP TO PLOT,WHAT LIMIT OF INTERPOLA
     1TION')
        READ(7,*)INTEM,ILIM
        DO 100 I=1,1000
        READ(5,*,END=110 ) NUM,DUM1,DUM2,IDEPTH(1),ITEMP(1),
     1IDEPTH(2),ITEMP(2),IDEPTH(3),
     1ITEMP(3),IDEPTH(4),ITEMP(4),IDEPTH(5),ITEMP(5),IDEPTH(6
     1),ITEMP(6)
        DO 30 K=1,6
        IF(ITEMP(K).EQ.INTEM) GOTO 50
        IF(ITEMP(K).LT.INTEM .AND. INTEM-ITEMP(K) .LE.ILIM
     1.AND. (ITEMP(K+1).GT.INTEM .OR. ITEMP(K+1).EQ.0)) GO TO 40
        IF(ITEMP(K).GT.INTEM .AND. ITEMP(K)-INTEM.LT.ILIM) GO
     1TO 70
```

```
30      CONTINUE
        GOTO 100
40      IF(ITEMP(K+1).EQ.0)THEN
             ICRCD=INTEM*IDEPTH(K)/ITEMP(K)
        ELSE
        ICRCD= (IDEPTH(K+1)-IDEPTH(K))*(INTEM-ITEMP(K))/
       1  (ITEMP(K+1)-ITEMP(K))+IDEPTH(K)
         END IF
50      WRITE(6,55) NUM,DUM1,DUM2,ICRCD
             NC=NC+1
55      FORMAT(1X,I5,2F13.1,I6)
60      GOTO 100
70      ICRCD=INTEM*IDEPTH(K)/ITEMP(K)
        GOTO 50
100     CONTINUE
110     WRITE(7,120)NC
120     FORMAT(1X,'THE NUMBER OF ENTRIES IS',I5)
        WRITE(6,130)NC
130     FORMAT(1X,'C** THE NUMBER OF ENTRIES IS',I5)
        STOP
        END
```

# APPENDIX D- KRIGING

*Author's note: Before embarking on the study of this appendix, you are hereby warned that the Kriging process is rather involved and will not be learned in a day, nor probably even in a week. You will first need: A basic knowledge of FORTRAN, data that are digitized using a cartesian system (eg. UTM), access to the programs covered herein(GAMM8B, NEWPLTB, NEWUKB, & MAPWB which are property of the UT Bureau of Economic Geology, Contact the Bureau's computer center) and familiarity with the computer on which you intend to run them.*

Kriging is a data smoothing technique which employs statistical methods to accomplish smoothing. The method can transform irregularly spaced or unevenly distributed data into regularly spaced points, each point being estimated from the actual data points surrounding it. A standard deviation at each of the estimated points is also calculated. The method was originally developed for estimating mineral recovery in mining operations, but has been applied to other geostatistical problems such as preparing data for contouring in cases where the reliability of the data is not absolute. In such cases, contouring the data without some way of first smoothing out the scatter can result in an impossibly

complex and unrealistic surface. Kriging allows one to average out the scatter while providing a measure of the reliability of the resulting estimated surface at each contoured point. In my work, the kriging technique has been employed to smooth bottom-hole temperature measurements for contouring subsurface isotherms.

The kriging process involves several steps. A computer is essential for handling the multitude of calculations required. This appendix does not attempt to explicitly review all the calculations needed. Presented is a general outline of the procedures, accompanied by instructions in the use of the various computer programs that I used to accomplish them. The programs were donated to the Bureau of Economic Geology of the University of Texas by Dr. Young C. Kim of the University of Arizona College of Mines.

## THE VARIOGRAM

Constructing a variogram is the first step in the kriging process. A variogram is a plot which graphically describes how the data varies on average at increasing distances away from any point within the data field. It can be thought of as a plot of the difference in value between some starting point and points increasing distances away from that starting point. A typical variogram is shown in figure D1 . The underlying assumption of the variogram, and hence the kriging process itself, is that the values of neighboring points influence each other. In other words, we expect the variogram to show the smallest differences at points closest to the starting point (represented on the variogram by

the origin), with the differences becoming greater at increasing distances away from the starting point. Data that behaves in this manner is termed regionalized. As distance increases, the regionalized influence diminishes and variation increases until some plateau is reached where differences become purely random.

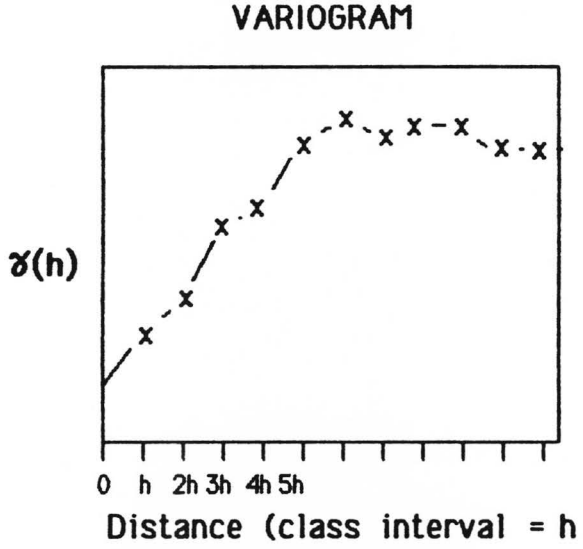


**Figure D1**. A typical variogram where the x's are γ(h)'s plotted at each multiple of h.

The variogram is an integral part of the Kriging process. In essence the kriging program I used constructs a regularly spaced grid over the data field and then finds values for the center of each block in the grid. It determines the value of each block center by averaging the surrounding data points. This is not a simple average because the kriging process weights each surrounding datum separately. This weight is based on its distance from the block center. The program knows how to weight the data by referring to the variogram as shown in figure D2. In general, points closest to the block center receive greater weight than those

farther away. In actuality, the kriging program cannot read the variogram directly. Instead, it must be given an equation of a curve which closely approximates the variogram. This curve is shown in figure D2 by the heavier line. The details of fitting a curve are supplied in the section on NEWPLOT.

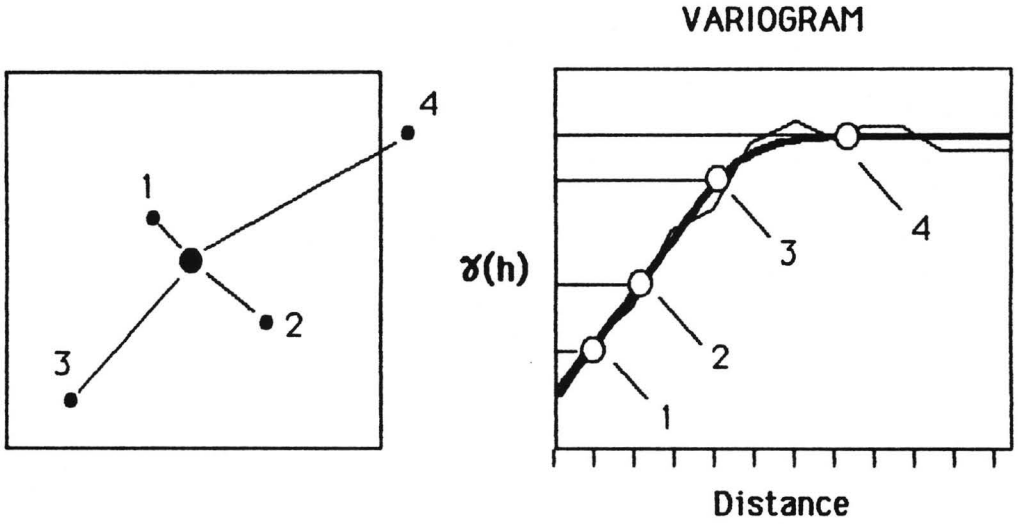


Figure D2 shows how a variogram is used to krig a block center (left). The data points 1-4 around the block center are weighted according to the variogram (right). The weighting values are derived from the $\gamma$'s read off the variogram, which in turn are approximated by fitting a curve to the actual variogram. The weighted values are then averaged yielding a value for the block center.

The variogram is constructed by surveying within a set distance around each data point, finding the average difference of the value between the point being surveyed and the points that occur within the set distance from it, and then averaging this result with those of all the other data points in the data field. This number is then plotted on the

variogram, with the average difference plotted along the y axis and the distance surveyed plotted along the x axis. The process is then repeated for multiples of the original surveying distance. The distance used in the original survey is set arbitrarily and is termed the *class interval.* Finding the optimum class interval is a trial and error process. The investigator guesses at the class interval until a proper looking variogram such as shown in figure D2 results. Note in the figure that the y axis is labeled gamma. Gamma is actually the standard deviation squared. The squaring eliminates the problem of dealing with both positive and negative variations. If this were not done, the average differences would be near zero as a result of the positive and negative variations cancelling each other. As one can now see, there is a staggering amount of calculation involved in finding all these averages for each data point, and then averaging these together. This technique would not be practical without the aid of a computer.

The above method is stated in equation form as follows:

$$\gamma[h] = \frac{1}{2N} \sum_{j=1}^{N} [f(x_j) - f(x_j + h)]^2$$

where N is the number of data points, $\gamma$ is the standard deviation squared, and h is the class interval. To construct the variogram, $\gamma$ is plotted against distances h and multiples of h.

## VARIOGRAM COMPUTER PROGRAM

### THE SEARCH WINDOW

When calculating $\gamma$ at multiples of class interval h, it is possible to control the direction of search. In otherwords, one need not necessarily sweep 360 degrees around each data point. In fact, since every data point is used as a starting point of search for each class interval, the search angle, also termed the *window*, need only be 90 degrees to cover the whole data base in all directions as shown in figure D3. By decreasing the window angle further and specifying a direction, such as N, NW, SE ect., a variogram showing behavior of the data in one direction is created (figure D4). This variogram can be compared to variograms resulting from different window orientations for the purpose of estimating anisotropy. The section Fitting A Curve contains some additional information on this. It is necessary to introduce the concept of the search window here since the following program requires that the window be specified.

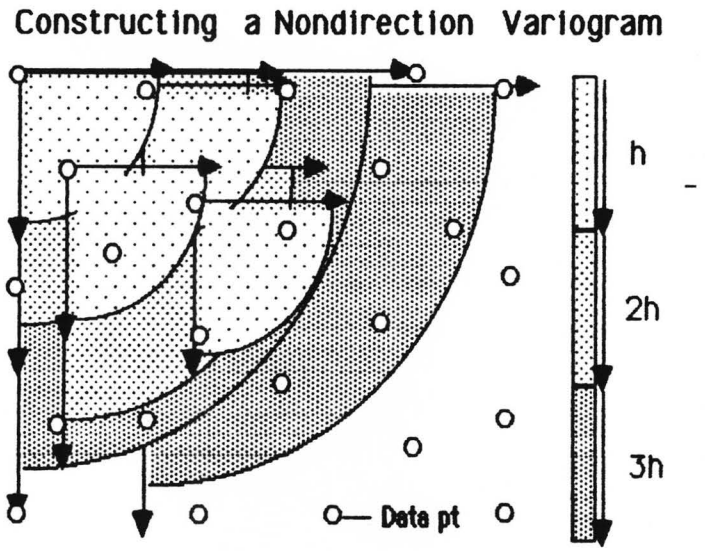


Figure D3 schematically showing sweeps of the data field for h, 2h and 3h intervals for a nondirectional variogram.

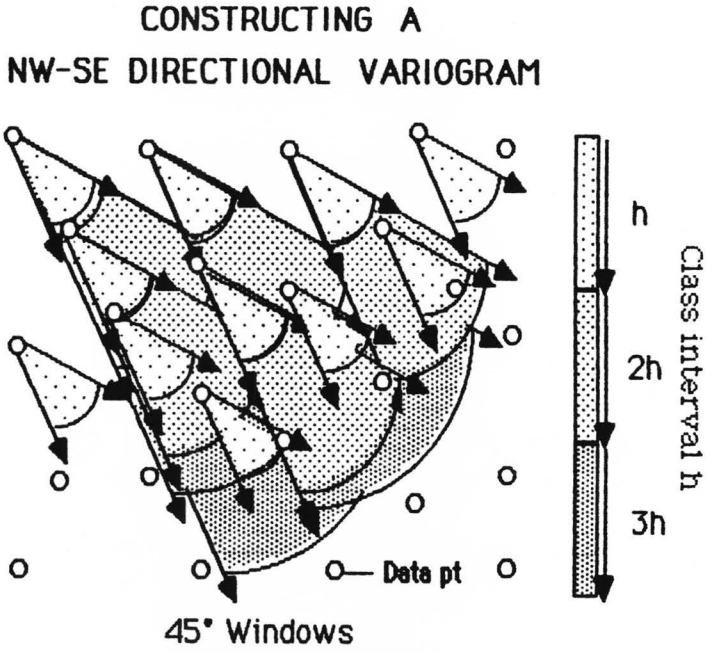


Figure D4 schematically showing sweeps of the data field for h, 2h and 3h intervals for a directional variogram.

## THE UTM COORDINATE SYSTEM

For all the programs used to analyize my data, a cartesian coordinate system is required as the means to locate the data points. The usual latitude and longitude will not work as these are not cartesian. Another mapping system was developed for this need and it is called the *Universal Transverse Mercator* system or *UTM* for short. Unfortunately, there are some problems with UTM that can make it difficult to use. UTM does not account for earth curvature, and for a very large area, say the size of the state of Texas, this can be a problem, depending on how accurately the data need to be located. For my study this was not a problem. Another problem occurs at central meridians, which occur every six degrees of longitude, where the UTM system is discontinous. This is a concern only if the Bureau's printed UTM listings are used. This may be convenient for some applications, but if data cross over one of these meridians, a program which the Bureau calls LLTRANB should be used to get your UTM coordinates.

## VARIOGRAM PROGRAM GAMM8

The following instructions apply to the use of the FORTRAN program GAMM8B which is the property of the Bureau of Economic Geology. This and other programs used in my thesis are not in the public domain and are not listed here for that reason. A knowledge of FORTRAN formating is assumed.

To use this program, one must create an input deck. The input deck contains information which controls the various options of the program as well as suppling basic information about the data. The data are then placed after this initial information. When running the program, the input deck must be specified as the input file. For those not familiar with constructing an input deck: The term *card* in the listing below refers to the now seldom used computer punch cards. An entry line on a terminal display is the modern equivilant of a card. There are 80 columns to a card and each column corresponds to one character. An input deck should have the following form (**Bold** type indicates the usual selections):

| CARD | COLUMN | FORMAT | SELECTION DESCRIPTION |
|---|---|---|---|
| Card 1 | 1-80 | 8A10 | Run Name |
| Card 2 | 3 | I1 | 1= Log Transform, **0**= no |
| | 4 | I1 | 1= Average variogram option: yes<br>**0**= " " " : no |
| | 5 | I1 | **1**= Punch for NEWPLOT, 0= no |
| | 6 | I1 | 1= Moment center, **0**=$\gamma(h)$ |
| | 7 | I1 | **1**=Auto Scale, 0= no |
| | 8 | I1 | 2= divide by variance<br>1= divide by mean square<br>**0**=neither |
| | 9 | I1 | 1- tape input, **0**= system |
| | 10 | I1 | No. of directions (max. 8) |
| | 11-20 | F10.0 | Class interval: 20 × |

| | | | |
|---|---|---|---|
| | | | class = max range |
| | 41-50 | F10.0 | Max vertical value to allow |
| Card 3 | You will need one of these cards for each Direction | | |
| | 1-10 | F10.0 | Direction<br>0. = E-W 45. = NE-SW<br>90.= N-S -45. = NW-SE |
| | 11-20 | F10.0 | Window in degrees |
| Card 4 | 1 | I1 | 1,2, or **3** (specifies order of occurence of value being Kriged on data line) |
| | 2 | I1 | 1,**2**, or 3 (specifies occur. of y coord. ie. Northing) |
| | 3 | I1 | **1**,2 or 3 (specifies occur. of x coord. ie. Easting) |
| | 4 | I1 | 1=flags definition of rectangular sub-area to confine variogram to follow:<br>**0**=no sub-area defined |
| | 11-20 | F10.0 | Minimum Northing (y) |
| | 21-30 | F10.0 | Maximum Northing |
| | 31-40 | F10.0 | Minimum Easting (x) |
| | 41-50 | F10.0 | Maximum Easting |
| Card 5 | 1-80 | 8A10 | Format of input on system enclosed in (paren.) |
| Card 6 | 1-80 | 8A10 | Title of Variogram for output |
| Card 7→n | | | |
| | Data. . . | | |

Each data point is represented by its own data card (7→n). Three values are being read in from each of these. They are the Easting, Northing,

and the value to be kriged in that order. Other numbers may exist on the data line as well, but formatting should ensure that just the three numbers being used are read in.

The output from the program is written to a file named OUTPUT and also to one named TAPE8. OUTPUT includes information on the variogram(s) just run and a character built plot of the variogram which comes off the line printer and provides a good, if not pretty, variogram plot. To get a copy of the results printed on an actual plotter, TAPE8 provides unformated plotting output. NEWPLOT, the next program described, will produce a ZETA plot file from the TAPE8 file, which in turn can be sent directly to a ZETA plotter for draft-quality plots.

PLOTTING PROGRAM NEWPLOT

Before running this program, output file TAPE8 discussed above must be modified. To run several variograms at once with GAMM8B, TAPE8 must contain plotting information for each variogram, each being separated by a blank card (line). For each plot, one card free-formated with the following data must be present:

Variogram value at the top of the graph
Variogram value at the bottom of the graph
Variogram value at the right of the graph
Variogram value at the left of the graph
Length of the x axis (distance) in inches
Length of the y axis ($\gamma$) in inches

These values should be seperated by spaces but contained within one line

and should be listed in order. Do not leave a blank card between this card and the TAPE8 group (plot). Each plot should have one of these cards at the top. Leave only one blank card between the end of one group and this top card for the following one.

To then run NEWPLTB on the CDC (Control Data Dual Cyber) you will need to first execute the following command (this procedure as of May, 1985):

LDSET,PRESET=ZERO,LIB=ZETLIBF

The computer than prompts you with:

LDR>

You then type:

NEWPLTB,TAPE8

The program then generates a file called PLOTR, which can be sent to a ZETA plotter by issuing the command:

DISPOSE PLOT=PLOTR,ID= *id site*

where *id site* is some printing site identification number, eg. Taylor Hall is 44.

Fitting A Curve. As mentioned in the section THE VARIOGRAM, and as shown in figure D2, you will need to fit a curve to the variogram. This curve will be the weighting curve that the kriging program will actually use. The kriging program presented in this appendix uses the so-called *spherical model* for this curve. To fit the curve, three characteristic measurements of the variogram plot must be estimated. These are the *nugget value, Co;* the *C value;* and the *range, a.* To read these values off the variogram, the variogram must first be plotted.

The line-printed plot will do (this can be done on a terminal screen). Figure D5 illustrates the proceedure. Draw a straight line along the slope described by the first three for four points. Then draw another straight line across the points that indicate a plateau (its normal for this plateau to slope back down at the far end of the x axis.) This second line should be nearly horizontal and should pass through or near the highest $\gamma$ values on the graph. If the shape of your variogram does not comply with this proceedure and does not resemble those shown in the various figures in this appendix, then the variogram needs to be redone chosing a different class interval. The y-intercept of the first sloping line is the nugget value (Co) and can be thought of as an indication of the accuracy of the data. Ideally this intercept should intersect the origin, though it almost never does. The y-intercept of the horizontal line is the sill value which is given as C + Co, C being the difference between the sill and the nugget values. The sill indicates the maximum variance of the data. The range (a) is calculated as 3/2 times the distance (measured off the x axis) from the origin of the intersection of the two lines which have been traced.

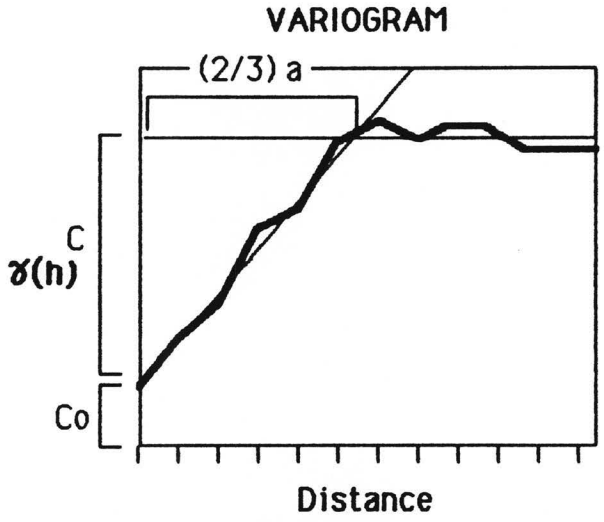


**Figure** D5. Optaining **C**, **Co** and **a** by construction. The sill is given by **C** + **Co**.

These three values alone are used to describe the fitted curve. Record these for future use in the kriging program. NEWPLOTB can plot the fitted curve on the variogram by further adding the following cards to the end of each data group on TAPE8:

| CARD | COLUMN | FORMAT | DESCRIPTION |
|---|---|---|---|
| Card1 | Blank | | |
| Card 2 | 1 | A1 | Type a "**3**" in this column |
| Card 3 | 1-10 | F10.0 | Nugget value (Co) |
| | 11-20 | F10.0 | Sill value (C) |
| | 21-30 | F10.0 | Range (a) |

The Anisotropy Ratio. If several variograms have been run in different directions as discussed in previous sections, the *anisotropy*

*ratio* can be calculated using the sill values. The ratio is given by the ratio of the maximum directional sill value to the minimum directional sill value. The anisotropy ratio is used by the kriging program. Since the program only allows integers for this ratio, if the ratio is less than 1.5, then the anisotropy should be ignored.

## THE KRIGING PROGRAM NEWUKB

The goal of constructing a variogram is to obtain the nugget, sill and range values for the nondirectional variogram, and also the anisotropy ratio if it is not less than 1.5. These will now be used as part of the input deck of the kriging program.

Kriging produces a rectangular grid of rows and columns. The centers of the blocks in this grid are the points for which the kriging program calculates values. One must therefore decide what size blocks to use. Considerations include how much resolution is desired, how many data points there are, and how much computer time can be dedicated to the procedure. In general, smaller blocks yield better resolution, but also require more computer time. However, a block will not be kriged with less than two points. If there are less than two points within the radius of search you specify, no value will be generated for that block.

The theory of kriging has been covered in the previous sections detailing the construction of the variogram. The procedure for executing the kriging program NEWUKB follows the same form as the previous programs. Here is the form for the input deck:

| CARD | COLUMN | FORMAT | SELECTION DESCRIPTION |
|---|---|---|---|
| Card 1 | 1-5 | I5 | Starting Column |
| | 6-10 | I5 | Ending Column |
| | 11-15 | I5 | Starting Row |
| | 16-20 | I5 | Ending Row |
| | 21-30 | F10.0 | Max. Northing (Row 1) |
| | 31-40 | F10.0 | Min. Easting (Col 1) |
| | 41-50 | F10.0 | Block Width-North direction |
| | 51-60 | F10.0 | Block Width-East direction |
| Card 2 | 1-5 | F5.0 | Max. dist. from block for hole to be included in kriging. This should be about half the distance across the data field. |
| | 6-10 | I5 | Max. no. of points to be used for each block ($\leq$ 50, usually 10 is enough). |
| | 11 | I1 | Debug output (1=yes, 0=no) |
| | 12 | I1 | List drill holes (1=yes, 0=no) |
| Card 3 | Card three is for mining applications and is used for kriging mineral-grade. You should set everything except the anisotropy ratio equal to zero. The ratio should be set at one. Card four, however is identical and was originally intended for vein thickness. For thickness, substitute the value you want to krig, eg. hydraulic heads. You should select the appropriate settings for card four. Bear in mind that in the output, the kriged values will be printed under the heading "thickness". | | |
| | 1-10 | F10.0 | Nugget Value (Co) |
| | 11-20 | F10.0 | Sill Value (C) |
| | 21-30 | F10.0 | Range (a) |
| | 31-40 | F10.0 | Angle of anisotropy (0 if none)<br>0. = E-W 45. = NE-SW<br>90.= N-S -45. = NW-SE |
| | 41-50 | F10.0 | Anisotropy Ratio (1 if none) |

| | | | |
|---|---|---|---|
| | 51-60 | F10.0 | Vertical anisotropy (for mining, set to **0** for 2D) |
| Card 4 | Same as Card 3. Use this card for you kriging values. | | |
| Card 5 | Format Card for your data (bracketted by paren.). You must format for the following variables in order (use tab format if necessary):<br>**Well identification**<br>**X coordinate** (Easting)<br>**Y coordinate** (Northing)<br>Z coordinate (supply a dummy variable, blanks should work; however, if you have problems, you might have to supply zeros)<br>Grade-thickness (another dummy)<br>**Thickness Value** (this is the value you are kriging) | | |
| Card | 6→n | Your Data (one data point per card). | |

To then run NEWUKB on the CDC the following command needs to be executed (this procedure as of May, 1985):

LDSET,PRESET=ZERO

The computer than prompts with:

LDR>

You then type:

NEWUKB, *datafile*

Where *datafile* is the name given to the input deck. The program then generates a file called OUTPUT, which contains the kriged grid, giving the kriged value for the block center under the column "thickness" and the

row and column for each block center. These block-centers can be displayed by using the following program MAPWB, which provides a crude line-printed map of the output. However, it will not handle more than approximately 30 blocks across. The output file can be used as input for a plotting package (eg. CPS1).

MAPWB

For a line-printed map of the kriged output used the output file in conjunction with the following cards:

| CARD | COLUMN | FORMAT | DESCRIPTION |
|---|---|---|---|
| Card 1 | 1-10 | F10.0 | North coord of upper edge (row 1) |
| | 11-20 | F10.0 | East coord of left edge (col 1) |
| | 21-25 | F5.0 | Block size y dimension |
| | 26-30 | F5.0 | Block size x dimension |
| | 31-35 | I5 | Beginning col. no. of area to be mapped |
| | 36-40 | I5 | Ending col. no. of area to be mapped |
| | 41-45 | I5 | Beginning row. no. of area to be mapped |
| | 46-50 | I5 | Ending row. no. of area to be mapped |
| Card 2 | 1-10 | F10.0 | Scale parameter to make variable1 an integer (usually 1) |
| | 11-20 | F10.0 | Scale parameter to make variable2 an integer (usually 1) |
| | 21-30 | F10.0 | Scale parameter to make variable3 an integer (usually 1) |

| | |
|---|---|
| Card 3 | Format Card for your data (bracketted by paren.). You must format for the following variables in order (use tab format if necessary):<br>**East coordinate** (as produced by NEWUKB)<br>**North coordinate** (as produced by NEWUKB)<br>**Variable 1** (thickness)<br>Variable 2 (dummy)<br>Variable 3 (dummy) |
| Card 4→ n | Data (from output of NEWUKB) |

# APPENDIX E-CPS1

The following files were used to execute the CPS1 graphics subroutines on the Dual Cyber computer. The command file was used to submit the job batch, ie., run CPS1 as a job on a queue independant of an interactive user. The command file is written in a command language which is specific to the operating system (called Taurus) on the CDC at the University of Texas. The verb files contain the commands (which they call verbs) to execute the CPS1 subroutines.

CPS1 turned out to be computation intensive. The contouring programs, for example, required an average of 300 seconds of central processing time. The isometric plots (3-D) took even longer. The boldface print indicates file names or variables that can be changed depending on the desired options and which files the user desires to be used for data input, etc.. . Because of the complexity of using CPS1, these files are presented without explanation. For descriptions of their construction and use, the reader is refered to a Taurus manual for the command files, and a CPS1 manual for the verb files.

# POSTING DATA

COMMAND FILE

```
READPF 4170 T400L50
READPF 4170 POSTYRB
RENAME T400L50 TAPE1
RFL 220000
CPS1 POSTYRB
CPS1TRN,,PLOT.
SKIPCC.
EXIT.
REVIEW L=DAY
SAVEPF 4170 5682 DAY OUTPUT P400L50=PLOT
ZAP
```

VERB FILE

```
 $YC JOB=1 $END
WELL LOCATONS FOR K400L50
 $YC AOI=1,YMIN=3014056.1,YMAX=3237605.5,XMIN=450501.3,XMAX=
718654.3, XINC=1.,YINC=1. $END
 $YC PDEF=1,XSCL=23000,YSCL=23000,IOPT=0 $END
 $YC POLY=1,NPC=27,ISMB=0,ISCL=1,IFMT=2 $END
(20X,F20.1,T1,F20.1)
     3014594.7      451204.7
     3014007.3      675797.4
     3055372.3      674940.5
               ect.....
     3112021.3      475036.1
     3112309.0      450669.8
     3014594.7      451204.7
 $YC FENC=1,NPC=27,IFMT=2,ISCL=1 $END
(20X,F20.1,T1,F20.1)
     3014594.7      451204.7
     3014007.3      675797.4
     3055372.3      674940.5
               ect....
     3112021.3      475036.1
     3112309.0      450669.8
     3014594.7      451204.7
 $CD FILD=0 $END
 $YC LGPT=1,ISMB=-6,SIZE=0.06,LUN=1,MODE=2 $END
 $CD FILD=1,SIZP=0.06,IPSN=1,NCLS=5 $END
(19X,2F10.0,T1,I1,T4,5A1)
 $YC NWPG=1 $END
 $YC STOP=1 $END
```

# CONTOURING

COMMAND FILE

```
READPF 5576 KRGCONB KRG350
RENAME KRG350 TAPE1
REWALLX
RFL,250000
CPS1 KRGCONB
CPS1TRN,,PLTCNT.
SKIPCC.
EXIT.
REVIEW,L=DAYCNT
SAVEPF 5576 8908 DAYCNT,K350L50=PLTCNT,OUTKRGB=OUTPUT
ZAP
```

VERB FILE

```
 $VC JOB=1 $END
K250L30
 $VC AOI=1,XMIN=450501.3,XMAX=718654.3,YMIN=3014056.1,YMAX=
3237605.5, XINC=5000.,YINC=5000. $END
 $VC MGRD=1,NCP=0,IFMT=2,LUN=1 $END
(19X,2F10.0,T56,F8.0)
 $VC STAT=1 $END
 $VC PDEF=1,XSCL=23000.,YSCL=23000.,MODE=1 $END
 $VC POLY=1,NPC=27,ISMB=0,ISCL=1,IFMT=2 $END
(20X,F20.1,T1,F20.1)
     3014594.7      451204.7
     3014007.3      675797.4
     3055372.3      674940.5
       ect...
     3112021.3      475036.1
     3112309.0      450669.8
     3014594.7      451204.7
 $VC FENC=1,NPC=27,IFMT=2,ISCL=1 $END
(20X,F20.1,T1,F20.1)
     3014594.7      451204.7
     3014007.3      675797.4
     3055372.3      674940.5
       ect...
     3112021.3      475036.1
     3112309.0      450669.8
     3014594.7      451204.7
 $CD FILD=0 $END
 $VC CTYP=1,NREF=0,BOLD=0,DIS1=4.,DIS2=2.,HSHR=0,LABR=1,SIZE=.08    $END
 $VC CLY4=1,ZIDA=1,CLMN=-5000.,DEL=-500.,NCY=30,ICRT=1 $END
 $VC STOP=1 $END
```

# ISOMETRIC PROJECTION

COMMAND FILE

```
READPF 5576 YRBISOC KRG350
RENAME KRG350 TAPE1
REWALLX
RFL,371000
CPS1 YRBISOC
CPS1TRN,,I350L50
SKIPCC
EXIT
REVIEW,L=DAYISO
SAVEPF 5576 8908 DAYISO,I350L50,OUTISO=OUTPUT
ZAP
```

VERB FILE

```
 $YC JOB=1 $END
LOOKING NORTHEAST,DEPTH TO 250 DEG F
 $YC AOI=1,YMIN=3014056.1,YMAX=3237605.5,XMIN=450501.3,XMAX=718654.3,
    XINC=8000.,YINC=8000. $END
 $YC MGRD=1,IFMT=2,LUN=1,NCP=0,NZ=1,IANL=1 $END
(18X,F10.0,F10.0,T56,F8.0)
 $YC STAT=1 $END
 $YC PDEF=1,XSCL=50000.,YSCL=50000. $END
 $YC RFIT=1,NREF=1,ZIDA=1,ITYP=1,ZIDB=0 $END
 $YC ISOM=1,ZIDA=1,ZSCL=2500.,ZMIN=-20000.,ZMAX=1000.,
    ISID=1,THET=65. $END
 $YC NWPG=1 $END
 $YC STOP=1 $END
```

# APPENDIX F - FLOW VELOCITY VECTOR FIELDS

The flow velocity vectors are listed for each triangular element. They appear by column, each column taking three lines in this listing. The columns are listed in order, as they appear from the left to right side of the mesh. The vectors for each element are listed in order starting at the bottom or basement of the mesh, and working toward the top. There are twenty-two elements in each column, and the vectors of the top two elements are all that appear on the third line for each column. The columns can be distinquished by this partial line.

## SIMULATION ONE-Horizontal component

0.64E-12 0.56E-12 0.72E-10 0.63E-10 0.76E-10 0.79E-10 0.93E-10 0.80E-10 0.86E-10 0.87E-10
0.10E-09 0.09E-10 0.72E-10 0.50E-10 0.50E-10 0.45E-10 0.51E-10 0.18E-10 0.58E-09 0.20E-09
0.18E-09 0.00E+00
0.11E-11 -0.15E-11 0.40E-10 0.27E-10 0.51E-10 0.34E-10 0.50E-10 0.34E-10 0.47E-10 0.38E-10
0.40E-10 0.31E-10 0.33E-10 0.21E-10 0.26E-10 0.15E-10 0.16E-10 0.98E-11 0.32E-09 0.16E-09
0.15E-09 0.00E+00
0.26E-11 0.34E-11 0.53E-11 -0.32E-11 0.25E-10 -0.11E-10 0.38E-10 0.50E-11 0.33E-10 0.15E-10
0.34E-10 0.18E-10 0.27E-10 0.16E-10 0.17E-10 0.81E-11 0.97E-11 0.42E-11 0.18E-09 0.78E-10
0.13E-09 0.25E-10
0.43E-12 0.11E-10 0.43E-11 -0.64E-11 0.61E-11 -0.27E-11 0.19E-10 0.24E-11 0.18E-10 0.72E-11
0.18E-10 0.83E-11 0.13E-10 0.51E-11 0.10E-10 0.33E-11 0.56E-11 0.20E-11 0.95E-10 0.50E-10
0.45E-10 0.00E+00
-0.15E-10 0.47E-10 0.50E-11 -0.24E-11 0.65E-11 -0.44E-11 0.36E-10 -0.41E-11 0.29E-10 0.55E-11
0.22E-10 0.31E-11 0.15E-10 0.36E-11 0.82E-11 0.12E-11 0.26E-11 0.32E-12 0.10E-10 -0.89E-11
0.14E-10 0.00E+00
-0.94E-10 0.16E-09 -0.12E-11 -0.11E-10 -0.14E-11 -0.65E-11 0.51E-10 0.28E-12 0.35E-10 0.24E-11
0.27E-10 0.90E-12 0.14E-10 -0.63E-12 0.76E-11 -0.26E-11 0.12E-11 -0.13E-11 -0.41E-10 -0.42E-10
-0.38E-10 -0.54E-11
-0.32E-09 0.57E-09 -0.73E-10 -0.40E-10 -0.40E-10 0.17E-10 0.10E-10 -0.18E-11 0.28E-10 -0.52E-11
0.21E-10 -0.63E-11 0.89E-11 -0.79E-11 0.19E-11 -0.11E-10 -0.52E-11 -0.77E-11 -0.20E-09 -0.14E-09
-0.13E-09 0.31E-10
-0.97E-09 0.79E-09 -0.98E-11 -0.19E-11 -0.16E-09 -0.43E-10 -0.11E-09 0.41E-10 0.48E-10 -0.45E-12
0.33E-10 -0.12E-10 0.19E-10 -0.19E-10 0.39E-11 -0.21E-10 -0.12E-10 -0.22E-10 -0.58E-09 -0.59E-09
-0.48E-09 -0.52E-10
-0.78E-09 0.41E-09 -0.73E-11 -0.11E-11 -0.34E-11 0.10E-11 -0.52E-10 0.12E-09 0.11E-09 0.55E-10
0.92E-10 0.32E-10 0.49E-10 0.10E-10 0.25E-10 -0.27E-10 -0.87E-11 -0.51E-10 -0.14E-08 -0.26E-08
-0.20E-08 -0.56E-08
-0.52E-09 0.68E-10 -0.68E-11 0.42E-11 0.11E-11 0.25E-11 0.41E-10 0.15E-09 0.35E-09 0.37E-09
0.35E-09 0.30E-09 0.29E-09 0.26E-09 0.24E-09 0.22E-09 0.17E-09 0.15E-09 0.45E-08 0.25E-08
0.22E-08 -0.58E-08
-0.46E-09 -0.20E-09 -0.22E-11 0.69E-11 0.18E-11 0.34E-11 0.17E-11 0.82E-13 -0.13E-09 0.97E-10
0.69E-09 0.79E-09 0.69E-09 0.86E-09 0.68E-09 0.79E-09 0.60E-09 0.73E-09 0.20E-07 0.24E-07
0.20E-07 0.31E-07
-0.44E-09 -0.40E-09 0.76E-12 -0.90E-12 -0.41E-11 0.55E-11 -0.17E-11 0.25E-11 0.12E-10 0.89E-10
-0.89E-09 -0.47E-10 -0.28E-09 0.13E-08 0.64E-09 0.66E-09 0.50E-09 0.58E-09 0.16E-07 0.22E-07
0.19E-07 0.34E-07
-0.45E-09 -0.61E-09 0.20E-12 -0.19E-10 -0.73E-11 -0.13E-10 -0.15E-10 -0.65E-13 -0.47E-11 0.14E-12
-0.18E-09 0.43E-10 -0.68E-09 -0.13E-09 -0.50E-09 -0.65E-09 -0.45E-09 -0.66E-09 -0.18E-07 -0.28E-07
-0.22E-07 -0.51E-07
-0.27E-09 -0.76E-09 -0.42E-11 -0.15E-10 -0.10E-10 -0.18E-10 -0.14E-10 -0.22E-10 -0.23E-10 -0.82E-11

-0.12E-10 -0.28E-11 -0.31E-09  0.31E-10 -0.55E-09 -0.64E-09 -0.44E-09 -0.52E-09 -0.15E-07 -0.19E-07
-0.17E-07 -0.21E-07
-0.11E-09 -0.88E-09 -0.41E-11 -0.16E-10 -0.12E-10 -0.19E-10 -0.15E-10 -0.23E-10 -0.19E-10 -0.23E-10
-0.24E-10 -0.53E-11 -0.24E-09  0.32E-10 -0.42E-09 -0.51E-09 -0.35E-09 -0.42E-09 -0.12E-07 -0.14E-07
-0.13E-07 -0.23E-07
 0.54E-10 -0.91E-09 -0.20E-11 -0.87E-11 -0.62E-11 -0.89E-11 -0.68E-11 -0.91E-11 -0.66E-11 -0.82E-11
-0.71E-11 -0.42E-11 -0.25E-09  0.77E-10 -0.31E-09 -0.32E-09 -0.21E-09 -0.22E-09 -0.65E-08 -0.71E-08
-0.62E-08 -0.71E-08
 0.13E-08 -0.74E-09 -0.26E-11 -0.62E-11 -0.39E-11 -0.83E-11 -0.49E-11 -0.80E-11 -0.55E-11 -0.51E-11
-0.38E-11 -0.32E-11 -0.20E-09  0.98E-11 -0.92E-10  0.18E-10  0.28E-10  0.81E-10  0.18E-08  0.43E-08
 0.37E-08  0.12E-07
 0.25E-08 -0.62E-09 -0.18E-11 -0.19E-11 -0.14E-11  0.56E-12  0.17E-11 -0.12E-12  0.20E-11 -0.19E-11
-0.19E-12 -0.27E-11 -0.12E-09  0.18E-10 -0.44E-10  0.27E-10  0.16E-09  0.17E-09  0.39E-08  0.76E-08
 0.65E-08  0.23E-07
 0.28E-08 -0.60E-09 -0.37E-11 -0.30E-11 -0.19E-11 -0.23E-11 -0.21E-11 -0.75E-11 -0.43E-11 -0.19E-11
-0.16E-11 -0.11E-11 -0.85E-10  0.73E-10 -0.62E-10  0.60E-10  0.14E-09  0.10E-09  0.31E-08  0.48E-08
 0.55E-08  0.00E+00
 0.31E-08 -0.48E-09 -0.19E-11 -0.23E-11 -0.20E-11 -0.48E-12 -0.43E-12  0.33E-11  0.30E-11  0.74E-12
 0.61E-12 -0.87E-12 -0.49E-10  0.50E-10 -0.24E-10  0.41E-10  0.18E-09  0.55E-10  0.23E-08  0.42E-08
 0.34E-09  0.00E+00
 0.30E-08 -0.37E-09 -0.42E-14  0.14E-11  0.13E-11  0.19E-11  0.17E-11  0.15E-11  0.13E-11  0.86E-12
 0.72E-12  0.50E-13  0.18E-11  0.11E-09 -0.22E-10  0.90E-10  0.51E-09  0.52E-09  0.43E-09  0.36E-09
 0.99E-08  0.54E-08
 0.29E-08 -0.20E-09 -0.23E-14  0.21E-12  0.19E-12  0.29E-12  0.26E-12  0.26E-12  0.23E-12  0.21E-12
 0.18E-12  0.11E-13  0.74E-11  0.83E-10 -0.76E-11  0.11E-09  0.68E-09  0.70E-09  0.53E-09  0.61E-09
 0.14E-07  0.19E-07
 0.28E-08 -0.37E-10 -0.43E-15 -0.18E-12 -0.17E-12 -0.35E-12 -0.32E-12 -0.43E-12 -0.38E-12 -0.64E-12
-0.55E-12 -0.83E-12 -0.85E-11 -0.38E-10 -0.29E-10  0.20E-10  0.62E-09  0.59E-09  0.49E-09  0.44E-09
 0.11E-07  0.71E-08
 0.27E-08  0.15E-09  0.17E-14 -0.76E-12 -0.70E-12 -0.17E-11 -0.16E-11 -0.26E-11 -0.24E-11 -0.37E-11
-0.33E-11 -0.49E-11 -0.43E-11 -0.62E-11 -0.51E-11  0.34E-12  0.62E-09  0.61E-09  0.48E-09  0.48E-09
 0.11E-07  0.15E-07
 0.24E-08  0.33E-09  0.39E-14  0.44E-12  0.41E-12  0.84E-12  0.79E-12  0.11E-11  0.98E-12  0.12E-11
 0.10E-11  0.12E-11  0.10E-11  0.98E-12  0.83E-12  0.27E-12  0.51E-09  0.50E-09  0.41E-09  0.40E-09
 0.10E-07  0.26E-07
 0.22E-08  0.44E-09  0.51E-14  0.17E-11  0.16E-11  0.33E-11  0.30E-11  0.43E-11  0.39E-11  0.52E-11
 0.45E-11  0.58E-11  0.48E-11  0.54E-11  0.45E-11  0.23E-12  0.43E-09  0.41E-09  0.33E-09  0.30E-09
 0.77E-08 -0.13E-07
 0.21E-08  0.50E-09  0.57E-14  0.25E-11  0.22E-11  0.46E-11  0.41E-11  0.59E-11  0.53E-11  0.76E-11
 0.65E-11  0.10E-10  0.84E-11  0.18E-10  0.15E-10  0.20E-12  0.38E-09  0.39E-09  0.31E-09  0.32E-09
 0.82E-08  0.26E-07

0.20E-09 0.36E-09 0.65E-10 0.32E-11 0.29E-11 0.58E-11 0.53E-11 0.71E-11 0.65E-11 0.82E-11
0.72E-11 0.84E-11 0.71E-11 0.89E-11 0.50E-11 0.20E-12 0.39E-09 0.38E-09 0.30E-09 0.30E-09
0.79E-08 0.14E-07
0.18E-08 0.65E-09 0.75E-10 0.30E-11 0.45E-11 0.89E-11 0.80E-11 0.11E-10 0.96E-11 0.12E-10
0.11E-10 0.13E-10 0.11E-10 0.48E-11 0.42E-11 0.18E-12 0.35E-09 0.32E-09 0.26E-09 0.22E-09
0.56E-09 0.00E+00
0.16E-08 0.74E-09 0.84E-10 0.85E-11 0.75E-11 0.15E-10 0.13E-10 0.18E-10 0.15E-10 0.19E-10
0.16E-10 0.95E-11 0.81E-11 0.14E-12 0.31E-09 0.30E-09 0.25E-09 0.26E-09 0.21E-09 0.21E-09
0.54E-09 0.00E+00
0.14E-08 0.77E-09 0.31E-12 0.13E-10 0.12E-10 0.23E-10 0.21E-10 0.31E-10 0.26E-10 0.14E-10
0.12E-10 0.29E-11 0.14E-09 0.11E-10 0.38E-09 0.37E-09 0.31E-09 0.32E-09 0.26E-09 0.26E-09
0.68E-09 0.00E+00
0.13E-09 0.77E-09 0.12E-10 0.19E-10 0.17E-10 0.26E-10 0.23E-10 0.83E-11 0.73E-11 0.18E-11
0.85E-10 0.20E-09 0.18E-09 0.13E-10 0.46E-09 0.45E-09 0.38E-09 0.39E-09 0.32E-09 0.36E-09
0.94E-09 0.26E-07
0.11E-08 0.70E-09 0.11E-10 0.99E-11 0.87E-11 0.70E-11 0.61E-11 0.30E-11 0.26E-11 0.13E-11
0.62E-10 0.13E-10 0.47E-09 0.44E-09 0.37E-09 0.37E-09 0.31E-09 0.30E-09 0.24E-09 0.25E-09
0.63E-08 0.49E-08
0.70E-09 0.53E-09 0.84E-11 0.58E-11 0.52E-11 0.26E-11 0.23E-11 0.16E-11 0.14E-11 0.88E-12
0.93E-10 0.95E-11 0.33E-09 0.31E-09 0.26E-09 0.25E-09 0.21E-09 0.20E-09 0.16E-09 0.14E-09
0.36E-08 0.33E-08
0.39E-09 0.39E-09 0.61E-11 0.43E-11 0.38E-11 0.19E-11 0.16E-11 0.12E-11 0.10E-11 0.63E-12
0.31E-10 0.57E-11 0.20E-09 0.17E-09 0.15E-09 0.12E-09 0.10E-09 0.86E-10 0.69E-10 0.48E-10
0.12E-08 0.36E-10
0.13E-09 0.29E-09 0.45E-11 0.57E-11 0.51E-11 0.20E-11 0.18E-11 0.11E-11 0.98E-12 0.46E-12
0.23E-10 0.25E-11 0.88E-10 0.72E-10 0.61E-10 0.50E-10 0.43E-10 0.32E-10 0.26E-10 0.14E-10
0.34E-09 0.17E-11

## SIMULATION ONE-Vertical component

-0.44E-13 -0.45E-13 -0.37E-11 -0.89E-11 -0.68E-11 -0.50E-11 0.46E-11 -0.11E-11 -0.10E-11 0.81E-12
0.21E-10 0.53E-11 0.15E-10 0.81E-11 0.11E-10 0.95E-11 0.50E-10 0.11E-10 0.35E-10 0.15E-10
0.25E-10 0.16E-10
-0.26E-13 -0.74E-13 0.91E-11 0.18E-12 0.54E-11 -0.24E-11 0.40E-11 -0.13E-11 0.53E-11 0.26E-11
0.53E-11 0.38E-11 0.70E-11 0.32E-11 0.88E-11 0.65E-11 0.10E-10 0.65E-11 0.13E-10 0.84E-11
0.15E-10 0.10E-10
-0.48E-13 -0.33E-13 0.17E-13 -0.15E-12 0.41E-11 -0.10E-10 0.49E-11 -0.53E-11 0.34E-11 -0.25E-11
0.38E-11 0.16E-12 0.41E-11 0.28E-11 0.39E-11 0.26E-11 0.46E-11 0.27E-11 0.59E-11 0.38E-11
0.79E-11 0.58E-11
0.11E-14 0.31E-12 -0.14E-12 -0.50E-12 0.56E-11 -0.11E-11 0.29E-11 -0.57E-11 0.19E-11 -0.51E-11
0.12E-11 -0.22E-11 0.79E-12 -0.22E-11 0.15E-11 -0.81E-12 0.18E-11 -0.49E-12 0.22E-11 0.11E-11
0.35E-11 0.14E-11

```
 0.39E-12  0.19E-11 -0.40E-12 -0.66E-12  0.22E-13 -0.36E-12  0.41E-11 -0.14E-10  0.35E-11 -0.88E-11
 0.19E-13 -0.66E-11  0.27E-12 -0.36E-11 -0.11E-11 -0.20E-11 -0.12E-11 -0.12E-11 -0.14E-11 -0.43E-12
 0.24E-12  0.13E-11
 0.21E-11  0.83E-11 -0.65E-12 -0.88E-12 -0.34E-12 -0.51E-12  0.91E-11 -0.16E-10  0.51E-11 -0.14E-10
 0.33E-11 -0.82E-11  0.12E-11 -0.52E-11  0.37E-13 -0.25E-11 -0.34E-12  0.58E-13  0.55E-13  0.21E-11
 0.15E-12  0.52E-11
 0.69E-11  0.23E-10 -0.86E-12 -0.75E-13 -0.49E-12  0.16E-11  0.13E-10  0.79E-11  0.11E-10 -0.11E-10
 0.60E-11 -0.65E-11  0.41E-11 -0.46E-11  0.23E-11 -0.16E-11  0.71E-12  0.17E-11  0.21E-11  0.69E-11
 0.28E-11  0.14E-10
 0.26E-10  0.27E-10  0.25E-14  0.74E-11  0.18E-11  0.58E-11  0.66E-13  0.45E-11  0.14E-10 -0.18E-10
 0.96E-11 -0.13E-10  0.71E-11 -0.84E-11  0.44E-11 -0.46E-11  0.20E-11 -0.19E-11  0.71E-11  0.91E-11
 0.13E-10  0.44E-10
 0.10E-10  0.10E-10  0.80E-11  0.13E-10  0.64E-11  0.15E-10  0.48E-11  0.10E-10  0.17E-10 -0.21E-10
 0.99E-11 -0.21E-10  0.45E-11 -0.23E-10 -0.18E-12 -0.24E-10 -0.21E-11 -0.28E-10  0.78E-11 -0.82E-10
 0.42E-10 -0.17E-09
 0.11E-10  0.11E-10  0.15E-10  0.23E-10  0.12E-10  0.14E-10  0.11E-10  0.14E-10  0.30E-10  0.49E-10
 0.10E-10 -0.10E-10 -0.39E-11 -0.21E-10 -0.18E-10 -0.25E-10 -0.35E-10 -0.44E-10 -0.85E-10 -0.23E-09
-0.18E-09 -0.62E-09
 0.13E-10  0.13E-10  0.86E-11  0.11E-10  0.16E-10  0.18E-10  0.15E-10  0.13E-10  0.18E-12  0.98E-11
 0.33E-10  0.95E-10  0.12E-10  0.15E-09 -0.21E-10  0.41E-10 -0.46E-10  0.52E-10 -0.23E-09  0.15E-10
-0.63E-09  0.12E-10
 0.14E-10  0.14E-10  0.12E-10  0.11E-10  0.67E-11  0.12E-10  0.11E-10  0.16E-10  0.97E-11  0.13E-10
 0.19E-12  0.92E-12  0.26E-12  0.18E-11  0.98E-10  0.68E-10  0.49E-10  0.12E-09  0.14E-10  0.49E-09
 0.88E-11  0.13E-08
 0.14E-10  0.14E-10  0.12E-10  0.95E-11  0.12E-10  0.10E-10  0.58E-11  0.10E-10  0.10E-10  0.15E-10
 0.10E-11  0.69E-11  0.19E-11  0.22E-11  0.56E-10  0.19E-11  0.12E-09  0.14E-11  0.49E-09 -0.12E-11
 0.13E-08 -0.34E-09
 0.15E-10  0.15E-10  0.98E-11  0.87E-11  0.11E-10  0.87E-11  0.11E-10  0.89E-11  0.53E-11  0.86E-11
 0.55E-11  0.13E-10  0.22E-11  0.64E-11 -0.74E-14 -0.17E-13 -0.37E-11 -0.19E-10 -0.56E-11 -0.13E-09
-0.35E-09 -0.46E-09
 0.15E-10  0.15E-10  0.87E-11  0.80E-11  0.90E-11  0.80E-11  0.93E-11  0.85E-11  0.88E-11  0.83E-11
 0.93E-11  0.70E-11  0.65E-11  0.85E-11 -0.25E-13 -0.22E-13 -0.24E-10 -0.26E-10 -0.13E-09 -0.17E-09
-0.46E-09 -0.59E-09
 0.14E-10  0.15E-10  0.81E-11  0.72E-11  0.84E-11  0.76E-11  0.87E-11  0.82E-11  0.86E-11  0.82E-11
 0.72E-11  0.80E-11  0.64E-11  0.11E-10 -0.29E-13 -0.16E-13 -0.29E-10 -0.25E-10 -0.17E-09 -0.19E-09
-0.60E-09 -0.62E-09
 0.15E-10  0.15E-10  0.74E-11  0.67E-11  0.78E-11  0.64E-11  0.85E-11  0.75E-11  0.85E-11  0.86E-11
 0.82E-11  0.84E-11  0.35E-11  0.48E-11 -0.18E-13  0.20E-11 -0.29E-10 -0.33E-11 -0.19E-09 -0.88E-10
-0.52E-09 -0.27E-09
 0.15E-10  0.15E-10  0.69E-11  0.70E-11  0.65E-11  0.70E-11  0.77E-11  0.73E-11  0.89E-11  0.80E-11
 0.85E-11  0.81E-11  0.48E-11  0.53E-11  0.20E-11  0.28E-11 -0.12E-10 -0.78E-12 -0.93E-10 -0.22E-10
-0.27E-09  0.15E-09
```

| | | | | | | | | | |
|---|---|---|---|---|---|---|---|---|---|
| 0.15E-10 | 0.16E-10 | 0.71E-11 | 0.72E-11 | 0.71E-11 | 0.71E-11 | 0.74E-11 | 0.68E-11 | 0.83E-11 | 0.86E-11 |
| 0.81E-11 | 0.82E-11 | 0.54E-11 | 0.57E-11 | 0.28E-11 | 0.36E-11 | -0.22E-11 | 0.29E-11 | -0.25E-10 | -0.60E-11 |
| 0.15E-09 | 0.95E-10 | | | | | | | | |
| 0.16E-10 | 0.16E-10 | 0.73E-11 | 0.72E-11 | 0.72E-11 | 0.76E-11 | 0.70E-11 | 0.80E-11 | 0.88E-11 | 0.82E-11 |
| 0.83E-11 | 0.81E-11 | 0.59E-11 | 0.63E-11 | 0.37E-11 | 0.46E-11 | -0.12E-11 | -0.16E-10 | -0.88E-11 | 0.23E-10 |
| 0.90E-10 | 0.17E-10 | | | | | | | | |
| 0.16E-10 | 0.16E-10 | 0.75E-11 | 0.80E-11 | 0.78E-11 | 0.81E-11 | 0.83E-11 | 0.82E-11 | 0.85E-11 | 0.83E-11 |
| 0.94E-11 | 0.82E-11 | 0.66E-11 | 0.79E-11 | 0.48E-11 | 0.75E-11 | -0.18E-10 | -0.72E-11 | 0.11E-10 | -0.11E-10 |
| 0.13E-10 | -0.19E-09 | | | | | | | | |
| 0.16E-10 | 0.17E-10 | 0.82E-11 | 0.84E-11 | 0.83E-11 | 0.84E-11 | 0.84E-11 | 0.85E-11 | 0.85E-11 | 0.85E-11 |
| 0.85E-11 | 0.84E-11 | 0.78E-11 | 0.84E-11 | 0.78E-11 | 0.11E-10 | -0.45E-11 | 0.10E-10 | -0.15E-10 | 0.17E-10 |
| -0.19E-09 | -0.73E-10 | | | | | | | | |
| 0.17E-10 | 0.17E-10 | 0.85E-11 | 0.85E-11 | 0.85E-11 | 0.85E-11 | 0.86E-11 | 0.86E-11 | 0.86E-11 | 0.86E-11 |
| 0.86E-11 | 0.85E-11 | 0.87E-11 | 0.85E-11 | 0.11E-10 | 0.13E-10 | 0.12E-10 | 0.50E-11 | 0.19E-10 | 0.11E-10 |
| -0.79E-10 | -0.15E-09 | | | | | | | | |
| 0.17E-10 | 0.17E-10 | 0.85E-11 | 0.80E-11 | 0.85E-11 | 0.78E-11 | 0.86E-11 | 0.76E-11 | 0.86E-11 | 0.74E-11 |
| 0.86E-11 | 0.71E-11 | 0.85E-11 | 0.69E-11 | 0.32E-11 | 0.64E-11 | 0.99E-11 | 0.11E-10 | 0.69E-11 | 0.15E-10 |
| -0.17E-09 | -0.65E-10 | | | | | | | | |
| 0.17E-10 | 0.16E-10 | 0.80E-11 | 0.78E-11 | 0.78E-11 | 0.76E-11 | 0.76E-11 | 0.73E-11 | 0.74E-11 | 0.70E-11 |
| 0.71E-11 | 0.67E-11 | 0.67E-11 | 0.63E-11 | 0.64E-11 | 0.60E-11 | 0.48E-11 | 0.97E-11 | 0.12E-10 | 0.18E-10 |
| -0.77E-10 | 0.17E-09 | | | | | | | | |
| 0.16E-10 | 0.16E-10 | 0.78E-11 | 0.79E-11 | 0.75E-11 | 0.77E-11 | 0.73E-11 | 0.75E-11 | 0.70E-11 | 0.72E-11 |
| 0.67E-11 | 0.69E-11 | 0.63E-11 | 0.63E-11 | 0.60E-11 | 0.48E-11 | 0.74E-11 | 0.88E-11 | 0.13E-10 | 0.12E-10 |
| 0.17E-09 | -0.36E-10 | | | | | | | | |
| 0.16E-10 | 0.16E-10 | 0.79E-11 | 0.81E-11 | 0.77E-11 | 0.79E-11 | 0.74E-11 | 0.76E-11 | 0.72E-11 | 0.74E-11 |
| 0.69E-11 | 0.73E-11 | 0.63E-11 | 0.74E-11 | 0.49E-11 | 0.29E-11 | 0.49E-11 | 0.11E-10 | 0.67E-11 | 0.14E-10 |
| -0.47E-10 | 0.55E-10 | | | | | | | | |
| 0.16E-10 | 0.15E-10 | 0.81E-11 | 0.84E-11 | 0.78E-11 | 0.82E-11 | 0.76E-11 | 0.79E-11 | 0.74E-11 | 0.76E-11 |
| 0.73E-11 | 0.73E-11 | 0.74E-11 | 0.69E-11 | 0.12E-10 | 0.69E-11 | 0.68E-11 | 0.94E-11 | 0.77E-11 | 0.16E-10 |
| 0.46E-10 | 0.12E-09 | | | | | | | | |
| 0.15E-10 | 0.15E-10 | 0.84E-11 | 0.99E-11 | 0.81E-11 | 0.95E-11 | 0.79E-11 | 0.91E-11 | 0.76E-11 | 0.86E-11 |
| 0.73E-11 | 0.82E-11 | 0.69E-11 | 0.43E-11 | 0.70E-11 | 0.62E-14 | 0.77E-11 | -0.22E-11 | 0.10E-10 | 0.98E-12 |
| 0.11E-09 | 0.12E-10 | | | | | | | | |
| 0.15E-10 | 0.15E-10 | 0.98E-11 | 0.12E-10 | 0.95E-11 | 0.12E-10 | 0.90E-11 | 0.11E-10 | 0.86E-11 | 0.10E-10 |
| 0.92E-11 | 0.57E-11 | 0.13E-10 | 0.47E-11 | 0.55E-12 | 0.40E-11 | -0.87E-11 | 0.49E-12 | -0.55E-11 | -0.33E-11 |
| 0.72E-12 | -0.77E-10 | | | | | | | | |
| 0.15E-10 | 0.15E-10 | 0.12E-10 | 0.15E-10 | 0.12E-10 | 0.14E-10 | 0.11E-10 | 0.14E-10 | 0.10E-10 | 0.68E-11 |
| 0.17E-10 | 0.10E-10 | 0.63E-11 | 0.41E-11 | -0.48E-13 | 0.41E-11 | -0.65E-11 | 0.11E-12 | -0.11E-10 | -0.59E-11 |
| -0.87E-10 | -0.15E-09 | | | | | | | | |
| 0.15E-10 | 0.13E-10 | 0.15E-10 | 0.15E-10 | 0.14E-10 | 0.17E-10 | 0.14E-10 | 0.75E-11 | 0.20E-10 | 0.14E-10 |
| 0.14E-10 | 0.17E-10 | 0.42E-11 | 0.10E-13 | -0.58E-12 | 0.59E-11 | -0.67E-11 | 0.78E-11 | -0.12E-10 | 0.14E-10 |
| -0.16E-09 | 0.12E-09 | | | | | | | | |

0.13E-10 0.11E-10 0.16E-10 0.15E-10 0.16E-10 0.16E-10 0.22E-10 0.16E-10 0.19E-10 0.15E-10
0.18E-10 0.15E-10 0.23E-10 0.36E-11 0.78E-11 0.12E-10 0.12E-10 0.15E-10 0.15E-10 0.25E-10
0.11E-09 0.80E-10
0.11E-10 0.10E-10 0.16E-10 0.19E-10 0.16E-10 0.14E-10 0.16E-10 0.14E-10 0.16E-10 0.14E-10
0.16E-10 0.14E-10 0.27E-10 0.10E-10 0.27E-10 0.15E-10 0.29E-10 0.19E-10 0.28E-10 0.23E-10
0.78E-10 0.76E-10
0.10E-10 0.10E-10 0.14E-10 0.13E-10 0.14E-10 0.13E-10 0.14E-10 0.13E-10 0.14E-10 0.13E-10
0.14E-10 0.13E-10 0.23E-10 0.11E-10 0.26E-10 0.14E-10 0.27E-10 0.17E-10 0.27E-10 0.21E-10
0.71E-10 0.40E-10
0.10E-10 0.11E-10 0.13E-10 0.14E-10 0.13E-10 0.11E-10 0.13E-10 0.11E-10 0.13E-10 0.11E-10
0.13E-10. 0.12E-10 0.18E-10 0.15E-10 0.20E-10 0.19E-10 0.21E-10 0.19E-10 0.22E-10 0.20E-10
0.36E-10 0.35E-10

## SIMULATION TWO-Horizontal component

0.98E-13 0.37E-12 0.40E-10 0.29E-10 0.47E-10 0.43E-10 0.59E-10 0.48E-10 0.58E-10 0.52E-10
0.43E-10 0.46E-10 0.50E-10 0.31E-10 0.34E-10 0.24E-10 0.96E-09 0.41E-09 0.38E-09 0.14E-09
0.13E-09 0.00E+00
-0.45E-12 0.23E-12 0.27E-10 -0.87E-11 0.23E-10 0.55E-11 0.24E-10 0.85E-11 0.23E-10 0.15E-10
0.19E-10 0.14E-10 0.16E-10 0.11E-10 0.15E-10 0.12E-10 0.48E-09 0.30E-09 0.28E-09 0.14E-09
0.13E-09 0.00E+00
-0.17E-11 0.83E-12 -0.35E-11 -0.54E-10 -0.34E-11 -0.36E-10 0.12E-10 -0.15E-10 0.13E-10 -0.31E-12
0.17E-10 0.78E-11 0.16E-10 0.11E-10 0.13E-10 0.99E-11 0.35E-09 0.19E-09 0.25E-09 0.96E-10
0.19E-09 0.12E-10
-0.38E-11 0.63E-11 -0.17E-10 -0.29E-10 -0.34E-12 -0.15E-10 0.97E-11 -0.32E-11 0.12E-10 0.37E-11
0.13E-10 0.73E-11 0.12E-10 0.66E-11 0.10E-10 0.69E-11 0.28E-09 0.16E-09 0.18E-09 0.94E-10
0.16E-10 0.00E+00
-0.27E-10 0.48E-11 -0.16E-10 0.86E-11 0.59E-10 0.15E-10 0.55E-10 0.13E-10 0.44E-10 0.19E-10
0.34E-10 0.14E-10 0.25E-10 0.11E-10 0.15E-10 0.83E-11 0.23E-09 0.15E-09 0.14E-09 0.64E-10
0.87E-10 0.00E+00
-0.66E-10 0.28E-10 -0.24E-10 0.35E-10 0.11E-09 0.85E-10 0.12E-09 0.46E-10 0.80E-10 0.34E-10
0.59E-10 0.19E-10 0.33E-10 0.11E-10 0.30E-10 0.99E-11 0.38E-09 0.19E-09 0.17E-09 0.11E-09
0.96E-10 0.41E-10
-0.19E-09 0.85E-10 -0.78E-10 0.36E-10 -0.28E-10 0.28E-10 0.17E-09 0.74E-10 0.12E-09 0.63E-10
0.91E-10 0.39E-10 0.53E-10 0.28E-10 0.36E-10 0.20E-10 0.71E-09 0.27E-09 0.29E-09 0.12E-09
0.11E-09 -0.63E-10
-0.41E-09 0.11E-09 -0.17E-09 0.99E-10 -0.15E-10 0.78E-10 0.13E-09 0.95E-10 0.12E-09 0.67E-10
0.97E-10 0.50E-10 0.72E-10 0.51E-10 0.62E-10 0.48E-10 0.15E-08 0.53E-09 0.55E-09 0.68E-10
0.14E-09 0.41E-10

```
-0.47E-09  0.68E-10 -0.25E-09  0.14E-09 -0.42E-10  0.11E-09 -0.81E-09  0.70E-09  0.18E-09  0.15E-09
 0.17E-09  0.14E-09  0.14E-09  0.13E-09  0.12E-09  0.11E-09  0.32E-08  0.12E-08  0.11E-08 -0.13E-08
-0.76E-09 -0.54E-08
-0.45E-09 -0.20E-09 -0.76E-11  0.39E-11 -0.43E-10 -0.38E-10 -0.17E-09  0.96E-10  0.38E-09  0.38E-09
 0.37E-09  0.33E-09  0.31E-09  0.29E-09  0.27E-09  0.26E-09  0.73E-08  0.61E-08  0.52E-08  0.25E-08
 0.23E-08 -0.57E-08
-0.34E-09 -0.34E-09 -0.52E-11 -0.48E-11 -0.89E-11  0.28E-11 -0.15E-09  0.53E-10 -0.12E-09  0.80E-10
 0.68E-09  0.67E-09  0.59E-09  0.54E-09  0.47E-09  0.45E-09  0.12E-07  0.17E-07  0.13E-07  0.20E-07
 0.17E-07  0.31E-07
-0.33E-09 -0.50E-09 -0.68E-11 -0.74E-11 -0.50E-11 -0.38E-11 -0.88E-11  0.62E-11 -0.61E-10  0.16E-09
-0.23E-09  0.11E-08  0.43E-09  0.35E-09  0.33E-09  0.30E-09  0.84E-08  0.13E-07  0.11E-07  0.20E-07
 0.17E-07  0.36E-07
-0.33E-09 -0.74E-09 -0.95E-11 -0.25E-10 -0.17E-10 -0.20E-10 -0.15E-10 -0.17E-10 -0.20E-10  0.56E-11
-0.27E-09  0.18E-09  0.57E-10 -0.13E-09 -0.39E-10 -0.13E-09 -0.17E-08 -0.10E-07 -0.60E-08 -0.25E-07
-0.18E-07 -0.52E-07
-0.29E-09 -0.83E-09 -0.14E-10 -0.45E-10 -0.33E-10 -0.37E-10 -0.31E-10 -0.28E-10 -0.73E-10 -0.81E-10
-0.29E-10  0.17E-10 -0.56E-13 -0.41E-11 -0.49E-10 -0.11E-09 -0.14E-08 -0.80E-08 -0.63E-08 -0.15E-07
-0.13E-07 -0.21E-07
-0.39E-09 -0.82E-09 -0.17E-10 -0.49E-10 -0.33E-10 -0.63E-10 -0.49E-10 -0.26E-10 -0.77E-10 -0.11E-10
-0.14E-09  0.14E-11  0.12E-11  0.61E-16  0.69E-10 -0.50E-10 -0.53E-09 -0.59E-08 -0.46E-08 -0.11E-07
-0.10E-07 -0.23E-07
-0.73E-09 -0.62E-09 -0.12E-10 -0.13E-10 -0.81E-11 -0.16E-10 -0.59E-11 -0.28E-10 -0.59E-10  0.79E-11
-0.91E-10  0.23E-09  0.32E-11  0.85E-12  0.86E-10 -0.91E-11  0.57E-09 -0.25E-08 -0.26E-08 -0.48E-08
-0.42E-08 -0.65E-08
-0.57E-11 -0.47E-10 -0.38E-11 -0.41E-11 -0.18E-11 -0.61E-11  0.26E-11 -0.10E-10  0.17E-10  0.13E-10
 0.80E-10  0.37E-09  0.44E-11  0.29E-11  0.39E-11  0.23E-11  0.29E-08  0.28E-08  0.13E-08  0.49E-08
 0.42E-08  0.12E-07
 0.68E-09  0.54E-09  0.67E-11  0.13E-10  0.11E-10  0.15E-10  0.17E-10  0.14E-10  0.93E-10 -0.83E-11
 0.14E-09  0.30E-11  0.42E-13  0.13E-13  0.16E-11  0.44E-11  0.45E-08  0.60E-08  0.23E-08  0.84E-08
 0.69E-08  0.23E-07
 0.37E-09  0.77E-09  0.92E-11  0.21E-10  0.19E-10  0.29E-10  0.89E-10  0.99E-10  0.13E-09  0.71E-11
 0.99E-10 -0.45E-10 -0.55E-09 -0.53E-09 -0.43E-09  0.49E-10  0.55E-08  0.67E-08  0.39E-08  0.66E-08
 0.61E-08  0.00E+00
 0.53E-09  0.87E-09  0.13E-10  0.21E-10  0.19E-10  0.27E-10  0.83E-10  0.86E-10  0.79E-10  0.18E-10
 0.25E-09 -0.50E-09 -0.62E-09 -0.96E-10 -0.92E-10  0.40E-10  0.52E-08  0.74E-08  0.47E-08  0.65E-08
 0.51E-08  0.00E+00
 0.29E-09  0.70E-09  0.11E-10  0.17E-10  0.16E-10  0.20E-10  0.62E-10  0.67E-10  0.60E-10  0.41E-10
 0.56E-09 -0.37E-09 -0.42E-09 -0.11E-09 -0.14E-09  0.11E-09  0.44E-08  0.89E-08  0.55E-08  0.81E-08
 0.63E-08  0.53E-08
 0.93E-09  0.57E-09  0.93E-11  0.19E-10  0.18E-10  0.29E-10  0.88E-10  0.61E-10  0.55E-10  0.41E-10
 0.58E-09  0.48E-11 -0.29E-09 -0.35E-09 -0.19E-10  0.14E-09  0.61E-09  0.55E-09  0.14E-07  0.14E-07
 0.86E-08  0.18E-07
```

| | | | | | | | | | |
|---|---|---|---|---|---|---|---|---|---|
| 0.93E-09 | 0.56E-09 | 0.92E-11 | 0.88E-11 | 0.82E-11 | 0.72E-11 | 0.22E-10 | 0.22E-10 | 0.21E-10 | 0.17E-10 |
| 0.25E-09 | 0.67E-11 | 0.19E-09 | 0.17E-09 | 0.33E-11 | 0.13E-10 | 0.40E-09 | 0.40E-09 | 0.11E-07 | 0.12E-07 |
| 0.10E-07 | 0.72E-08 | | | | | | | | |
| 0.89E-09 | 0.52E-09 | 0.87E-11 | 0.19E-11 | 0.18E-11 | -0.52E-11 | -0.17E-10 | 0.47E-11 | 0.45E-11 | 0.15E-11 |
| 0.24E-10 | 0.95E-11 | 0.34E-09 | 0.76E-09 | 0.28E-12 | 0.20E-12 | 0.36E-09 | 0.36E-09 | 0.99E-08 | 0.13E-07 |
| 0.98E-08 | 0.16E-07 | | | | | | | | |
| 0.73E-09 | 0.51E-09 | 0.85E-11 | 0.39E-11 | 0.36E-11 | -0.38E-12 | -0.12E-11 | -0.82E-11 | -0.77E-11 | -0.25E-11 |
| -0.39E-10 | 0.11E-10 | 0.40E-09 | 0.56E-09 | 0.48E-09 | 0.31E-09 | 0.26E-09 | 0.27E-09 | 0.77E-08 | 0.12E-07 |
| 0.90E-08 | 0.26E-07 | | | | | | | | |
| 0.67E-09 | 0.52E-09 | 0.83E-11 | 0.51E-11 | 0.46E-11 | 0.12E-11 | 0.37E-11 | -0.65E-11 | -0.57E-11 | 0.22E-10 |
| 0.19E-10 | 0.29E-10 | 0.40E-09 | 0.57E-09 | 0.48E-09 | 0.80E-11 | 0.27E-09 | 0.19E-09 | 0.56E-08 | 0.91E-08 |
| 0.68E-08 | -0.13E-07 | | | | | | | | |
| 0.65E-09 | 0.53E-09 | 0.84E-11 | 0.63E-11 | 0.56E-11 | 0.29E-11 | 0.87E-11 | 0.74E-11 | 0.65E-11 | 0.24E-10 |
| 0.20E-10 | 0.30E-10 | 0.42E-09 | 0.60E-09 | 0.51E-09 | 0.38E-10 | 0.13E-08 | 0.14E-08 | 0.12E-08 | 0.56E-09 |
| 0.15E-07 | 0.26E-07 | | | | | | | | |
| 0.68E-09 | 0.53E-09 | 0.87E-11 | 0.77E-11 | 0.70E-11 | 0.69E-11 | 0.64E-11 | 0.65E-11 | 0.20E-10 | 0.27E-10 |
| 0.24E-10 | 0.30E-10 | 0.43E-09 | 0.34E-10 | 0.12E-08 | 0.77E-09 | 0.67E-09 | 0.68E-09 | 0.56E-09 | 0.51E-09 |
| 0.13E-07 | 0.14E-07 | | | | | | | | |
| 0.65E-09 | 0.54E-09 | 0.87E-11 | 0.91E-11 | 0.82E-11 | 0.89E-11 | 0.80E-11 | 0.88E-11 | 0.26E-10 | 0.36E-10 |
| 0.30E-10 | 0.96E-12 | 0.54E-09 | 0.12E-08 | 0.48E-12 | 0.24E-12 | 0.47E-09 | 0.45E-09 | 0.37E-09 | 0.34E-09 |
| 0.88E-08 | 0.00E+00 | | | | | | | | |
| 0.61E-09 | 0.55E-09 | 0.87E-11 | 0.94E-11 | 0.84E-11 | 0.81E-11 | 0.72E-11 | 0.57E-11 | 0.50E-11 | 0.11E-12 |
| 0.20E-09 | 0.51E-09 | 0.20E-12 | 0.24E-12 | 0.47E-09 | 0.43E-09 | 0.36E-09 | 0.36E-09 | 0.29E-09 | 0.28E-09 |
| 0.74E-08 | 0.00E+00 | | | | | | | | |
| 0.60E-09 | 0.55E-09 | 0.87E-11 | 0.12E-10 | 0.11E-10 | 0.15E-10 | 0.13E-10 | 0.15E-10 | 0.14E-10 | 0.35E-11 |
| 0.17E-09 | 0.33E-09 | 0.53E-11 | 0.21E-12 | 0.41E-09 | 0.42E-09 | 0.36E-09 | 0.38E-09 | 0.31E-09 | 0.31E-09 |
| 0.82E-08 | 0.00E+00 | | | | | | | | |
| 0.60E-09 | 0.53E-09 | 0.86E-11 | 0.15E-10 | 0.14E-10 | 0.22E-10 | 0.20E-10 | 0.14E-10 | 0.13E-10 | 0.11E-10 |
| 0.94E-11 | 0.71E-11 | 0.35E-09 | 0.15E-10 | 0.53E-09 | 0.53E-09 | 0.46E-09 | 0.46E-09 | 0.38E-09 | 0.39E-09 |
| 0.10E-07 | 0.26E-07 | | | | | | | | |
| 0.53E-09 | 0.47E-09 | 0.73E-11 | 0.68E-11 | 0.60E-11 | 0.48E-11 | 0.42E-11 | 0.21E-11 | 0.18E-11 | 0.78E-12 |
| 0.37E-10 | 0.15E-10 | 0.52E-09 | 0.49E-09 | 0.41E-09 | 0.40E-09 | 0.34E-09 | 0.32E-09 | 0.26E-09 | 0.26E-09 |
| 0.67E-08 | 0.48E-08 | | | | | | | | |
| 0.39E-09 | 0.36E-09 | 0.56E-11 | 0.39E-11 | 0.34E-11 | 0.17E-11 | 0.15E-11 | 0.10E-11 | 0.88E-12 | 0.57E-12 |
| 0.28E-10 | 0.96E-11 | 0.33E-09 | 0.31E-09 | 0.26E-09 | 0.25E-09 | 0.21E-09 | 0.20E-09 | 0.16E-09 | 0.15E-09 |
| 0.37E-08 | 0.33E-08 | | | | | | | | |
| 0.25E-09 | 0.29E-09 | 0.45E-11 | 0.32E-11 | 0.28E-11 | 0.13E-11 | 0.12E-11 | 0.79E-12 | 0.70E-12 | 0.44E-12 |
| 0.22E-10 | 0.58E-11 | 0.20E-09 | 0.17E-09 | 0.14E-09 | 0.12E-09 | 0.10E-09 | 0.82E-10 | 0.67E-10 | 0.49E-10 |
| 0.12E-08 | 0.32E-10 | | | | | | | | |
| 0.82E-10 | 0.25E-09 | 0.39E-11 | 0.53E-11 | 0.47E-11 | 0.17E-11 | 0.15E-11 | 0.88E-12 | 0.78E-12 | 0.37E-12 |
| 0.18E-10 | 0.26E-11 | 0.91E-10 | 0.73E-10 | 0.62E-10 | 0.50E-10 | 0.43E-10 | 0.32E-10 | 0.26E-10 | 0.14E-10 |
| 0.34E-09 | 0.12E-11 | | | | | | | | |

## SIMULATION TWO-Vertical component

-0.68E-14 0.21E-14 -0.20E-11 -0.25E-10 -0.38E-11 -0.14E-10 0.97E-11 -0.48E-11 0.60E-11 -0.26E-11
0.31E-10 0.56E-11 0.27E-10 0.91E-11 0.24E-10 0.94E-11 0.40E-10 0.11E-10 0.27E-10 0.15E-10
0.20E-10 0.15E-10
0.26E-13 0.46E-13 0.32E-10 -0.19E-10 0.19E-10 -0.74E-11 0.10E-10 -0.62E-11 0.10E-10 0.33E-11
0.38E-11 0.49E-11 0.39E-11 0.67E-11 0.61E-11 0.89E-11 0.93E-11 0.54E-11 0.13E-10 0.83E-11
0.13E-10 0.90E-11
0.82E-13 0.14E-12 0.20E-10 -0.43E-10 0.12E-10 -0.32E-10 0.12E-10 -0.16E-10 0.42E-11 -0.82E-11
0.32E-11 -0.13E-11 0.19E-11 0.49E-11 -0.81E-13 0.27E-11 0.22E-11 -0.20E-12 0.58E-11 0.19E-11
0.67E-11 0.35E-11
0.19E-12 0.63E-12 0.23E-10 0.16E-11 0.16E-10 -0.22E-10 0.73E-11 -0.14E-10 0.32E-11 -0.13E-10
-0.46E-12 -0.50E-11 -0.33E-11 -0.63E-11 -0.20E-11 -0.28E-11 -0.19E-11 -0.53E-11 0.12E-12 -0.41E-11
0.12E-11 -0.44E-11
0.74E-12 0.16E-11 0.42E-13 0.80E-12 0.24E-10 -0.70E-10 0.10E-10 -0.51E-10 0.85E-11 -0.35E-10
-0.25E-11 -0.28E-10 -0.16E-11 -0.18E-10 -0.59E-11 -0.83E-11 -0.71E-11 -0.97E-11 -0.66E-11 -0.90E-11
-0.57E-11 -0.88E-11
0.19E-11 0.49E-11 0.93E-12 0.27E-11 0.54E-10 0.56E-11 0.35E-10 -0.87E-10 0.20E-10 -0.75E-10
0.13E-10 -0.51E-10 0.52E-11 -0.30E-10 -0.32E-11 -0.12E-10 -0.88E-11 -0.12E-10 -0.89E-11 -0.12E-10
-0.10E-10 -0.11E-10
0.57E-11 0.14E-10 0.32E-11 0.65E-11 0.12E-12 0.27E-11 0.76E-10 -0.11E-09 0.64E-10 -0.72E-10
0.42E-10 -0.49E-10 0.24E-10 -0.26E-10 0.71E-11 -0.13E-10 -0.11E-10 -0.22E-10 -0.12E-10 -0.25E-10
-0.13E-10 -0.23E-10
0.98E-11 0.18E-10 0.74E-11 0.14E-10 0.31E-11 0.71E-11 0.11E-09 0.67E-10 0.74E-10 -0.40E-10
0.51E-10 -0.23E-10 0.28E-10 -0.88E-11 0.13E-10 0.23E-11 -0.21E-10 -0.47E-10 -0.25E-10 -0.55E-10
-0.25E-10 -0.29E-10
0.20E-10 0.26E-10 0.93E-11 0.16E-10 0.76E-11 0.15E-10 0.92E-13 0.15E-11 0.53E-10 -0.13E-10
0.34E-10 -0.92E-12 0.17E-10 -0.42E-12 0.21E-11 -0.31E-11 -0.52E-10 -0.11E-09 -0.57E-10 -0.24E-09
-0.32E-10 -0.31E-09
0.95E-11 0.10E-10 0.55E-11 0.85E-11 0.15E-10 0.16E-10 0.16E-11 0.11E-10 0.31E-10 0.28E-10
0.40E-11 -0.56E-10 -0.76E-11 -0.34E-10 -0.15E-10 -0.17E-10 -0.12E-09 -0.15E-09 -0.25E-09 -0.43E-09
-0.32E-09 -0.76E-09
0.12E-10 0.12E-10 0.93E-11 0.94E-11 0.34E-11 0.92E-11 0.72E-11 0.12E-10 0.14E-12 0.99E-11
0.57E-10 0.49E-10 0.17E-10 -0.11E-09 -0.11E-10 -0.20E-10 -0.15E-09 0.14E-10 -0.44E-09 0.77E-10
-0.77E-09 0.44E-10
0.13E-10 0.13E-10 0.11E-10 0.11E-10 0.11E-10 0.11E-10 0.45E-11 0.11E-10 0.70E-11 0.14E-10
0.18E-12 0.16E-11 0.10E-09 -0.75E-10 0.51E-10 0.30E-10 0.25E-10 0.22E-09 0.86E-10 0.89E-09
0.91E-10 0.16E-08
0.14E-10 0.13E-10 0.12E-10 0.93E-11 0.13E-10 0.12E-10 0.13E-10 0.13E-10 0.52E-11 0.14E-10
0.12E-11 0.99E-11 0.21E-09 -0.28E-10 0.84E-10 0.14E-10 0.23E-09 0.34E-10 0.89E-09 0.21E-10
0.16E-08 -0.33E-09

```
 0.42E-10  0.40E-10  0.10E-10  0.57E-11  0.13E-10  0.12E-10  0.13E-10  0.14E-10  0.15E-10  0.15E-10
 0.36E-11  0.15E-10  0.95E-10  0.11E-10  0.81E-11  0.88E-11  0.25E-10 -0.50E-10  0.16E-10 -0.24E-09
-0.34E-09 -0.54E-09
 0.41E-10  0.40E-10  0.21E-10  0.15E-10  0.12E-10  0.82E-11  0.15E-10  0.17E-10  0.15E-10  0.18E-10
 0.16E-10  0.16E-10  0.23E-10 -0.17E-11 -0.69E-11 -0.52E-11 -0.59E-10 -0.81E-10 -0.24E-09 -0.33E-09
-0.54E-09 -0.70E-09
 0.68E-10  0.70E-10  0.28E-10  0.28E-10  0.26E-10  0.19E-10  0.17E-10  0.12E-10  0.18E-10  0.24E-10
 0.16E-10  0.18E-10  0.40E-11 -0.53E-10  0.27E-11 -0.34E-10 -0.83E-10 -0.11E-09 -0.34E-09 -0.41E-09
-0.71E-09 -0.78E-09
 0.72E-10  0.72E-10  0.29E-10  0.29E-10  0.34E-10  0.27E-10  0.39E-10  0.27E-10  0.25E-10  0.25E-10
 0.19E-10  0.21E-10  0.60E-10  0.11E-10  0.52E-10  0.19E-10 -0.11E-09 -0.95E-10 -0.42E-09 -0.27E-09
-0.79E-09 -0.47E-09
 0.72E-10  0.72E-10  0.30E-10  0.34E-10  0.28E-10  0.33E-10  0.29E-10  0.27E-10  0.26E-10  0.19E-10
 0.21E-10  0.21E-10  0.87E-10  0.68E-10  0.72E-10  0.19E-09 -0.10E-09 -0.75E-10 -0.28E-09 -0.17E-09
-0.47E-09 -0.56E-10
 0.43E-10  0.43E-10  0.35E-10  0.39E-10  0.33E-10  0.38E-10  0.27E-10  0.28E-10  0.19E-10  0.15E-10
 0.21E-10  0.20E-10  0.50E-10  0.13E-09  0.90E-13  0.36E-11 -0.81E-10 -0.59E-10 -0.17E-09 -0.15E-09
-0.59E-10 -0.12E-09
 0.14E-10  0.15E-10  0.23E-10  0.27E-10  0.23E-10  0.27E-10  0.28E-10  0.28E-10  0.44E-10  0.29E-10
 0.20E-10  0.18E-10  0.61E-13  0.10E-10  0.37E-11  0.58E-11 -0.69E-10 -0.36E-10 -0.15E-09 -0.12E-09
-0.13E-09 -0.24E-09
 0.14E-10  0.16E-10  0.26E-10  0.33E-10  0.27E-10  0.32E-10  0.28E-10  0.31E-10  0.29E-10  0.21E-10
 0.17E-10  0.11E-10  0.22E-11  0.44E-11  0.58E-11  0.14E-10 -0.47E-10  0.41E-10 -0.13E-09 -0.70E-10
-0.24E-09 -0.28E-09
 0.16E-10  0.14E-10  0.11E-10  0.14E-10  0.11E-10  0.15E-10  0.10E-10  0.59E-11  0.21E-10  0.14E-10
 0.34E-10  0.22E-10  0.14E-10  0.14E-10  0.27E-11  0.38E-11  0.68E-10  0.21E-10 -0.83E-10 -0.69E-10
-0.29E-09  0.24E-10
 0.14E-10  0.13E-10  0.14E-10  0.14E-10  0.15E-10  0.14E-10  0.30E-10  0.29E-10  0.24E-10  0.21E-10
 0.37E-10  0.28E-10  0.23E-10  0.23E-10  0.39E-11  0.38E-11 -0.78E-12  0.23E-11 -0.77E-10 -0.44E-10
 0.22E-10 -0.34E-10
 0.13E-10  0.10E-10  0.14E-10  0.10E-10  0.14E-10  0.10E-10  0.58E-11  0.95E-11  0.12E-10  0.10E-10
 0.17E-10  0.15E-10  0.13E-10  0.13E-10  0.38E-11  0.36E-11  0.69E-11  0.73E-11 -0.53E-10  0.35E-10
-0.42E-10  0.11E-09
 0.10E-10  0.94E-11  0.10E-10  0.86E-11  0.10E-10  0.84E-11  0.95E-11  0.81E-11  0.99E-11  0.11E-10
 0.50E-11  0.47E-11  0.43E-11  0.39E-11  0.36E-11  0.34E-11 -0.15E-10  0.17E-10  0.32E-10  0.12E-09
 0.10E-09  0.38E-09
 0.93E-11  0.90E-11  0.86E-11  0.80E-11  0.84E-11  0.77E-11  0.81E-11  0.72E-11  0.36E-11  0.56E-11
 0.49E-11  0.54E-11  0.39E-11  0.45E-11  0.34E-11  0.12E-11  0.83E-11 -0.58E-10  0.12E-09  0.17E-09
 0.38E-09  0.19E-09
 0.89E-11  0.89E-11  0.79E-11  0.78E-11  0.77E-11  0.74E-11  0.72E-11  0.72E-11  0.57E-11  0.63E-11
 0.55E-11  0.59E-11  0.46E-11  0.49E-11  0.12E-11  0.15E-12 -0.67E-10  0.48E-11  0.33E-09  0.10E-09
 0.17E-09  0.24E-09
```

0.98E-11 0.69E-11 0.77E-11 0.74E-11 0.74E-11 0.72E-11 0.72E-11 0.70E-11 0.64E-11 0.66E-11
0.59E-11 0.61E-11 0.49E-11 0.31E-11 0.75E-12 0.53E-12 -0.98E-11 0.33E-10 0.77E-10 0.60E-10
0.23E-09 0.20E-09
0.83E-11 0.79E-11 0.74E-11 0.75E-11 0.72E-11 0.74E-11 0.70E-11 0.73E-11 0.66E-11 0.79E-11
0.61E-11 0.22E-11 0.31E-11 0.32E-11 0.54E-12 0.28E-13 0.31E-10 0.25E-10 0.40E-10 0.35E-10
0.25E-09 0.92E-10
0.78E-11 0.77E-11 0.74E-11 0.75E-11 0.73E-11 0.72E-11 0.73E-11 0.67E-11 0.79E-11 0.60E-11
0.66E-11 0.68E-11 0.99E-11 0.10E-10 0.63E-10 0.23E-10 0.14E-10 0.24E-10 0.15E-10 0.23E-10
0.91E-10 -0.28E-10
0.76E-11 0.75E-11 0.76E-11 0.82E-11 0.72E-11 0.78E-11 0.67E-11 0.72E-11 0.60E-11 0.33E-11
0.68E-11 0.89E-11 0.17E-10 0.11E-10 0.22E-11 0.22E-10 0.42E-12 0.13E-10 -0.26E-11 0.74E-11
-0.39E-10 -0.12E-09
0.74E-11 0.70E-11 0.82E-11 0.98E-11 0.78E-11 0.10E-10 0.72E-11 0.47E-11 0.98E-11 0.77E-11
0.15E-10 0.10E-10 0.11E-10 -0.12E-13 -0.46E-11 -0.69E-11 -0.10E-10 0.55E-12 -0.17E-10 0.11E-10
-0.13E-09 0.13E-09
0.70E-11 0.67E-11 0.98E-11 0.96E-11 0.10E-10 0.95E-11 0.14E-10 0.95E-11 0.13E-10 0.93E-11
0.11E-10 0.94E-11 0.10E-10 -0.45E-10 0.16E-11 -0.19E-10 0.57E-11 -0.90E-11 0.98E-11 0.18E-10
0.13E-09 0.84E-10
0.68E-11 0.67E-11 0.98E-11 0.95E-11 0.98E-11 0.85E-11 0.98E-11 0.84E-11 0.98E-11 0.83E-11
0.99E-11 0.83E-11 0.52E-10 -0.18E-10 0.41E-10 -0.71E-11 0.40E-10 0.26E-11 0.28E-10 0.15E-10
0.81E-10 0.72E-10
0.68E-11 0.71E-11 0.87E-11 0.91E-11 0.86E-11 0.79E-11 0.86E-11 0.78E-11 0.85E-11 0.77E-11
0.96E-11 0.76E-11 0.52E-10 -0.10E-10 0.44E-10 -0.24E-11 0.37E-10 0.44E-11 0.26E-10 0.13E-10
0.67E-10 0.43E-10
0.71E-11 0.82E-11 0.81E-11 0.89E-11 0.79E-11 0.62E-11 0.78E-11 0.63E-11 0.78E-11 0.63E-11
0.78E-11 0.68E-11 0.28E-10 0.97E-11 0.26E-10 0.14E-10 0.23E-10 0.14E-10 0.18E-10 0.16E-10
0.32E-10 0.31E-10

## SIMULATION THREE-Horizontal component

0.10E-12 0.36E-12 0.40E-10 0.28E-10 0.47E-10 0.43E-10 0.59E-10 0.48E-10 0.58E-10 0.52E-10
0.63E-10 0.46E-10 0.50E-10 0.31E-10 0.34E-10 0.24E-10 0.96E-09 0.41E-09 0.38E-09 0.14E-09
0.13E-09 0.00E+00
-0.41E-12 0.16E-12 0.26E-10 -0.85E-11 0.23E-10 0.56E-11 0.24E-10 0.87E-11 0.23E-10 0.15E-10
0.19E-10 0.14E-10 0.17E-10 0.12E-10 0.15E-10 0.12E-10 0.48E-09 0.31E-09 0.28E-09 0.14E-09
0.13E-09 0.00E+00
-0.16E-11 0.70E-12 -0.23E-11 -0.53E-10 -0.25E-11 -0.35E-10 0.13E-10 -0.15E-10 0.13E-10 -0.21E-13
0.18E-10 0.79E-11 0.16E-10 0.11E-10 0.13E-10 0.90E-11 0.35E-09 0.19E-09 0.25E-09 0.95E-10
0.15E-09 0.12E-10

-0.54E-11 0.75E-11 -0.15E-10 -0.27E-10 0.13E-11 -0.14E-10 0.11E-10 -0.25E-11 0.12E-10 0.41E-11
0.14E-10 0.74E-11 0.12E-10 0.66E-11 0.11E-10 0.68E-11 0.27E-09 0.16E-09 0.18E-09 0.94E-10
0.95E-10 0.00E+00
-0.25E-10 0.46E-11 -0.15E-10 0.83E-11 0.62E-10 0.17E-10 0.57E-10 0.14E-10 0.45E-10 0.20E-10
0.35E-10 0.17E-10 0.25E-10 0.11E-10 0.15E-10 0.81E-11 0.29E-09 0.15E-09 0.14E-09 0.64E-10
0.96E-10 0.00E+00
-0.62E-10 0.27E-10 -0.22E-10 0.33E-10 0.10E-09 0.81E-10 0.11E-09 0.44E-10 0.78E-10 0.33E-10
0.58E-10 0.19E-10 0.33E-10 0.11E-10 0.20E-10 0.10E-10 0.38E-09 0.19E-09 0.17E-09 0.11E-09
0.98E-10 0.42E-10
-0.18E-09 0.80E-10 -0.74E-10 0.34E-10 -0.26E-10 0.26E-10 0.16E-09 0.68E-10 0.12E-09 0.60E-10
0.87E-10 0.37E-10 0.52E-10 0.28E-10 0.36E-10 0.21E-10 0.72E-09 0.28E-09 0.30E-09 0.12E-09
0.11E-09 -0.64E-10
-0.39E-09 0.10E-09 -0.16E-09 0.93E-10 -0.14E-10 0.73E-10 0.12E-09 0.93E-10 0.12E-09 0.67E-10
0.95E-10 0.50E-10 0.72E-10 0.52E-10 0.62E-10 0.49E-10 0.15E-08 0.54E-09 0.55E-09 0.72E-10
0.15E-09 0.41E-10
-0.44E-09 0.55E-10 -0.23E-09 0.13E-09 -0.39E-10 0.11E-09 -0.75E-09 0.68E-09 0.18E-09 0.15E-09
0.17E-09 0.14E-09 0.14E-09 0.13E-09 0.12E-09 0.11E-09 0.32E-08 0.12E-08 0.11E-08 -0.13E-08
-0.77E-09 -0.54E-08
-0.42E-09 -0.19E-09 -0.71E-11 0.37E-11 -0.39E-10 -0.34E-10 -0.16E-09 0.91E-10 0.39E-09 0.38E-09
0.38E-09 0.33E-09 0.31E-09 0.29E-09 0.27E-09 0.26E-09 0.72E-08 0.61E-08 0.52E-08 0.25E-08
0.23E-08 -0.57E-08
-0.32E-09 -0.32E-09 -0.48E-11 -0.45E-11 -0.83E-11 0.27E-11 -0.14E-09 0.51E-10 -0.11E-09 0.84E-10
0.68E-09 0.66E-09 0.58E-09 0.53E-09 0.47E-09 0.45E-09 0.12E-07 0.17E-07 0.13E-07 0.20E-07
0.17E-07 0.31E-07
-0.31E-09 -0.47E-09 -0.64E-11 -0.70E-11 -0.47E-11 -0.36E-11 -0.83E-11 0.58E-11 -0.57E-10 0.15E-09
-0.20E-09 0.10E-08 0.42E-09 0.35E-09 0.32E-09 0.30E-09 0.84E-08 0.13E-07 0.11E-07 0.20E-07
0.17E-07 0.36E-07
-0.30E-09 -0.70E-09 -0.88E-11 -0.24E-10 -0.16E-10 -0.18E-10 -0.15E-10 -0.16E-10 -0.19E-10 0.51E-11
-0.25E-09 0.16E-09 0.31E-10 -0.14E-09 -0.46E-10 -0.13E-09 -0.17E-08 -0.10E-07 -0.60E-08 -0.25E-07
-0.18E-07 -0.52E-07
-0.26E-09 -0.78E-09 -0.13E-10 -0.42E-10 -0.31E-10 -0.34E-10 -0.29E-10 -0.27E-10 -0.69E-10 -0.79E-10
-0.28E-10 0.16E-10 -0.45E-12 -0.40E-11 -0.52E-10 -0.11E-09 -0.14E-08 -0.79E-08 -0.62E-08 -0.15E-07
-0.13E-07 -0.21E-07
-0.35E-09 -0.77E-09 -0.16E-10 -0.45E-10 -0.31E-10 -0.58E-10 -0.46E-10 -0.25E-10 -0.73E-10 -0.13E-10
-0.15E-09 0.75E-12 0.62E-12 -0.25E-12 0.57E-10 -0.47E-10 -0.54E-09 -0.58E-08 -0.46E-08 -0.11E-07
-0.99E-08 -0.23E-07
-0.65E-09 -0.58E-09 -0.11E-10 -0.13E-10 -0.78E-11 -0.15E-10 -0.58E-11 -0.26E-10 -0.56E-10 0.36E-11
-0.10E-09 0.22E-09 0.24E-11 0.61E-12 0.73E-10 -0.34E-11 0.57E-09 -0.24E-08 -0.26E-08 -0.48E-08
-0.42E-08 -0.65E-08
0.15E-09 -0.41E-10 -0.32E-11 -0.42E-11 -0.20E-11 -0.62E-11 0.18E-11 -0.10E-10 0.12E-10 0.59E-11
0.42E-10 0.36E-09 0.42E-11 0.30E-11 0.38E-11 0.25E-11 0.29E-08 0.28E-08 0.13E-08 0.49E-08
0.42E-08 0.12E-07

0.94E-09 0.48E-09 0.62E-11 0.11E-10 0.95E-11 0.12E-10 0.14E-10 0.10E-10 0.77E-10 -0.16E-10
0.74E-10 0.20E-11 0.29E-13 0.55E-14 0.11E-11 0.46E-11 0.46E-08 0.60E-08 0.23E-08 0.84E-08
0.69E-08 0.23E-07
0.71E-09 0.67E-09 0.84E-11 0.18E-10 0.16E-10 0.23E-10 0.71E-10 0.79E-10 0.11E-09 0.16E-11
0.21E-10 -0.98E-10 -0.58E-09 -0.56E-09 -0.45E-09 0.53E-10 0.57E-08 0.67E-08 0.38E-08 0.65E-08
0.51E-08 0.00E+00
0.92E-09 0.70E-09 0.12E-10 0.22E-10 0.19E-10 0.19E-10 0.57E-10 0.66E-10 0.59E-10 0.10E-10
0.14E-09 -0.57E-09 -0.67E-09 -0.11E-09 -0.11E-09 0.44E-10 0.54E-08 0.73E-08 0.47E-08 0.65E-08
0.51E-08 0.00E+00
0.52E-09 0.40E-09 0.36E-09 0.13E-09 0.12E-09 0.74E-10 0.41E-11 0.36E-10 0.32E-10 0.30E-10
0.41E-09 -0.44E-09 -0.48E-09 -0.14E-09 -0.17E-09 0.12E-09 0.46E-08 0.89E-08 0.55E-08 0.81E-08
0.62E-08 0.53E-08
0.85E-09 0.38E-09 0.35E-09 0.17E-09 0.16E-09 0.11E-09 0.60E-11 0.55E-10 0.49E-10 0.40E-10
0.57E-09 0.43E-11 -0.40E-09 -0.42E-09 -0.21E-10 0.16E-09 0.63E-09 0.56E-09 0.14E-07 0.14E-07
0.86E-08 0.18E-07
0.65E-09 0.36E-09 0.33E-09 0.13E-09 0.13E-09 0.27E-09 0.16E-10 0.20E-10 0.19E-10 0.16E-10
0.25E-09 0.14E-10 0.17E-09 0.17E-09 0.34E-11 0.13E-10 0.40E-09 0.40E-09 0.11E-07 0.12E-07
0.10E-07 0.73E-08
0.61E-09 0.61E-09 0.10E-10 0.19E-10 0.18E-10 0.23E-10 0.74E-10 0.21E-10 0.21E-10 0.42E-11
0.67E-10 0.11E-10 0.41E-09 0.84E-09 0.32E-12 0.19E-12 0.36E-09 0.35E-09 0.99E-08 0.13E-07
0.98E-08 0.16E-07
0.53E-09 0.58E-09 0.96E-11 0.85E-11 0.79E-11 0.54E-11 0.17E-10 0.10E-12 0.98E-13 -0.13E-12
-0.21E-11 0.17E-10 0.47E-09 0.62E-09 0.53E-09 0.31E-09 0.26E-09 0.27E-09 0.77E-08 0.12E-07
0.30E-08 0.26E-07
0.51E-09 0.57E-09 0.91E-11 0.75E-11 0.67E-11 0.43E-11 0.13E-10 0.29E-11 0.26E-11 0.31E-10
0.27E-10 0.33E-10 0.47E-09 0.63E-09 0.53E-09 0.80E-11 0.27E-09 0.19E-09 0.56E-08 0.91E-08
0.68E-08 -0.13E-07
0.51E-09 0.57E-09 0.90E-11 0.80E-11 0.71E-11 0.49E-11 0.15E-10 0.14E-10 0.12E-10 0.31E-10
0.26E-10 0.35E-10 0.48E-09 0.66E-09 0.55E-09 0.37E-10 0.13E-08 0.14E-08 0.12E-08 0.56E-09
0.15E-07 0.26E-07
0.55E-09 0.56E-09 0.91E-11 0.90E-11 0.82E-11 0.89E-11 0.82E-11 0.84E-11 0.26E-10 0.32E-10
0.28E-10 0.34E-10 0.49E-09 0.37E-10 0.13E-08 0.77E-09 0.67E-09 0.68E-09 0.56E-09 0.51E-09
0.13E-07 0.14E-07
0.55E-09 0.56E-09 0.89E-11 0.97E-11 0.87E-11 0.96E-11 0.86E-11 0.95E-11 0.28E-10 0.37E-10
0.31E-10 0.11E-11 0.60E-09 0.13E-08 0.52E-12 0.24E-12 0.46E-09 0.45E-09 0.36E-09 0.34E-09
0.88E-08 0.00E+00
0.53E-09 0.55E-09 0.87E-11 0.94E-11 0.84E-11 0.82E-11 0.73E-11 0.58E-11 0.51E-11 0.11E-12
0.20E-09 0.55E-09 0.21E-12 0.24E-12 0.47E-09 0.43E-09 0.37E-09 0.36E-09 0.29E-09 0.28E-09
0.74E-08 0.00E+00
0.53E-09 0.54E-09 0.86E-11 0.12E-10 0.11E-10 0.14E-10 0.13E-10 0.15E-10 0.13E-10 0.36E-11
0.17E-09 0.35E-09 0.56E-11 0.21E-12 0.42E-09 0.43E-09 0.37E-09 0.38E-09 0.31E-09 0.31E-09
0.82E-08 0.00E+00

0.54E-09 0.53E-09 0.84E-11 0.13E-10 0.13E-10 0.22E-10 0.20E-10 0.14E-10 0.13E-10 0.11E-10
0.96E-11 0.72E-11 0.30E-09 0.15E-10 0.53E-09 0.53E-09 0.46E-09 0.46E-09 0.38E-09 0.39E-09
0.10E-07 0.26E-07
0.49E-09 0.46E-09 0.71E-11 0.66E-11 0.58E-11 0.47E-11 0.41E-11 0.21E-11 0.18E-11 0.77E-12
0.37E-10 0.15E-10 0.52E-09 0.49E-09 0.41E-09 0.40E-09 0.34E-09 0.32E-09 0.26E-09 0.26E-09
0.67E-08 0.48E-08
0.36E-09 0.35E-09 0.55E-11 0.38E-11 0.33E-11 0.16E-11 0.14E-11 0.98E-12 0.86E-12 0.56E-12
0.27E-10 0.95E-11 0.33E-09 0.31E-09 0.26E-09 0.24E-09 0.21E-09 0.19E-09 0.16E-09 0.15E-09
0.37E-08 0.33E-08
0.23E-09 0.28E-09 0.44E-11 0.31E-11 0.27E-11 0.13E-11 0.11E-11 0.78E-12 0.68E-12 0.43E-12
0.21E-10 0.57E-11 0.20E-09 0.17E-09 0.14E-09 0.12E-09 0.10E-09 0.82E-10 0.66E-10 0.49E-10
0.12E-08 0.32E-10
0.77E-10 0.25E-09 0.39E-11 0.53E-11 0.46E-11 0.17E-11 0.15E-11 0.88E-12 0.78E-12 0.37E-12
0.18E-10 0.26E-11 0.90E-10 0.73E-10 0.62E-10 0.50E-10 0.42E-10 0.32E-10 0.26E-10 0.14E-10
0.34E-09 0.12E-11

## SIMULATION THREE-Vertical component

-0.72E-14 0.11E-14 -0.20E-11 -0.25E-10 -0.38E-11 -0.13E-10 0.97E-11 -0.47E-11 0.60E-11 -0.25E-11
0.31E-10 0.57E-11 0.27E-10 0.91E-11 0.24E-10 0.94E-11 0.40E-10 0.11E-10 0.27E-10 0.15E-10
0.20E-10 0.14E-10
0.25E-13 0.42E-13 0.32E-10 -0.18E-10 0.18E-10 -0.74E-11 0.98E-11 -0.62E-11 0.10E-10 0.32E-11
0.37E-11 0.48E-11 0.38E-11 0.66E-11 0.60E-11 0.88E-11 0.92E-11 0.53E-11 0.13E-10 0.82E-11
0.13E-10 0.90E-11
0.78E-13 0.13E-12 0.20E-10 -0.99E-10 0.11E-10 -0.32E-10 0.12E-10 -0.16E-10 0.40E-11 -0.86E-11
0.31E-11 -0.14E-11 0.18E-11 0.45E-11 -0.21E-12 0.26E-11 0.21E-11 -0.28E-12 0.58E-11 0.19E-11
0.67E-11 0.34E-11
0.18E-12 0.59E-12 0.23E-10 0.15E-11 0.16E-10 -0.23E-10 0.79E-11 -0.15E-10 0.32E-11 -0.14E-10
-0.43E-12 -0.56E-11 -0.33E-11 -0.67E-11 -0.21E-11 -0.31E-11 -0.19E-11 -0.53E-11 0.95E-13 -0.41E-11
0.11E-11 -0.43E-11
0.70E-12 0.15E-11 0.44E-13 0.75E-12 0.25E-10 -0.71E-10 0.12E-10 -0.52E-10 0.94E-11 -0.36E-10
-0.18E-11 -0.28E-10 -0.11E-11 -0.18E-10 -0.56E-11 -0.81E-11 -0.70E-11 -0.94E-11 -0.66E-11 -0.89E-11
-0.56E-11 -0.87E-11
0.18E-11 0.46E-11 0.89E-12 0.25E-11 0.56E-10 0.53E-11 0.37E-10 -0.84E-10 0.22E-10 -0.72E-10
0.14E-10 -0.48E-10 0.59E-11 -0.28E-10 -0.26E-11 -0.10E-10 -0.85E-11 -0.12E-10 -0.87E-11 -0.12E-10
-0.10E-10 -0.11E-10
0.54E-11 0.13E-10 0.30E-11 0.62E-11 0.12E-12 0.25E-11 0.73E-10 -0.10E-09 0.62E-10 -0.67E-10
0.41E-10 -0.45E-10 0.23E-10 -0.24E-10 0.66E-11 -0.12E-10 -0.11E-10 -0.22E-10 -0.12E-10 -0.25E-10
-0.13E-10 -0.23E-10
0.92E-11 0.17E-10 0.69E-11 0.19E-10 0.29E-11 0.66E-11 0.10E-09 0.62E-10 0.68E-10 -0.41E-10
0.46E-10 -0.24E-10 0.24E-10 -0.11E-10 0.10E-10 0.52E-12 -0.22E-10 -0.48E-10 -0.26E-10 -0.55E-10

```
 0.12E-10  0.25E-10  0.68E-11  0.17E-10  0.72E-11  0.14E-10  0.89E-13  0.14E-11  0.52E-10 -0.19E-10
 0.32E-10 -0.52E-11  0.16E-10 -0.38E-11  0.93E-12 -0.45E-11 -0.53E-10 -0.11E-09 -0.57E-10 -0.24E-09
-0.33E-10 -0.31E-09
 0.90E-11  0.97E-11  0.52E-11  0.80E-11  0.14E-10  0.15E-10  0.16E-11  0.10E-10  0.36E-10  0.27E-10
 0.72E-11 -0.56E-10 -0.52E-11 -0.34E-10 -0.15E-10 -0.17E-10 -0.12E-09 -0.15E-09 -0.25E-09 -0.43E-09
-0.32E-09 -0.76E-09
 0.11E-10  0.11E-10  0.88E-11  0.89E-11  0.33E-11  0.87E-11  0.68E-11  0.11E-10  0.14E-12  0.93E-11
 0.56E-10  0.47E-10  0.18E-10 -0.99E-10 -0.11E-10 -0.17E-10 -0.15E-09  0.15E-10 -0.44E-09  0.77E-10
-0.77E-09  0.44E-10
 0.12E-10  0.12E-10  0.10E-10  0.10E-10  0.10E-10  0.11E-10  0.42E-11  0.11E-10  0.66E-11  0.13E-10
 0.17E-12  0.15E-11  0.98E-10 -0.62E-10  0.48E-10  0.35E-10  0.24E-10  0.22E-09  0.86E-10  0.89E-09
 0.41E-10  0.16E-08
 0.13E-10  0.12E-10  0.11E-10  0.86E-11  0.12E-10  0.11E-10  0.12E-10  0.12E-10  0.48E-11  0.13E-10
 0.11E-11  0.93E-11  0.19E-09 -0.22E-10  0.74E-10  0.13E-10  0.23E-09  0.31E-10  0.88E-09  0.19E-10
 0.16E-08 -0.33E-09
 0.39E-10  0.37E-10  0.93E-11  0.63E-11  0.12E-10  0.11E-10  0.12E-10  0.13E-10  0.14E-10  0.14E-10
 0.39E-11  0.14E-10  0.79E-10  0.91E-11  0.42E-11  0.79E-11  0.24E-10 -0.50E-10  0.14E-10 -0.24E-09
-0.34E-09 -0.54E-09
 0.38E-10  0.37E-10  0.20E-10  0.15E-10  0.11E-10  0.75E-11  0.13E-10  0.16E-10  0.14E-10  0.16E-10
 0.15E-10  0.15E-10  0.24E-10  0.69E-11 -0.48E-11  0.13E-11 -0.59E-10 -0.80E-10 -0.24E-09 -0.33E-09
-0.54E-09 -0.70E-09
 0.62E-10  0.64E-10  0.25E-10  0.25E-10  0.23E-10  0.17E-10  0.16E-10  0.11E-10  0.17E-10  0.22E-10
 0.15E-10  0.17E-10  0.11E-12 -0.33E-10 -0.17E-12 -0.23E-10 -0.84E-10 -0.11E-09 -0.34E-09 -0.41E-09
-0.71E-09 -0.78E-09
 0.65E-10  0.63E-10  0.26E-10  0.25E-10  0.30E-10  0.23E-10  0.35E-10  0.24E-10  0.23E-10  0.22E-10
 0.18E-10  0.20E-10  0.43E-10  0.12E-10  0.42E-10  0.18E-10 -0.11E-09 -0.99E-10 -0.42E-09 -0.27E-09
-0.78E-09 -0.47E-09
 0.63E-10  0.59E-10  0.26E-10  0.29E-10  0.25E-10  0.27E-10  0.25E-10  0.23E-10  0.23E-10  0.17E-10
 0.20E-10  0.20E-10  0.79E-10  0.70E-10  0.67E-10  0.21E-09 -0.11E-09 -0.80E-10 -0.28E-09 -0.17E-09
-0.47E-09 -0.59E-10
 0.35E-10  0.35E-10  0.29E-10  0.33E-10  0.28E-10  0.32E-10  0.23E-10  0.24E-10  0.17E-10  0.13E-10
 0.20E-10  0.20E-10  0.62E-10  0.20E-09  0.99E-13  0.39E-11 -0.86E-10 -0.66E-10 -0.18E-09 -0.15E-09
-0.61E-10 -0.13E-09
 0.12E-10  0.11E-10  0.20E-10  0.24E-10  0.19E-10  0.18E-10  0.24E-10  0.26E-10  0.39E-10  0.28E-10
 0.19E-10  0.17E-10  0.89E-13  0.11E-10  0.39E-11  0.63E-11 -0.75E-10 -0.43E-10 -0.16E-09 -0.12E-09
-0.13E-09 -0.24E-09
 0.33E-10  0.31E-10  0.40E-10  0.32E-10  0.31E-10  0.29E-10  0.27E-10  0.42E-10  0.28E-10  0.27E-10
 0.18E-10  0.12E-10  0.24E-11  0.50E-11  0.66E-11  0.15E-10 -0.44E-10  0.40E-10 -0.13E-09 -0.69E-10
-0.25E-09 -0.28E-09
 0.31E-10  0.25E-10  0.32E-10  0.26E-10  0.29E-10  0.27E-10  0.14E-10  0.22E-10  0.27E-10  0.23E-10
 0.38E-10  0.25E-10  0.16E-10  0.16E-10  0.31E-11  0.44E-11  0.85E-10  0.20E-10 -0.82E-10 -0.68E-10
-0.29E-09  0.27E-10
```

0.24E-10 0.21E-10 0.21E-10 0.19E-10 0.27E-10 0.30E-10 0.22E-10 0.21E-10 0.23E-10 0.21E-10
0.43E-10 0.33E-10 0.20E-10 0.25E-10 0.45E-11 0.43E-11 0.45E-11 0.45E-11 -0.76E-10 -0.42E-10
0.25E-10 -0.31E-10
0.69E-11 0.68E-11 0.38E-11 0.80E-11 0.60E-11 0.85E-11 0.21E-10 0.10E-10 0.21E-10 0.11E-10
0.20E-10 0.16E-10 0.15E-10 0.14E-10 0.43E-11 0.40E-11 0.63E-11 0.77E-11 -0.52E-10 0.37E-10
-0.40E-10 0.12E-09
0.68E-11 0.67E-11 0.80E-11 0.74E-11 0.85E-11 0.74E-11 0.10E-10 0.75E-11 0.11E-10 0.99E-11
0.55E-11 0.51E-11 0.47E-11 0.43E-11 0.40E-11 0.37E-11 -0.15E-10 0.18E-10 0.32E-10 0.12E-09
0.11E-09 0.39E-09
0.67E-11 0.68E-11 0.74E-11 0.71E-11 0.74E-11 0.69E-11 0.75E-11 0.67E-11 0.33E-11 0.54E-11
0.51E-11 0.54E-11 0.43E-11 0.49E-11 0.37E-11 0.13E-11 0.68E-11 -0.58E-10 0.12E-09 0.17E-09
0.38E-09 0.19E-09
0.67E-11 0.68E-11 0.70E-11 0.70E-11 0.69E-11 0.67E-11 0.67E-11 0.67E-11 0.54E-11 0.61E-11
0.55E-11 0.58E-11 0.49E-11 0.53E-11 0.14E-11 0.18E-12 -0.68E-10 0.51E-11 0.33E-09 0.10E-09
0.18E-09 0.24E-09
0.68E-11 0.67E-11 0.70E-11 0.68E-11 0.67E-11 0.67E-11 0.67E-11 0.66E-11 0.61E-11 0.64E-11
0.59E-11 0.61E-11 0.52E-11 0.32E-11 0.91E-12 0.62E-12 -0.99E-11 0.33E-10 0.77E-10 0.60E-10
0.23E-09 0.26E-09
0.67E-11 0.67E-11 0.68E-11 0.70E-11 0.66E-11 0.69E-11 0.65E-11 0.69E-11 0.64E-11 0.76E-11
0.60E-11 0.21E-11 0.32E-11 0.34E-11 0.64E-12 0.31E-13 0.31E-10 0.28E-10 0.41E-10 0.37E-10
0.25E-09 0.94E-10
0.66E-11 0.67E-11 0.70E-11 0.72E-11 0.69E-11 0.68E-11 0.69E-11 0.63E-11 0.76E-11 0.56E-11
0.62E-11 0.63E-11 0.10E-10 0.10E-10 0.70E-10 0.23E-10 0.17E-10 0.24E-10 0.17E-10 0.24E-10
0.83E-10 -0.27E-10
0.67E-11 0.67E-11 0.71E-11 0.77E-11 0.68E-11 0.74E-11 0.63E-11 0.67E-11 0.56E-11 0.31E-11
0.63E-11 0.87E-11 0.17E-10 0.11E-10 0.28E-11 0.22E-10 0.11E-11 0.13E-10 -0.18E-11 0.76E-11
-0.38E-10 -0.12E-09
0.66E-11 0.64E-11 0.77E-11 0.93E-11 0.73E-11 0.96E-11 0.67E-11 0.44E-11 0.92E-11 0.73E-11
0.14E-10 0.10E-10 0.11E-10 -0.11E-13 -0.44E-11 -0.65E-11 -0.98E-11 0.96E-12 -0.17E-10 0.11E-10
-0.13E-09 0.13E-09
0.64E-11 0.62E-11 0.93E-11 0.91E-11 0.96E-11 0.91E-11 0.13E-10 0.90E-11 0.12E-10 0.89E-11
0.10E-10 0.89E-11 0.10E-10 -0.43E-10 0.11E-11 -0.17E-10 0.54E-11 -0.81E-11 0.97E-11 0.18E-10
0.13E-09 0.84E-10
0.64E-11 0.63E-11 0.93E-11 0.91E-11 0.93E-11 0.80E-11 0.93E-11 0.79E-11 0.93E-11 0.78E-11
0.94E-11 0.78E-11 0.50E-10 -0.17E-10 0.39E-10 -0.65E-11 0.39E-10 0.29E-11 0.27E-10 0.15E-10
0.81E-10 0.72E-10
0.64E-11 0.68E-11 0.83E-11 0.76E-11 0.82E-11 0.75E-11 0.81E-11 0.74E-11 0.81E-11 0.72E-11
0.81E-11 0.72E-11 0.49E-10 -0.10E-10 0.42E-10 -0.26E-11 0.36E-10 0.42E-11 0.25E-10 0.13E-10
0.67E-10 0.43E-10
0.67E-11 0.78E-11 0.77E-11 0.85E-11 0.75E-11 0.58E-11 0.74E-11 0.58E-11 0.73E-11 0.58E-11
0.74E-11 0.63E-11 0.27E-10 0.92E-11 0.25E-10 0.13E-10 0.22E-10 0.13E-10 0.17E-10 0.15E-10
0.31E-10 0.30E-10

# REFERENCES

Andrews, C.B., Anderson, M.P.; 1979, Thermal Alteration of Groundwater Caused by Seepage From a Cooling Lake; Water Resour. Res., v 15, no 3, p 595-602.

Barker, Colin; 1972, Aquathermal Pressuring - Role of Temperature in Development of Abnormal Pressure Zones; American Association of Petroleum Geologists Bulletin, v 56, no 10, p 2068-2071.

Bjorlykke, K.; 1983, Diagenetic Reactions in Sandstones, in Parke, A., and Seliwood, B.W., eds., Sediment Diagenesis; D. Reidel, p 169-213.

Blanchard, P.E., and Sharp, J.M. Jr.; 1985, Possible Free Convection in Thick Gulf Coast Sandstone Sequences; in C.L. McNulty and J.G. McPherson, eds., Transactions Southwest Section American Association of Petroleum Geologists; Fort Worth Geological Society, p6-12.

Bodner,D.P, Blanchard, P.E.,Sharp, J.M. Jr.; 1985, Variations in Gulf Coast Heat Flow Created by Groundwater Flow; Gulf Coast Association of Geological Societies Transactions; v35, p19-28.

Boles, J.R.; 1980, Calcium Budget in Frio Sandstones, Southwest Texas; American Association of Petroleum Geologists Bulletin, v 64, n 678, abstract.

Bonham,L.G.; 1980, Migration of Hydrocarbons in Compacting Basins; American Association of Petroleum Geologists Bulletin, v 64, no 4, p 549-556.

Bredehoeft,J.D., and Hanshaw,B.B; 1968, On the Maintenace of Anomalous Fluid Pressures: I. Thick Sedimentary Sequences; Geological Society of America Bulletin, v 79, no 9, p 1097-1106.

Bruce, C.H.; 1984; Smectite Dehydration-Its relation to Sturctural Devlopment and Hydrocarbon Accumulation in Northern Gulf of Mexico Basin; American Association of Petroleum Geologists Bulletin, v 68, p 673-683.

Burst, J.F. Jr.; 1969, Diagensis of Gulf Coast Clayey Sediments and its Possible Relations to Petroleum Migration; American Association of Petroleum Geologists Bulletin, v 53, no 1, p 73-93.

Dickinson, G.; 1953, Geological Aspects of Abnormal Reservoir Pressures in Gulf Coast Louisiana; American Association of Petroleum Geologists Bulletin, v 37, p 410-423.

Epp, D., Grim, P.J., and Langseth, M.G.; 1970, Heat Flow in the Caribbean and Gulf of Mexico; Journal of Geophysical Research, v 75, no 29, p 5655-5669.

Fisher, S.R.; 1982, Diagenetic History of Eocene Wilcox Sandstones and Associated Formation Waters, South-Central Texas; Phd Dissertation, Univ. of Texas at Austin.

Fyfe, W.S., Price, N.J., and Thompson, A.B.; 1978, Fluids in the Earth's Crust; Elsevier, Amsterdam, 383p.

Galloway, W.E.; 1984, Hydrogeologic Regimes of Sandstone Diagenesis; in D.A. McDonald and E.L. Surdam, eds., Clastic Diagenesis, American Association of Petroleum Geologists Memoir 37, p3-13.

Galloway, W.E., and Hobday, D.K.; 1983, Terrigenous Clastic Depositional Systems; Applications to Petrolium, Coal, and Urnaium Exploration, Springer-Verlag, 423 p.

Gibson, R.E.; 1958, The Progress of Consolidation in a Clay Layer Increasing in Thickness with Time; Geotechnique, v18, p171-182.

Hedberg, H.D.; 1980, Methane Generation and Petroleum Migration; in Problems of Petroleum Migration, (eds. Roberts, W.H. III and Cordell, R.J.) American Association of Petroleum Geologists Studies in Geology, no 10, p 179-206.

Jaeger, J.C. and Cook, N.G.; 1979, Fundamentals of Rock Mechanics (3rd Ed.); Chapman and Hall, London, 593p.

Jones, P.H.; 1969, Hydrology of Neogene deposits in the Northern Gulf of Mexico Basin; Louisiana Water Resource Institute Bulletin, #GT-2, 105p.

Keenan, J.H., Keyes, F.G., Hill, P.G.,and Moore, J.G.; 1978, Steam Tables - Thermodynamic Properties of Water Including Vapor, Liquid, and Solid Phases; John Wiley & Sons, N.Y..

Kehle, R.O.; 1971, Geothermal Survey of North America, 1971 Annual Progress Report; Research Committee American Association of Petroleum Geologists (unpub.), 31p.

Keith, L.A., and Rimstidt, J.D.; 1985, A Numerical Compaction Model of Overpressuring in Shales; Mathematical Geology, v 17, p 115-136.

Kharaka, Y.K., Lico, M.S., Carothers, W.W.; 1980, Predicted Corrosion and Scale-Formation Properties of Geopressured Geothermal Waters of the Northern Gulf of Mexico Basin, Journal of Petroleum Technology, v 32, no 2, p 319-324.

Kim, Young C; 1984, Geostatistics in Research Short Course Notes, Bureau of Economic Geology, University of Texas at Austin, Oct. 10-12, 1984.

Kingston, J; 1985, Long Term Effects of In Situ Leach Mining Restoration in the Oakville Aquifer System Near George West, Texas; Gullf Coast Association of Geological Societies Transactions, v35, p 151-159.

Land, L.S; 1984, Frio Sandstone Diagenesis, Texas Gulf Coast: A Regional Isotopic Study, in D.A. McDonald and R.C. Surdam, eds., Clastic Diagenesis; American Association of Petroleum Geologists Memoir 37, pp. 47-62.

Land, L.S. and Dutton, S.P.; 1979, Reply: Cementation of Sandstones; Journal of Sedimentary Petrology, v49, p 1359-1361.

Lewis, C.R., and Rose, S.C.; 1970, A Theory Relating High Temperatures and Overpressures; Journal of Petroleum Technology; v 22, p 11-16.

Li, T.M.C.; 1980, Axisymmetric Numerical Simulation of Hydrothermal Systems, Including Changes in Porosity and Permeability Due to the Quartz-Qater Reaction; Ph.D. thesis, Penn State Univ., 240 pp.

Loucks, R.G., Dodge, M.M., and Galloway, W.E.; 1979, Sandstone Consolidation Analysis to Delineate Areas of High-Quality Reservoirs Suitable for Production of Geopressured Geothermal Energy Along the Texas Gulf Coast; Bureau of Economic Geology, Contract Report #EG-77-505-5554, January.

Magara, Kinji; 1976, Water Expulsion from Calstic Sediments During Compaction-Directions and Volumes; American Association of Petroleum Geologists, v 60, no 4, p 543-553.

Mercer, J.W., Pinder, G.F., and Donaldson, I.G.; 1975, A Galerkin Finite Element Analysis of the Hydrothermal System at Wairakei, New Zealand; J. Geophy. Res., v 80, n 17, pp 2608-2621.

Mumme,S.T., and Ferrel, R.E.; 1979, Geopressure in the Houma and Hooywood Fields, Louisiana; Gulf Coast Association of Geological Societies Transactions,v29, p 321-327.

Philippi, G.T.; 1965, On the depths, Time and Mechanism of Petroleum Generation; Geochimica et Cosmochimica Acta, v 29, p 1021-1051.

Pinder, G.F., Gray, W.; 1977, Finite Element Simulation in Surface and Subsurface Hydrology; Academic, New York.

Price, L.C.; 1976, Aqueous Solubility of Petroleum as Applied to Its Origin in Primary Migration; American Association of Petroleum Geologists Bulletin, v 60, no 2, p 213-244.

Reiter, M, Toverar, R.J.C.; 1982, Estimates of Terrestrial Heat Flow in Northern Chihuahua, Mexico, Based on Petroleum Bottom-Hole Temperature Measurements; Geological Society of America Bulletin, 1982, v 93, p 613-624.

Richmann, D.L., Milliken, K.L., Loucks, R.G., and Dodge, M.M.; 1980, Relationship Between Mineraolgy, Diagenesis, and Porosity in Vicksburg Sandstones, McAllen Ranch Field, Hidalgo County, Texas; Gulf Coast Assoc. Geol. Soc. Trans, annual meeting 1980.

Royden, L., Sclater, J.G., Von Her, R.P.; 1980, Continental Margin Subsidence and Heat Flow: Important Parameters in Formation of Petroleum Hydrocarbons; American Association of Petroleum Geologists, v 64, no 2, p173-187.

Russel, K.L.; 1971, Fresher Intersitital Waters From Normal Marine Shales; Abstract, Am. Geophys. Union Trans.; v 52, p 929.

Sass, J.H., Luchenbruch, A.H., and Munroe, R.J.; 1971, Heat Flow in the Western United States; Journal of Geophys Research, v 76, p 6376-6413.

Schmidt, G.W.; 1973, Interstitial Water Composition and Geochemistry of Deep Gulf Coast Shales and Sandstones; American Association of Petroleum Geologists Bulletin, v 57, no 2, p 321-337.

Sharp, J.M. Jr., 1976, Momentum and Energy Balance Equations for Compacting Sediments, Mathematical Geology, v 8, no 3, p305-322.

Sharp, J.M. Jr., and Domenico, P.A.; 1976, Energy Transport in Thick Sequences of Compacting Sediment. Geological Society of America Bulletin, v 87, p 3.

Sibley, D.F. and Blatt, H.; 1976, Intragranular Pressure Solution and Cementation of the Tuscarora Orthoquartzite; Journal of Sedimentary Petrology, v 46, p 881-896.

Smith, G.E., Galloway, W.E., and Henry, C.D.; 1982, Regional Hydrodynamics and Hydrochemistry of the Uranium-Bearing Oakville Aquifer (Miocene) of South Texas; Texas Bureau of Economic Geology Report of Investigations, 124, 31p.

Smith,L; December 1984, Program Canshaft, Simulataneous Heat and Fluid Transport; University of Briish Columbia, unpublished.

Smith, L., and Chapman, D.S.; 1983, On the Thermal Effects of Groundwater Flow 1. Regional Scale Systems; Jour Geophys Res., v 88, no B1, p 593-608.

Wang, H.F., Anderson, M.P.; 1982, Introduction to Groundwater Modeling, Finite Difference and Finite Element Methods; W.H. Freeman and Company, New York, 237p.

Watson, J.T., Basu, R.S., and Sengers, J.V.; 1980, An Improved Representative Equation for the Dynamic Viscosity of Water Substance; Jour of Phys. Chem. Ref. Data, v 9, no 4, pp 1255-1279.

Weaver, C.E., and Beck, K.C.; 1971, Clay Water Diagensis During Burial: How Mud Becomes Gneiss, Geological Society of America Special Paper 134, p 1-78.

Wessleman, J.B.; 1983, Structure, Temperature, Pressure, and Salinity of Cenozoic Aquifers of South Texas, Hydrological Atlas, USGS HA-654.

Wood, J.R., and Hewett, T.A.; 1982, Fluid Convection and Mass Transfer in Porous Sandstones - A Theoretical model; Geochimica et Cosmochimica Acta, v46, p 1707-1713.

The vita has been removed from the digitized version of this document.

# WELL LOCATIONS OF COMPLETE DATA BASE

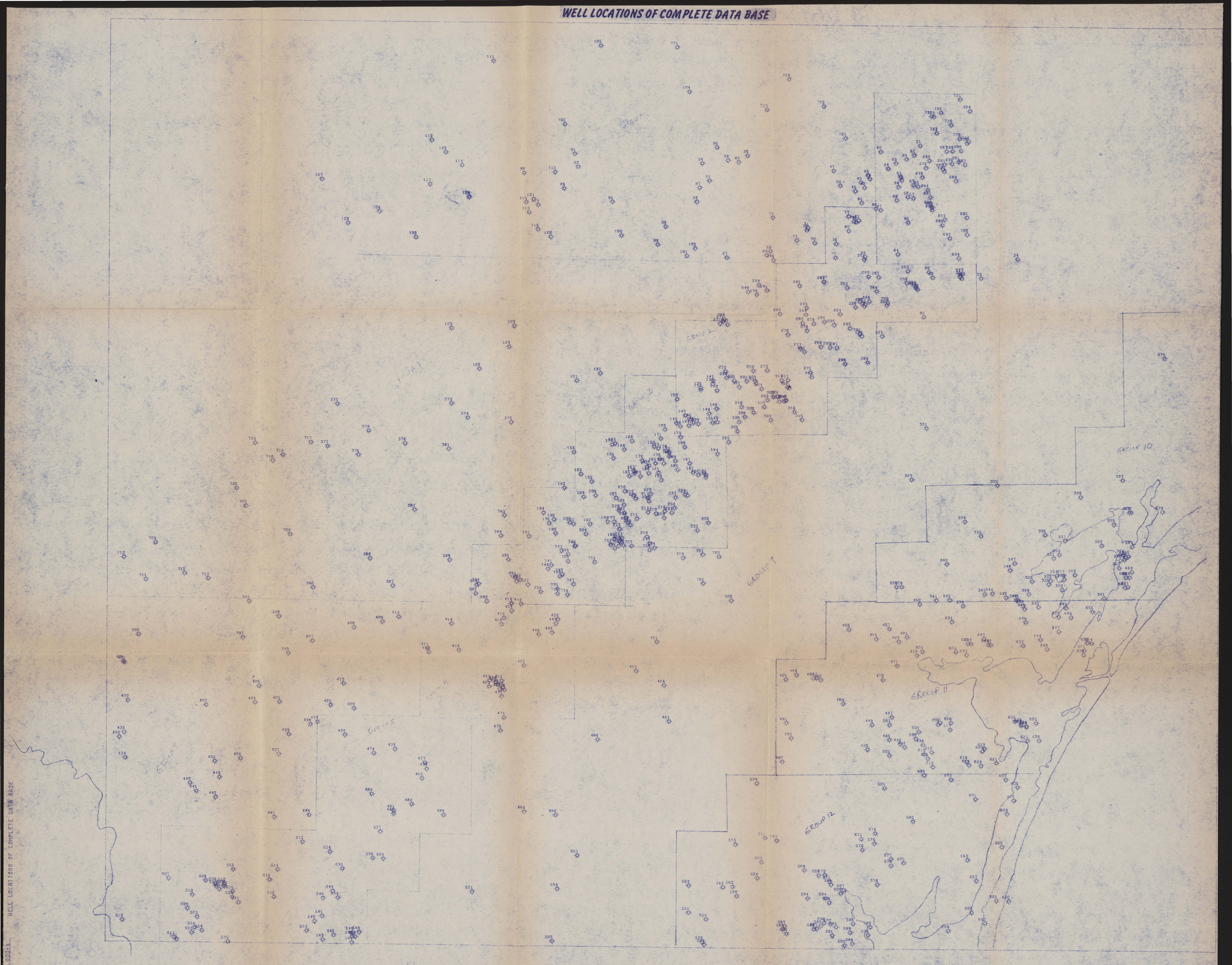


WELL LOCATIONS OF COMPLETE DATA BASE